National Library of Canada
Acquisitions and Bibliographic Services Branch
395 Wellington Street
Ottawa, Ontario
K1A 0N4

Bibliothèque nationale du Canada
Direction des acquisitions et des services bibliographiques
395, rue Wellington
Ottawa (Ontario)
K1A 0N4

Your file Votre référence

Our file Notre référence

NOTICE

The quality of this microform is heavily dependent upon the quality of the original thesis submitted for microfilming. Every effort has been made to ensure the highest quality of reproduction possible.

If pages are missing, contact the university which granted the degree.

Some pages may have indistinct print especially if the original pages were typed with a poor typewriter ribbon or if the university sent us an inferior photocopy.

Reproduction in full or in part of this microform is governed by the Canadian Copyright Act, R.S.C. 1970, c. C-30, and subsequent amendments.

AVIS

La qualité de cette microforme dépend grandement de la qualité de la thèse soumise au microfilmage. Nous avons tout fait pour assurer une qualité supérieure de reproduction.

S'il manque des pages, veuillez communiquer avec l'université qui a conféré le grade.

La qualité d'impression de certaines pages peut laisser à désirer, surtout si les pages originales ont été dactylographiées à l'aide d'un ruban usé ou si l'université nous a fait parvenir une photocopie de qualité inférieure.

La reproduction, même partielle, de cette microforme est soumise à la Loi canadienne sur le droit d'auteur, SRC 1970, c. C-30, et ses amendements subséquents.

Canada

Modelling and Simulation of Electric Mining Shovels

by

Hongjin Wu

B.Sc. M.Eng.

Department of Mining and Metallurgical Engineering
McGill University,
Montréal, Québec, Canada

A thesis submitted to the Faculty of Graduate Studies and Research
in partial fulfillment of the requirements for the degree of
Doctor of Philosophy

May 18, 1995

© Hongjin Wu

National Library of Canada
Acquisitions and Bibliographic Services Branch
395 Wellington Street
Ottawa, Ontario
K1A 0N4

Bibliothèque nationale du Canada
Direction des acquisitions et des services bibliographiques
395, rue Wellington
Ottawa (Ontario)
K1A 0N4

Your file Votre référence

Our file Notre référence

THE AUTHOR HAS GRANTED AN IRREVOCABLE NON-EXCLUSIVE LICENCE ALLOWING THE NATIONAL LIBRARY OF CANADA TO REPRODUCE, LOAN, DISTRIBUTE OR SELL COPIES OF HIS/HER THESIS BY ANY MEANS AND IN ANY FORM OR FORMAT, MAKING THIS THESIS AVAILABLE TO INTERESTED PERSONS.

L'AUTEUR A ACCORDE UNE LICENCE IRREVOCABLE ET NON EXCLUSIVE PERMETTANT A LA BIBLIOTHEQUE NATIONALE DU CANADA DE REPRODUIRE, PRETER, DISTRIBUER OU VENDRE DES COPIES DE SA THESE DE QUELQUE MANIERE ET SOUS QUELQUE FORME QUE CE SOIT POUR METTRE DES EXEMPLAIRES DE CETTE THESE A LA DISPOSITION DES PERSONNE INTERESSEES.

THE AUTHOR RETAINS OWNERSHIP OF THE COPYRIGHT IN HIS/HER THESIS. NEITHER THE THESIS NOR SUBSTANTIAL EXTRACTS FROM IT MAY BE PRINTED OR OTHERWISE REPRODUCED WITHOUT HIS/HER PERMISSION.

L'AUTEUR CONSERVE LA PROPRIETE DU DROIT D'AUTEUR QUI PROTEGE SA THESE. NI LA THESE NI DES EXTRAITS SUBSTANTIELS DE CELLE-CI NE DOIVENT ETRE IMPRIMES OU AUTREMENT REPRODUITS SANS SON AUTORISATION.

ISBN 0-612-05815-8

Canada

Dedicated to my father, Qingming Wu, my mother, Hanfen Huang, my wife, Suming Su, and my son, Di Wu

ABSTRACT

The electric mining shovel is the main rock loading machine at the majority of surface mining operations. The performance and utilization of these multi-million dollar machines can govern an entire mining operation. Despite their significance, they remain largely unexplored in terms of their potential. The thesis discusses the development of the forward and inverse kinematic models, the Newton-Euler dynamics, and the actuator dynamics for an electric mining shovel. The thesis relates to work undertaken towards the development of a mining shovel simulator, the purpose of which is to explore productivity and machine performance issues as a function of the interaction of the shovel with the ground. Both the parametric and nonparametric system identification results are presented, based on field test data collected from an operating mining shovel. Simulator results describing analytical and empirical models, as well as continuous-time controller and disturbance rejection are also presented. The thesis concludes with a discussion of planned continuing work.

ABSTRACT

La pelle mécanique électrique représente l'outil de chargement le plus utilisé dans la plupart des opérations de surface dans le domaine minier. L'utilisation et la performance de ces machines pouvant valoir jusqu'à plusieurs millions de dollars ont un impact déterminant sur les activités d'une mine. Malgré leur rôle crucial, leur potentiel reste largement inexploité.

L'objet de cette thèse consiste à discuter le développement de modèles de cinématique inverse, de la dynamique Newton-Euler et de la dynamique des actuateurs d'une pelle électrique. La thèse relate le travail entrepris afin de développer un simulateur de pelle mécanique électrique dont le but est d'étudier la productivité et la performance en fonction du degré d'interaction de la pelle avec le sol.

On présentera ici les résultats de l'identification paramétrique et non-paramétrique du système basée sur l'analyse des résultats expérimentaux. On présentera également les résultats provenant de simulateurs fondés sur deux approches différentes, l'une analytique et l'autre empirique. Les deux modèles utilisent des méthodes de contrôle en temps continu ainsi que des techniques de rejet des perturbations. La thèse se termine avec un aperçu des développements à venir.

ACKNOWLEDGEMENTS

I wish to express my sincere gratitude to my thesis supervisor, Professor Laeeque K. Daneshmend, for his continued support (from M.Eng. to Ph.D.), confidence, and guidance during the course of the investigation.

I wish to thank my cosupervisor, Professor Carl Handricks, for his advice and help. Particularly, he taught me mining knowledge and gave me some valuable mining material which had great help to me, a student with electrical engineering background.

I wish to thank Professor Malcolm Scoble for his assistance and advice. He actually introduced me to my first open pit mine, the asbestos mine, in Black Lake, Quebec.

Financial support for this work was provided by a Strategic Project Grant from the Natural Sciences and Engineering Research Council of Canada. I wish to thank the above three professors for arranging my financial support from this grant.

I wish to thank Professor N. Hori, for taking time to discuss some interesting issues about the research with me.

I wish to thank P&H Ltd. for providing much valuable data and material. I could not have completed this work without this collaborative assistance.

I would also like to thank the staff and students at the Canadian Centre for Automation and Robotics in Mining (CCARM), and at the McGill Research Centre for Intelligent Machines (McRCIM), for providing excellent facilities and a stimulating research environment. In particular, I wish to thank Prof.J. Mossop, Mr.C. Aboujaoude, Mr.M. Amjad, Mr.X. Huang, Mr.X. Luo, Mr.P. Knight, and Mr.A. Maluf, for their various help. I also thank Mr.E. Garant, who translated my English Abstract to French Abstract.

Finally, I wish to thank my father, Qingming Wu, my mother, Hanfen Huang, for their long time education and encouragement. Meanwhile, I wish to thank my wife, Suming Su, and my son, Di Wu, for their love, understanding and patience.

CLAIM OF ORIGINALITY

The following original contributions were made.

- Systematic investigation of the electric mining shovel using robotics and control theory
- Creation of a model of the entire shovel, including forward and inverse kinematics, Jacobian, rigid body dynamics, and actuator dynamics
- Complete analysis of the friction and impact between bucket and muckpile, and its effect on the shovel and its actuators
- Use of nonparametric system identification techniques to analyse the behaviour of the shovel digging process
- Establishment of both analytical and empirical shovel simulators, and validation of the overall system model using empirical data.

Contents

List of Figures

List of Tables

Symbols

A coefficient matrix of state-space equation

a_i distance from Z_i to Z_{i+1} measured along X_i

B coefficient matrix of state-space equation

B_1 coefficient matrix of state-space equation

b mechanical damping constant of DC motor

b_e electrical damping constant of DC motor

b_i viscous damping coefficient

C coefficient matrix of state-space equation

c_1 friction coefficient of the crowd DC motor

c_2 friction coefficient of the hoist DC motor

c_3 friction coefficient of the swing DC motor

c_1 $\cos(\theta_1)$

c_2 $\cos(\theta_2)$

c_3 $\cos(\theta_3)$

D Maximum digging distance

D_1 bucket length

d_i distance from X_i to X_{i+1} measured along Z_i

d_4 translation of dipper handle

$\dot{d}_4$ translational velocity of dipper handle

E_a back emf

$e(t)$ white noise

F impact forces

F_I impacts along x_5

F_{II} impacts along z_5

F_{max} maximum impact

${}^1F_i$ inertial force acting at the center of mass of each link

f friction forces

f_p payload gravity

f_1 bottom surface friction of outer bucket

f_2 bottom surface friction of inner bucket

f_3 two-side surface friction of outer bucket

f_4 two-side surface friction of inner bucket

${}^i\mathbf{f_i}$ force vector exerted on the ith joint

$G(q)$ transfer function

$\hat{G}_N(e^{i\omega})$ estimation function

$\hat{\bar{G}}_N(e^{i\omega})$ estimation function

g gravity acceleration

H actual depth of material in bucket

H_{fa} final average depth of material in bucket

I unit matrix

I_m sum of the actuator and gearbox inertias

I_a actuator inertia

I_g gearbox inertia

$^{c_i}I_i$ inertia tensor

I_{xxi} scalar element of inertia tensor

I_{yyi} scalar element of inertia tensor

I_{zzi} scalar element of inertia tensor

i_a armature current of DC motor

i_f field current of DC motor

i_l total current of DC motor

J Jacobian

K coefficient matrix of state-space equation

k_p passive pressure coefficient

k_r factor due to gravity(from nomograms)

K_1 $\frac{1}{M_1} + \frac{1}{M_2}$

K_2 deformation coefficient

k_{ii} gain(i=1,2,3,4,5,etc.)

k_1 torque constant of swing motor

k_2 back emf constant of swing motor

k_3 torque constant of hoist motor

k_4 back emf constant of hoist motor

k_5 torque constant of crowd motor

k_6 back emf of crowd motor

L lip friction force

L_a armature winding inductance

L_f field winding inductance

L_i length of link i

M_b bucket mass

M_p payload

M_1 bucket mass

M_2 muckpile mass

m_i rigid body i mass

${}^iN_i$ inertial torque acting at the center of mass of each link

n length number of bucket

n_1 number of teeth or lips

${}^i\mathbf{n_i}$ moment vector exerted on the ith joint

P payload

P_p lateral thrust per length of wall(N/m)

P_x X coordinate of the cutting head frame {5} relative to frame {0}

P_y Y coordinate of the cutting head frame {5} relative to frame {0}

P_z Z coordinate of the cutting head frame {5} relative to frame {0}

${}^i\mathbf{P_{i+1}}$ vector from the origin of frame i toward the origin of frame $i+1$

$^{i}\mathbf{P}_{ci}$ center of mass for each link

Q controllability matrix

Q_i geometry constant

q shift operator

R resistive force on blade

R_a armature winding resistance

R_f field winding resistance

$^{i}_{i+1}\mathbf{R}$ rotation part of the coordinate $i+1$ with respect to the coordinate i

r_i gearbox ratio

S Laplace transform

s_1 $\sin(\theta_1)$

s_2 $\sin(\theta_2)$

s_3 $\sin(\theta_3)$

T tooth friction force

T_m torque generated by the DC motor

T_{di} disturbance torque to the DC motor

$^{i-1}_{i}T$ transformation from frame $\{i\}$ to the frame $\{i-1\}$ for each link

U_N $\frac{1}{\sqrt{N}}\sum_{t=1}^{N} u(t)e^{-it\omega}$

$u(t)$ system input

V_1 bucket motion velocity

V_2 muckpile velocity

v_i input voltage of DC motor

${}^i v_{i+1}$ rigid body i+1's linear velocity with respect to rigid body i

${}^i \dot{v}_{i+1}$ rigid body i+1's linear acceleration with respect to rigid body i

${}^i \dot{v}_{ci}$ linear acceleration of the center of mass of each link

Δv $v_i - v_i^*$

W_i weighting function

w blade width

w_L width of the lips

w_T width of the teeth

X_0 X coordinate of frame 6 origin relative to frame 0

x_1 state variable representation of θ for swing motor

x_2 state variable representation of ω for swing motor

x_3 state variable representation of i_a for swing motor

x_4 state variable representation of θ for hoist motor

x_5 state variable representation of ω for hoist motor

x_6 state variable representation of i_a for hoist motor

x_7 state variable representation of θ for crowd motor

x_8 state variable representation of ω for crowd motor

x_9 state variable representation of i_a for crowd motor

x_i^* steady-state values of state-space variable

Δx $x_i - x_i^*$

Δx_6 $x_{61} - x_{60}$

Y_N $\frac{1}{\sqrt{N}} \sum_{t=1}^{N} y(t) e^{-it\omega}$

Y_0 Y coordinate of frame 6 origin relative to frame 0

$y(t)$ system output

Δy_6 $y_{61} - y_{60}$

Z_0 Z coordinate of frame 6 origin relative to frame 0

${}^{i+1}\hat{Z}_{i+1}$ along the Z-axis direction

Δz_6 $z_{61} - z_{60}$

$(x_{61} y_{61} z_{61})$ destination of bucket digging

$(x_{60} y_{60} z_{60})$ start of bucket digging

Greek letters

α_{i-1} angle between Z_i and Z_{i+1} measured about X_i

γ unit weight of the fill material(N/m)

δ_i material dependent constant

θ rotor position(radians)

θ_i angle between X_{i-1} and X_i measured about Z_i

θ_1 rotatory angle of swing motor

θ_3 rotatory angle of hoist motor

$\dot{\theta}_i$ angular velocity of DC motor

$\ddot{\theta}_i$ angular acceleration of DC motor

$\hat{\theta}_i$ estimator

μ coefficient of friction

τ_1 time constant, $\frac{L_a}{R_a}$

τ_2 time constant, $\frac{I_m}{b}$

$\hat{\phi}_v^N(\omega)$ noise spectrum

φ digging angle

χ blade tip depth

ω $2\pi k/N, k = 1, ..., N$

ω_i angular velocity of DC motor

ω_{1r} reference angular velocity for swing motor

ω_{2r} reference angular velocity for hoist motor

ω_{3r} reference angular velocity for crowd motor

${}^i\omega_{i+1}$ rigid body i+1's rotational velocity with respect to rigid body i

${}^i\dot{\omega}_{i+1}$ rigid body i+1's rotational acceleration with respect to rigid body i

Chapter 1

Introduction

This thesis is an application of robotics and control theory to the operation of the electric mining shovel. It is also a detailed description to the electric mining shovel from the points of view of mining, electricity, and mechanics.

1.1 Overview

Surface mining represents one of the world's largest industries. The mining shovel plays a key role in many surface mining operations. It is used as a production machine in conjunction with drill and blast operations to move waste rock or ore. The rate and efficiency with which mining shovels operate in loading haul trucks will largely determine the efficiency of the overall mining operation. Hence, most surface mining operations tend to evaluate their productivity based on the performance of their primary loading equipment. There exists considerable scope for productivity enhancement in surface mine extraction through the optimized use and operation of current excavation equipment.

There are two types of mining shovels used in current mining industry, i.e., the hydraulic shovel and the electric shovel.

The typical hydraulic shovel is illustrated in Figure 1.1. The machine has versatile features, and it is well adapted to selective mining methods. It has a wrist action of the dipper, and is able to separate waste from ore in order to reduce the cost of ore processing. Although the hydraulic shovel has many merits, the electric shovel is preferred in the hard digging environments, due to its power and capacity.

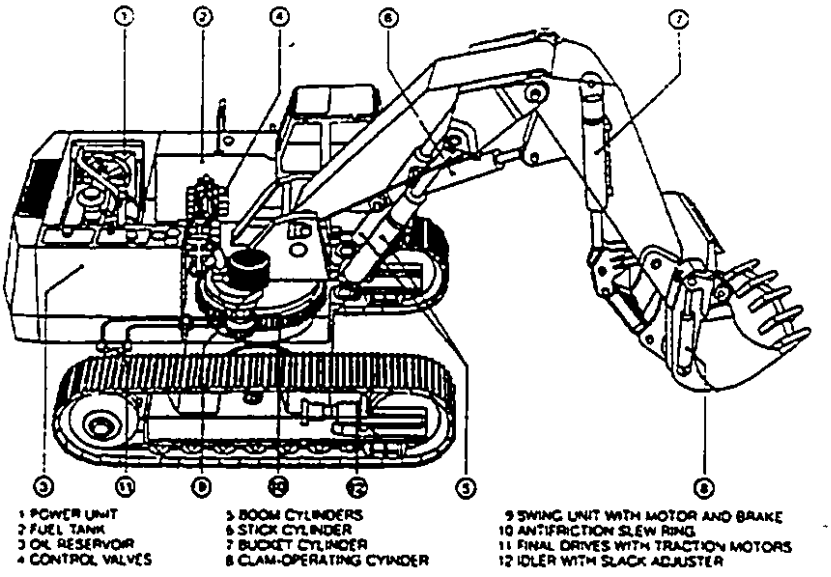

Figure 1.1: Typical Hydraulic Mining Shovel (Source: Demag Corp.)

An typical electric shovel is illustrated in Figure 1.2. The machine consists of two major sub-systems: the mechanical and electrical systems. From a mechanical viewpoint, the shovel has three main parts: the crawler and gantry structure; the boom and rope assembly; the dipper handle and dipper. Corresponding to the three mechanical parts, there are also three major electrical parts: the swing motor, which drives the gantry structure rotation; the hoist motor, which drives the rope assembly payout and retraction; and the crowd motor, which drives the linear displacement of the dipper handle and dipper. This thesis will focus on the electric shovel.

1.2 Previous Shovel Research

Research of the actual performance of an electric mining shovel was initially undertaken by Keller (1978). His system used a microprocessor based monitoring system to enhance the performance of electric mining shovels in the coal industry. Keller's work included shovel monitoring, but did not relate to data analysis and shovel responses

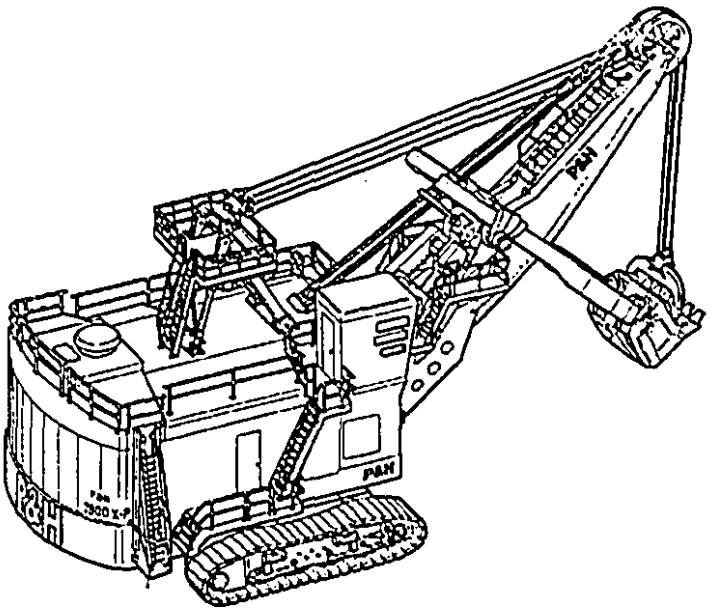

Figure 1.2: Typical Electric Mining Shovel (Source: P&H Inc.)

to variations in muckpile diggability. Williamson et al.(1983) and Mol et al.(1987) undertook investigations into muckpile diggability by monitoring shovel performance. Their work measured blast efficiency through the performance monitoring of an electric mining shovel. Their work was undertaken in separate uncontrolled geologic and blast environments, and did not account for several uncontrollable variables. In addition, no data on dipper trajectory was recorded assist in assessing muckpile diggability. Carl Hendricks et al. (1989) investigated another electric mining shovel operation. This work included geologic investigation and blast design, post blast evaluation, data acquisition, and analysis of monitored shovel performance parameters. This research demonstrated the relationships between shovel performance and muckpile diggability and the significance of the digging trajectory. Although there has not been any research directly relating to the friction of shovel buckets so far, Rowlands' thesis (1991) investigated the friction of a dragline bucket. His work provided some basis to our research on the friction model of a shovel bucket. Hadjigeorgiou J. et al. (1993) developed an empirical classification system which was used to assess the ease of excavation. He took inertial effects into consideration in his model.

1.3 Research Goals

No prior work has assembled a total system model of an electric shovel. Our work focuses on mathematic modelling of the system. It uses up-to-date robotic and automatic techniques to solve some very practical issues, such as the relationship between digging and the DC motors of the shovel. Moreover, advanced system identification and spectrum analysis techniques are used to analyze data collected and to assess rock fragmentation and diggability. The overall goal of the research is to increase the productivity and raise the efficiency of electric shovels through a better understanding of the machine operational limitations and its interaction with the rock. The methodology that is proposed relies upon both analytical and experimental studies of the behaviour of the machine and its performance while digging. In the scope of this thesis, these studies are related to the model of the complete shovel, including forward and inverse kinematics; Jacobian; rigid body dynamics; actuator/transmission dynamics; full analysis of the interactive effect of friction and impact between bucket and muckpile; introduction of the parametric and nonparametric system identification to the shovel and its digging process; and establishment of both analytical and empirical model simulators.

The research is aimed to advance mining technology in two ways. In the medium term, the thesis should assist the optimization of shovel productivity. In the long term, however, it should contribute to the fully automated operation of the electric mining shovel with a computer vision guidance system. Overall system model could contribute to computer control design which would make a shovel fully automated. Kinematics model could contribute to trajectory planning/task planning which would enable the shovel to follow a human operator's guidance. Figure 1.3 summarizes the research goals and steps.

The thesis investigation includes three phases: analytical modelling; empirical modelling; and system simulation. In the analytical phase, mathematical models parameterized with actual data from a P&H 2300XPA shovel were built (Help was received from the P&H Company, see Chapter 5). In the empirical modelling phase,

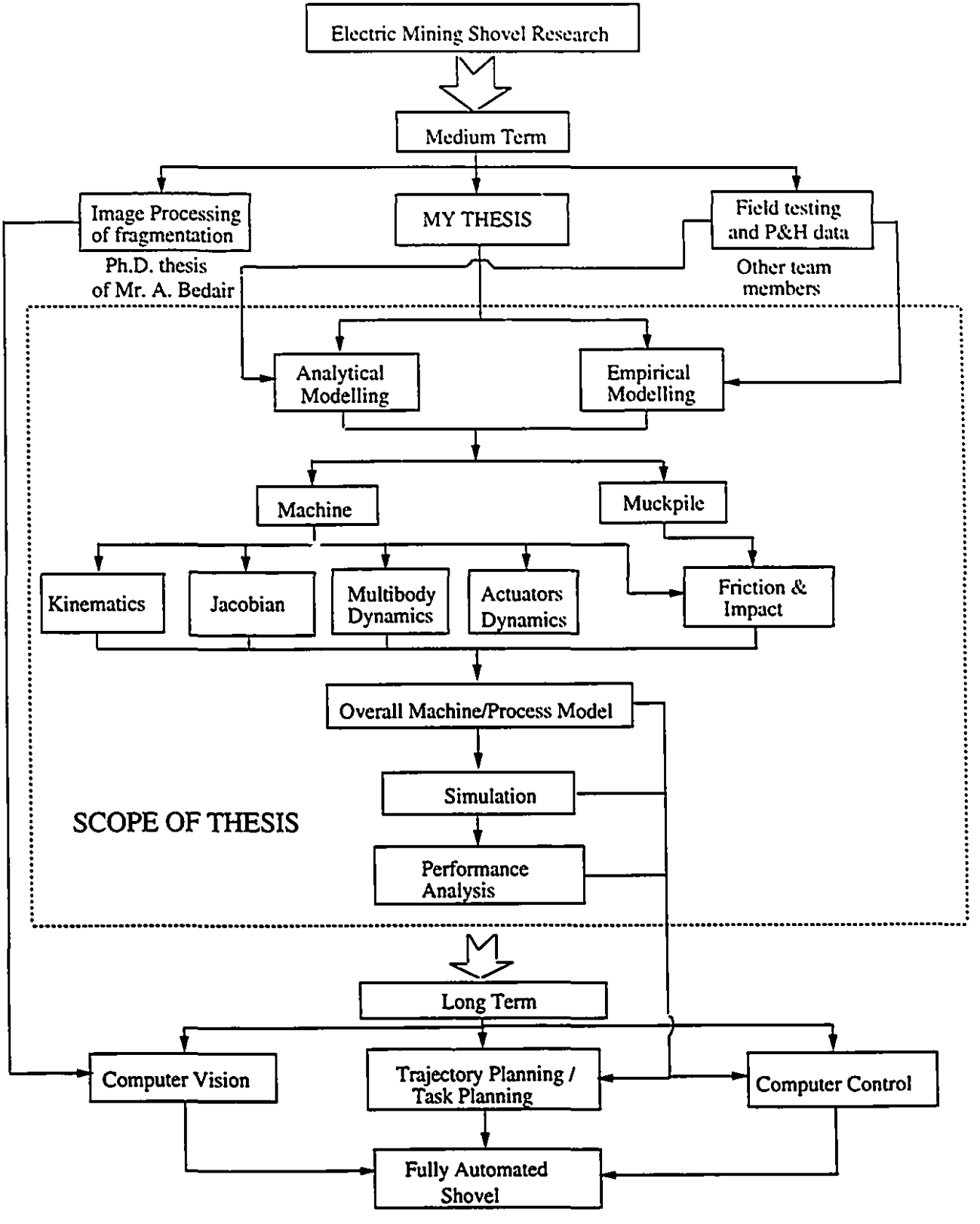

Figure 1.3: Research Goals and Steps

field tests and data acquisition were undertaken. The parametric and nonparametric system identification was implemented so that an empirical model could be built. In the simulation phase, both the analytical and empirical models were set up and used to simulate and validate the electric shovel operation.

1.4 Thesis Outline

In Chapter 2, the forward and inverse kinematics which establish the relationship between the bucket and all joints are obtained. This relationship lays a foundation for the bucket tracking calculation and trajectory control. The shovel Jacobian, which is the foundation for shovel speed calculation and control, is included in Chapter 3. In Chapter 4, the rigid body dynamics are calculated. The dynamics enables us to relate the digging forces and rigid body motion forces to the load torques of the shovel actuators. Chapter 5 examines the shovel actuators and their system parameters, which are components of our simulators. Friction and impact are investigated in Chapter 6. Based on Rowlands's work, we develop a more complete friction model of the shovel bucket. In addition, the impact effects of the bucket encountering large fragments are investigated. The experimental investigation and parameter system identification are described in Chapter 7. Both the least square identification for actuator transfer function and the maximum likelihood system identification for actuator state-space function are presented. Chapter 8 gives the nonparametric system identification to the analysis of the armature currents with and without digging, as well as easy and hard digging. Moreover, the position noise with and without digging is also depicted. Both the analytical and the empirical model simulators are developed in Chapter 9. Final simulation results are also presented in this chapter. Conclusions are given in Chapter 10, which also reviews achievements and suggestions for future work.

Chapter 2

Forward and Inverse Kinematics of Shovel

Kinematics is concerned with defining an object's motion, i.e. an object's position, orientation, velocity and acceleration, in terms of geometrical properties. Since the joints in the shovel are connected to each other, the motion of one joint will affect the motion of the other joints. Kinematics consists of forward kinematics and inverse kinematics.

2.1 Forward Kinematics of Shovel

The forward kinematics of a shovel need to be derived in order to solve the trajectory generation problem of the machine. Its trajectory is dependent on the swing, hoist and crowd motor motions. The trajectory also contributes to the calculation of friction between the bucket and muckpile. This issue is considered in detail in Chapter 6.

The forward kinematics problem is as follows: given the joint angle vector [θ_1, θ_2, θ_3, d_4], find the position and orientation of the end effector of the shovel in the work location coordinate system, which has been determined with respect to a reference coordinate system. Figure 2.1 is the coordinate set diagram of the shovel with several coordinates fixed on it. If one considers the base of the machine to be fixed when the shovel is digging, the frame {0} is the world coordinate frame; frames {1}, {2}, {3}, {4}, and {5} are fixed on the shovel and the frame {6} is fixed on the location where the shovel is working.

In terms of the Denavit-Hartenberg notation, the shovel can be described kinematically by assigning four values to each link. Two values are for the link and the

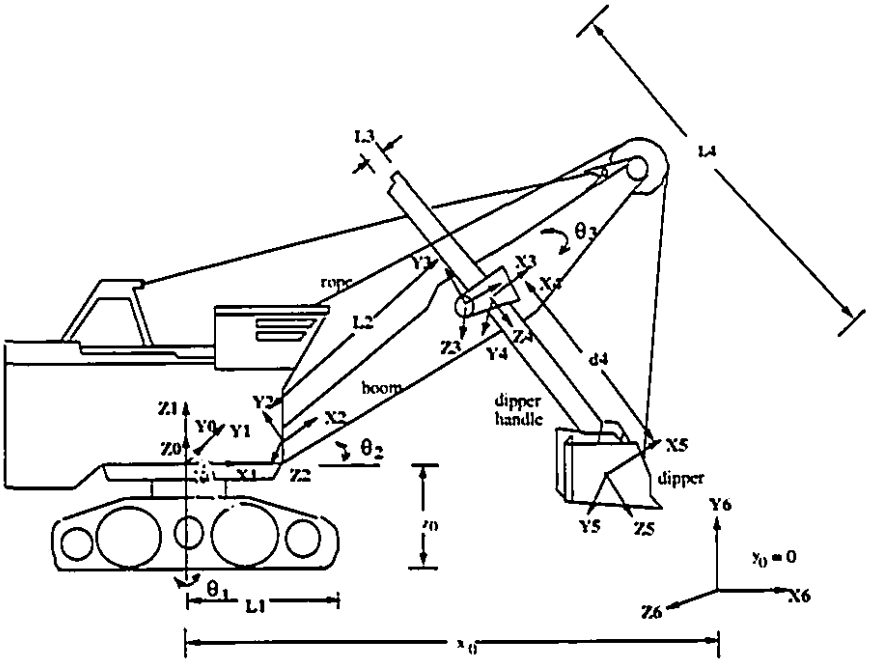

Figure 2.1: The Coordinate Set Diagram

i	α_{i-1}	a_{i-1}	d_i	θ_i
1	0	0	0	θ_1
2	90°	L_1	0	45°
3	0	L_2	0	θ_3
4	90°	L_3	0	0
5	0	0	d_4	0

Table 2.1: Link Parameters

other two values are for the connection between the links. Usually, three variables, α_{i-1}, a_{i-1} and d_i, are fixed link parameters but θ_i is a variable for rotational case. Three variables, α_{i-1}, a_{i-1}, and θ_i are fixed link parameters but d_i is a variable for translational case. Based on this foundation, one can determine the shovel's coordinate structure. Table 2.1 describes the link parameters, where

L_1 is the length of link 1;
L_2 is the length of link 2;
L_3 is the length of link 3;
L_4 is the length of link 4;
d_4 is the arm extension of dipper handle;
θ_1 is the joint 1 (swing motor) rotational angle;
θ_2 is the joint 2 angle; it is fixed ($\theta_2 = 45°$).
θ_3 is the joint 3 (hoist motor) rotational angle, corresponding to rope position.

θ_1, θ_3, and d_4 are variables; while other parameters are all constants. The physical meanings of the parameters or variables are also shown in Figure 2.1.

Computing the individual transformations for each link which defines frame $\{i\}$ relative to the frame $\{i-1\}$, one can use the formula [12]:

$$ {}^{i-1}_{i}T = \begin{pmatrix} c\theta_i & -s\theta_i & 0 & a_{i-1} \\ s\theta_i c\alpha_{i-1} & c\theta_i c\alpha_{i-1} & -s\alpha_{i-1} & -s\alpha_{i-1} d_i \\ s\theta_i s\alpha_{i-1} & c\theta_i s\alpha_{i-1} & c\alpha_{i-1} & c\alpha_{i-1} d_i \\ 0 & 0 & 0 & 1 \end{pmatrix} \tag{2.1} $$

thus,

$$ {}^{0}_{1}T = \begin{pmatrix} c_1 & -s_1 & 0 & 0 \\ s_1 & c_1 & 0 & 0 \\ 0 & 0 & 1 & 0 \\ 0 & 0 & 0 & 1 \end{pmatrix} \tag{2.2} $$

Because link 2 is fixed, $\theta_2 = 45°$

$$ {}^{1}_{2}T = \begin{pmatrix} \frac{\sqrt{2}}{2} & -\frac{\sqrt{2}}{2} & 0 & L_1 \\ 0 & 0 & -1 & 0 \\ \frac{\sqrt{2}}{2} & \frac{\sqrt{2}}{2} & 0 & 0 \\ 0 & 0 & 0 & 1 \end{pmatrix} \tag{2.3} $$

$$ {}^{2}_{3}T = \begin{pmatrix} c_3 & -s_3 & 0 & L_2 \\ s_3 & c_3 & 0 & 0 \\ 0 & 0 & 1 & 0 \\ 0 & 0 & 0 & 1 \end{pmatrix} \tag{2.4} $$

$$ {}^{3}_{4}T = \begin{pmatrix} 1 & 0 & 0 & L_3 \\ 0 & 0 & -1 & 0 \\ 0 & 1 & 0 & 0 \\ 0 & 0 & 0 & 1 \end{pmatrix} \tag{2.5} $$

$$ {}^{4}_{5}T = \begin{pmatrix} 1 & 0 & 0 & 0 \\ 0 & 1 & 0 & 0 \\ 0 & 0 & 1 & d_4 \\ 0 & 0 & 0 & 1 \end{pmatrix} \tag{2.6} $$

Multiplying equation (2.2) by (2.3), and we get

$$ {}^{0}_{1}T\ {}^{1}_{2}T = \begin{pmatrix} c_1 & -s_1 & 0 & 0 \\ s_1 & c_1 & 0 & 0 \\ 0 & 0 & 1 & 0 \\ 0 & 0 & 0 & 1 \end{pmatrix} \begin{pmatrix} \frac{\sqrt{2}}{2} & -\frac{\sqrt{2}}{2} & 0 & L_1 \\ 0 & 0 & -1 & 0 \\ \frac{\sqrt{2}}{2} & \frac{\sqrt{2}}{2} & 1 & 0 \\ 0 & 0 & 0 & 1 \end{pmatrix} \tag{2.7} $$

$$ = \begin{pmatrix} \frac{\sqrt{2}}{2}c_1 & -\frac{\sqrt{2}}{2}c_1 & -s_1 & L_1c_1 \\ \frac{\sqrt{2}}{2}s_1 & -\frac{\sqrt{2}}{2}s_1 & -c_1 & L_1s_1 \\ \frac{\sqrt{2}}{2} & \frac{\sqrt{2}}{2} & 1 & 0 \\ 0 & 0 & 0 & 1 \end{pmatrix} \tag{2.8} $$

Then, multiplying (2.8) by (2.4), and we get

$$ {}^{0}_{1}T\ {}^{1}_{2}T\ {}^{2}_{3}T = \begin{pmatrix} \frac{\sqrt{2}}{2}c_1 & -\frac{\sqrt{2}}{2}c_1 & -s_1 & L_1c_1 \\ \frac{\sqrt{2}}{2}s_1 & -\frac{\sqrt{2}}{2}s_1 & -c_1 & L_1s_1 \\ \frac{\sqrt{2}}{2} & \frac{\sqrt{2}}{2} & 0 & 0 \\ 0 & 0 & 0 & 1 \end{pmatrix} \begin{pmatrix} c_3 & -s_3 & 0 & L_2 \\ s_3 & c_3 & 0 & 0 \\ 0 & 0 & 1 & 0 \\ 0 & 0 & 0 & 1 \end{pmatrix} \tag{2.9} $$

$$= \begin{pmatrix} \frac{\sqrt{2}}{2}c_1c_3 - \frac{\sqrt{2}}{2}c_1s_3 & -\frac{\sqrt{2}}{2}c_1s_3 - \frac{\sqrt{2}}{2}c_1c_3 & -s_1 & \frac{\sqrt{2}}{2}c_1L_2 + L_1c_1 \\ \frac{\sqrt{2}}{2}s_1c_3 - \frac{\sqrt{2}}{2}s_1s_3 & -\frac{\sqrt{2}}{2}s_1s_3 - \frac{\sqrt{2}}{2}s_1c_3 & -c_1 & \frac{\sqrt{2}}{2}L_2s_1 + L_1s_1 \\ \frac{\sqrt{2}}{2}c_3 + \frac{\sqrt{2}}{2}s_3 & -\frac{\sqrt{2}}{2}s_3 + \frac{\sqrt{2}}{2}c_3 & 0 & \frac{\sqrt{2}}{2}L_2 \\ 0 & 0 & 0 & 1 \end{pmatrix} \tag{2.10}$$

Finally, multiplying (2.10) by (2.6), and we get

$${}^0_4T = {}^0_1T\,{}^1_2T\,{}^2_3T\,{}^3_4T$$

$$= \begin{pmatrix} \frac{\sqrt{2}}{2}c_1c_3 - \frac{\sqrt{2}}{2}c_1s_3 & -\frac{\sqrt{2}}{2}c_1s_3 - \frac{\sqrt{2}}{2}c_1c_3 & -s_1 & \frac{\sqrt{2}}{2}c_1L_2 + L_1c_1 \\ \frac{\sqrt{2}}{2}s_1c_3 - \frac{\sqrt{2}}{2}s_1s_3 & -\frac{\sqrt{2}}{2}s_1s_3 - \frac{\sqrt{2}}{2}s_1c_3 & -c_1 & \frac{\sqrt{2}}{2}L_2s_1 + L_1s_1 \\ \frac{\sqrt{2}}{2}c_3 + \frac{\sqrt{2}}{2}s_3 & -\frac{\sqrt{2}}{2}s_3 + \frac{\sqrt{2}}{2}c_3 & 0 & \frac{\sqrt{2}}{2}L_2 \\ 0 & 0 & 0 & 1 \end{pmatrix} \begin{pmatrix} 1 & 0 & 0 & L_3 \\ 0 & 0 & -1 & 0 \\ 0 & 1 & 0 & 0 \\ 0 & 0 & 0 & 1 \end{pmatrix}$$

$$= \begin{pmatrix} \frac{\sqrt{2}}{2}c_1c_3 - \frac{\sqrt{2}}{2}c_1s_3 & -s_1 & \frac{\sqrt{2}}{2}c_1s_3 + \frac{\sqrt{2}}{2}c_1c_3 & \frac{\sqrt{2}}{2}c_1L_2 + L_1c_1 + L_3(\frac{\sqrt{2}}{2}c_1c_3 - \frac{\sqrt{2}}{2}c_1s_3) \\ \frac{\sqrt{2}}{2}s_1c_3 - \frac{\sqrt{2}}{2}s_1s_3 & -c_1 & \frac{\sqrt{2}}{2}s_1s_3 + \frac{\sqrt{2}}{2}s_1c_3 & \frac{\sqrt{2}}{2}L_2s_1 + L_1s_1 + L_3(\frac{\sqrt{2}}{2}s_1c_3 - \frac{\sqrt{2}}{2}s_1s_3) \\ \frac{\sqrt{2}}{2}c_3 + \frac{\sqrt{2}}{2}s_3 & 0 & \frac{\sqrt{2}}{2}s_3 - \frac{\sqrt{2}}{2}c_3 & \frac{\sqrt{2}}{2}L_2 + L_3(\frac{\sqrt{2}}{2}c_3 + \frac{\sqrt{2}}{2}s_3) \\ 0 & 0 & 0 & 1 \end{pmatrix} \tag{2.11}$$

Because

$${}^0_5T = {}^0_4T\,{}^4_5T \quad . \tag{2.12}$$

one has

$${}^0_5T = {}^0_4T \begin{pmatrix} 1 & 0 & 0 & 0 \\ 0 & 1 & 0 & 0 \\ 0 & 0 & 1 & d_4 \\ 0 & 0 & 0 & 1 \end{pmatrix}$$

$$= \begin{pmatrix} \frac{\sqrt{2}}{2}c_1c_3 - \frac{\sqrt{2}}{2}c_1s_3 & -s_1 & \frac{\sqrt{2}}{2}c_1s_3 + \frac{\sqrt{2}}{2}c_1c_3 & t_{51} \\ \frac{\sqrt{2}}{2}s_1c_3 - \frac{\sqrt{2}}{2}s_1s_3 & -c_1 & \frac{\sqrt{2}}{2}s_1s_3 + \frac{\sqrt{2}}{2}s_1c_3 & t_{52} \\ \frac{\sqrt{2}}{2}c_3 + \frac{\sqrt{2}}{2}s_3 & 0 & \frac{\sqrt{2}}{2}s_3 - \frac{\sqrt{2}}{2}c_3 & t_{53} \\ 0 & 0 & 0 & 1 \end{pmatrix} \quad , \tag{2.13}$$

where

$$t_{51} = \frac{\sqrt{2}}{2}d_4c_1(s_3 + c_3) + \frac{\sqrt{2}}{2}c_1L_3(c_3 - s_3) + \frac{\sqrt{2}}{2}c_1L_2 + L_1c_1 \tag{2.14}$$

$$t_{52} = \frac{\sqrt{2}}{2}d_4s_1(s_3 + c_3) + \frac{\sqrt{2}}{2}s_1L_3(c_3 - s_3) + \frac{\sqrt{2}}{2}s_1L_2 + L_1s_1 \tag{2.15}$$

$$t_{53} = \frac{\sqrt{2}}{2}d_4(s_3 - c_3) + \frac{\sqrt{2}}{2}L_3(c_3 + s_3) + \frac{\sqrt{2}}{2}L_2 \quad . \tag{2.16}$$

Because

$$ {}^{0}_{6}T\,{}^{6}_{5}T = {}^{0}_{5}T \quad . \tag{2.17} $$

therefore

$$ {}^{6}_{5}T = {}^{0}_{6}T^{-1}\,{}^{0}_{5}T \quad . \tag{2.18} $$

Yet,

$$ {}^{0}_{6}T = \begin{pmatrix} 1 & 0 & 0 & x_0 \\ 0 & 0 & 1 & y_0 \\ 0 & -1 & 0 & z_0 \\ 0 & 0 & 0 & 1 \end{pmatrix} \tag{2.19} $$

where $\{x_0, y_0, z_0\}$ is the origin of the coordinate $\{6\}$ with respect to the coordinate $\{0\}$. $x_0 = 9$, $y_0 = 0$, $z_0 = -1.5$.

$$ {}^{0}_{6}T^{-1} = \begin{pmatrix} 1 & 0 & 0 & x_0 \\ 0 & 0 & 1 & y_0 \\ 0 & -1 & 0 & z_0 \\ 0 & 0 & 0 & 1 \end{pmatrix}^{-1} = \begin{pmatrix} 1 & 0 & 0 & -x_0 \\ 0 & 0 & -1 & z_0 \\ 0 & 1 & 0 & -y_0 \\ 0 & 0 & 0 & 1 \end{pmatrix} \tag{2.20} $$

Hence, one has

$$ {}^{6}_{5}T = {}^{0}_{6}T^{-1}\,{}^{0}_{5}T $$

$$ \begin{aligned} &= \begin{pmatrix} 1 & 0 & 0 & -x_0 \\ 0 & 0 & -1 & z_0 \\ 0 & 1 & 0 & -y_0 \\ 0 & 0 & 0 & 1 \end{pmatrix} \begin{pmatrix} \frac{\sqrt{2}}{2}c_1c_3 - \frac{\sqrt{2}}{2}c_1s_3 & -s_1 & \frac{\sqrt{2}}{2}c_1s_3 + \frac{\sqrt{2}}{2}c_1c_3 & t_{51} \\ \frac{\sqrt{2}}{2}s_1c_3 - \frac{\sqrt{2}}{2}s_1s_3 & -c_1 & \frac{\sqrt{2}}{2}s_1s_3 + \frac{\sqrt{2}}{2}s_1c_3 & t_{52} \\ \frac{\sqrt{2}}{2}c_3 + \frac{\sqrt{2}}{2}s_3 & 0 & \frac{\sqrt{2}}{2}s_3 - \frac{\sqrt{2}}{2}c_3 & t_{53} \\ 0 & 0 & 0 & 1 \end{pmatrix} \\ &= \begin{pmatrix} \frac{\sqrt{2}}{2}c_1(c_3 - s_3) & -s_1 & \frac{\sqrt{2}}{2}c_1(c_3 + s_3) & t_{61} \\ -\frac{\sqrt{2}}{2}(c_3 + s_3) & 0 & \frac{\sqrt{2}}{2}(c_3 - s_3) & t_{62} \\ \frac{\sqrt{2}}{2}s_1(c_3 - s_3) & -c_1 & \frac{\sqrt{2}}{2}s_1(c_3 + s_3) & t_{63} \\ 0 & 0 & 0 & 1 \end{pmatrix} \end{aligned} \tag{2.21} $$

where,

$$ t_{61} = \frac{\sqrt{2}}{2}c_1(d_4(s_3 + c_3) + L_3(c_3 - s_3)) + c_1(L_2\frac{\sqrt{2}}{2} + L_1) - x_0 \tag{2.22} $$

$$ t_{62} = -\frac{\sqrt{2}}{2}(d_4(s_3 - c_3) + L_3(s_3 + c_3)) - \frac{\sqrt{2}}{2}L_2 + z_0 \tag{2.23} $$

$$ t_{63} = \frac{\sqrt{2}}{2}s_1(d_4(s_3 + c_3) + L_3(c_3 - s_3)) + s_1(\frac{\sqrt{2}}{2}L_2 + L1) - y_0 \tag{2.24} $$

After the above lengthy algebraic manipulation, one can obtain the bucket position with respect to the work-site (muck-pile) reference coordinate $\{6\}$, as long as one knows the joint position θ_1, θ_3, d_4. This is the forward kinematics shown as follows:

$$x_6 = \frac{\sqrt{2}}{2}c_1(d_4(s_3+c_3)+L_3(c_3-s_3)) + c_1(\frac{\sqrt{2}}{2}L_2+L_1) - x_0 \quad (2.25)$$

$$y_6 = -\frac{\sqrt{2}}{2}(d_4(s_3-c_3)+L_3(c_3+s_3)) - \frac{\sqrt{2}}{2}L_2 + z_0 \quad (2.26)$$

$$z_6 = \frac{\sqrt{2}}{2}s_1(d_4(s_3+c_3)+L_3(c_3-s_3)) + s_1(\frac{\sqrt{2}}{2}L_2+L_1) - y_0 \quad (2.27)$$

If $\theta_1 = 0$, $c_1 = 1, s_1 = 0$, i.e. shovel stands on its original central position, we have

$$x_6 = \frac{\sqrt{2}}{2}(d_4(s_3+c_3)+L_3(c_3-s_3)) + \frac{\sqrt{2}}{2}L_2 + L_1 - X_0 \quad (2.28)$$

$$y_6 = -\frac{\sqrt{2}}{2}(d_4(s_3-c_3)+L_3(c_3+s_3)) - \frac{\sqrt{2}}{2}L_2 + Z_0 \quad (2.29)$$

$$z_6 = 0 \quad (2.30)$$

2.2 Inverse Kinematics of Shovel

The inverse kinematics of shovel has not been used in our system simulation. But because it is a fundamental work to our fully-automated shovel in future, we still show its manipulation here.

The inverse kinematics problem of the shovel is as follows: given the desired Cartesian position and orientation of the last link of the machine relative to the work location, calculate a set of joint angles which can achieve the desired position and orientation. In order to solve this problem, one must first perform coordinate transformation to obtain the bucket coordinate $\{5\}$, relative to the coordinate $\{1\}$, and then use the inverse kinematics to solve the joint angles.

Multiplying (2.3) by (2.4) and we get

$${}^1_2T\,{}^2_3T = \begin{pmatrix} \frac{\sqrt{2}}{2} & -\frac{\sqrt{2}}{2} & 0 & L_1 \\ 0 & 0 & -1 & 0 \\ \frac{\sqrt{2}}{2} & \frac{\sqrt{2}}{2} & 0 & 0 \\ 0 & 0 & 0 & 1 \end{pmatrix} \begin{pmatrix} c_3 & -s_3 & 0 & L_2 \\ s_3 & c_3 & 0 & 0 \\ 0 & 0 & 1 & 0 \\ 0 & 0 & 0 & 1 \end{pmatrix}$$

$$= \begin{pmatrix} \frac{\sqrt{2}}{2}(c_3 - s_3) & -\frac{\sqrt{2}}{2}(s_3 - c_3) & 0 & \frac{\sqrt{2}}{2}L_2 + L_1 \\ 0 & 0 & -1 & 0 \\ \frac{\sqrt{2}}{2}(c_3 + s_3) & \frac{\sqrt{2}}{2}(c_3 - s_3) & 0 & \frac{\sqrt{2}}{2}L_2 \\ 0 & 0 & 0 & 1 \end{pmatrix} \tag{2.31}$$

Multiplying (2.31) by (2.5), and we get

$$ {}^1_2T\ {}^2_3T\ {}^3_4T = \begin{pmatrix} \frac{\sqrt{2}}{2}(c_3 - s_3) & -\frac{\sqrt{2}}{2}(s_3 - c_3) & 0 & \frac{\sqrt{2}}{2}L_2 + L_1 \\ 0 & 0 & -1 & 0 \\ \frac{\sqrt{2}}{2}(c_3 + s_3) & \frac{\sqrt{2}}{2}(c_3 - s_3) & 0 & \frac{\sqrt{2}}{2}L_2 \\ 0 & 0 & 0 & 1 \end{pmatrix} \begin{pmatrix} 1 & 0 & 0 & L_3 \\ 0 & 0 & -1 & 0 \\ 0 & 1 & 0 & 0 \\ 0 & 0 & 0 & 1 \end{pmatrix} $$

$$= \begin{pmatrix} \frac{\sqrt{2}}{2}(c_3 - s_3) & 0 & -\frac{\sqrt{2}}{2}(c_3 - s_3) & \frac{\sqrt{2}}{2}(c_3 - s_3)L_3 + \frac{\sqrt{2}}{2}L_2 + L_1 \\ 0 & -1 & 0 & 0 \\ \frac{\sqrt{2}}{2}(c_3 + s_3) & 0 & -\frac{\sqrt{2}}{2}(c_3 - s_3) & \frac{\sqrt{2}}{2}(c_3 + s_3)L_3 + \frac{\sqrt{2}}{2}L_2 \\ 0 & 0 & 0 & 1 \end{pmatrix} \tag{2.32}$$

Multiplying (2.32) by (2.6) and we get

$$ {}^1_5T\ {}^1_2T\ {}^2_3T\ {}^3_4T\ {}^4_5T $$

$$= \begin{pmatrix} \frac{\sqrt{2}}{2}(c_3 - s_3) & 0 & -\frac{\sqrt{2}}{2}(c_3 - s_3) & t_{02} \\ 0 & -1 & 0 & 0 \\ \frac{\sqrt{2}}{2}(c_3 + s_3) & 0 & -\frac{\sqrt{2}}{2}(c_3 - s_3) & t_{03} \\ 0 & 0 & 0 & 1 \end{pmatrix} \begin{pmatrix} 1 & 0 & 0 & 0 \\ 0 & 1 & 0 & 0 \\ 0 & 0 & 1 & d_4 \\ 0 & 0 & 0 & 1 \end{pmatrix}$$

$$= \begin{pmatrix} \frac{\sqrt{2}}{2}(c_3 - s_3) & 0 & -\frac{\sqrt{2}}{2}(c_3 - s_3) & t_{12} \\ 0 & -1 & 0 & 0 \\ \frac{\sqrt{2}}{2}(c_3 + s_3) & 1 & -\frac{\sqrt{2}}{2}(c_3 - s_3) & t_{13} \\ 0 & 0 & 0 & 1 \end{pmatrix} \tag{2.33}$$

Where,

$$t_{02} = \frac{\sqrt{2}}{2}(c_3 - s_3)L_3 + \frac{\sqrt{2}}{2}L_2 + L_1 \tag{2.34}$$

$$t_{03} = \frac{\sqrt{2}}{2}(c_3 + s_3)L_3 + \frac{\sqrt{2}}{2}L_2 \tag{2.35}$$

$$t_{12} = -\frac{\sqrt{2}}{2}(c_3 - s_3)d_4 + \frac{\sqrt{2}}{2}(c_3 - s_3)L_3 + \frac{\sqrt{2}}{2}L_2 + L_1 \tag{2.36}$$

$$t_{13} = -\frac{\sqrt{2}}{2}(c_3 - s_3)d_4 + \frac{\sqrt{2}}{2}(c_3 + s_3)L_3 + \frac{\sqrt{2}}{2}L_2 \tag{2.37}$$

Because

$$ {}^{0}_{1}T^{-1} = \begin{pmatrix} c_1 & -s_1 & 0 & 0 \\ s_1 & c_1 & 0 & 0 \\ 0 & 0 & 1 & 0 \\ 0 & 0 & 0 & 1 \end{pmatrix}^{-1} = \begin{pmatrix} c_1 & s_1 & 0 & 0 \\ -s_1 & c_1 & 0 & 0 \\ 0 & 0 & 1 & 0 \\ 0 & 0 & 0 & 1 \end{pmatrix} \tag{2.38} $$

$$ {}^{1}_{5}T = {}^{0}_{1}T^{-1}\, {}^{0}_{5}T \tag{2.39} $$

Assuming

$$ {}^{0}_{5}T = \begin{pmatrix} r_{11} & r_{12} & r_{13} & P_x \\ r_{21} & r_{22} & r_{23} & P_y \\ r_{31} & r_{32} & r_{33} & P_z \\ 0 & 0 & 0 & 1 \end{pmatrix} \tag{2.40} $$

Where P_x, P_y, and P_z are end effector positions with respect to the world coordinate {0}. From (2.38), (2.39), and (2.40), one has

$$ {}^{1}_{5}T = \begin{pmatrix} c_1 & s_1 & 0 & 0 \\ -s_1 & c_1 & 0 & 0 \\ 0 & 0 & 1 & 0 \\ 0 & 0 & 0 & 1 \end{pmatrix} \begin{pmatrix} r_{11} & r_{12} & r_{13} & P_x \\ r_{21} & r_{22} & r_{23} & P_y \\ r_{31} & r_{32} & r_{33} & P_z \\ 0 & 0 & 0 & 1 \end{pmatrix} \tag{2.41} $$

Equating the (2,4) element of equations (2.33) and (2.41), one has:

$$ c_1 P_y - s_1 P_x = 0 $$

$$ \theta_1 = \arctan \frac{P_y}{P_x} \tag{2.42} $$

Equating the (1,4) element of equations (2.33) and (2.41), one has:

$$ c_1 P_x + s_1 P_y = -\frac{\sqrt{2}}{2} d_4 (c_3 - s_3) + \frac{\sqrt{2}}{2} L_3 (c_3 - s_3) + \frac{\sqrt{2}}{2} L_2 + L_1 \tag{2.43} $$

Equating the (3,4) element of equations (2.33) and (2.41), one has:

$$ P_z = -\frac{\sqrt{2}}{2} d_4 (c_3 - s_3) + \frac{\sqrt{2}}{2} L_3 (c_3 + s_3) + \frac{\sqrt{2}}{2} L_2 \tag{2.44} $$

Subtracting (2.43) from (2.44), one gets

$$ c_1 P_x + s_1 P_y - P_z = -\sqrt{2} s_3 L_3 + L_1 \tag{2.45} $$

Arranging (2.45), one has

$$s_3 = \frac{c_1 P_x + s_1 P_y - P_z - L_1}{-\sqrt{2} L_3} \tag{2.46}$$

Meanwhile, one has

$$c_3 = \pm\sqrt{1 - {s_3}^2} \tag{2.47}$$

Transfering (2.46) into angle form, one has

$$\theta_3 = \arcsin \frac{L_1 + P_z - c_1 P_x - s_1 P_y}{\sqrt{2} L_3} \tag{2.48}$$

Arranging (2.44), one gets

$$\begin{aligned} d_4 &= \frac{P_z - \frac{\sqrt{2}}{2}(c_3 + s_3) L_3 - \frac{\sqrt{2}}{2} L_2}{-\frac{\sqrt{2}}{2}(c_3 - s_3)} \\ &= \frac{(c_3 + s_3) L_3 + L_2 - \sqrt{2} P_z}{c_3 - s_3} \end{aligned} \tag{2.49}$$

In short, one can obtain the joint position θ_1, θ_3, d_4 as long as one knows bucket position P_x,P_y,P_z. This is the inverse kinematics shown as follows:

$$\theta_1 = \arctan \frac{P_y}{P_x} \tag{2.50}$$

$$\theta_3 = \arctan \frac{L_1 + P_z - c_1 P_x - s_1 P_y}{\sqrt{2} L_3} \tag{2.51}$$

$$d_4 = \frac{(c_3 + s_3) L_3 + L_2 - \sqrt{2} P_z}{c_3 - s_3} \tag{2.52}$$

Chapter 3

Shovel Jacobian

In order to analyze the motion of a manipulator, the "Jacobian" concept is commonly utilized. The Jacobian describes the relation between the linear and angular velocity of rigid body. It is also the basis for the formulation of the shovel's dynamics which will be described in the next chapter. Furthermore, when one calculates the impact in Chapter 6, one will use the shovel Jacobian.

3.1 Linear and Rotational Velocity of Rigid Bodies

The angular velocity and linear velocity propagation from joint to joint can be expressed by the formulae [12]:

For a rotational motion,

$$^{i+1}\omega_{i+1} = {}^{i+1}_{i}\mathbf{R}\,{}^{i}\omega_i + \dot{\theta}_{i+1}\,{}^{i+1}\hat{\mathbf{Z}}_{i+1} \tag{3.1}$$

$$^{i+1}\mathbf{v}_{i+1} = {}^{i+1}_{i}\mathbf{R}({}^{i}\mathbf{v}_i + {}^{i}\omega_i \times {}^{i}\mathbf{P}_{i+1}) \tag{3.2}$$

For a translational motion,

$$^{i+1}\omega_{i+1} = {}^{i+1}_{i}\mathbf{R}\,{}^{i}\omega_i + \dot{\theta}_{i+1}\,{}^{i+1}\hat{\mathbf{Z}}_{i+1} \tag{3.3}$$

$$^{i+1}\mathbf{v}_{i+1} = {}^{i+1}_{i}\mathbf{R}({}^{i}\mathbf{v}_i + {}^{i}\omega_i \times {}^{i}\mathbf{P}_{i+1}) + \dot{d}_i\hat{\mathbf{Z}}_i \tag{3.4}$$

From (2.2), (2.3), (2.4), (2.5), and (2.6), one can obtain

$$ {}^{0}_{1}R = \begin{pmatrix} c_1 & -s_1 & 0 \\ s_1 & c_1 & 0 \\ 0 & 0 & 1 \end{pmatrix}, \qquad {}^{1}_{2}R = \begin{pmatrix} \frac{\sqrt{2}}{2} & -\frac{\sqrt{2}}{2} & 0 \\ 0 & 0 & -1 \\ \frac{\sqrt{2}}{2} & \frac{\sqrt{2}}{2} & 1 \end{pmatrix} \tag{3.5}$$

$$ {}^2_3R = \begin{pmatrix} c_3 & -s_3 & 0 \\ s_3 & c_3 & 0 \\ 0 & 0 & 1 \end{pmatrix}, \qquad {}^3_4R = \begin{pmatrix} 1 & 0 & 0 \\ 0 & 0 & -1 \\ 0 & 1 & 0 \end{pmatrix} \tag{3.6} $$

$$ {}^4_5R = \begin{pmatrix} 1 & 0 & 0 \\ 0 & 1 & 0 \\ 0 & 0 & 1 \end{pmatrix} \tag{3.7} $$

Using (3.1) and (3.2) for rotational motion,

$$ {}^1\omega_1 = \begin{pmatrix} 0 \\ 0 \\ \dot{\theta}_1 \end{pmatrix} \tag{3.8} $$

$$ {}^1\mathbf{V}_1 = \begin{pmatrix} 0 \\ 0 \\ 0 \end{pmatrix} \tag{3.9} $$

$$ {}^2\omega_2 = \begin{pmatrix} \frac{\sqrt{2}}{2} & 0 & \frac{\sqrt{2}}{2} \\ -\frac{\sqrt{2}}{2} & 0 & \frac{\sqrt{2}}{2} \\ 0 & -1 & 0 \end{pmatrix} \begin{pmatrix} 0 \\ 0 \\ \dot{\theta}_1 \end{pmatrix} + \begin{pmatrix} 0 \\ 0 \\ 0 \end{pmatrix} = \begin{pmatrix} \frac{\sqrt{2}}{2}\dot{\theta}_1 \\ \frac{\sqrt{2}}{2}\dot{\theta}_1 \\ 0 \end{pmatrix} \tag{3.10} $$

$$ {}^2\mathbf{V}_2 = \begin{pmatrix} \frac{\sqrt{2}}{2} & 0 & \frac{\sqrt{2}}{2} \\ -\frac{\sqrt{2}}{2} & 0 & \frac{\sqrt{2}}{2} \\ 0 & -1 & 0 \end{pmatrix} \left(\begin{pmatrix} 0 \\ 0 \\ 0 \end{pmatrix} + \begin{pmatrix} 0 \\ 0 \\ \dot{\theta}_1 \end{pmatrix} \times \begin{pmatrix} L_1 \\ 0 \\ 0 \end{pmatrix} \right) = \begin{pmatrix} 0 \\ 0 \\ -L_1\dot{\theta}_1 \end{pmatrix} \tag{3.11} $$

$$ {}^3\omega_3 = \begin{pmatrix} c_3 & s_3 & 0 \\ -s_3 & c_3 & 0 \\ 0 & 0 & 1 \end{pmatrix} \begin{pmatrix} \frac{\sqrt{2}}{2}\dot{\theta}_1 \\ \frac{\sqrt{2}}{2}\dot{\theta}_1 \\ 0 \end{pmatrix} + \begin{pmatrix} 0 \\ 0 \\ \dot{\theta}_3 \end{pmatrix} = \begin{pmatrix} \frac{\sqrt{2}}{2}\dot{\theta}_1(c_3 + s_3) \\ \frac{\sqrt{2}}{2}\dot{\theta}_1(c_3 - s_3) \\ \dot{\theta}_1 + \dot{\theta}_3 \end{pmatrix} \tag{3.12} $$

$$ {}^3\mathbf{V}_3 = \begin{pmatrix} c_3 & s_3 & 0 \\ -s_3 & c_3 & 0 \\ 0 & 0 & 1 \end{pmatrix} \left(\begin{pmatrix} 0 \\ 0 \\ -L_1\dot{\theta}_1 \end{pmatrix} + \begin{pmatrix} \frac{\sqrt{2}}{2}\dot{\theta}_1 \\ \frac{\sqrt{2}}{2}\dot{\theta}_1 \\ 0 \end{pmatrix} \times \begin{pmatrix} L_2 \\ 0 \\ 0 \end{pmatrix} \right) $$

$$ = \begin{pmatrix} c_3 & s_3 & 0 \\ -s_3 & c_3 & 0 \\ 0 & 0 & 1 \end{pmatrix} \begin{pmatrix} 0 \\ 0 \\ -L_1\dot{\theta}_1 - \frac{\sqrt{2}}{2}L_2\dot{\theta}_1 \end{pmatrix} = \begin{pmatrix} 0 \\ 0 \\ -\dot{\theta}_1(L_1 + \frac{\sqrt{2}}{2}L_2) \end{pmatrix} \tag{3.13} $$

$$
{}^4\omega_4 = \begin{pmatrix} 1 & 0 & 0 \\ 0 & 0 & 1 \\ 0 & -1 & 0 \end{pmatrix} \begin{pmatrix} \frac{\sqrt{2}}{2}\dot{\theta}_1(c_3+s_3) \\ \frac{\sqrt{2}}{2}\dot{\theta}_1(c_3-s_3) \\ \dot{\theta}_3 \end{pmatrix} + \begin{pmatrix} 0 \\ 0 \\ 0 \end{pmatrix} = \begin{pmatrix} \frac{\sqrt{2}}{2}\dot{\theta}_1(c_3+s_3) \\ \dot{\theta}_3 \\ \frac{\sqrt{2}}{2}\dot{\theta}_1(s_3-c_3) \end{pmatrix} \tag{3.14}
$$

$$
\begin{aligned}
{}^4\mathbf{V}_4 &= \begin{pmatrix} 1 & 0 & 0 \\ 0 & 0 & 1 \\ 0 & -1 & 0 \end{pmatrix} \left(\begin{pmatrix} 0 \\ 0 \\ -\dot{\theta}_1(L_1 + \frac{\sqrt{2}}{2}L_2) \end{pmatrix} + \begin{pmatrix} \frac{\sqrt{2}}{2}\dot{\theta}_1(c_3+s_3) \\ \frac{\sqrt{2}}{2}\dot{\theta}_1(c_3-s_3) \\ \dot{\theta}_3 \end{pmatrix} \times \begin{pmatrix} L_3 \\ 0 \\ 0 \end{pmatrix} \right) \\
&= \begin{pmatrix} 1 & 0 & 0 \\ 0 & 0 & 1 \\ 0 & -1 & 0 \end{pmatrix} \begin{pmatrix} 0 \\ L_3\dot{\theta}_3 \\ -\dot{\theta}_1(L_1 + \frac{\sqrt{2}}{2}L_2) + \frac{\sqrt{2}}{2}L_3\dot{\theta}_1(s_3-c_3) \end{pmatrix} \\
&= \begin{pmatrix} 0 \\ -\dot{\theta}_1(L_1 + \frac{\sqrt{2}}{2}L_2) + \frac{\sqrt{2}}{2}L_3\dot{\theta}_1(s_3-c_3) \\ L_3\dot{\theta}_3 \end{pmatrix}
\end{aligned} \tag{3.15}
$$

Using (3.3) and (3.4) for translational motion

$$
{}^5\omega_5 = \begin{pmatrix} 1 & 0 & 0 \\ 0 & 1 & 0 \\ 0 & 0 & 1 \end{pmatrix} \begin{pmatrix} \frac{\sqrt{2}}{2}\dot{\theta}_1(c_3+s_3) \\ \dot{\theta}_3 \\ \frac{\sqrt{2}}{2}\dot{\theta}_1(s_3-c_3) \end{pmatrix} = \begin{pmatrix} \frac{\sqrt{2}}{2}\dot{\theta}_1(c_3+s_3) \\ \dot{\theta}_3 \\ \frac{\sqrt{2}}{2}\dot{\theta}_1(s_3-c_3) \end{pmatrix} \tag{3.16}
$$

$$
\begin{aligned}
{}^5\mathbf{V}_5 &= \begin{pmatrix} 0 \\ -\dot{\theta}_1(L_1 + \frac{\sqrt{2}}{2}L_2) + \frac{\sqrt{2}}{2}L_3\dot{\theta}_1(s_3-c_3) \\ L_3\dot{\theta}_3 \end{pmatrix} \\
&\quad + \begin{pmatrix} \frac{\sqrt{2}}{2}\dot{\theta}_1(c_3+s_3) \\ \dot{\theta}_3 \\ \frac{\sqrt{2}}{2}\dot{\theta}_1(s_3-c_3) \end{pmatrix} \times \begin{pmatrix} 0 \\ 0 \\ d_4 \end{pmatrix} + \begin{pmatrix} 0 \\ 0 \\ \dot{d}_4 \end{pmatrix} \\
&= \begin{pmatrix} d_4\dot{\theta}_3 \\ -\dot{\theta}_1(L_1 + \frac{\sqrt{2}}{2}L_2) + \frac{\sqrt{2}}{2}L_3\dot{\theta}_1(s_3-c_3) - \frac{\sqrt{2}}{2}d_4\dot{\theta}_1(c_3+s_3) \\ L_3\dot{\theta}_3 + \dot{d}_4 \end{pmatrix}
\end{aligned} \tag{3.17}
$$

3.2 Jacobian

The Jacobian is a multidimensional form of the derivative. In shovel case, it is a three dimensional derivative. From (2.10), one knows

$$ {}^0_5R = \begin{pmatrix} \frac{\sqrt{2}}{2}c_1(c_3 - s_3) & -s_1 & \frac{\sqrt{2}}{2}c_1(c_3 + s_3) \\ \frac{\sqrt{2}}{2}s_1(c_3 - s_3) & -c_1 & \frac{\sqrt{2}}{2}s_1(c_3 + s_3) \\ \frac{\sqrt{2}}{2}(c_3 + s_3) & 0 & -\frac{\sqrt{2}}{2}(c_3 - s_3) \end{pmatrix} \tag{3.18} $$

Because

$$ {}^0\mathbf{V}_5 = {}^0_5\mathbf{R}\ {}^5\mathbf{V}_5 \tag{3.19} $$

from (3.17) and (3.18), one has

$$ {}^0\mathbf{V}_5 = {}^0_5\mathbf{R} \begin{pmatrix} d_4\dot{\theta}_3 \\ -\dot{\theta}_1(L_1 + \frac{\sqrt{2}}{2}L_2) + \frac{\sqrt{2}}{2}L_3\dot{\theta}_1(s_3 - c_3) - \frac{\sqrt{2}}{2}d_4\dot{\theta}_1(c_3 + s_3) \\ L_3\dot{\theta}_3 + \dot{d}_4 \end{pmatrix} $$

$$ = \begin{pmatrix} V_{51} \\ V_{52} \\ V_{53} \end{pmatrix} \tag{3.20} $$

where,

$$ V_{51} = \frac{\sqrt{2}}{2}c_1((c_3 - s_3)d_4 + (c_3 + s_3)L_3)\dot{\theta}_3 + \frac{\sqrt{2}}{2}c_1(c_3 + s_3)\dot{d}_4 $$

$$ + s_1((L_1 + \frac{\sqrt{2}}{2}L_2) - \frac{\sqrt{2}}{2}L_3(s_3 - c_3)\dot{\theta}_1 \tag{3.21} $$

$$ V_{52} = \frac{\sqrt{2}}{2}s_1((d_4(c_3 - s_3) + L_3(c_3 + s_3))\dot{\theta}_3 + \frac{\sqrt{2}}{2}s_1(c_3 + s_3)\dot{d}_4 $$

$$ + c_1((L_1 + \frac{\sqrt{2}}{2}L_2)) - \frac{\sqrt{2}}{2}L_3(s_3 - c_3) + \frac{\sqrt{2}}{2}d_4(c_3 + s_3))\dot{\theta}_1 \tag{3.22} $$

$$ V_{53} = \frac{\sqrt{2}}{2}((c_3 + s_3)d_4 + (s_3 - c_3)L_3)\dot{\theta}_3 - \frac{\sqrt{2}}{2}(c_3 - s_3)\dot{d}_4 \tag{3.23} $$

Arranging (3.20), (3.21), (3.22), and (3.23), one has

$$ {}^0V_5 = \begin{pmatrix} x_{11} & x_{12} & x_{13} \\ x_{21} & x_{22} & x_{23} \\ x_{31} & x_{32} & x_{33} \end{pmatrix} \begin{pmatrix} \dot{\theta}_1 \\ \dot{\theta}_3 \\ \dot{d}_4 \end{pmatrix} \tag{3.24} $$

where,

$$x_{11} = s_1((L_1 + \frac{\sqrt{2}}{2}L_2) - \frac{\sqrt{2}}{2}L_3(s_3 - c_3)) \quad (3.25)$$

$$x_{12} = \frac{\sqrt{2}}{2}c_1((c_3 - s_3)d_4 + (c_3 + s_3)L_3) \quad (3.26)$$

$$x_{13} = \frac{\sqrt{2}}{2}s_1(c_3 + s_3) \quad (3.27)$$

$$x_{21} = s_1((L_1 + \frac{\sqrt{2}}{2}L_2) - \frac{\sqrt{2}}{2}L_3(s_3 - c_3)) \quad (3.28)$$

$$x_{22} = \frac{\sqrt{2}}{2}s_1((d_4(c_3 - s_3) + L_3(c_3 + s_3)) \quad (3.29)$$

$$x_{23} = \frac{\sqrt{2}}{2}c_1(c_3 + s_3) \quad (3.30)$$

$$x_{31} = 0 \quad (3.31)$$

$$x_{32} = \frac{\sqrt{2}}{2}((c_3 + s_3)d_4 + (s_3 - c_3)L_3) \quad (3.32)$$

$$x_{33} = -\frac{\sqrt{2}}{2}(c_3 - s_3) \quad (3.33)$$

The variables are the components of the Jacobian. The shovel Jacobian is

$${}^0\mathbf{J}(\theta) = \begin{pmatrix} x_{11} & x_{12} & x_{13} \\ x_{21} & x_{22} & x_{23} \\ x_{31} & x_{32} & x_{33} \end{pmatrix} \quad (3.34)$$

Finally, one can get the relationship between the shovel's linear velocity and angular velocity

$${}^0\mathbf{V}_5 = {}^0\mathbf{J}(\theta)\dot{\theta} \quad (3.35)$$

Chapter 4

Rigid Body Dynamics

Dynamics is the study of the relationships between forces, torques, and motions. The motion of the shovel arises from torques generated by the actuators, and by external forces. The Newton-Euler formulation can be applied to calculate the torque vector, τ, if one knows the trajectory point, θ, $\dot{\theta}$, and $\ddot{\theta}$. One can also calculate θ, $\dot{\theta}$, and $\ddot{\theta}$, if one knows the torque vector, τ. The vectors which locate the center of mass for each link of shovel are:

$$ {}^{1}P_{c1} = 0\hat{x}_1, \qquad {}^{2}P_{c2} = \frac{L_2}{2}\hat{x}_2 \tag{4.1} $$

$$ {}^{3}P_{c3} = \frac{L_3}{2}\hat{x}_3, \qquad {}^{4}P_{c4} = \frac{d_4}{2}\hat{z}_4 \tag{4.2} $$

The inertia is a very complex issue. Considering that each link has symmetry (although there are some asymmetrical elements, compared to the major element, in engineering, one can neglect the asymmetrical elements), one can choose the principal axes of inertia; therefore, the inertia tensors are as follows:

$$ {}^{c_1}I_1 = \begin{pmatrix} I_{xx1} & 0 & 0 \\ 0 & I_{yy1} & 0 \\ 0 & 0 & I_{zz1} \end{pmatrix}, \qquad {}^{c_2}I_2 = \begin{pmatrix} I_{xx2} & 0 & 0 \\ 0 & I_{yy2} & 0 \\ 0 & 0 & I_{zz2} \end{pmatrix} \tag{4.3} $$

$$ {}^{c_3}I_3 = \begin{pmatrix} I_{xx3} & 0 & 0 \\ 0 & I_{yy3} & 0 \\ 0 & 0 & I_{zz3} \end{pmatrix}, \qquad {}^{c_4}I_4 = \begin{pmatrix} I_{xx4} & 0 & 0 \\ 0 & I_{yy4} & 0 \\ 0 & 0 & I_{zz4} \end{pmatrix} \tag{4.4} $$

The rotations between neighbouring link frames are described by formulae (3.5), (3.6), and (3.7).

By applying of the analysis to the bucket (Chapter 6 will introduce this issue), one can consider the effects of the external forces and moments acting on the bucket as follows:

$$\mathbf{f}_5 = \begin{pmatrix} f_{51} \\ f_{52} \\ f_{53} \end{pmatrix} = \begin{pmatrix} f_{51} \\ 0 \\ f_{53} \end{pmatrix}, \qquad \mathbf{n}_5 = \begin{pmatrix} n_{51} \\ n_{52} \\ n_{53} \end{pmatrix} = \begin{pmatrix} 0 \\ 0 \\ 0 \end{pmatrix} \tag{4.5}$$

The complete algorithm for manipulating shovel rigid body dynamics consists of two parts: first, forward recursion for the velocities and accelerations of the joints; second, backward recursion for the calculation of the generalized forces. They will be discussed individually below.

4.1 Forward Recursion for the Velocities and Accelerations of the Joints

For the shovel with four links, one can compute link i: 0→4 [12]:

$${}^{i+1}\omega_{i+1} = {}^{i+1}_{i}R\,{}^{i}\omega_i + \dot{\theta}_{i+1}\,{}^{i+1}\hat{\mathbf{Z}}_{i+1} \tag{4.6}$$

$${}^{i+1}\dot{\omega}_{i+1} = {}^{i+1}_{i}R\,{}^{i}\dot{\omega}_i + {}^{i+1}_{i}R\,{}^{i}\omega_i \times \dot{\theta}_{i+1}\,{}^{i+1}\hat{\mathbf{Z}}_{i+1} + \ddot{\theta}_{i+1}\,{}^{i+1}\hat{\mathbf{Z}}_{i+1} \tag{4.7}$$

$${}^{i+1}\dot{\mathbf{v}}_{i+1} = {}^{i+1}_{i}R({}^{i}\dot{\omega}_i \times {}^{i}\mathbf{P}_{i+1} + {}^{i}\omega_i \times ({}^{i}\omega_i \times {}^{i}\mathbf{P}_{i+1}) + {}^{i}\dot{\mathbf{v}}_i) \tag{4.8}$$

$${}^{i+1}\dot{\mathbf{v}}_{c_{i+1}} = {}^{i+1}\dot{\omega}_{i+1} \times {}^{i+1}\mathbf{P}_{c_{i+1}} + {}^{i+1}\omega_{i+1} \times ({}^{i+1}\omega_{i+1} \times {}^{i+1}\mathbf{P}_{c_{i+1}}) + {}^{i+1}\dot{\mathbf{v}}_{i+1} \tag{4.9}$$

$$^{i+1}\mathbf{F}_{i+1} = m_{i+1}{}^{i+1}\dot{\mathbf{v}}_{c_{i+1}} \tag{4.10}$$

$$^{i+1}\mathbf{N}_{i+1} = {}^{c_{i+1}}I_{i+1}{}^{i+1}\dot{\omega}_{i+1} + {}^{i+1}\omega_{i+1} \times {}^{c_{i+1}}I_{i+1}{}^{i+1}\omega_{i+1} \tag{4.11}$$

Let us concretely manipulate the forward recursion of the shovel. The gravity effect is calculated as:

$$^{0}\dot{\mathbf{v}}_0 = g\hat{\mathbf{z}}_0 \tag{4.12}$$

The base of the shovel machine is not rotating, therefore one has:

$$\omega_0 = 0, \qquad \dot{\omega}_0 = 0 \tag{4.13}$$

The forward recursions for link 1 are as follows:

$$^{1}\omega_1 = \dot{\theta}_1{}^{1}\hat{\mathbf{Z}}_1 = \begin{pmatrix} 0 \\ 0 \\ \dot{\theta}_1 \end{pmatrix} \tag{4.14}$$

$$^{1}\dot{\omega}_1 = \ddot{\theta}_1{}^{1}\hat{\mathbf{Z}}_1 = \begin{pmatrix} 0 \\ 0 \\ \ddot{\theta}_1 \end{pmatrix} \tag{4.15}$$

$$^{1}\dot{\mathbf{v}}_1 = \begin{pmatrix} c_1 & s_1 & 0 \\ -s_1 & c_1 & 0 \\ 0 & 0 & 1 \end{pmatrix} \begin{pmatrix} 0 \\ 0 \\ g \end{pmatrix} = \begin{pmatrix} 0 \\ 0 \\ g \end{pmatrix} \tag{4.16}$$

$$^{1}\dot{\mathbf{v}}_{c1} = \begin{pmatrix} 0 \\ 0 \\ \ddot{\theta}_1 \end{pmatrix} \times \begin{pmatrix} 0 \\ 0 \\ 0 \end{pmatrix} + \begin{pmatrix} 0 \\ 0 \\ \dot{\theta}_1 \end{pmatrix} \times \left(\begin{pmatrix} 0 \\ 0 \\ \dot{\theta}_1 \end{pmatrix} \times \begin{pmatrix} 0 \\ 0 \\ 0 \end{pmatrix} \right) + \begin{pmatrix} 0 \\ 0 \\ g \end{pmatrix} = \begin{pmatrix} 0 \\ 0 \\ g \end{pmatrix} \tag{4.17}$$

$$^{1}\mathbf{F}_1 = m_1 \begin{pmatrix} 0 \\ 0 \\ g \end{pmatrix} = \begin{pmatrix} 0 \\ 0 \\ m_1 g \end{pmatrix} = \begin{pmatrix} F_{11} \\ F_{12} \\ F_{13} \end{pmatrix} \tag{4.18}$$

$$
{}^{1}\mathbf{N}_1 = \begin{pmatrix} I_{xx1} & 0 & 0 \\ 0 & I_{yy1} & 0 \\ 0 & 0 & I_{zz1} \end{pmatrix} \begin{pmatrix} 0 \\ 0 \\ \ddot{\theta}_1 \end{pmatrix} + \begin{pmatrix} 0 \\ 0 \\ \dot{\theta}_1 \end{pmatrix} \times \begin{pmatrix} I_{xx1} & 0 & 0 \\ 0 & I_{yy1} & 0 \\ 0 & 0 & I_{zz1} \end{pmatrix} \begin{pmatrix} 0 \\ 0 \\ \dot{\theta}_1 \end{pmatrix}
$$

$$
= \begin{pmatrix} 0 \\ 0 \\ I_{zz1}\ddot{\theta}_1 \end{pmatrix} = \begin{pmatrix} N_{11} \\ N_{12} \\ N_{13} \end{pmatrix} \tag{4.19}
$$

The forward recursions for link 2 are as follows:

$$
{}^{2}\omega_2 = \begin{pmatrix} \frac{\sqrt{2}}{2} & 0 & \frac{\sqrt{2}}{2} \\ -\frac{\sqrt{2}}{2} & 0 & \frac{\sqrt{2}}{2} \\ 0 & -1 & 0 \end{pmatrix} \begin{pmatrix} 0 \\ 0 \\ \dot{\theta}_1 \end{pmatrix} + 0 = \begin{pmatrix} \frac{\sqrt{2}}{2}\dot{\theta}_1 \\ \frac{\sqrt{2}}{2}\dot{\theta}_1 \\ 0 \end{pmatrix} \tag{4.20}
$$

$$
{}^{2}\dot{\omega}_2 = \begin{pmatrix} \frac{\sqrt{2}}{2} & 0 & \frac{\sqrt{2}}{2} \\ -\frac{\sqrt{2}}{2} & 0 & \frac{\sqrt{2}}{2} \\ 0 & -1 & 0 \end{pmatrix} \begin{pmatrix} 0 \\ 0 \\ \ddot{\theta}_1 \end{pmatrix} = \begin{pmatrix} \frac{\sqrt{2}}{2}\ddot{\theta}_1 \\ \frac{\sqrt{2}}{2}\ddot{\theta}_1 \\ 0 \end{pmatrix} \tag{4.21}
$$

$$
\begin{aligned}
{}^{2}\dot{\mathbf{v}}_2 \;=\; & \begin{pmatrix} \frac{\sqrt{2}}{2} & 0 & \frac{\sqrt{2}}{2} \\ -\frac{\sqrt{2}}{2} & 0 & \frac{\sqrt{2}}{2} \\ 0 & -1 & 0 \end{pmatrix} \Bigg(\begin{pmatrix} 0 \\ 0 \\ \ddot{\theta}_1 \end{pmatrix} \times \begin{pmatrix} L_1 \\ 0 \\ 0 \end{pmatrix} + \begin{pmatrix} 0 \\ 0 \\ \dot{\theta}_1 \end{pmatrix} \times \Bigg(\begin{pmatrix} 0 \\ 0 \\ \dot{\theta}_1 \end{pmatrix} \times \begin{pmatrix} L_1 \\ 0 \\ 0 \end{pmatrix} \Bigg) \\
& + \begin{pmatrix} 0 \\ 0 \\ g \end{pmatrix} \Bigg) = \begin{pmatrix} \frac{\sqrt{2}}{2} & 0 & \frac{\sqrt{2}}{2} \\ -\frac{\sqrt{2}}{2} & 0 & \frac{\sqrt{2}}{2} \\ 0 & -1 & 0 \end{pmatrix} \begin{pmatrix} -L_1\dot{\theta}_1^{\,2} \\ L_1\ddot{\theta}_1 \\ g \end{pmatrix} = \begin{pmatrix} \frac{\sqrt{2}}{2}(g - L_1\dot{\theta}_1^{\,2}) \\ \frac{\sqrt{2}}{2}(L_1\dot{\theta}_1^{\,2} + g) \\ -L_1\ddot{\theta}_1 \end{pmatrix}
\end{aligned} \tag{4.22}
$$

$$
\begin{aligned}
{}^{2}\dot{\mathbf{v}}_{c2} \;=\; & \begin{pmatrix} \frac{\sqrt{2}}{2}\ddot{\theta}_1 \\ \frac{\sqrt{2}}{2}\ddot{\theta}_1 \\ 0 \end{pmatrix} \times \begin{pmatrix} \frac{L_2}{2} \\ 0 \\ 0 \end{pmatrix} + \begin{pmatrix} \frac{\sqrt{2}}{2}\dot{\theta}_1 \\ \frac{\sqrt{2}}{2}\dot{\theta}_1 \\ 0 \end{pmatrix} \times \Bigg(\begin{pmatrix} \frac{\sqrt{2}}{2}\dot{\theta}_1 \\ \frac{\sqrt{2}}{2}\dot{\theta}_1 \\ 0 \end{pmatrix} \times \begin{pmatrix} \frac{L_2}{2} \\ 0 \\ 0 \end{pmatrix} \Bigg) \\
& + \begin{pmatrix} \frac{\sqrt{2}}{2}(g - L_1\dot{\theta}_1^{\,2}) \\ \frac{\sqrt{2}}{2}(L_1\dot{\theta}_1^{2} + g) \\ -L_1\ddot{\theta}_1 \end{pmatrix} = \begin{pmatrix} (-\frac{\sqrt{2}L_1}{2} - \frac{L_2}{4})\dot{\theta}_1^{\,2} + \frac{\sqrt{2}}{2}g \\ (\frac{\sqrt{2}L_1}{2} + \frac{L_2}{4})\dot{\theta}_1^{\,2} + \frac{\sqrt{2}}{2}g \\ (-L_1 - \frac{\sqrt{2}L_2}{4})\ddot{\theta}_1 \end{pmatrix}
\end{aligned} \tag{4.23}
$$

$$
{}^2\mathbf{F_2} = m_2{}^2\dot{\mathbf{v}}_{c2} = \begin{pmatrix} (-\frac{\sqrt{2}L_1}{2} - \frac{L_2}{4})m_2\dot{\theta}_1^{\,2} + \frac{\sqrt{2}}{2}m_2 g \\ +(\frac{\sqrt{2}L_1}{2} + \frac{L_2}{4})m_2\dot{\theta}_1^{\,2} + \frac{\sqrt{2}}{2}m_2 g \\ (-L_1 - \frac{\sqrt{2}L_2}{4})m_2\ddot{\theta}_1 \end{pmatrix} = \begin{pmatrix} F_{21} \\ F_{22} \\ F_{23} \end{pmatrix} \tag{4.24}
$$

$$
\begin{aligned}
{}^2\mathbf{N_2} &= \begin{pmatrix} I_{xx2} & 0 & 0 \\ 0 & I_{yy2} & 0 \\ 0 & 0 & I_{zz2} \end{pmatrix} \begin{pmatrix} \frac{\sqrt{2}}{2}\ddot{\theta}_1 \\ \frac{\sqrt{2}}{2}\ddot{\theta}_1 \\ 0 \end{pmatrix} + \begin{pmatrix} \frac{\sqrt{2}}{2}\dot{\theta}_1 \\ \frac{\sqrt{2}}{2}\dot{\theta}_1 \\ 0 \end{pmatrix} \times \begin{pmatrix} I_{xx2} & 0 & 0 \\ 0 & I_{yy2} & 0 \\ 0 & 0 & I_{zz2} \end{pmatrix} \begin{pmatrix} \frac{\sqrt{2}}{2}\dot{\theta}_1 \\ \frac{\sqrt{2}}{2}\dot{\theta}_1 \\ 0 \end{pmatrix} \\
&= \begin{pmatrix} \frac{\sqrt{2}}{2}I_{xx2}\ddot{\theta}_1 \\ \frac{\sqrt{2}}{2}I_{yy2}\ddot{\theta}_1 \\ \frac{1}{2}\dot{\theta}_1^{\,2}(I_{yy2} - I_{xx2}) \end{pmatrix} = \begin{pmatrix} N_{21} \\ N_{22} \\ N_{23} \end{pmatrix}
\end{aligned} \tag{4.25}
$$

The forward recursions for link 3 are as follows:

$$
{}^3\omega_3 = \begin{pmatrix} c_3 & s_3 & 0 \\ -s_3 & c_3 & 0 \\ 0 & 0 & 1 \end{pmatrix} \begin{pmatrix} \frac{\sqrt{2}}{2}\dot{\theta}_1 \\ \frac{\sqrt{2}}{2}\dot{\theta}_1 \\ 0 \end{pmatrix} + \begin{pmatrix} 0 \\ 0 \\ \dot{\theta}_3 \end{pmatrix} = \begin{pmatrix} (c_3 + s_3)\frac{\sqrt{2}}{2}\dot{\theta}_1 \\ (c_3 - s_3)\frac{\sqrt{2}}{2}\dot{\theta}_1 \\ \dot{\theta}_3 \end{pmatrix} \tag{4.26}
$$

$$
\begin{aligned}
{}^3\dot{\omega}_3 &= \begin{pmatrix} c_3 & s_3 & 0 \\ -s_3 & c_3 & 0 \\ 0 & 0 & 1 \end{pmatrix} \begin{pmatrix} \frac{\sqrt{2}}{2}\ddot{\theta}_1 \\ \frac{\sqrt{2}}{2}\ddot{\theta}_1 \\ 0 \end{pmatrix} + \begin{pmatrix} c_3 & s_3 & 0 \\ -s_3 & c_3 & 0 \\ 0 & 0 & 1 \end{pmatrix} \begin{pmatrix} \frac{\sqrt{2}}{2}\dot{\theta}_1 \\ \frac{\sqrt{2}}{2}\dot{\theta}_1 \\ 0 \end{pmatrix} \times \begin{pmatrix} 0 \\ 0 \\ \dot{\theta}_3 \end{pmatrix} \\
&\quad + \begin{pmatrix} 0 \\ 0 \\ \ddot{\theta}_3 \end{pmatrix} = \begin{pmatrix} \frac{\sqrt{2}}{2}(c_3 + s_3)\ddot{\theta}_1 + \frac{\sqrt{2}}{2}(c_3 - s_3)\dot{\theta}_1\dot{\theta}_3 \\ \frac{\sqrt{2}}{2}(c_3 - s_3)\ddot{\theta}_1 - \frac{\sqrt{2}}{2}(c_3 + s_3)\dot{\theta}_1\dot{\theta}_3 \\ \ddot{\theta}_3 \end{pmatrix}
\end{aligned} \tag{4.27}
$$

$$
\begin{aligned}
{}^3\dot{\mathbf{v}}_3 &= \begin{pmatrix} c_3 & s_3 & 0 \\ -s_3 & c_3 & 0 \\ 0 & 0 & 1 \end{pmatrix} \Big(\begin{pmatrix} \frac{\sqrt{2}}{2}\ddot{\theta}_1 \\ \frac{\sqrt{2}}{2}\ddot{\theta}_1 \\ 0 \end{pmatrix} \times \begin{pmatrix} L_2 \\ 0 \\ 0 \end{pmatrix} + \begin{pmatrix} \frac{\sqrt{2}}{2}\dot{\theta}_1 \\ \frac{\sqrt{2}}{2}\dot{\theta}_1 \\ 0 \end{pmatrix} \\
&\quad \times \Big(\begin{pmatrix} \frac{\sqrt{2}}{2}\dot{\theta}_1 \\ \frac{\sqrt{2}}{2}\dot{\theta}_1 \\ 0 \end{pmatrix} \times \begin{pmatrix} L_2 \\ 0 \\ 0 \end{pmatrix} \Big) + \begin{pmatrix} \frac{\sqrt{2}}{2}(g - L_1\dot{\theta}_1^2) \\ \frac{\sqrt{2}}{2}(g + L_1\dot{\theta}_1^2) \\ -L_1\ddot{\theta}_1 \end{pmatrix} \Big)
\end{aligned}
$$

$$= \begin{pmatrix} (\frac{\sqrt{2}}{2}(g - L_1\dot{\theta}_1^2) - \frac{1}{2}L_2\dot{\theta}_1^2)c_3 + (\frac{\sqrt{2}}{2}(L_1\dot{\theta}_1^2 + g) + \frac{1}{2}L_2\dot{\theta}_1^2)s_3 \\ -(\frac{\sqrt{2}}{2}(g - L_1\dot{\theta}_1^2) - \frac{1}{2}L_2\dot{\theta}_1^2)s_3 + (\frac{\sqrt{2}}{2}(L_1\dot{\theta}_1^2 + g) + \frac{1}{2}L_2\dot{\theta}_1^2)c_3 \\ -L_1\ddot{\theta}_1 - \frac{\sqrt{2}}{2}L_2\ddot{\theta}_1 \end{pmatrix} \quad (4.28)$$

$$^3\dot{\mathbf{v}}_{\mathbf{c_3}} = \begin{pmatrix} \frac{\sqrt{2}}{2}(c_3 + s_3)\ddot{\theta}_1 + \frac{\sqrt{2}}{2}(c_3 - s_3)\dot{\theta}_1\dot{\theta}_3 \\ \frac{\sqrt{2}}{2}(c_3 - s_3)\ddot{\theta}_1 - \frac{\sqrt{2}}{2}(c_3 + s_3)\dot{\theta}_1\dot{\theta}_3 \\ \ddot{\theta}_3 \end{pmatrix} \times \begin{pmatrix} \frac{L_3}{2} \\ 0 \\ 0 \end{pmatrix} + \begin{pmatrix} (c_3 + s_3)\frac{\sqrt{2}}{2}\dot{\theta}_1 \\ (c_3 - s_3)\frac{\sqrt{2}}{2}\dot{\theta}_1 \\ \dot{\theta}_3 \end{pmatrix} \times$$
$$(\begin{pmatrix} (c_3 + s_3)\frac{\sqrt{2}}{2}\dot{\theta}_1 \\ (c_3 - s_3)\frac{\sqrt{2}}{2}\dot{\theta}_1 \\ \dot{\theta}_3 \end{pmatrix} \times \begin{pmatrix} \frac{L_3}{2} \\ 0 \\ 0 \end{pmatrix}) + {}^3\dot{\mathbf{v}}_3 = \begin{pmatrix} v_{31} \\ v_{32} \\ v_{33} \end{pmatrix} \quad (4.29)$$

where,

$$v_{31} = -\frac{L_3}{2}(\frac{1}{2}\dot{\theta}_1^2(c_3 - s_3)^2 + \dot{\theta}_3^2) + (\frac{\sqrt{2}}{2}(g - L_1\dot{\theta}_1^2) - \frac{1}{2}L_2\dot{\theta}_1^2)c_3$$
$$+(\frac{\sqrt{2}}{2}(L_1\dot{\theta}_1^2 + g) + \frac{1}{2}L_2\dot{\theta}_1)s_3 \quad (4.30)$$

$$v_{32} = \frac{L_3}{2}\ddot{\theta}_3 - (\frac{\sqrt{2}}{2}(g - L_1\dot{\theta}_1^2) - \frac{1}{2}L_2\dot{\theta}_1)s_3$$
$$+(\frac{\sqrt{2}}{2}(L_1\dot{\theta}_1^2 + g) + \frac{1}{2}L_2\dot{\theta}_1^2)c_3 \quad (4.31)$$

$$v_{33} = -\frac{L_3}{2}(\frac{\sqrt{2}}{2}\ddot{\theta}_1(c_3 - s_3) - \frac{\sqrt{2}}{2}\dot{\theta}_1\dot{\theta}_3(c_3 + s_3)) - (\frac{\sqrt{2}}{2}L_2 + L_1)\ddot{\theta}_1 \quad (4.32)$$

$$^3F_3 = \begin{pmatrix} m_3v_{31} \\ m_3v_{32} \\ m_3v_{33} \end{pmatrix} = \begin{pmatrix} F_{31} \\ F_{32} \\ F_{33} \end{pmatrix} \quad (4.33)$$

$$^3\mathbf{N_3} = \begin{pmatrix} I_{xx3} & 0 & 0 \\ 0 & I_{yy3} & 0 \\ 0 & 0 & I_{zz3} \end{pmatrix} \begin{pmatrix} \frac{\sqrt{2}}{2}(c_3 + s_3)\ddot{\theta}_1 + \frac{\sqrt{2}}{2}(c_3 - s_3)\dot{\theta}_1\dot{\theta}_3 \\ \frac{\sqrt{2}}{2}(c_3 - s_3)\ddot{\theta}_1 - \frac{\sqrt{2}}{2}(c_3 + s_3)\dot{\theta}_1\dot{\theta}_3 \\ \ddot{\theta}_3 \end{pmatrix}$$
$$+ \begin{pmatrix} (c_3 + s_3)\frac{\sqrt{2}}{2}\dot{\theta}_1 \\ (c_3 - s_3)\frac{\sqrt{2}}{2}\dot{\theta}_1 \\ \dot{\theta}_3 \end{pmatrix} \times \begin{pmatrix} I_{xx3} & 0 & 0 \\ 0 & I_{yy3} & 0 \\ 0 & 0 & I_{zz3} \end{pmatrix} \begin{pmatrix} (c_3 + s_3)\frac{\sqrt{2}}{2}\dot{\theta}_1 \\ (c_3 - s_3)\frac{\sqrt{2}}{2}\dot{\theta}_1 \\ \dot{\theta}_3 \end{pmatrix}$$
$$= \begin{pmatrix} \frac{\sqrt{2}}{2}I_{xx3}(\ddot{\theta}_1(c_3 + s_3) + \dot{\theta}_1\dot{\theta}_3(c_3 - s_3)) + \frac{\sqrt{2}}{2}\dot{\theta}_1(c_3 - s_3) + \dot{\theta}_3(I_{zz3} - I_{yy3}) \\ \frac{\sqrt{2}}{2}I_{yy3}(\ddot{\theta}_1(c_3 - s_3) - \dot{\theta}_1\dot{\theta}_3(c_3 + s_3)) - \frac{\sqrt{2}}{2}\dot{\theta}_1(c_3 + s_3)\dot{\theta}_3(I_{zz3} - I_{yy3}) \\ I_{zz3}\ddot{\theta}_3 + \frac{\sqrt{2}}{2}\dot{\theta}_1^2(c_3 + s_3)(c_3 - s_3)(I_{yy3} - I_{xx3}) \end{pmatrix}$$

$$= \begin{pmatrix} N_{31} \\ N_{32} \\ N_{33} \end{pmatrix} \tag{4.34}$$

The forward recursions for link 4 are as follows:

$${}^4\omega_4 = \begin{pmatrix} 1 & 0 & 0 \\ 0 & 0 & 1 \\ 0 & -1 & 0 \end{pmatrix} \begin{pmatrix} (c_3+s_3)\frac{\sqrt{2}}{2}\dot{\theta}_1 \\ (c_3-s_3)\frac{\sqrt{2}}{2}\dot{\theta}_1 \\ \dot{\theta}_3 \end{pmatrix} = \begin{pmatrix} \frac{\sqrt{2}}{2}\dot{\theta}_1(c_3+s_3) \\ \dot{\theta}_3 \\ \frac{\sqrt{2}}{2}\dot{\theta}_1(s_3-c_3) \end{pmatrix} \tag{4.35}$$

$$\begin{aligned} {}^4\dot{\omega}_4 &= \begin{pmatrix} 1 & 0 & 0 \\ 0 & 0 & 1 \\ 0 & -1 & 0 \end{pmatrix} \begin{pmatrix} \frac{\sqrt{2}}{2}(c_3+s_3)\ddot{\theta}_1 + \frac{\sqrt{2}}{2}(c_3-s_3)\dot{\theta}_1\dot{\theta}_3 \\ \frac{\sqrt{2}}{2}(c_3-s_3)\ddot{\theta}_1 - \frac{\sqrt{2}}{2}(c_3+s_3)\dot{\theta}_1\dot{\theta}_3 \\ \ddot{\theta}_3 \end{pmatrix} \\ &= \begin{pmatrix} \frac{\sqrt{2}}{2}\ddot{\theta}_1(c_3+s_3) + \frac{\sqrt{2}}{2}\dot{\theta}_1\dot{\theta}_3(c_3-s_3) \\ \ddot{\theta}_3 \\ -\frac{\sqrt{2}}{2}\ddot{\theta}_1(c_3-s_3) + \frac{\sqrt{2}}{2}\dot{\theta}_1\dot{\theta}_3(c_3+s_3) \end{pmatrix} \end{aligned} \tag{4.36}$$

$$\begin{aligned} {}^4\dot{v}_4 &= \begin{pmatrix} 1 & 0 & 0 \\ 0 & 0 & 1 \\ 0 & -1 & 0 \end{pmatrix} \left(\begin{pmatrix} (c_3+s_3)\frac{\sqrt{2}}{2}\dot{\theta}_1 \\ (c_3-s_3)\frac{\sqrt{2}}{2}\dot{\theta}_1 \\ \dot{\theta}_3 \end{pmatrix} \times \begin{pmatrix} d_4 \\ 0 \\ 0 \end{pmatrix} + \begin{pmatrix} (c_3+s_3)\frac{\sqrt{2}}{2}\dot{\theta}_1 \\ (c_3-s_3)\frac{\sqrt{2}}{2}\dot{\theta}_1 \\ \dot{\theta}_3 \end{pmatrix} \right. \\ &\left. \times \left(\begin{pmatrix} (c_3+s_3)\frac{\sqrt{2}}{2}\dot{\theta}_1 \\ (c_3-s_3)\frac{\sqrt{2}}{2}\dot{\theta}_1 \\ \dot{\theta}_3 \end{pmatrix} \times \begin{pmatrix} d_4 \\ 0 \\ 0 \end{pmatrix} \right) + {}^3\dot{\mathbf{v}}_3 \right) = \begin{pmatrix} v_{41} \\ v_{42} \\ v_{43} \end{pmatrix} \end{aligned} \tag{4.37}$$

where,

$$\begin{aligned} v_{41} &= -\frac{d_4}{2}\dot{\theta}_1^2(c_3-s_3)^2 - d_4\dot{\theta}_3^2 + \left(\frac{\sqrt{2}}{2}(g-L_1\dot{\theta}_1)^2 - \frac{1}{2}L_2\dot{\theta}_1^2\right)c_3 \\ &\quad + \left(\frac{\sqrt{2}}{2}(L_1\dot{\theta}_1^2+g) + \frac{1}{2}L_2\dot{\theta}_1^2\right)s_3 \end{aligned} \tag{4.38}$$

$$\begin{aligned} v_{42} &= -\frac{\sqrt{2}d_4}{2}\dot{\theta}_1(c_3-s_3) + \frac{\sqrt{2}d_4}{2}\dot{\theta}_1\dot{\theta}_3(c_3+s_3) \\ &\quad -L_1\ddot{\theta}_1 - \frac{\sqrt{2}}{2}L_2\ddot{\theta}_1 \end{aligned} \tag{4.39}$$

$$v_{43} = -d_4\dot{\theta}_3 - \frac{d_4}{2}\dot{\theta}_1^2(c_3^2 - s_3^2) + (\frac{\sqrt{2}}{2}(g - L_1\dot{\theta}_1^2) - \frac{1}{2}L_2\dot{\theta}_1^2)s_3$$
$$-(\frac{\sqrt{2}}{2}(L_1\dot{\theta}_1^2 + g) + \frac{1}{2}L_2\dot{\theta}_1^2)c_3 \tag{4.40}$$

$${}^4\dot{\mathbf{v}}_{\mathbf{c4}} = \begin{pmatrix} \frac{\sqrt{2}}{2}\ddot{\theta}_1(c_3 + s_3) + \frac{\sqrt{2}}{2}\dot{\theta}_1\dot{\theta}_3(c_3 - s_3) \\ \ddot{\theta}_3 \\ -\frac{\sqrt{2}}{2}\ddot{\theta}_1(c_3 - s_3) + \frac{\sqrt{2}}{2}\dot{\theta}_1\dot{\theta}_3(c_3 + s_3) \end{pmatrix} \times \begin{pmatrix} 0 \\ 0 \\ \frac{d_4}{2} \end{pmatrix} + \begin{pmatrix} \frac{\sqrt{2}}{2}\dot{\theta}_1(c_3 + s_3) \\ \dot{\theta}_3 \\ \frac{\sqrt{2}}{2}\dot{\theta}_1(s_3 - c_3) \end{pmatrix}$$
$$\times(\begin{pmatrix} \frac{\sqrt{2}}{2}\dot{\theta}_1(c_3 + s_3) \\ \dot{\theta}_3 \\ \frac{\sqrt{2}}{2}\dot{\theta}_1(s_3 - c_3) \end{pmatrix} \times \begin{pmatrix} 0 \\ 0 \\ \frac{d_4}{2} \end{pmatrix}) + {}^4\dot{\mathbf{v}}_4 = \begin{pmatrix} v_{4c1} \\ v_{4c2} \\ v_{4c3} \end{pmatrix} \tag{4.41}$$

$$v_{4c1} = \frac{d_4}{2}\ddot{\theta}_3 + \frac{d_4}{4}\dot{\theta}_1^2(s_3^2 - c_3^2) + v_{41} \tag{4.42}$$

$$v_{4c2} = -\frac{\sqrt{2}d_4}{4}(\ddot{\theta}_1(c_3 + s_3) + \dot{\theta}_1\dot{\theta}_3(c_3 - s_3)) + \frac{\sqrt{2}d_4}{4}\dot{\theta}_1\dot{\theta}_3(s_3 - c_3)$$
$$+v_{42} \tag{4.43}$$

$$v_{4c3} = -\frac{d_4}{2}(\frac{1}{2}\dot{\theta}_1^2(c_3 + s_3)^2 + \dot{\theta}_3^2) + v_{43} \tag{4.44}$$

$${}^4F_4 = \begin{pmatrix} m_4v_{4c1} \\ m_4v_{4c2} \\ m_4v_{4c3} \end{pmatrix} = \begin{pmatrix} F_{41} \\ F_{42} \\ F_{43} \end{pmatrix} \tag{4.45}$$

$${}^4\mathbf{N}_4 = \begin{pmatrix} I_{xx4} & 0 & 0 \\ 0 & I_{yy4} & 0 \\ 0 & 0 & I_{zz4} \end{pmatrix} \begin{pmatrix} \frac{\sqrt{2}}{2}\ddot{\theta}_1(c_3 + s_3) + \frac{\sqrt{2}}{2}\dot{\theta}_1\dot{\theta}_3(c_3 - s_3) \\ \ddot{\theta}_3 \\ -\frac{\sqrt{2}}{2}\ddot{\theta}_1(c_3 - s_3) + \frac{\sqrt{2}}{2}\dot{\theta}_1\dot{\theta}_3(c_3 + s_3) \end{pmatrix}$$
$$+\begin{pmatrix} \frac{\sqrt{2}}{2}\dot{\theta}_1(c_3 + s_3) \\ \dot{\theta}_3 \\ \frac{\sqrt{2}}{2}\dot{\theta}_1(s_3 - c_3) \end{pmatrix} \times \begin{pmatrix} I_{xx4} & 0 & 0 \\ 0 & I_{yy4} & 0 \\ 0 & 0 & I_{zz4} \end{pmatrix} \begin{pmatrix} \frac{\sqrt{2}}{2}\dot{\theta}_1(c_3 + s_3) \\ \dot{\theta}_3 \\ \frac{\sqrt{2}}{2}\dot{\theta}_1(s_3 - c_3) \end{pmatrix}$$
$$= \begin{pmatrix} \frac{\sqrt{2}}{2}I_{xx4}(\ddot{\theta}_1(c_3 + s_3) + \dot{\theta}_1\dot{\theta}_3(c_3 - s_3)) + \frac{\sqrt{2}}{2}\dot{\theta}_1(s_3 - c_3)\dot{\theta}_3(I_{zz4} - I_{yy4}) \\ I_{yy4}\ddot{\theta}_3 - \frac{1}{2}\dot{\theta}_1{}^2(s_3{}^2 - c_3{}^2)(I_{zz4} - I_{xx4}) \\ \frac{\sqrt{2}}{2}I_{zz4}((s_3 - c_3) + \dot{\theta}_1\dot{\theta}_3(c_3 + s_3)) + \frac{\sqrt{2}}{2}\dot{\theta}_1\dot{\theta}_3(c_3 + s_3)(I_{yy4} - I_{xx4}) \end{pmatrix}$$
$$= \begin{pmatrix} N_{41} \\ N_{42} \\ N_{43} \end{pmatrix} \tag{4.46}$$

4.2 Backward Recursion for the Calculation of the Forces and Torques

For the shovel with four links, we can compute: i: 5→1[12]:

$$^{i}\mathbf{f}_{i} = {}^{i+1}_{i}\mathbf{R}\,{}^{i+1}\mathbf{f}_{i+1} + {}^{i}\mathbf{F}_{i} \tag{4.47}$$

$$^{i}\mathbf{n}_{i} = {}^{i}\mathbf{N}_{i} + {}^{i}_{i+1}R\,{}^{i+1}\mathbf{n}_{i+1} + {}^{i}\mathbf{P}_{c_i} \times {}^{i}\mathbf{F}_{i} + {}^{i}\mathbf{P}_{i+1} \times {}^{i}_{i+1}R\,{}^{i+1}\mathbf{f}_{i+1} \tag{4.48}$$

If link i is translational, then

$$\tau_i = {}^{i}\mathbf{f}_{i}^{\mathbf{T}i}\hat{\mathbf{Z}}_{i} + b_i\dot{d}_i \tag{4.49}$$

If link i is rotational, then

$$\tau_i = {}^{i}\mathbf{n}_{i}^{\mathbf{T}i}\hat{\mathbf{Z}}_{i} + b_i\dot{\theta}_i \tag{4.50}$$

where b_i is the appropriate viscous damping coefficient. Backward recursions for link 4 are as follows:

$$^{4}\mathbf{f}_{4} = \begin{pmatrix} 1 & 0 & 0 \\ 0 & 1 & 0 \\ 0 & 0 & 1 \end{pmatrix} \begin{pmatrix} f_{51} \\ 0 \\ f_{53} \end{pmatrix} + {}^{4}\mathbf{F}_{4} = \begin{pmatrix} f_{51} + m_4 v_{4c1} \\ m_4 v_{4c2} \\ f_{53} + m_4 v_{4c3} \end{pmatrix} = \begin{pmatrix} f_{41} \\ f_{42} \\ f_{43} \end{pmatrix} \tag{4.51}$$

$$\begin{aligned} {}^{4}\mathbf{n}_{4} &= {}^{4}\mathbf{N}_{4} + \begin{pmatrix} n_{51} \\ n_{52} \\ n_{53} \end{pmatrix} + \begin{pmatrix} 0 \\ 0 \\ \frac{d_4}{2} \end{pmatrix} \times \begin{pmatrix} m_4 v_{4c1} \\ m_4 v_{4c2} \\ m_4 v_{4c3} \end{pmatrix} + \begin{pmatrix} 0 \\ 0 \\ \frac{d_4}{2} \end{pmatrix} \times \begin{pmatrix} f_{51} \\ 0 \\ f_{53} \end{pmatrix} \\ &= \begin{pmatrix} N_{41} - \frac{d_4}{2} m_4 v_{4c2} \\ N_{42} + \frac{d_4}{2} m_4 v_{4c1} + d_4 f_{51} \\ N_{43} \end{pmatrix} = \begin{pmatrix} n_{41} \\ n_{42} \\ n_{43} \end{pmatrix} \end{aligned} \tag{4.52}$$

As link 4 has a prismatic joint, we have:

$$T_{d4} = f_{43} + b_4\dot{d}_4 \tag{4.53}$$

Backward recursions for link 3 are as follows:

$$^{3}\mathbf{f}_{3} = \begin{pmatrix} 1 & 0 & 0 \\ 0 & 0 & -1 \\ 0 & 1 & 0 \end{pmatrix} \begin{pmatrix} f_{51} + m_4 v_{4c1} \\ m_4 v_{4c2} \\ f_{53} + m_4 v_{4c3} \end{pmatrix} + {}^{3}\mathbf{F}_{3}$$

$$= \begin{pmatrix} f_{51} + m_4 v_{4c1} + F_{31} \\ -f_{53} - m_4 v_{4c3} + F_{32} \\ m_4 v_{4c2} + F_{33} \end{pmatrix} = \begin{pmatrix} f_{31} \\ f_{32} \\ f_{33} \end{pmatrix} \quad (4.54)$$

$$\begin{aligned} {}^3\mathbf{n_3} &= \begin{pmatrix} N_{31} \\ N_{32} \\ N_{33} \end{pmatrix} + \begin{pmatrix} 1 & 0 & 0 \\ 0 & 0 & -1 \\ 0 & 1 & 0 \end{pmatrix} \begin{pmatrix} N_{41} - \frac{d_4}{2} m_4 v_{4c2} \\ N_{42} + \frac{d_4}{2} m_4 v_{4c1} + d_4 f_{51} \\ N_{43} \end{pmatrix} \\ &+ \begin{pmatrix} 0 \\ 0 \\ \frac{L_3}{2} \end{pmatrix} \times \begin{pmatrix} F_{31} \\ F_{32} \\ F_{33} \end{pmatrix} + \begin{pmatrix} 0 \\ 0 \\ L_3 \end{pmatrix} \times \begin{pmatrix} 1 & 0 & 0 \\ 0 & 0 & -1 \\ 0 & 1 & 0 \end{pmatrix} \begin{pmatrix} f_{51} + m_4 v_{4c1} \\ m_4 v_{4c2} \\ f_{53} + m_4 v_{4c3} \end{pmatrix} \\ &= \begin{pmatrix} N_{31} + n_{41} - \frac{d_4}{2} m_4 v_{4c2} - \frac{L_3}{2} F_{32} + L_3 f_{53} + L_3 m_4 v_{4c3} \\ N_{32} - N_{43} + \frac{L_3}{2} F_{31} + L_3 f_{51} + L_3 m_4 v_{4c1} \\ N_{33} + N_{42} + \frac{d_4}{2} m_4 v_{4c1} + d_4 f_{51} \end{pmatrix} = \begin{pmatrix} n_{31} \\ n_{32} \\ n_{33} \end{pmatrix} \end{aligned} \quad (4.55)$$

As link 3 has a rotational joint, we have:

$$T_{d3} = n_{33} + b_3 \dot{\theta}_3 \quad (4.56)$$

Backward recursions for link 2 are as follows:

$${}^2\mathbf{f_2} = \begin{pmatrix} c_3 & -s_3 & 0 \\ s_3 & c_3 & 0 \\ 0 & 0 & 1 \end{pmatrix} \begin{pmatrix} f_{51} + m_4 v_{4c1} + F_{31} \\ -f_{53} - m_4 v_{4c3} + F_{32} \\ m_4 v_{4c2} + F_{33} \end{pmatrix} + \begin{pmatrix} F_{21} \\ F_{22} \\ F_{23} \end{pmatrix}$$

$$= \begin{pmatrix} c_3(f_{51} + m_4 v_{4c1} + F_{31}) + s_3(f_{53} + m_4 v_{4c3} - F_{32}) + F_{21} \\ s_3(f_{51} + m_4 v_{4c1} + F_{31}) + c_3(-f_{53} - m_4 v_{4c3} + F_{32}) + F_{22} \\ m_4 v_{4c2} + F_{33} + F_{23} \end{pmatrix} = \begin{pmatrix} f_{21} \\ f_{22} \\ f_{23} \end{pmatrix} \quad (4.57)$$

$$\begin{aligned} {}^2\mathbf{n_2} &= \begin{pmatrix} N_{21} \\ N_{22} \\ N_{23} \end{pmatrix} + \begin{pmatrix} c_3 & -s_3 & 0 \\ s_3 & c_3 & 0 \\ 0 & 0 & 1 \end{pmatrix} \begin{pmatrix} n_{31} \\ n_{32} \\ n_{33} \end{pmatrix} + \begin{pmatrix} \frac{L_2}{2} \\ 0 \\ 0 \end{pmatrix} \times \begin{pmatrix} F_{21} \\ F_{22} \\ F_{23} \end{pmatrix} + \begin{pmatrix} L_2 \\ 0 \\ 0 \end{pmatrix} \times \\ &\begin{pmatrix} c_3 & -s_3 & 0 \\ s_3 & c_3 & 0 \\ 0 & 0 & 1 \end{pmatrix} \begin{pmatrix} f_{31} \\ f_{32} \\ f_{33} \end{pmatrix} = \begin{pmatrix} N_{21} + c_3 n_{31} - s_3 n_{32} \\ N_{22} + s_3 n_{31} + c_3 n_{32} - \frac{L_2}{2} F_{23} - L_2 f_{33} \\ N_{23} + n_{33} + \frac{L_2}{2} F_{22} + L_2(s_3 f_{31} + c_3 f_{32}) \end{pmatrix} \\ &= \begin{pmatrix} n_{21} \\ n_{22} \\ n_{23} \end{pmatrix} \end{aligned} \quad (4.58)$$

As link 2 is fixed, therefore,

$$T_{d2} = 0 \tag{4.59}$$

Backward recursions for link 1 are as follows:

$$\begin{aligned} {}^1\mathbf{f}_1 &= \begin{pmatrix} \frac{\sqrt{2}}{2} & -\frac{\sqrt{2}}{2} & 0 \\ 0 & 0 & -1 \\ \frac{\sqrt{2}}{2} & \frac{\sqrt{2}}{2} & 0 \end{pmatrix} \begin{pmatrix} f_{21} \\ f_{22} \\ f_{23} \end{pmatrix} + \begin{pmatrix} 0 \\ 0 \\ m_1 g \end{pmatrix} \\ &= \begin{pmatrix} \frac{\sqrt{2}}{2}(f_{21} - f_{22}) \\ -f_{23} \\ \frac{\sqrt{2}}{2}(f_{21} + f_{22}) + m_1 g \end{pmatrix} = \begin{pmatrix} f_{11} \\ f_{12} \\ f_{13} \end{pmatrix} \end{aligned} \tag{4.60}$$

$$\begin{aligned} {}^1\mathbf{n}_1 &= \begin{pmatrix} 0 \\ 0 \\ I_{zz1}\ddot{\theta}_1 \end{pmatrix} + \begin{pmatrix} \frac{\sqrt{2}}{2} & -\frac{\sqrt{2}}{2} & 0 \\ 0 & 0 & -1 \\ \frac{\sqrt{2}}{2} & \frac{\sqrt{2}}{2} & 0 \end{pmatrix} \begin{pmatrix} n_{21} \\ n_{22} \\ n_{23} \end{pmatrix} \\ &+ \begin{pmatrix} L_1 \\ 0 \\ 0 \end{pmatrix} \times \begin{pmatrix} \frac{\sqrt{2}}{2} & -\frac{\sqrt{2}}{2} & 0 \\ 0 & 0 & -1 \\ \frac{\sqrt{2}}{2} & \frac{\sqrt{2}}{2} & 0 \end{pmatrix} \begin{pmatrix} f_{21} \\ f_{22} \\ f_{23} \end{pmatrix} \\ &= \begin{pmatrix} \frac{\sqrt{2}}{2}(n_{21} - n_{22}) \\ -n_{23} - \frac{\sqrt{2}}{2}L_1(f_{21} + f_{22}) \\ I_{zz1}\ddot{\theta}_1 + \frac{\sqrt{2}}{2}(n_{21} + n_{22}) - L_1 f_{23} \end{pmatrix} = \begin{pmatrix} n_{11} \\ n_{12} \\ n_{13} \end{pmatrix} \end{aligned} \tag{4.61}$$

As link 1 also has a rotational joint, we have,

$$T_{d1} = n_{13} + b_1\dot{\theta}_1 \tag{4.62}$$

The T_{d1}, T_{d3}, and T_{d4} are the load torques which act on the swing, hoist, and crowd motors respectively.

Chapter 5

Analytical Actuator Dynamics and Shovel Parameters

This research project received excellent collaboration from the P&H company. Its chief mechanical and electrical engineers met our team members and provided a lot of data, such as various mass, size of machine, and DC motors' currents and voltages and so forth. In the following sections, these data will be used to calculate parameters of the analytical model.

5.1 Analytical Actuator Dynamics

The swing, hoist, and crowd motors on the type of electric shovel being modelled are all DC shunt motors. The circuit diagram for the DC shunt motor is shown in Figure 5.1.

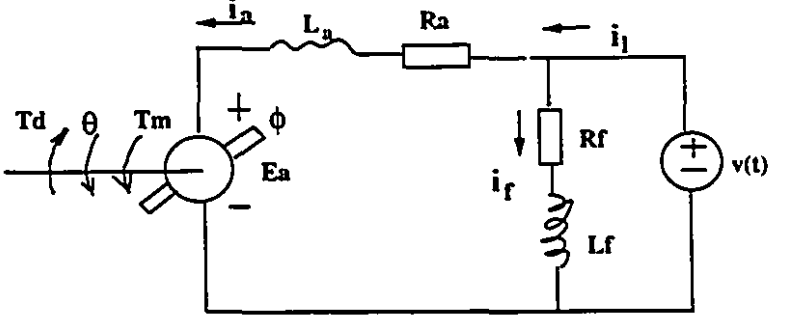

Figure 5.1: Circuit Diagram for DC Shunt Motor

The notations in Figure 5.1 have the following physical significance:

v(t) armature voltage

i_t total current

L_f field winding inductance

R_f — field winding resistance

i_f — field current

L_a — armature winding inductance

R_a — armature winding resistance

i_a — armature current

E_a — back emf

θ — rotor position(radians)

ω — rotational velocity

T_m — generated torque

T_d — load torque

ϕ — magnetic flux due to stator

The lumped model of a single link with actuator/gear train is illustrated Figure 5.2. The equation for the armature current is:

$$v - E_a = L_a \frac{di_a}{dt} + R_a i_a \tag{5.1}$$

The torque balancing equation is:

$$T_m = I_m \dot{\omega} + b\omega + T_d \tag{5.2}$$

where b is the mechanical damping constant. Since the flux ϕ is constant, the torque developed by the motor is:

$$T_m = k_m \phi i_a = k_1 i_a \tag{5.3}$$

where k_1 is the torque constant. The back emf relation is

$$E_a = k_b\omega = k_2\omega = k_2\frac{d\theta}{dt} \tag{5.4}$$

where k_2 is the back emf constant. When using a gearbox with gearbox ratio r, the

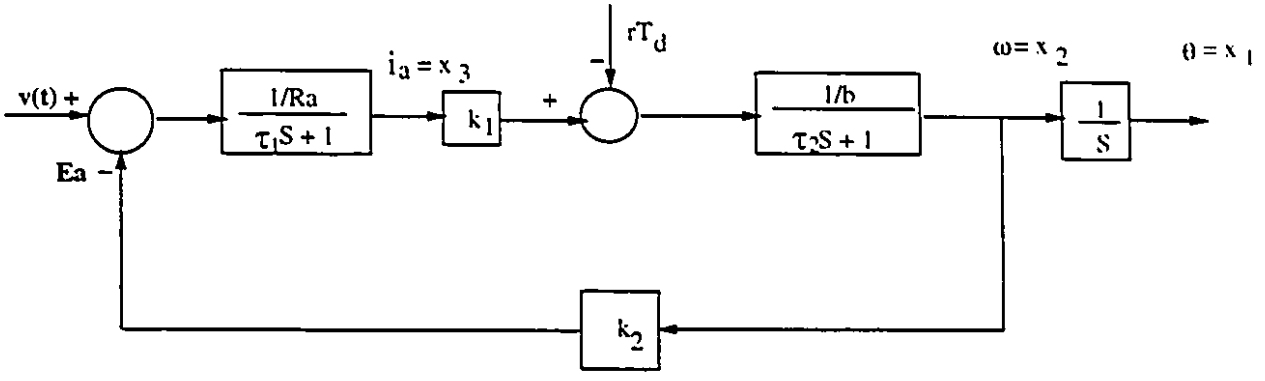

Figure 5.2: DC Shunt Motor System Block

sum of the actuator and gearbox inertias is as follows:

$$I_m = I_a + I_g \tag{5.5}$$

From equations (5.2) and (5.3), we have

$$I_m\frac{d^2\theta}{dt^2} + b\frac{d\theta}{dt} = T_m - rT_d = k_1 i_a - rT_d \tag{5.6}$$

Considering (5.1) and (5.4), we have

$$v - k_2\frac{d\theta}{dt} = L_a\frac{di_a}{dt} + R_a i_a \tag{5.7}$$

Taking $\tau_1 = \frac{L_a}{R_a}$, $\tau_2 = \frac{I_m}{b}$, (5.6) and (5.7) become

$$\tau_2\frac{d^2\theta}{dt^2} + \frac{d\theta}{dt} = \frac{k_1}{b}i_a - \frac{r}{b}T_d \tag{5.8}$$

$$\frac{v}{R_a} - \frac{k_2}{R_a}\frac{d\theta}{dt} = \tau_1\frac{di_a}{dt} + i_a \tag{5.9}$$

Taking $x_1 = \theta$, $x_2 = \omega$, $x_3 = i_a$, and arranging the formulas (5.8) and (5.9), we have the state space representation of the DC motor:

$$\dot{x_1} = x_2 \tag{5.10}$$

$$\dot{x_2} = -\frac{1}{\tau_2}x_2 + \frac{k_1}{b\tau_2}x_3 - \frac{r}{b\tau_2}T_d \tag{5.11}$$

$$\dot{x_3} = -\frac{k_2}{R_a\tau_1}x_2 - \frac{1}{\tau_1}x_3 + \frac{1}{R_a\tau_1}v \tag{5.12}$$

5.2 DC Motor Parameters

1. Calculating armature winding resistance, R_a:

Considering equation (5.1),

$$v - E_a = L_a \frac{di_a}{dt} + R_a i_a \tag{5.13}$$

When the motor is stalled, $E_a = 0$, $L_a = 0$,

$$R_a = \frac{v}{i_a} \tag{5.14}$$

From $P\&H$'s data, we can get:

$$R_a = \frac{600V}{1450A} = 0.41 \ \Omega \qquad (swing\ motor) \tag{5.15}$$

$$R_a = \frac{550V}{2000A} = 0.28 \ \Omega \qquad (hoist\ motor) \tag{5.16}$$

$$R_a = \frac{550V}{1719A} = 0.32 \ \Omega \qquad (crowd\ motor) \tag{5.17}$$

2. Calculating the torque constant, k_1:

From equation (5.3), we have

$$T_m = k_m \phi i_a = k_1 i_a \tag{5.18}$$

$$k_1 = \frac{T_m}{i_a} \tag{5.19}$$

From P&H's data, we can get(the field current $I_f = 100 \ A.$)

$$k_1 = \frac{2460}{1400} \ ft.lb./A. \qquad (swing\ motor) \tag{5.20}$$

$$k_1 = \frac{9000}{2000} \ ft.lb./A. \qquad (hoist\ motor) \tag{5.21}$$

$$k_1 = \frac{4750}{1125} \ ft.lb./A. \qquad (crowd\ motor) \tag{5.22}$$

Because

1 ft. = 30.48 cm. = 0.3048 m.

1 lb. = 0.454 kg.

1 kg. = 9.8 N.

therefore,

$$k_1 = \frac{2460 \times 0.3048 \times 0.454 \times 9.8}{1400} = 2.383\ N.m./A. \quad (swing\ motor) \quad (5.23)$$

$$k_1 = \frac{9000 \times 0.3048 \times 0.454 \times 9.8}{2000} = 6.103\ N.m./A. \quad (hoist\ motor) \quad (5.24)$$

$$k_1 = \frac{4750 \times 0.3048 \times 0.454 \times 9.8}{1125} = 5.726\ N.m./A. \quad (crowd\ motor) \quad (5.25)$$

3. Calculating the back emf constant, k_2:

From equation (5.1) and (5.4), considering very small L_a, we have

$$v - E_a = R_a i_a \quad (5.26)$$

$$E_a = k_b \phi \omega = k_2 \omega = k_2 \frac{d\theta}{dt} = k_2 \omega \quad (5.27)$$

Thus

$$k_2 = \frac{v - R_a i_a}{\omega} \quad (5.28)$$

From P&H's data, one can get(the field current $I_f = 100\ \ A.$)

$$k_2 = \frac{275 - 0.41 \times 600}{108.85} = 0.27\ \ v.sec. \quad (swing\ motor) \quad (5.29)$$

$$k_2 = \frac{550 - 0.28 \times 1000}{78.5} = 3.44\ \ v.sec. \quad (hoist\ motor) \quad (5.30)$$

$$k_2 = \frac{550 - 0.49 \times 1000}{87.92} = 0.68\ \ v.sec. \quad (crowd\ motor) \quad (5.31)$$

4. Calculating the inertia on the DC motor shaft, I_m:

$$I_m = I_a + I_g \quad (5.32)$$

(1) Inertia of Swing Motor, I_m:

From P&H's data, one can get:

$$I_a = 100\ lb.ft.^2 = 100 \times 0.454 \times 0.3048^2 = 4.22\ \ kg.m.^2 \tag{5.33}$$

$$I_g = 20\ \ kg.m.^2 \tag{5.34}$$

$$I_m = 4.22 + 20 = 24.22\ \ kg.m.^2 \tag{5.35}$$

(2) Inertia of Hoist Motor, I_m:

From P&H's data, one can get:

$$I_a = 925\ lb.ft.^2 = 925 \times 0.454 \times 0.3048^2 = 39.02\ \ kg.m.^2 \tag{5.36}$$

$$I_g = \frac{MR^2}{2} = \frac{200 \times (56 \times 2.54 \times 10^{-2})^2}{2} = 202.32\ \ kg.m.^2 \tag{5.37}$$

$$I_m = 39.02 + 202.32 = 241.34\ \ kg.m.^2 \tag{5.38}$$

(3) Inertia of Crowd Motor, I_m:

From P&H's data, one can get:

$$I_a = 295\ lb.ft.^2 = 295 \times 0.454 \times 0.3048^2 = 12.44\ \ kg.m.^2 \tag{5.39}$$

$$I_g = \frac{MR^2}{2} = \frac{100 \times (20.50 \times 2.54 \times 10^{-2})^2}{2} = 13.56\ \ kg.m.^2 \tag{5.40}$$

$$I_m = 12.44 + 13.56 = 26\ \ kg.m.^2 \tag{5.41}$$

5. Friction Coefficients of DC Motor:

The electrical damping constant b_e can be expressed[66]

$$b_e = \frac{k_1 k_2}{R_a} \tag{5.42}$$

The mechanical damping constant b can be expressed[66]

$$b = \frac{P}{\omega^2} - b_e \tag{5.43}$$

where P is the power of the DC motor.

(1) Friction coefficient of swing motor:

$$b_e = \frac{k_1 k_2}{R_a} = \frac{2.383 \times 0.27}{0.41} = 1.57\ \ N.m.sec. \tag{5.44}$$

$$b = \frac{2700 \times 10^3}{108.85^2} - 1.57 = 226.31 \quad N.m.sec. \tag{5.45}$$

(2) Friction coefficient of hoist motor:

$$b_e = \frac{k_1 k_2}{R_a} = \frac{6.103 \times 3.44}{0.28} = 74.98 \quad N.m.sec. \tag{5.46}$$

$$b = \frac{2700 \times 10^3}{78.5^2} - 74.98 = 363.17 \quad N.m.sec. \tag{5.47}$$

(3) Friction coefficient of crowd motor:

$$b_e = \frac{k_1 k_2}{R_a} = \frac{5.726 \times 0.68}{0.32} = 12.17 \quad N.m.sec. \tag{5.48}$$

$$b = \frac{2700 \times 10^3}{87.92^2} - 12.17 = 337.12 \quad N.m.sec. \tag{5.49}$$

6. Time Constant, τ_1:

Taking $L_a = 0.01$,

$$\tau_1 = \frac{L_a}{R_a} = \frac{0.01}{0.41} = 0.024 \quad sec. \qquad (swing\ motor) \tag{5.50}$$

$$\tau_1 = \frac{L_a}{R_a} = \frac{0.01}{0.28} = 0.036 \quad sec. \qquad (hoist\ motor) \tag{5.51}$$

$$\tau_1 = \frac{L_a}{R_a} = \frac{0.01}{0.32} = 0.031 \quad sec. \qquad (crowd\ motor) \tag{5.52}$$

7. Time Constant, τ_2:

$$\tau_2 = \frac{I_m}{b} = \frac{24.22}{226.31} = 0.107 \quad sec. \qquad (swing\ motor) \tag{5.53}$$

$$\tau_2 = \frac{I_m}{b} = \frac{241.34}{363.17} = 0.67 \quad sec. \qquad (hoist\ motor) \tag{5.54}$$

$$\tau_2 = \frac{I_m}{b} = \frac{26}{337.12} = 0.077 \ \ sec. \qquad (crowd \ \ motor) \tag{5.55}$$

8. Gear box ratio, r:

$$r = \frac{1}{382.3692} = 0.0026 \qquad (swing \ \ motor) \tag{5.56}$$

$$r = \frac{1}{47.8647} = 0.02 \qquad (hoist \ \ motor) \tag{5.57}$$

$$r = \frac{1}{42.1513} = 0.024 \qquad (crowd \ \ motor) \tag{5.58}$$

5.3 Rigid Body Mechanical Parameters

From P&H's data, we can get:

$$L_1 = 132.00 \ in. = 11 \ ft. = 3.4528 \ m. \tag{5.59}$$

$$m_1 = 341000 \ lb. = 154814 \ kg. \ (gantry \ \ mass) \tag{5.60}$$

$$L_2 = 240.00 \ in. = 20 \ ft. = 6.096 \ m. \tag{5.61}$$

$$m_2 = 135000 \ lb. = 61290 \ kg. \ (boom \ \ mass) \tag{5.62}$$

$$L_3 = 250.00 \ in. - 240.00 \ in. = 10 \ in.$$

$$= 0.833 \ ft. = 0.2539 \ m. \tag{5.63}$$

$$m_3 = 100 \ lb. = 45.4 \ kg. \ (saddle \ \ block \ \ mass) \tag{5.64}$$

$$L_4 = 354.25 \ in. = 29.52 \ ft. = 8.96 \ m. \tag{5.65}$$

$$m_4 = 44.000 \ lb. = 19976 \ kg. \ (dipper \ \ handle \ \ mass) \tag{5.66}$$

$$m_5 = 87000 \ lb. = 39498 \ kg. \ (dipper \ \ mass) \tag{5.67}$$

where the physical significance of L_1, L_2, L_3, and L_4 are shown in Figure 2.1.

5.4 Rigid Body Inertias

Inertia of the rectangular prism is (see Figure 5.3):

$$I_{xx} = \frac{m}{12}(b^2 + c^2) \tag{5.68}$$

$$I_{yy} = \frac{m}{12}(a^2 + c^2) \tag{5.69}$$

$$I_{zz} = \frac{m}{12}(a^2 + b^2) \tag{5.70}$$

1. Gantry Frame Inertia

The gantry frame is a rectangular prism, therefore we have,

$$I_{zz1} = \frac{m_1(a^2 + c^2)}{12} = \frac{154814((300 \times \frac{0.3048}{12})^2 + (200 \times \frac{0.3048}{12})^2)}{12}$$

$$= \frac{154814 \times (58.06 + 25.81)}{12} = 1082021 \quad kg.m.^2 \tag{5.71}$$

2. Boom Inertias We can approximately consider the boom as a rectangular prism.

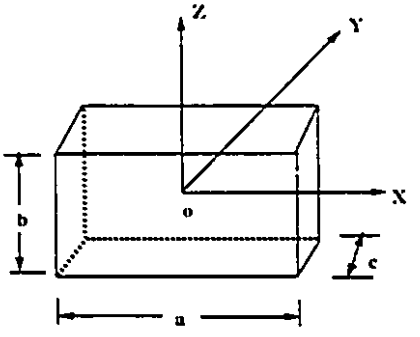

Figure 5.3: Rectangular Prism

Therefore, we have:

$$I_{xx2} = \frac{m_2}{12}(b^2 + c^2) = \frac{61290}{12}(1^2 + 1^2) = 10215 \quad kg.m.^2 \tag{5.72}$$

$$I_{yy2} = \frac{m_2}{12}(a^2 + c^2) = \frac{61290}{12}(15.17^2 + 1^2) = 1180490.86 \quad kg.m.^2 \tag{5.73}$$

$$I_{zz2} = \frac{m_2}{12}(a^2 + b^2) = \frac{61290}{12}(15.17^2 + 1^2) = 1180490.86 \quad kg.m.^2 \tag{5.74}$$

where a = 600 in. = 15.17 m., b = 1 m., c = 1 m.

3. Saddle Block Inertias

The saddle block has a complex trapezoidal shape. We use the fundamental inertia calculation formulae to solve the problem.

$$I_{xx3} = \int\int\int (y^2 + z^2)\rho dx dy dz$$

$$= \int_0^h \int_0^w \int_{\frac{w(x+a)}{a-b}}^{\frac{w(x-a)}{b-a}} (y^2 + z^2)\rho dy dx dz \tag{5.75}$$

On the x-y plane (see Figure 5.4), the right side of the trapezoid has:

$$\frac{w-0}{-b+a} = \frac{y-0}{x+a} \tag{5.76}$$

$$y = \frac{w(x+a)}{a-b} = \frac{w}{a-b}x + \frac{wa}{a-b} \tag{5.77}$$

The left side of the trapezoid has:

$$\frac{w-0}{b-a} = \frac{y-0}{x-a} \tag{5.78}$$

$$y = \frac{w(x-a)}{b-a} \tag{5.79}$$

Since $m = (a+b)wh\rho$ (ρ is material density), therefore,

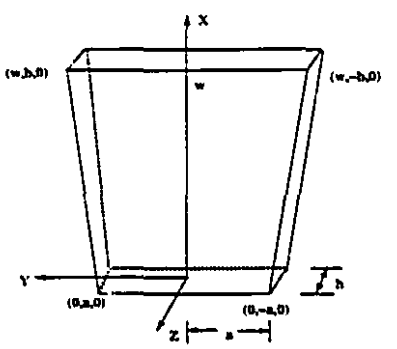

Figure 5.4: Saddle Block

$$\begin{aligned} I_{xx3} &= \int_0^h \int_0^w (z^2 \frac{w(x-a)}{b-a} - z^2 \frac{w(x+a)}{a-b} + \frac{1}{3}(\frac{w(x-a)}{b-a})^3 - \frac{1}{3}(\frac{w(x+a)}{a-b})^3)\rho dx dz \\ &= 27.33 \ \ kg.m.^2 \end{aligned} \tag{5.80}$$

$$\begin{aligned} I_{yy3} &= \int\int\int (x^2 + z^2)\rho dx dy dz \\ &= \int_0^h \int_0^w \int_{\frac{w(x+a)}{a-b}}^{\frac{w(x-a)}{b-a}} (x^2 + z^2)\rho dy dx dz \\ &= 214.5 \ \ kg.m.^2 \end{aligned} \tag{5.81}$$

$$I_{zz3} = \int\int\int (x^2+y^2)\rho dxdydz = \int_0^h \int_0^w \int_{\frac{w(x+a)}{b-a}}^{\frac{w(x+a)}{a-b}} (x^2+y^2)\rho dydxdz$$
$$= 2175.34 \ \ kg.m.^2 \tag{5.82}$$

According to the centre mass formula for a trapezoid,

$$\begin{pmatrix} x_c \\ y_c \\ z_c \end{pmatrix} = \begin{pmatrix} \frac{w(2a+b)}{3(a+b)} \\ 0 \\ 0 \end{pmatrix} \tag{5.83}$$

In terms of the parallel axis theorem,

$${}^cI_{xx3} = I_{xx3} - m_3({y_c}^2 + {z_c}^2) = I_{xx3} = 27.33 \ \ kg.m.^2 \tag{5.84}$$

$${}^cI_{yy3} = I_{yy3} - m_3({x_c}^2 + {z_c}^2) = I_{yy3} - m_3(\frac{w(2a+b)}{3(a+b)})^2$$
$$= 214.5 - 100(\frac{1.5(2\times 0.5+1)}{3(0.5+1)})^2 = 302.056 \ \ kg.m.^2 \tag{5.85}$$

$${}^cI_{zz3} = I_{zz3} - m_3({x_c}^2 + {y_c}^2) = 2175.34 - m_3(\frac{w(2a+b)}{3(a+b)})^2$$
$$= 2175.34 - 100(\frac{1.5(2\times 0.5+1)}{3(0.5+1)})^2 = 2130.8955 \ \ kg.m.^2 \tag{5.86}$$

In all the above calculations, we choose:

$$m_3 = 100\ kg., \ \ a = 0.5\ m., \ \ b = 1.0\ m. \tag{5.87}$$
$$w = 1.5\ m., \ \ h = 0.3\ m. \tag{5.88}$$

4. Dipper Handle and Dipper Inertias

We can separate a rigid body into two parts: dipper handle and dipper. Each part can be considered as an approximate a rectangular prism.

(1) Handle:

$$a = 354.25\ in. = 8.96\ m. \tag{5.89}$$
$$b = 41.00\ in. = 1.037\ m. \tag{5.90}$$
$$c = 0.4\ m. \tag{5.91}$$

$$I_{xx4}{}^{1} = \frac{m_4}{12}(8.96^2 + 0.4^2) = \frac{19976}{12}(8.96^2 + 0.4^2) = 133905.79 \ \ kg.m.^2 \quad (5.92)$$

$$I_{yy4}{}^{1} = \frac{m_4}{12}(8.96^2 + 1.04^2) = \frac{19976}{12}(8.96^2 + 1.04^2) = 135429.57 \ \ kg.m.^2 (5.93)$$

$$I_{zz4}{}^{1} = \frac{m_4}{12}(1.037^2 + 0.4^2) = \frac{19976}{12}(0.16 + 1.075) = 2056.48 \ \ kg.m.^2 \quad (5.94)$$

(2) Dipper:

$$a = 147\ in. = 3.72\ m. \quad (5.95)$$

$$b = 117\ in. = 2.96\ m. \quad (5.96)$$

$$c = 147\ in. = 3.72\ m. \quad (5.97)$$

$$I_{xx4}{}^{2} = \frac{m_5}{12}(3.72^2 + 3.72^2) = \frac{39498}{12} \times 2 \times 3.72^2 = 91098.19 \ \ kg.m.^2 \quad (5.98)$$

$$I_{yy4}{}^{2} = \frac{m_5}{12}(3.72^2 + 2.96^2) = \frac{39498}{12}(13.84 + 8.76) = 74393.17 \ \ kg.m.^2 \ (5.99)$$

$$I_{zz4}{}^{2} = \frac{m_5}{12}(2.96^2 + 3.72^2) = \frac{39498}{12}(8.76 + 13.84) = 74387.9 \ \ kg.m.^2 \ (5.100)$$

The distance between the mass centre point of the combined body (i.e. dipper handle and dipper together) and the mass centre point of the dipper handle is D_1; the distance between the mass centre point of the combined body and the mass centre point of the dipper is D_2. Thus,

$$\begin{pmatrix} x_c{}^{1} \\ y_c{}^{1} \\ z_c{}^{1} \end{pmatrix} = \begin{pmatrix} 0 \\ 0 \\ D_1 \end{pmatrix} \quad (5.101)$$

$$\begin{pmatrix} x_c{}^{2} \\ y_c{}^{2} \\ z_c{}^{2} \end{pmatrix} = \begin{pmatrix} 0 \\ 0 \\ D_2 \end{pmatrix} \quad (5.102)$$

In terms of the parallel axis theorem,

$${}^{c}I_{xx4}{}^{1} = I_{xx4}{}^{1} - m_4((y_c{}^{1})^2 + (z_c{}^{1})^2)$$

$$= I_{xx4}{}^{1} - m_4 D_1{}^2 = 133905.79 - 19976 \times 0.5^2$$
$$= 128911.79 \ \ kg.m.^2 \tag{5.103}$$

$$^cI_{yy4}{}^1 = I_{yy4}{}^1 - m_4((x_c{}^1)^2 + (z_c{}^1)^2)$$
$$= I_{yy4}{}^1 - m_4 D_1{}^2 = 135429.57 - 19976 \times 0.5^2$$
$$= 130435.57 \ \ kg.m.^2 \tag{5.104}$$

$$^cI_{zz4}{}^1 = I_{zz4}{}^1 - m_4((x_c{}^1)^2 + (y_c{}^1)^2) = I_{zz4}{}^1 = 2056.48 \ \ kg.m.^2 \tag{5.105}$$

$$^cI_{xx4}{}^2 = I_{xx4}{}^2 - m_5((y_c{}^2)^2 + (z_c{}^2)^2) = I_{xx4}{}^2 - m_5 D_2{}^2$$
$$= 91098.19 - 39498 \times 0.3^2 = 87543.37 \ \ kg.m.^2 \tag{5.106}$$

$$^cI_{yy4}{}^2 = I_{yy4}{}^2 - m_5((x_c{}^2)^2 + (z_c{}^2)^2) = I_{yy4}{}^2 - m_5 D_2{}^2$$
$$= 74393.17 - 39498 \times 0.3^2 = 70838.35 \ \ kg.m.^2 \tag{5.107}$$

$$^cI_{zz4}{}^2 = I_{zz4}{}^2 - m_5((x_c{}^2)^2 + (y_c{}^2)^2)$$
$$= I_{zz4}{}^2 = 74393.17 \ \ kg.m.^2 \tag{5.108}$$

$$^cI_{xx4} = {}^cI_{xx4}{}^1 + {}^cI_{xx4}{}^2 = 128911.79 + 87543.37 = 216455.16 \ \ kg.m.^2 \tag{5.109}$$

$$^cI_{yy4} = {}^cI_{yy4}{}^1 + {}^cI_{yy4}{}^2 = 130435.57 + 70838.35$$
$$= 201273.92 \ \ kg.m.^2 \tag{5.110}$$

$$^cI_{zz4} = {}^cI_{zz4}{}^1 + {}^cI_{zz4}{}^2 = 2056.48 + 74393.17$$
$$= 76449.65 \ \ kg.m.^2 \tag{5.111}$$

At this point, we must note that these analytical calculation of inertias are approximate. The precise results must come from actually measuring and estimating.

Chapter 6

Friction and Impact between Bucket and Muckpile

When the shovel is digging in the muckpile and loading rock, a digging interaction between the bucket and the rock exists and affects the overall machine motion and performance. Therefore, this interaction is an important issue which must be addressed by any model of shovel operation. The interaction actually includes two aspects, friction and impact. This interaction has not been studied extensively by anybody to date. Rowlands, (1991), however, has studied the friction of dragline buckets, and we can obtain some insight from his work. Based on his work, we have developed these friction models into a general coordinate space representation. In addition, we have also studied the impact effects relevant to larger fragments of rock.

6.1 Friction

When the bucket digs in the muckpile, the torque acting on the shovel bucket is zero; the forces acting on the shovel are shown in Figure 6.1. The physical significance of these notations are as follows:

P — payload weight

T — tooth friction force

L — lip friction force

f — friction forces; this includes friction of the bucket bottom's outer surface(f_1);

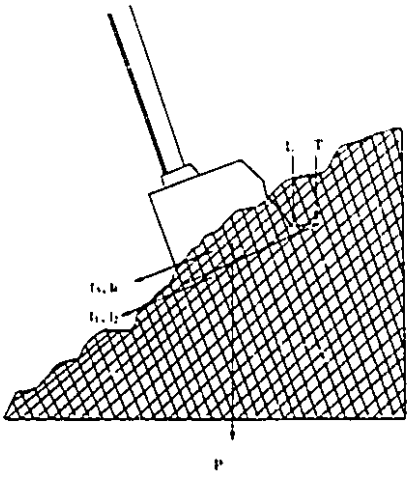

Figure 6.1: Forces Acting on Shovel Machine

friction of the bucket bottom's inner surface(f_2); the outer surface friction of two bucket sides(f_3); the inner surface friction of two bucket sides(f_4).

1. Frictions on the Bucket Bottom's Outer and Inner Surfaces

One can assume that the normal load increases at a constant rate due to the payload. The friction of the bucket bottom's outer surface(f_1) can be expressed by:

$$f_1(\Delta x_6, \Delta y_6, \Delta z_6) = (M_b + \frac{M_p}{D}\sqrt{\Delta x_6^2 + \Delta y_6^2 + \Delta z_6^2})g\mu\cos\varphi \quad , \quad (6.1)$$

where M_b is bucket mass; M_p is final payload; D is maximum digging distance; $\sqrt{\Delta x_6^2 + \Delta y_6^2 + \Delta z_6^2}$ is actual digging distance in work location coordinate {6}. ($\Delta x_6 = x_{61} - x_{60}$, $\Delta y_6 = y_{61} - y_{60}$, $\Delta z_6 = z_{61} - z_{60}$), $(x_{61}y_{61}z_{61})$ is destination of bucket digging; $(x_{60}y_{60}z_{60})$ is start of bucket digging; φ is digging angle; μ is coefficient of friction.

The friction of the bucket bottom's inner surface(f_2) can be expressed as follows:

$$f_2(\Delta x_6, \Delta y_6, \Delta z_6) = (\frac{M_p}{D_1}\sqrt{\Delta x_6^2 + \Delta y_6^2 + \Delta z_6^2})g\mu\cos\varphi \quad , \quad (6.2)$$

where D_1 is the bucket length.

2. Friction on two Bucket Sides' Outer and Inner Surfaces

The outer and inner surface friction of two bucket sides (f_3,f_4) can be described by the passive thrust per unit length along a stiff retaining wall [70]:

$$P_p = \frac{\gamma H^2 k_p}{2} \tag{6.3}$$

where, P_p is lateral thrust per length of wall, γ is unit weight of the fill material, H is actual depth of material, and k_p is passive pressure coefficient. The outer surface friction of two bucket sides, f_3, is:

$$f_3(\Delta x_6, \Delta y_6, \Delta z_6) = \frac{\gamma n k_p}{2}(\frac{H_{fa}}{D})^2(\Delta x_6^2 + \Delta y_6^2 + \Delta z_6^2)\mu \tag{6.4}$$

where H_{fa} is the final average depth of material in the bucket. n is length number of bucket.

The inner surface friction of the two bucket sides, f_4, is:

$$f_4(\Delta x_6, \Delta y_6, \Delta z_6) = \frac{\gamma n k_p}{2}(\frac{H_{fa}}{D_1})^2(\Delta x_6^2 + \Delta y_6^2 + \Delta z_6^2)\mu \tag{6.5}$$

3. Friction on Teeth and Lips

The friction across the teeth and lips of the bucket is a very complex problem. A model [30] was proposed by Hettiaratchi and Reech as follows:

$$R = \gamma \chi^2 w k_r \tag{6.6}$$

where R is resistive force on blade, χ is blade tip depth, w is blade width, and k_r is a factor due to gravity derived from nomograms. Thus, one can obtain teeth force as follows:

$$T(\Delta x_6, \Delta y_6, \Delta z_6) = n_1 \gamma w_T k_r(\frac{H_{fa}}{D})^2(\Delta x_6^2 + \Delta y_6^2 + \Delta z_6^2)\mu \tag{6.7}$$

Similarly, lip force is:

$$L(\Delta x_6, \Delta y_6, \Delta z_6) = n_1 \gamma w_L k_r(\frac{H_{fa}}{D})^2(\Delta x_6^2 + \Delta y_6^2 + \Delta z_6^2)\mu \tag{6.8}$$

where n_1 is number of teeth or lips and w_T and w_L represent the width of the teeth and lips respectively.

By and large, in the above three parts of friction, some parameters are constant (e.g. M_b D_1, etc.), and some parameters can be obtained by engineering manual (e.g. k_p and k_r). As soon as we know Δx_6, Δy_6, and Δz_6 via forward kinematics of the shovel, equations 2.25, 2.26, and 2.27, we can calculate these frictions. The relevant simulating work has been included in our simulator.

Rowlands used similar formulae to calculate his friction models for dragline bucket, but he omitted the friction coefficient, μ, in his formulae. Therefore, his models are unreasonable because of the different physical meaning on both sides of his formulae. In addition, he only considered the one dimension case; here, three dimensions based on real world coordinates are introduced.

6.2 Impact

During the digging process, the shovel often meets with large fragments which enter and interact with the bucket in a style different from smaller fragments: they produce impact on the bucket and the whole machine. The impacts acting on the shovel are shown in Figure 6.2.

In terms of the laws of motion, the impact between two colliding bodies is:

$$F = -M_1\dot{V}_1 = -M_2\dot{V}_2 \tag{6.9}$$

where 1 represents bucket and 2 represents fragment. Therefore, M_1 is mass of bucket; V_1 is velocity of bucket; M_2 is mass of fragment; V_2 is velocity of fragment. We can define colliding compression, Υ. It should have:

$$\dot{\Upsilon} = V_1 + V_2 \tag{6.10}$$

When two bodies collide, the deformation force is expressed by the Hertz Law [20]:

$$F = K_2\Upsilon^{3/2} \tag{6.11}$$

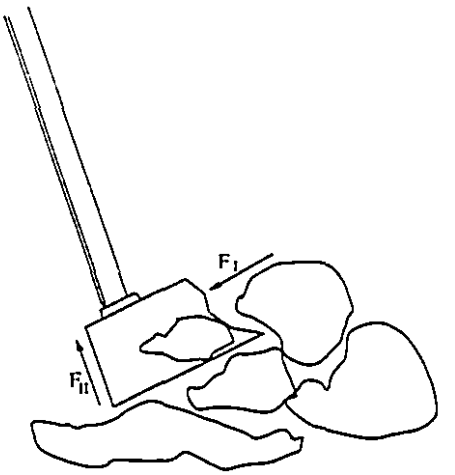

Figure 6.2: Impacts Acting on Shovel Machine

where $K_2 = \frac{4Q_3}{3(\delta_1+\delta_2)\sqrt{Q_1+Q_2}}$, $\delta_1 + \delta_2$ are material-dependent constants and Q_1, Q_2, and Q_3 are geometry constants. Differentiating equation (6.10), and considering equations (6.9) and (6.11), we get:

$$\ddot{\Upsilon} = -\frac{F}{M_1} - \frac{F}{M_2} = -K_1 K_2 \Upsilon^{3/2} \tag{6.12}$$

where $K_1 = \frac{1}{M_1} + \frac{1}{M_2}$. When two bodies begin to collide, $\Upsilon = 0$, $\dot{\Upsilon} = V_1$. The integration of equation (6.12) is:

$$\frac{1}{2}(\dot{\Upsilon}^2 - {V_1}^2) = -\frac{2}{5} K_1 K_2 \Upsilon^{5/2} \tag{6.13}$$

When a collision is completed, the relative velocity $\dot{\Upsilon} = 0$, and the compression has a maximum value. From equation (6.13), we have:

$$\Upsilon = (\frac{5{V_1}^2}{4K_1K_2})^{2/5} \tag{6.14}$$

Substituting (6.14) into (6.11), we have maximum impact:

$$F = K_2(\frac{5V_1^2}{4K_1K_2})^{3/5} \approx \eta V_1 \tag{6.15}$$

where $\eta = K_2(\frac{5}{4K_1K_2})^{3/5}$.

From equation (3.24), we can get the impact along the x_5 and z_5 directions, i.e.,

$$F_I = (x_{11}\dot{\theta}_1 + x_{12}\dot{\theta}_3 + x_{13}\dot{d}_4)\eta \tag{6.16}$$

$$F_{II} = (x_{31}\dot{\theta}_1 + x_{32}\dot{\theta}_3 + x_{33}\dot{d}_4)\eta \tag{6.17}$$

In short, in equation (6.15), we know K_2, M_1, and V_1 can be calculated by the Shovel Jacobian. Therefore, as soon as we know the mass or dimension of the fragment (i.e. M_2), we can calculate the impact. Normally, if M_2 increases, K_1 will decrease, and from equation (6.15), impact F will increase. That means that larger fragments will have larger impacts on the shovel. The relevant account has been included in our simulator.

6.3 All External Forces and Their Calculations

1. All External Forces

We put all external forces together and get:

$$f_1(x_6) = (M_b + \frac{M_p}{D}\sqrt{x_6^2 + y_6^2})g\mu\cos\varphi \tag{6.18}$$

$$f_2(x_6) = \frac{M_p}{D_1}\sqrt{x_6^2 + y_6^2}g\mu\cos\varphi \tag{6.19}$$

$$f_3(x_6) = \frac{\gamma K_p}{2}(\frac{H_{fa}}{D})^2(x_6^2 + y_6^2)\mu \tag{6.20}$$

$$f_4(x_6) = \frac{\gamma K_p}{2}(\frac{H_{fa}}{D_1})^2(x_6^2 + y_6^2)\mu \tag{6.21}$$

$$T(x_6) = n\gamma w_T k_r(\frac{H_{fa}}{D})^2(x_6^2 + y_6^2)\mu \tag{6.22}$$

$$L(x_6) = n\gamma w_L K_r(\frac{H_{fa}}{D})^2(x_6^2 + y_6^2)\mu \tag{6.23}$$

$$F_I = (x_{11}\dot{\theta}_1 + x_{12}\dot{\theta}_3 + x_{13}\dot{d}_4)\eta \tag{6.24}$$

$$F_{II} = (x_{31}\dot{\theta}_1 + x_{32}\dot{\theta}_3 + x_{33}\dot{d}_4)\eta \tag{6.25}$$

The payload gravity can be divided into:

$$\mathbf{f}_p = \mathbf{f}_{px5} + \mathbf{f}_{pz5} \tag{6.26}$$

$$|\mathbf{f}_{px5}| = M_p g \sin\varphi \tag{6.27}$$

$$|\mathbf{f}_{pz5}| = M_p g \cos\varphi \tag{6.28}$$

Thus, the total force acting on the bucket is:

$$\mathbf{F} = \mathbf{F}_{x5} + \mathbf{F}_{z5} \tag{6.29}$$

$$\mathbf{F}_{x5} = \mathbf{f}_1 + \mathbf{f}_2 + \mathbf{f}_3 + \mathbf{f}_4 + \mathbf{T} + \mathbf{L} + \mathbf{f}_{px5} + \mathbf{F}_I \tag{6.30}$$

$$\mathbf{F}_{z5} = \mathbf{f}_{pz5} + \mathbf{F}_{II} \tag{6.31}$$

The scalar values are:

$$F_{x5} = -f_1 - f_2 - f_3 - f_4 - T - L - f_{px5} - F_I \tag{6.32}$$

$$F_{z5} = f_{pz} - F_{II} \tag{6.33}$$

If there are no large fragments of rock, $F_I = F_{II} = 0$.

2. Calculations of All Forces

According to P&H's data, we have:

$$\begin{aligned} M_b &= 87000\ lb = 39498\ kg, & M_p &= 10000\ kg \\ H &= 1\ m, & n &= 6 \\ \varphi &= 20^\circ, & k_p &= 4.5 \\ \gamma &= 15500\ N/m^3, & w_T &= 0.42\ m \\ w_L &= 0.35\ m \end{aligned} \tag{6.34}$$

Therefore, for a complete digging process, the final force effects on the bucket are:

$$f_1 = (39498 + 10000) \times 9.8 \times 0.58 \times 0.939 = 264184.5\ N. \tag{6.35}$$

$$f_2 = 10000 \times 9.8 \times 0.58 \times 0.939 = 53372.76\ N. \tag{6.36}$$

$$f_3 = \frac{15500 \times 4.5}{2} \times 1^2 \times 0.58 = 20227.5\ N. \tag{6.37}$$

$$f_4 = \frac{15500 \times 4.5}{2} \times 1^2 \times 0.58 = 20227.5\ N. \tag{6.38}$$

$$T = 6 \times 15500 \times 0.42 \times 4.5 \times 1^2 = 175770\ N. \tag{6.39}$$

$$L = 6 \times 15500 \times 0.35 \times 4.5 \times 1^2 = 146475\ N. \quad (6.40)$$

$$f_{px} = 10000 \times 9.8 \times 0.342 = 33517.9\ N. \quad (6.41)$$

$$f_{pz} = 10000 \times 9.8 \times 0.9397 = 92089.9\ N. \quad (6.42)$$

$$F_{x5} = -264184.5 - 53372.76 - 20227.5 - 20227.5$$
$$- 175770 - 146475 - 33517.9 = -713775.16\ N. \quad (6.43)$$

$$F_{z5} = 92089.9\ N. \quad (6.44)$$

In case of impact, we assume $F_I = 9800\ N.$, $F_{II} = 4900\ N.$, then add these values into F_{x5} and F_{z5}. Inside our simulator,

$$f_{51} = F_{x5} \quad (6.45)$$

$$f_{53} = F_{z5} \quad (6.46)$$

where f_{51} and f_{53} are the force elements acting on the shovel. These external forces have been included in our simulator.

Chapter 7

Data Acquisition and System Identifications of Actuator Parameters

In this chapter, we will focus on three actuator models (swing motor, hoist motor, and crowd motor). They are one of our main research objectives, because the rigid body dynamic and kinematic effects, digging process influence, and the control system design all relate directly to these models. The work consists of three parts: the first is data acquisition; the second is analysing three transfer function models by using the ARX method; the third is setting up state space models by using the MLE method. The software MATLAB is used in system identification.

7.1 Overview of Data Acquisition

The field tests were undertaken to acquire data for use in system identification and subsequent validation of the shovel simulator. The data acquisition was conducted at a Western Canadian coal mine. The tests involved monitoring and data logging using a PC-based data acquisition system. The data sampling rate was 100 Hz. The basic structure of the data acquisition system is shown in Figure 7.1.

7.2 System Identifications of Transfer Functions

To get precise actuator models is the main advantage of the system identification of transfer functions. Typically, we use ARX and ARMAX model identification methods. They are stated as follows:

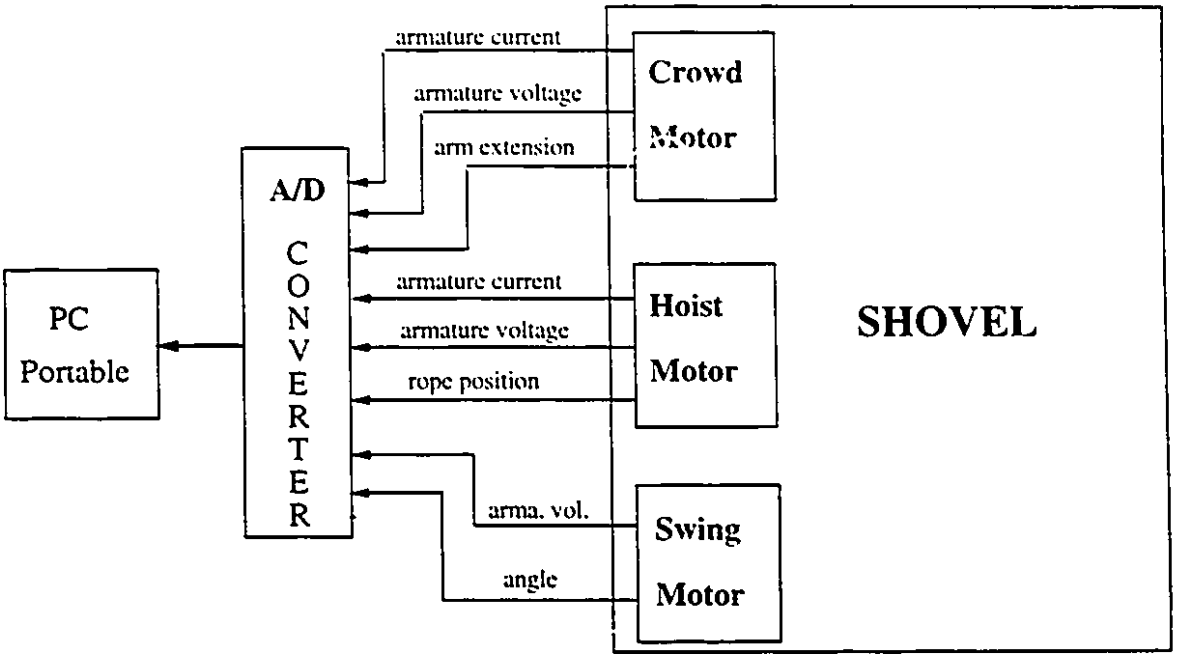

Figure 7.1: Data Acquisition System for Shovel Machine

If the system has input u, output y, and outside disturbance e, the relationship can be written

$$y(t) = G(q)u(t) + H(q)e(t) \quad , \tag{7.1}$$

where q is the shift operator and G(q)u(t) should be:

$$G(q)u(t) = \sum_{k=1}^{\infty} g(k)u(t-k) \tag{7.2}$$

and

$$G(q) = \sum_{k=1}^{\infty} g(k)q^{-k} \tag{7.3}$$

e(t) is white noise with variance λ and $\phi_v(\omega) = \lambda|H(e^{i\omega})|^2$. The above system can be represented by a general parametric model.

$$A(q)y(t) = \frac{B(q)}{F(q)}u(t-nk) + \frac{C(q)}{D(q)}e(t) \tag{7.4}$$

The general model structure can be divided into concrete models such as ARX and ARMAX. The ARX model is:

$$G(q) = q^{-nk}\frac{B(q)}{A(q)} \tag{7.5}$$

$$H(q) = \frac{1}{A(q)} \tag{7.6}$$

where B and A are polynomials in the delay operator q^{-1}:

$$A(q) = 1 + a_1 q^{-1} + ... + a_{na} q^{-na} \tag{7.7}$$

$$B(q) = b_1 + b_2 q^{-1} + ... + b_{nb} q^{-nb+1} \tag{7.8}$$

where the na and nb are the order of the polynomials. The nk is the delay from input to output. We can write the model to a standard form

$$A(q)y(t) = B(q)u(t - nk) + e(t) \tag{7.9}$$

The ARMAX model is

$$G(q) = q^{-nk} \frac{B(q)}{A(q)} \tag{7.10}$$

$$H(q) = \frac{C(q)}{A(q)} \tag{7.11}$$

Thus, the model has a structure

$$A(q)y(t) = B(q)u(t - nk) + C(q)e(t) \tag{7.12}$$

where $A(q)$ and $B(q)$ have same meaning as ARX model, while

$$C(q) = 1 + c_1 q^{-1} + ... + c_{nc} q^{-nc} \tag{7.13}$$

In this section, we mainly used the ARX method, while the ARMAX method was used as a reference. The typical methods and steps for the system identification of the transfer function in our research are as follows:

Subtract sample means from acquired data; compute loss functions for a set of different model structures and obtain the pole-zero plot; select the model order (structure); use the ARX or ARMAX method; compare real data to model output data; if not satisfactory, try again and until satisfactory. The relevant system identification procedures of the transfer function are shown in Figure 7.2.

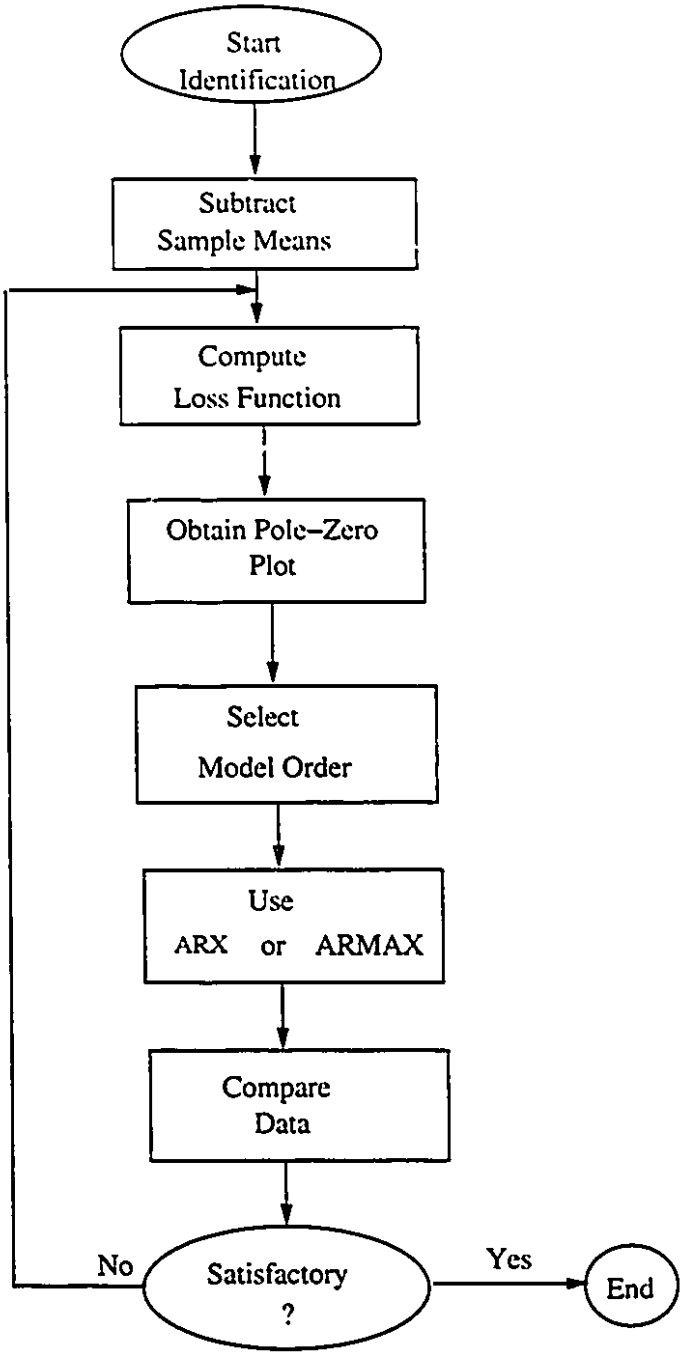

Figure 7.2: System Identification Procedure of Transfer Functions

In our experiment, input data came from an operator's input and we cannot produce high/low frequency signals in input data. Therefore, the input-output data can be unsuitable because there is not enough information, typically due to lack of frequency content. When we do system identification using the data, our estimation can still converge to a solution – model, i.e. model simulated output can match actual output, but this model does not match the true system parameters. In order to obtain more accurate model which can match true system parameters, we even need design our experiments again before processing the procedure of system identification in Figure 7.2.

(1) Swing Motor:

According to the procedure in Figure 7.2, the transfer function of the swing motor is identified as follows:

At first, we choose voltage as input, swing motor angle as output, and remove the sample mean. Then we compute loss functions and show the pole-zero plot. This is the key step in deciding the order of the model. The pole-zero plot of the swing motor is shown in Figure 7.3.

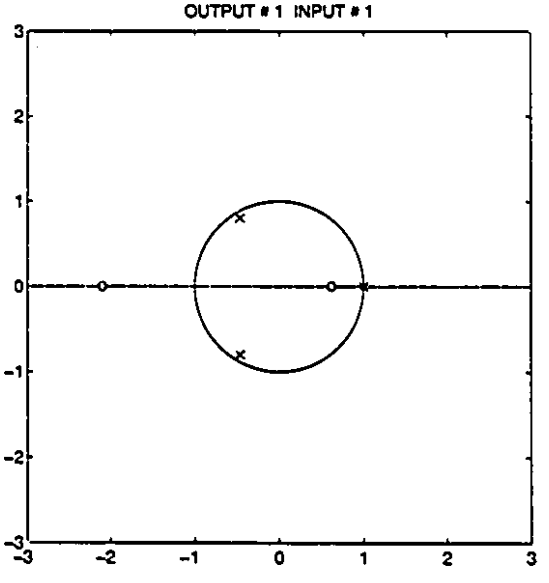

Figure 7.3: Pole-Zero Plot of the Swing Motor

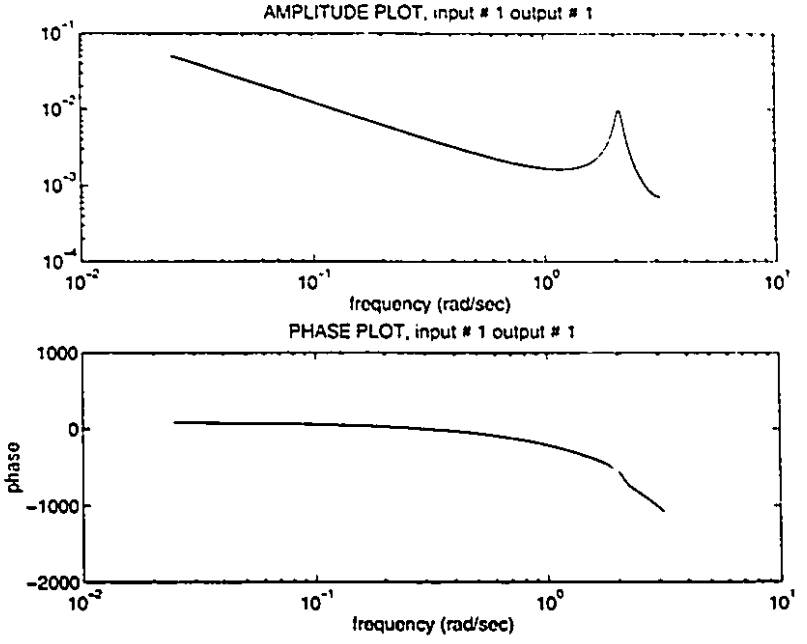

Figure 7.4: Frequency Response Plot of the Swing Motor in Discrete-Time

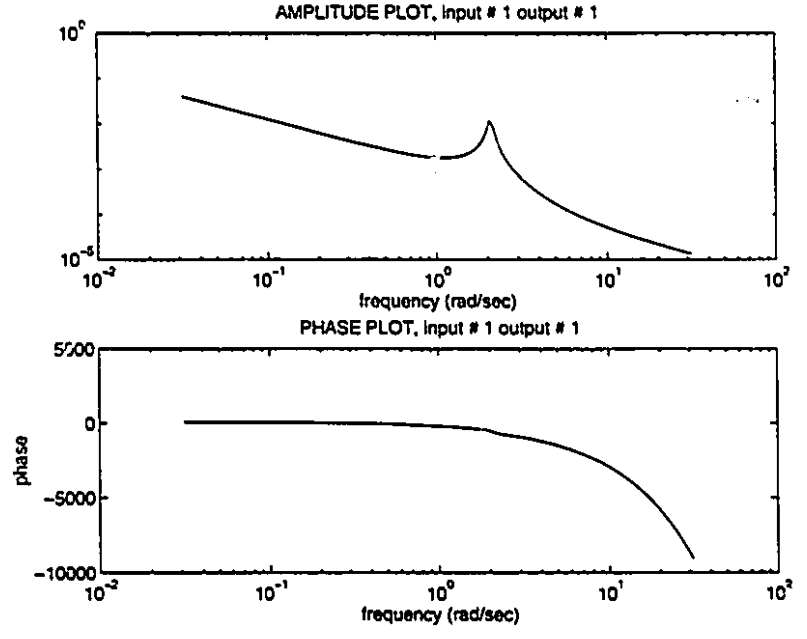

Figure 7.5: Frequency Response Plot of the Swing Motor in Continuous-Time

In Figure 7.3, one can see that there are only three poles. Therefore, the system becomes third-order. After using the ARX method, one obtains the transfer function of the swing motor as follows: (a) Discrete Time Transfer Function:

$$G(z) = \frac{-0.0011z - 0.0024}{z^3 - 0.0694z^2 - 0.0699z - 0.8602} \tag{7.14}$$

The frequency response plot, i.e. Bode Plot, in the discrete-time, is shown in Figure 7.4.

(b) Continuous Time Transfer Function:

$$G(s) = \frac{0.0004s^2 - 0.0016s - 0.0055}{s^3 + 0.1506s^2 + 4.3997s + 0.0008} \tag{7.15}$$

The frequency response plot, i.e. Bode Plot, in continuous-time, is shown in Figure 7.5.

(2) Hoist Motor: Similarly, one can choose voltage as input, rope position as output,

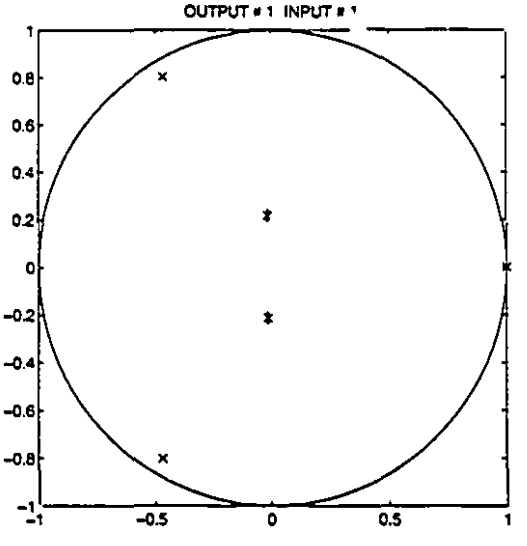

Figure 7.6: Pole-Zero Plot of Hoist Motor

and obtain the pole-zero plot of the hoist motor shown in Figure 7.6. One can find that there are one pair of symmetric zeroes and one pair of symmetric poles. Both pairs can be deleted. As a result, there are only three poles. Therefore, the system becomes third-order. One can obtain the transfer function of the hoist motor:

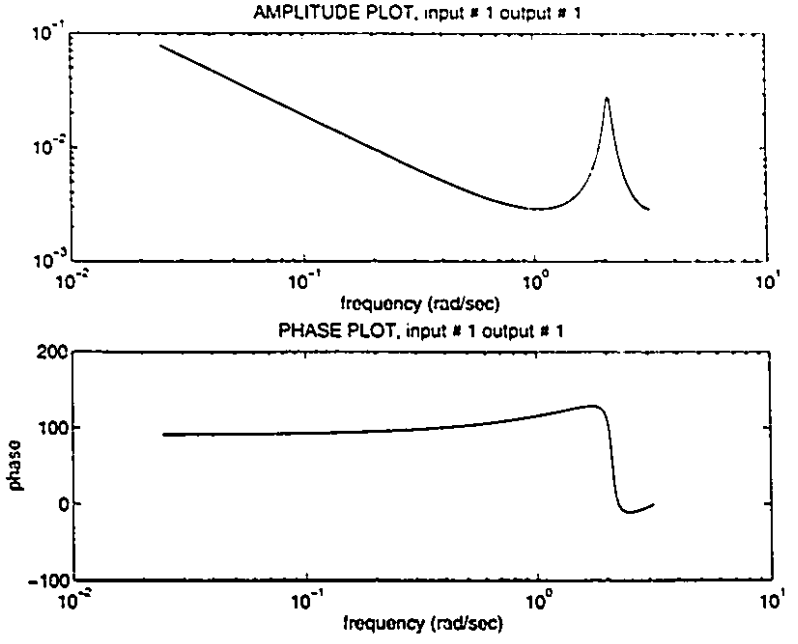

Figure 7.7: Frequency Response Plot of Hoist Motor in Discrete-Time

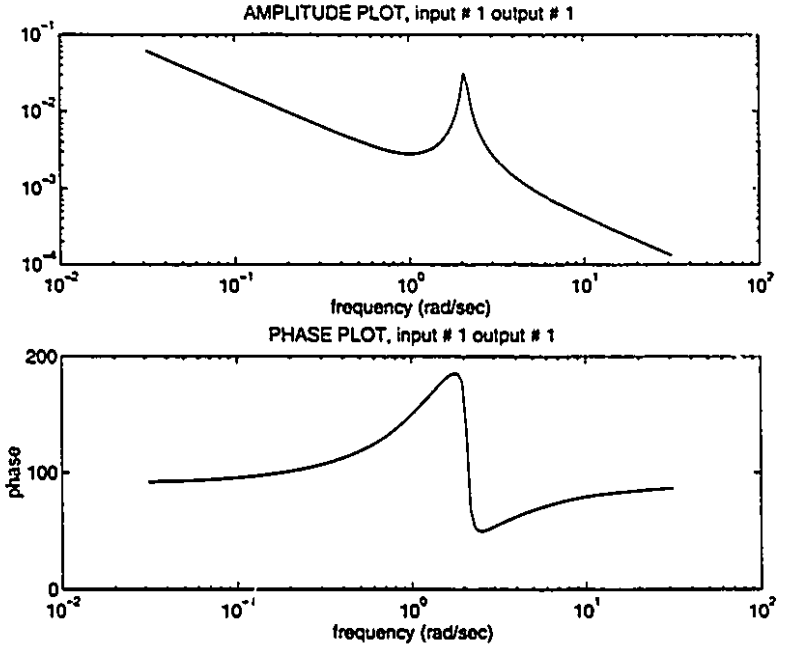

Figure 7.8: Frequency Response Plot of the Hoist Motor in Continuous-Time

(a) Discrete Time Transfer Function:

$$G(z) = \frac{-0.0054z^2}{z^3 - 0.064z^2 - 0.0639z - 0.8718} \tag{7.16}$$

The frequency response plot, i.e. Bode Plot, in discrete-time, is shown in Figure 7.7.

(b) Continuous Time Transfer Function:

$$G(s) = \frac{-0.0041s^2 - 0.0084s - 0.0085}{s^3 + 0.1372s^2 + 4.3968s + 0.0005} \tag{7.17}$$

The frequency response plot, i.e. Bode Plot, in continuous-time, is shown in Figure 7.8.

(3) Crowd Motor:

Similarly, one can choose voltage as input, arm extension as output, and also obtain the pole-zero plot of the crowd motor shown in Figure 7.9.

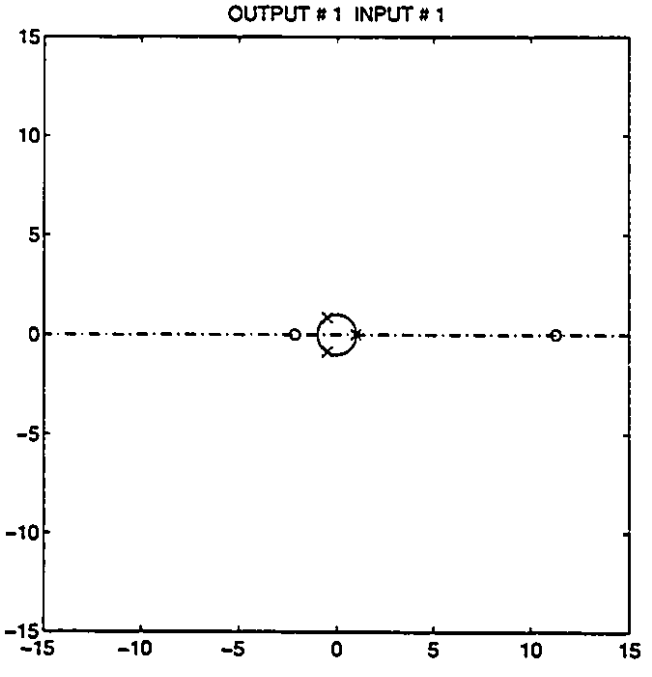

Figure 7.9: Pole-Zero Plot of Crowd Motor

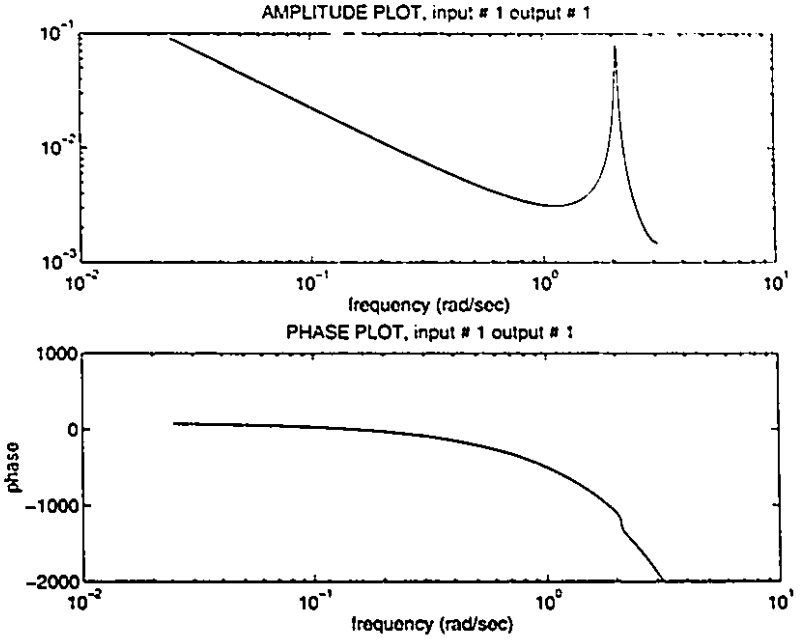

Figure 7.10: Frequency Response Plot of Crowd Motor in Discrete-Time

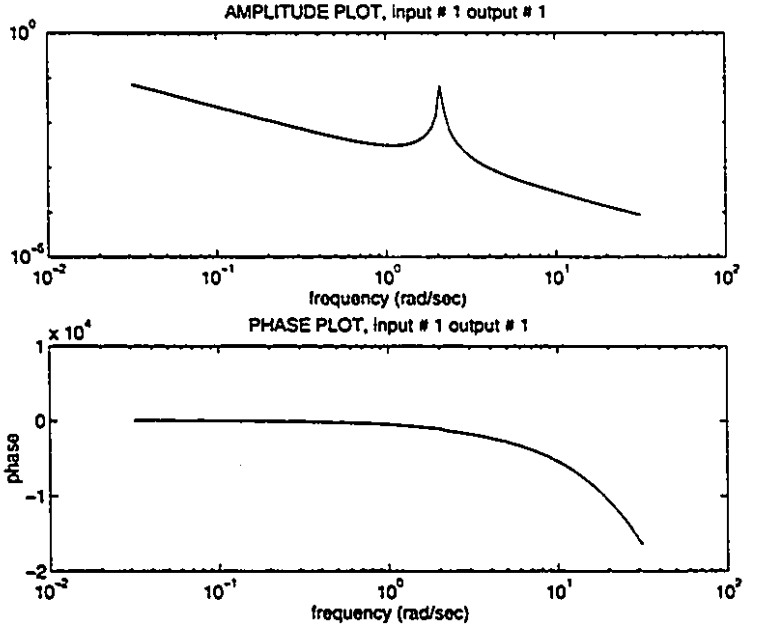

Figure 7.11: Frequency Response Plot of Crowd Motor in Continuous-Time

In Figure 7.9, one can find that there are three poles. Therefore, the system is third-order. After using the ARX method, one can obtain the transfer function of the crowd motor as follows:

(a) Discrete Time Transfer Function:

$$G(z) = \frac{0.0002z^2 - 0.00019z - 0.005}{z^3 - 0.0168z^2 - 0.0169z - 0.9654} \tag{7.18}$$

The frequency response plot, i.e. Bode Plot, in discrete-time, is shown in Figure 7.10.

(b) Continuous Time Transfer Function:

$$G(s) = \frac{-0.0027s^2 + 0.0077s - 0.0099}{s^3 + 0.0352s^2 + 4.3873s + 0.0013} \tag{7.19}$$

The frequency response plot, i.e. Bode Plot, in continuous-time, is shown in Figure 7.11.

The above motor frequency responses exhibit a resonant peak at 2 *rad/sec.* Upon inspection of the experimental data, it was determined that this peak was an artifact due to system and measurement noise. Hence, an alternative technique for determining the motor models, which is not acceptable to such noise, must be found. Therefore, we chose the maximun likelihood estimate while the models obtained by using ARX method are used as a reference.

7.3 System Identifications of State Space Models

The maximun likelihood estimate is usually used to identify the state space model in available System Identification Toolbox of MATLAB. In addition, we use Simulink in Matlab as our simulation tool. In order to use the tool, we must know a variety of parameters of state space model exactly for the DC motor. Usage of the simulation tool will be covered further in Chapter 9.

Recall the typical DC motor's third order system, (5.9), (5.10), and (5.11) as follows:

$$\dot{x}_1 = x_2 \tag{7.20}$$

$$\dot{x}_2 = -\frac{1}{\tau_2}x_2 + \frac{k_1}{b\tau_2}x_3 - \frac{1}{b\tau_2}T_d \tag{7.21}$$

$$\dot{x}_3 = -\frac{k_2}{R_a\tau_1}x_2 - \frac{1}{\tau_1}x_3 + \frac{1}{R_a\tau_1}v \tag{7.22}$$

The coefficient matrixes are

$$A = \begin{pmatrix} 0 & 1 & 0 \\ 0 & -\frac{1}{\tau_2} & \frac{k_1}{b\tau_2} \\ 0 & -\frac{k_2}{R_a\tau_1} & -\frac{1}{\tau_1} \end{pmatrix}, B = \begin{pmatrix} 0 \\ 0 \\ \frac{1}{R_a\tau_1} \end{pmatrix}, K = \begin{pmatrix} 0 \\ -\frac{1}{b\tau_2} \\ 0 \end{pmatrix} \tag{7.23}$$

$$C = (1 \quad 0 \quad 0) \tag{7.24}$$

One uses the Maximun Likelihood Estimation (MLE) for the identification. The fundamental principle of the maximun likelihood estimation is: suppose that the observations are represented by the random variable $z^n = (z(1), z(2), ..., z(N))$ that takes values in $\mathbf{R^N}$. Therefore, the probability density function is

$$f(\theta; z_1, z_2, ..., z_N) = f_z(\theta; z^N) \tag{7.25}$$

The probability is

$$P_z = \int f_z(\theta; z^N) dz^N \tag{7.26}$$

The purpose of the observation is in fact to estimate the vector θ using z^N. This is accomplished by an estimator $\hat{\theta}(z^N)$. If z^N is the actually observed value, the resulting estimate is $\hat{\theta}* = \hat{\theta}(z^N*)$. There may be a variety of estimators, i.e. $\hat{\theta_1}$, $\hat{\theta_2}$, ..., $\hat{\theta_n}$. Substituting these values into equation (7.25), we have $f_z(\hat{\theta_1}; z^N)$, $f_z(\hat{\theta_2}; z^N)$, ..., $f_z(\hat{\theta_N}; z^N)$, etc. This function, $f_z(\hat{\theta_2}; z^N)$, is called the likelihood function. It reflects the "likelihood" that observed events have taken place. A reasonable estimator of θ should be selected so that the likelihood of the observed event becomes "as maximum as possible", i.e.

$$\hat{\theta}_{ML}(z^N*) = \underbrace{arg\ max}_{\theta} f_z(\theta; z^N*) \tag{7.27}$$

This is the maximum likelihood estimator.

Now, we begin to estimate those parameters which need to be identified. In terms of (7.23), we assume some coefficient matrixes as follows:

$$A = \begin{pmatrix} 0 & 1 & 0 \\ 0 & NaN & NaN \\ 0 & NaN & NaN \end{pmatrix}, B = \begin{pmatrix} 0 \\ 0 \\ NaN \end{pmatrix}, K = \begin{pmatrix} 0 \\ NaN \\ 0 \end{pmatrix} \tag{7.28}$$

Then, according to the parameters offered by P&H Ltd, we assume these initial values:

$$guess = (-2.78 \quad 6 \quad -30 \quad -30 \quad 5); \tag{7.29}$$

Meanwhile, we define a state-space structure with unknown elements. Before we use the maximum likelihood method, we package standard state-space parameterizations into the *theta* model format (MATLAB's structure). We obtain detailed parameter values using the maximum likelihood method. Finally, the estimated values will be compared with actual values. If the residuals are too big, we can renew the *guess* value and repeat the above steps. After identifying three actuators, we can get their state space parameters as follows:

(1) Swing Motor:

$$\frac{1}{\tau_2} = 14.2542 \tag{7.30}$$

$$\frac{k_1}{b\tau_2} = 6.6362 \tag{7.31}$$

$$\frac{k_2}{R_a\tau_1} = 32.5403 \tag{7.32}$$

$$\frac{1}{\tau_1} = 31.3358 \tag{7.33}$$

$$\frac{1}{R_a\tau_1} = 11.9410 \tag{7.34}$$

From (7.30), we get $\tau_2 = 0.07$. From (7.33), we get $\tau_1 = 0.0319$. From (7.34), we get

$$R_a = \frac{1}{0.0319 \times 11.941} = 2.6242 \tag{7.35}$$

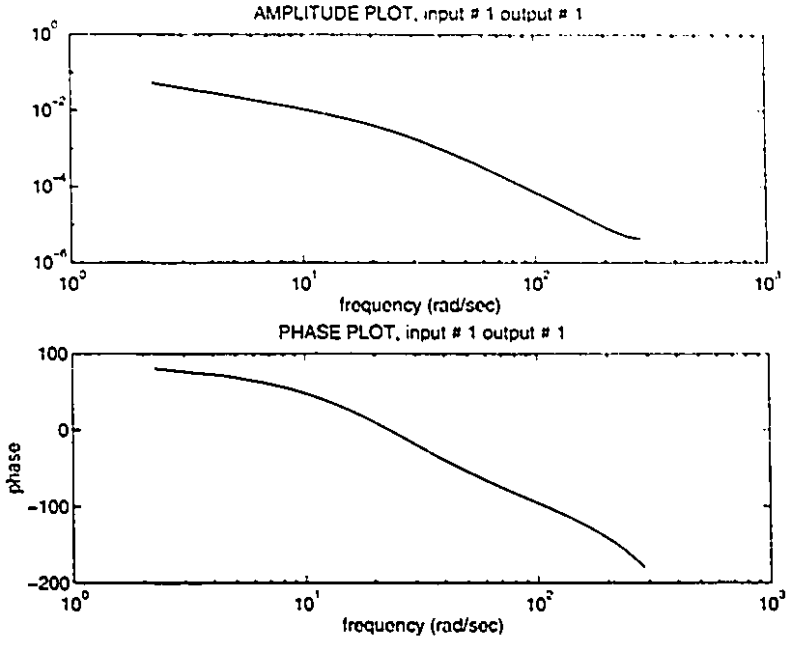

Figure 7.12: Frequency Response Plot of the Swing Motor in Discrete-Time

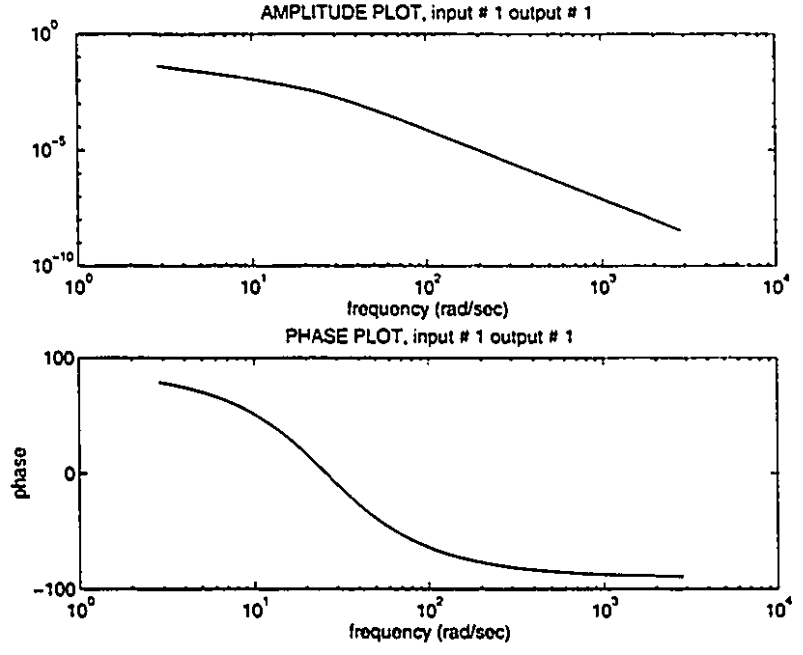

Figure 7.13: Frequency Response Plot of the Swing Motor in Continuous-Time

Substituting (7.35) into (7.32), we get

$$k_2 = 32.5403 \times 0.0319 \times 2.6242 = 2.725 \tag{7.36}$$

Because $\tau_2 = \frac{I}{b}$, we have

$$b = \frac{I}{\tau_2} = \frac{24.22}{0.07} = 346 \tag{7.37}$$

Substituting (7.37) into (7.31), we get

$$k_1 = 6.6362 \times b\tau_2 = 6.6362 \times 346 \times 0.07 = 106.73 \tag{7.38}$$

The frequency response plot, i.e. Bode Plot, in the discrete-time, is shown in Figure 7.12. The frequency response plot, i.e. Bode Plot, in continuous-time, is shown in Figure 7.13. Comparing the two figures with Figure 7.4 and Figure 7.5, we can find that there are no resonance (at 2 *rad/sec*) in Figure 7.12 and Figure 7.13. This is a reason that we choose MLE (Maximum Likelihood Estimate) method to investigate the actuator models. The relevant comparison curve is shown in Figure 7.14.

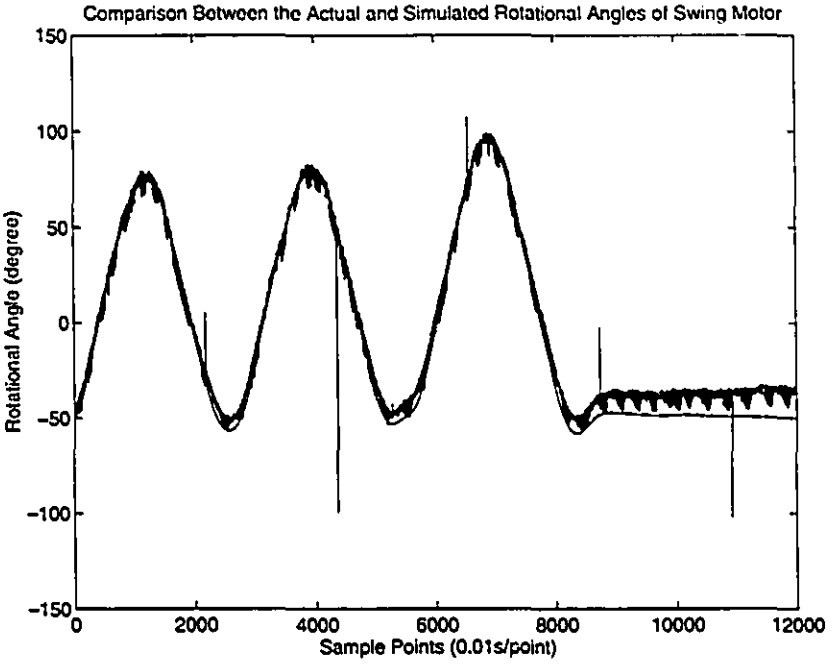

Figure 7.14: Comparison Between the Actual and Simulated Rotational Angles of Swing Motor

(2) Hoist Motor:

$$\frac{1}{\tau_2} = 3.6061 \tag{7.39}$$

$$\frac{k_1}{b\tau_2} = 0.3142 \tag{7.40}$$

$$\frac{k_2}{R_a\tau_1} = 53.0812 \tag{7.41}$$

$$\frac{1}{\tau_1} = 4.0743 \tag{7.42}$$

$$\frac{1}{R_a\tau_1} = 11.2947 \tag{7.43}$$

From (7.39), we get $\tau_2 = 0.2773$. From (7.42), we get $\tau_1 = 0.2454$. From (7.43), we get

$$R_a = \frac{1}{0.2454 \times 11.2947} = 0.36 \tag{7.44}$$

Substituting (7.44) into (7.41), we get

$$k_2 = 53.0812 \times 0.36 \times 0.2454 = 4.6997 \tag{7.45}$$

Because $\tau_2 = \frac{I}{b}$, we have

$$b = \frac{I}{\tau_2} = \frac{241.34}{0.2773} = 870.32 \tag{7.46}$$

Substituting (7.46) into (7.40), we get

$$k_1 = 0.3142 \times b\tau_2 = 0.3142 \times 870.32 \times 0.2773 = 75.829 \tag{7.47}$$

The frequency response plot, i.e. Bode Plot, in discrete-time, is shown in Figure 7.15. The frequency response plot, i.e. Bode Plot, in continuous-time, is shown in Figure 7.16. There are no resonance (at 2 *rad/sec*) in these frequency response plots. The relevant comparison curve is shown in Figure 7.17.

Note that the above physical parameters derived from the identified model are not necessarily correct, since input-output matching can occur even if the models are different.

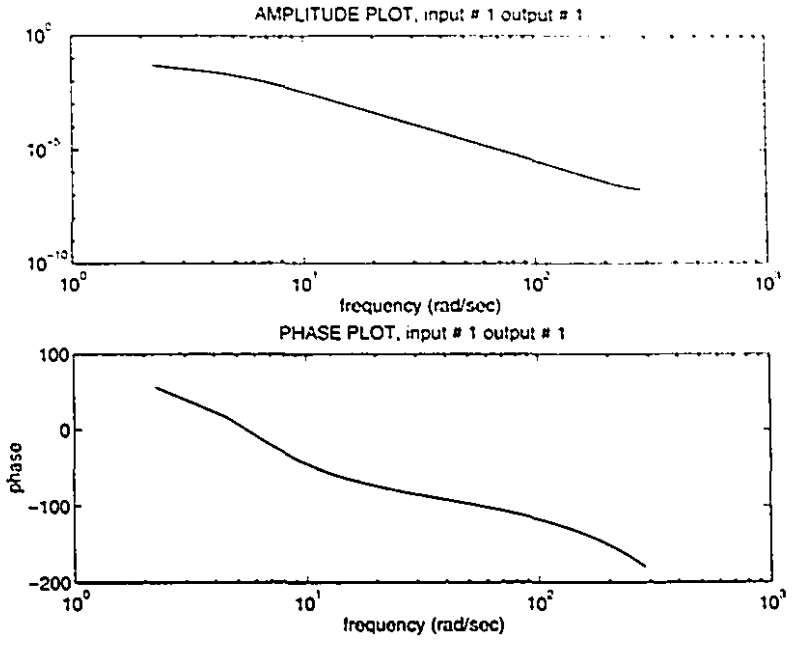

Figure 7.15: Frequency Response Plot of Hoist Motor in Discrete-Time

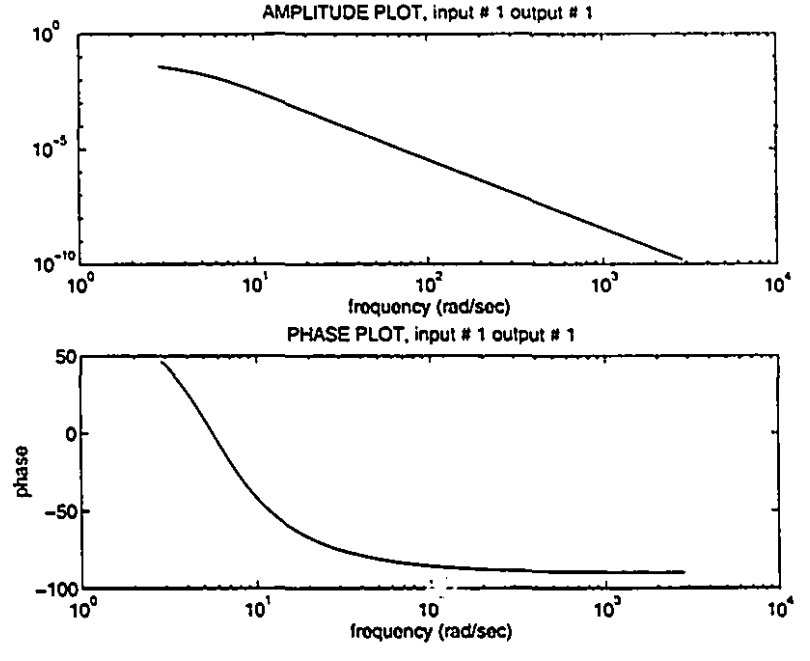

Figure 7.16: Frequency Response Plot of the Hoist Motor in Continuous-Time

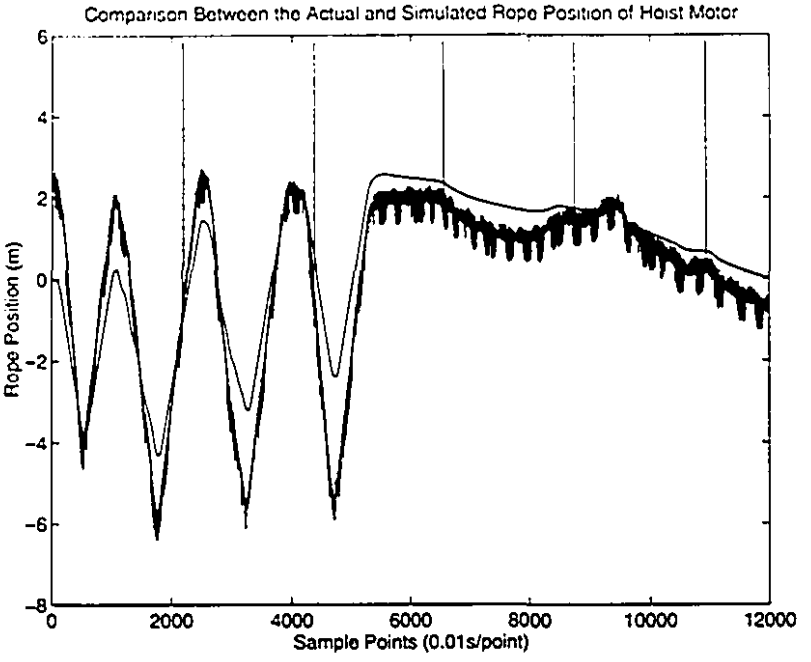

Figure 7.17: Comparison Between the Actual and Simulated Rope Positions of Hoist Motor

(3) Crowd Motor:

$$\frac{1}{\tau_2} = 11.9917 \tag{7.48}$$

$$\frac{k_1}{b\tau_2} = 2.7145 \tag{7.49}$$

$$\frac{k_2}{R_a\tau_1} = 30.4554 \tag{7.50}$$

$$\frac{1}{\tau_1} = 40.6672 \tag{7.51}$$

$$\frac{1}{R_a\tau_1} = 30.9475 \tag{7.52}$$

From (7.48), we get $\tau_2 = 0.083$. From (7.51), we get $\tau_1 = 0.025$. From (7.52), we get

$$R_a = \frac{1}{30.9475 \times 0.025} = 1.2925 \tag{7.53}$$

Substituting (7.53) into (7.50), we get

$$k_2 = 30.4554 \times 1.2925 \times 0.025 = 0.984 \tag{7.54}$$

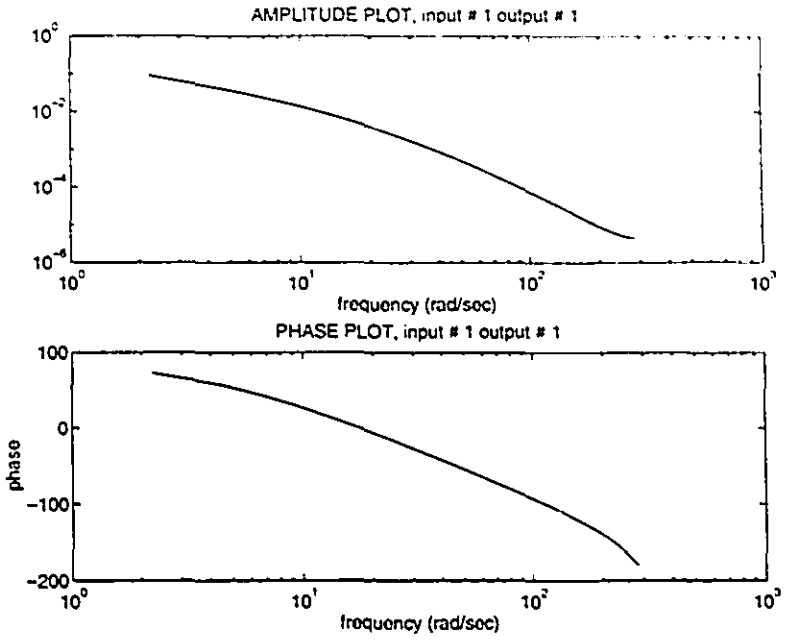

Figure 7.18: Frequency Response Plot of Crowd Motor in Discrete-Time

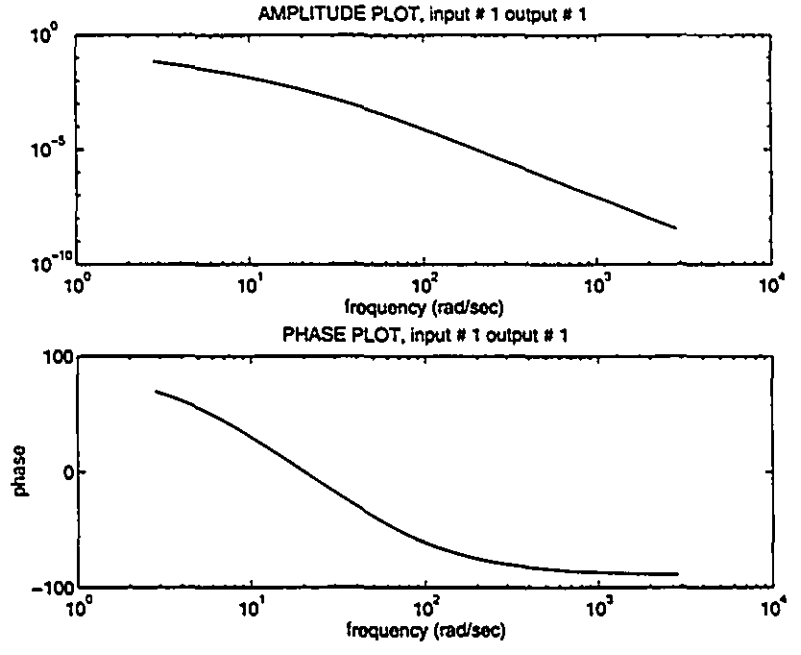

Figure 7.19: Frequency Response Plot of Crowd Motor in Continuous-Time

Because $\tau_2 = \frac{I}{b}$, we have

$$b = \frac{I}{\tau_2} = \frac{26}{0.083} = 313.25 \tag{7.55}$$

Substituting (7.55) into (7.49), we get

$$k_1 = 2.7145 \times b\tau_2 = 2.7145 \times 313.25 \times 0.083 = 70.577 \tag{7.56}$$

The frequency response plot, i.e. Bode Plot, in discrete-time, is shown in Figure 7.18. The frequency response plot, i.e. Bode Plot, in continuous-time, is shown in Figure 7.19. There are not noises (at 2 rad/sec) in these frequency response plots. The relevant comparison curve is shown in Figure 7.20.

In Figures 7.14, 7.17, and 7.20, we can see some large spikes, which are due to shot-type noise, probably due to large contactor transient on the shovel. These spikes do not represent the actual characteristics of these DC motors. In Chapter 9, we will see some spikes also exist in current and voltage signals. These spikes are also due to the same shot-type noise. In Figures 7.14, 7.17, and 7.20, we can see good input-output match, but does not necessarily indicate correct physical model parameters.

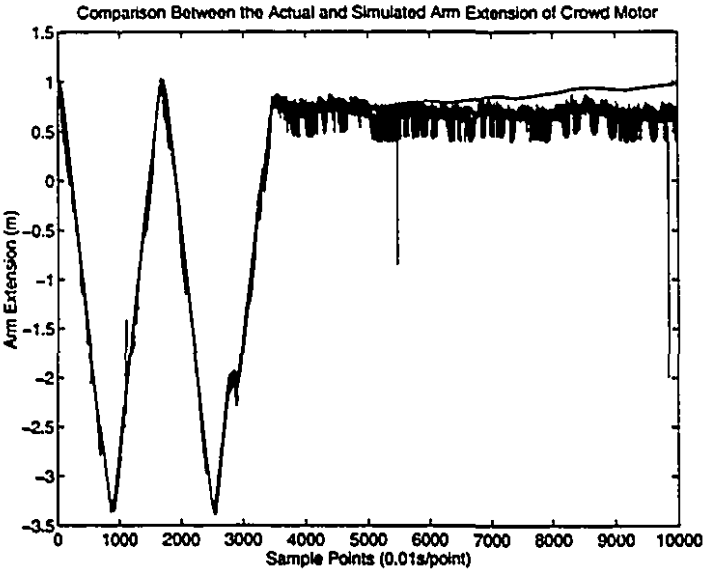

Figure 7.20: Comparison Between the Actual and Simulated Arm Extensions of Crowd Motor

7.4 Parametric Comparison

The DC motor parameters of the analytical model were obtained by the P&H company's data curves and our calculation. The DC motor parameters of the empirical model are obtained by the field test and system identification. Their comparisons are shown in Table 7.1. In the table, we choose empirical inertias are equal to analytical inertias, because the mechanical components are reliable. From these tables, one can find that some parameters have similar values, while some other parameters (e.g. k_1) have bigger differences. As being indicated in section 7.2, although our estimation still converges to a model and input-output matching can occur, the parameters of model can be inaccurate. For example, in Table 7.1, the swing motor $R_a = 2.6242$ is unreasonable high, which will results in low armature current. The reason of this problem is because we had not suitable input-output data which can produce true system parameters. But for our system simulation, the models are good enough.

$SwingParameters$	$R_a(\Omega)$	$I(kg.m^2)$	b	$k_1(N.m/A)$	$k_2(v.sec.)$	$\tau_1(sec.)$	$\tau_2(sec.)$
$AnalyticalModel$	0.41	24.22	226.31	2.383	0.27	0.024	0.107
$EmpiricalModel$	2.6242	24.22	346	106.73	2.725	0.0319	0.07
$HoistParameters$	$R_a(\Omega)$	$I(kg.m^2)$	b	$k_1(N.m/A)$	$k_2(v.sec.)$	$\tau_1(sec.)$	$\tau_2(sec.)$
$AnalyticalModel$	0.28	241.34	363.17	6.103	3.44	0.036	0.67
$EmpiricalModel$	0.36	241.34	870.32	75.829	4.6997	0.2454	0.2773
$CrowdParameters$	$R_a(\Omega)$	$I(kg.m^2)$	b	$k_1(N.m/A)$	$k_2(v.sec.)$	$\tau_1(sec.)$	$\tau_2(sec.)$
$AnalyticalModel$	0.32	26	337.12	5.726	0.68	0.031	0.077
$EmpiricalModel$	1.2925	26	313.25	70.577	0.984	0.025	0.083

Table 7.1: Parametric Comparison of Swing, Hoist, and Crowd Motors

Chapter 8

Nonparametric System Identification of Digging Process

In order to completely understand the shovel's work and real time monitoring/controlling of the electric mining shovel as well, the nonparametric system identification of the digging process is imperative. The work consists of two parts. First, nonparametric identification of the rigid body load; second, nonparametric identification of the both the rigid body load and the digging process. Actually, the nonparametric identification in our research is mainly to identify the armature currents and the positions of the DC motors.

8.1 Empirical Transfer-Function Estimation (ETFE)

System has inputs $u(t)$ and outputs $y(t)$, $t = 1, 2, ..., N$. One can define [46]:

$$U_N(\omega) = \frac{1}{\sqrt{N}} \sum_{t=1}^{N} u(t) e^{-it\omega} \tag{8.1}$$

$$Y_N(\omega) = \frac{1}{\sqrt{N}} \sum_{t=1}^{N} y(t) e^{-it\omega} \tag{8.2}$$

where $\omega = 2\pi k/N, k = 1, ..., N$. A transfer function based on data over the interval $1 \leq t \leq N$ is:

$$\hat{\hat{G}}_N(e^{i\omega}) = \frac{Y_N(\omega)}{U_N(\omega)} \tag{8.3}$$

where $\hat{\hat{G}}$ represents the estimation function.

Here, we mainly consider the digging process. When the shovel is digging ore, the swing motor is not needed to contribute to the digging work. Therefore, we

only study armature current for the hoist and crowd motor. Using the ETFE, we obtain transfer function curves based on input armature voltage and output armature current. The transfer function of hoist motor armature are shown in Figure 8.1 and the transfer function of crowd motor armature are shown in Figure 8.2.

8.2 Spectral Analysis Estimation (SAE)

Spectral Analysis Estimation has a smoother estimating curve than that of Empirical Transfer-Function Estimation. The transfer function is [46]:

$$\hat{G}_N(e^{i\omega}) = \frac{\int_{-\pi}^{\pi} W_\gamma(\xi-\omega)|U_N(\xi)|^2 \hat{G}_N(e^{i\xi})d\xi}{\int_{-\pi}^{\pi} W_\gamma(\xi-\omega)|U_N(\xi)|^2 d\xi} \tag{8.4}$$

The noise spectrum is:

$$\hat{\Phi}_v^N(\omega) = \int_{-\pi}^{\pi} W_\gamma(\xi-\omega)|Y_N(\xi) - \hat{G}_N(e^{i\xi})U_N(\xi)|^2 d\xi \tag{8.5}$$

where W_γ is weighting function. This method is different from the first method because it includes not only the frequency response of the transfer function but also the noise spectrum analysis. The latter part, however, is the important point of our analysis in the chapter. The transfer function curves are also based on input armature voltage and output armature current. The transfer function of the hoist motor armature is shown in Figure 8.3. The noise spectrum of the hoist motor armature current is shown in Figure 8.4. The transfer function of the crowd motor armature is shown in Figure 8.5. The noise spectrum of the crowd motor armature current is shown in Figure 8.6.

8.3 Lag Window Choice

As the Spectral Analysis Estimation includes the noise spectrum analysis, we focus our research on this method. In spectral analysis, the weighting function $W_\gamma(\xi)$ in equations (8.4) and (8.5) is called the frequency window. In our research, we chose the "Hamming" window, due to available MATLAB function.

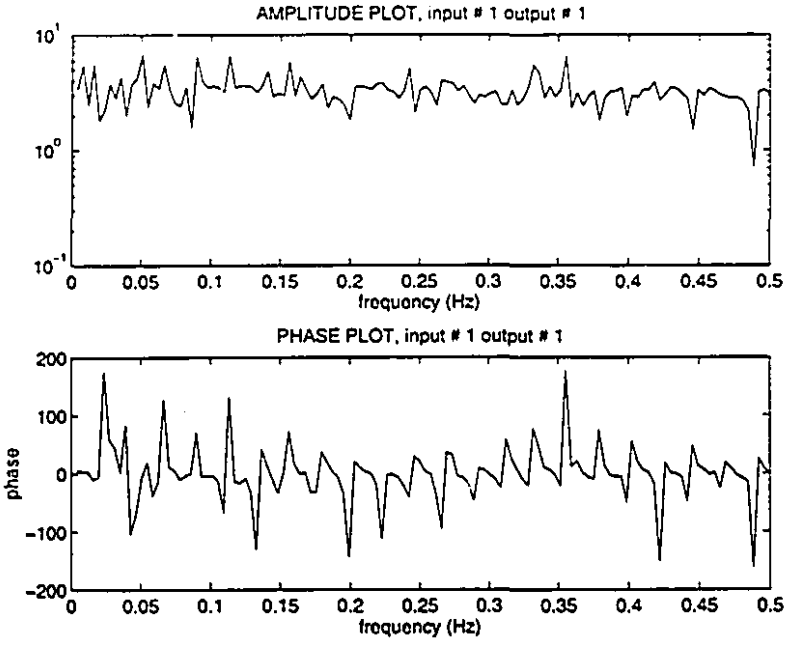

Figure 8.1: Transfer Functions of Hoist Motor Armature (ETFE)

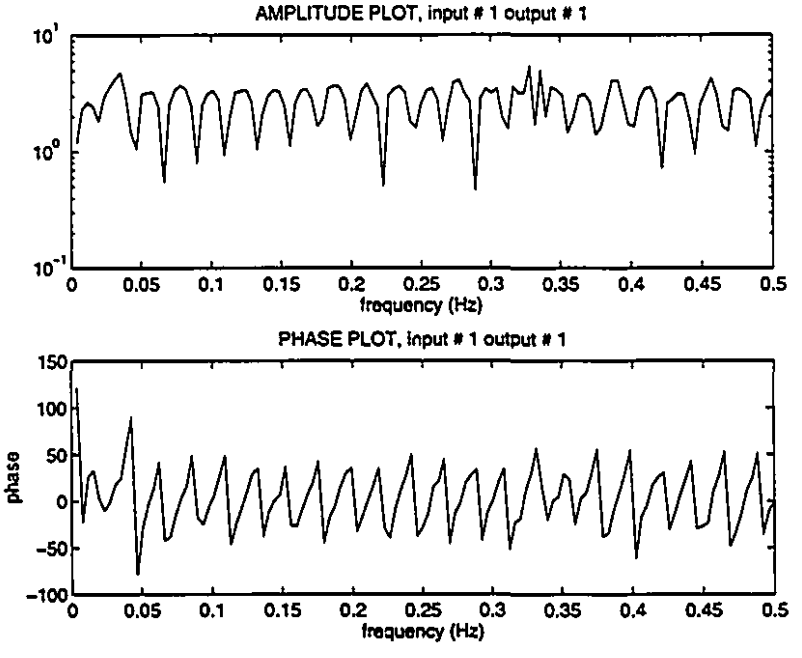

Figure 8.2: Transfer Functions of Crowd Motor Armature (ETFE)

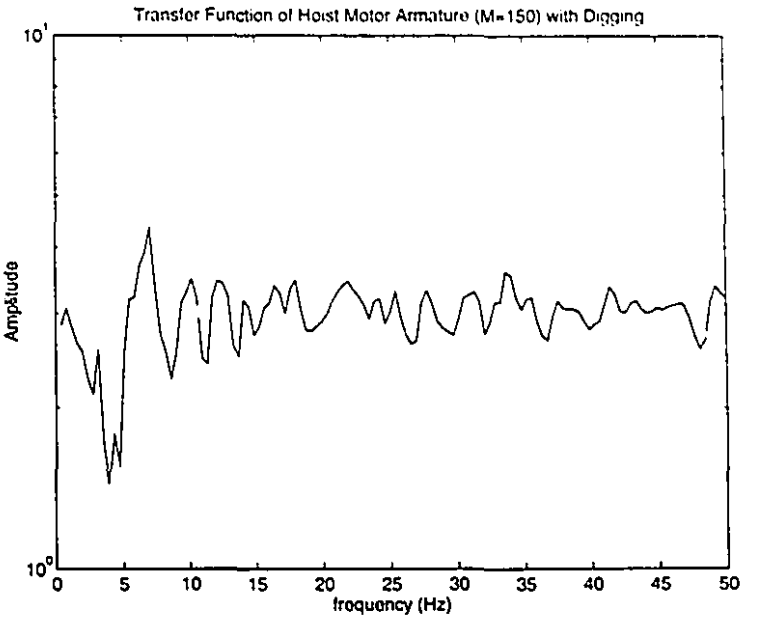

Figure 8.3: Transfer Function of Hoist Motor Armature (SAE)

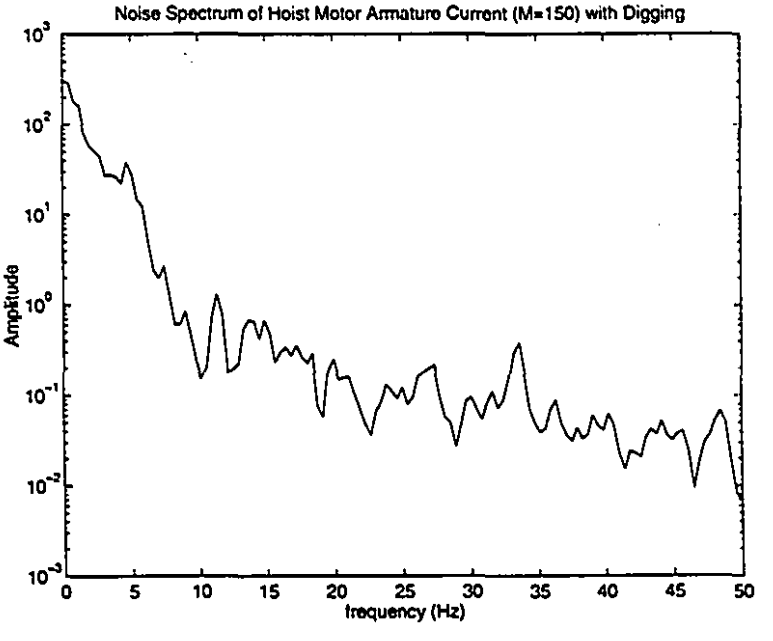

Figure 8.4: Noise Spectrum of Hoist Motor Armature Current (SAE)

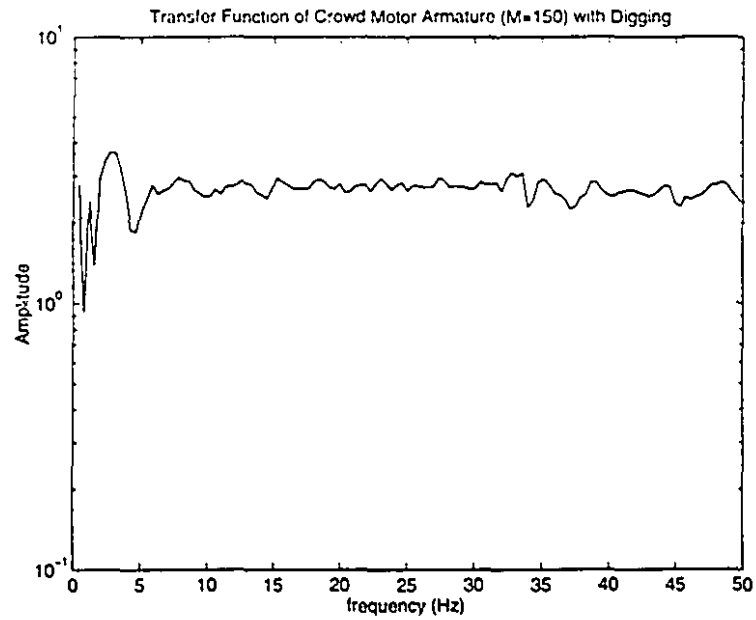

Figure 8.5: Transfer Function of Crowd Motor Armature (SAE)

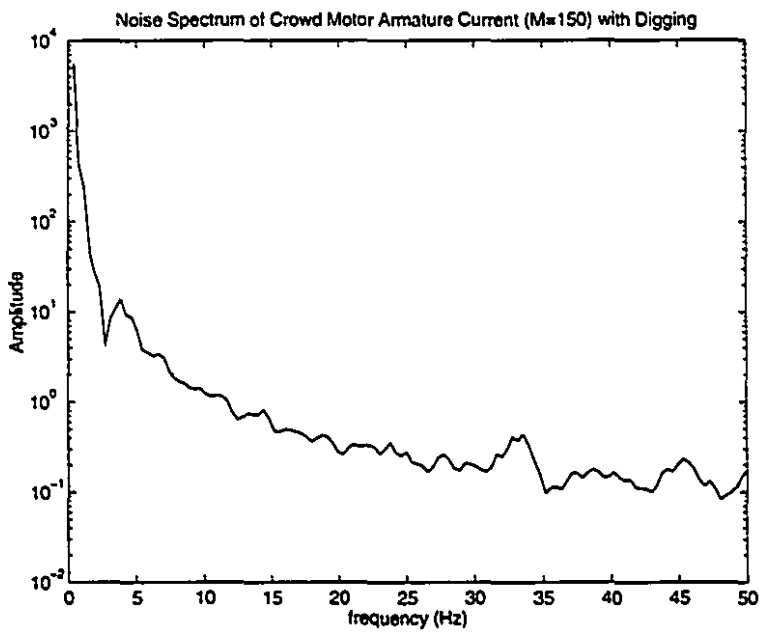

Figure 8.6: Noise Spectrum of Crowd Motor Armature Current (SAE)

The "Hamming" window has the following characteristics [46]:

$$\int_{-\pi}^{\pi} \xi^2 W_\gamma(\xi) d\xi = M(\gamma) \tag{8.6}$$

$$M(\gamma) \approx \frac{\pi^3}{\gamma^2} \tag{8.7}$$

The parameters γ and $M(\gamma)$ are used to evaluate the width of the window. As γ decrease (the frequency window gets wider), the number $M(\gamma)$ increases. The wider window will include frequencies which may deviate far from the central frequency ω_0, i.e. bring in a large bias, but lead to a small variance of $G_0(e^{i\omega_0})$. In order to better process the estimates, we must trade off between the variance and the bias.

In the following figures (from Figure 8.7 to Figure 8.12), we choose different $M(\gamma)$, and get different noise spectrum estimates. In our case, we chose $M = 150$, which seems suitable.

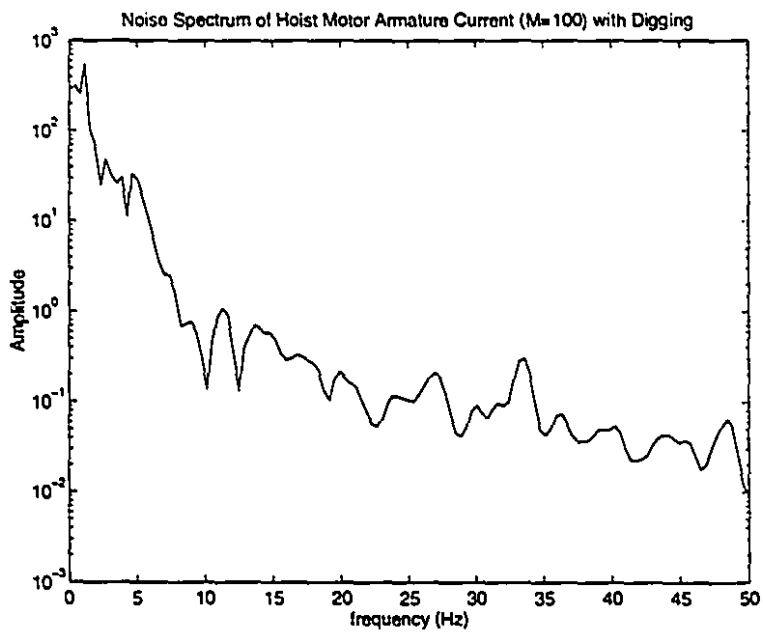

Figure 8.7: Noise Spectrum of Hoist Motor Armature Current (M=100)

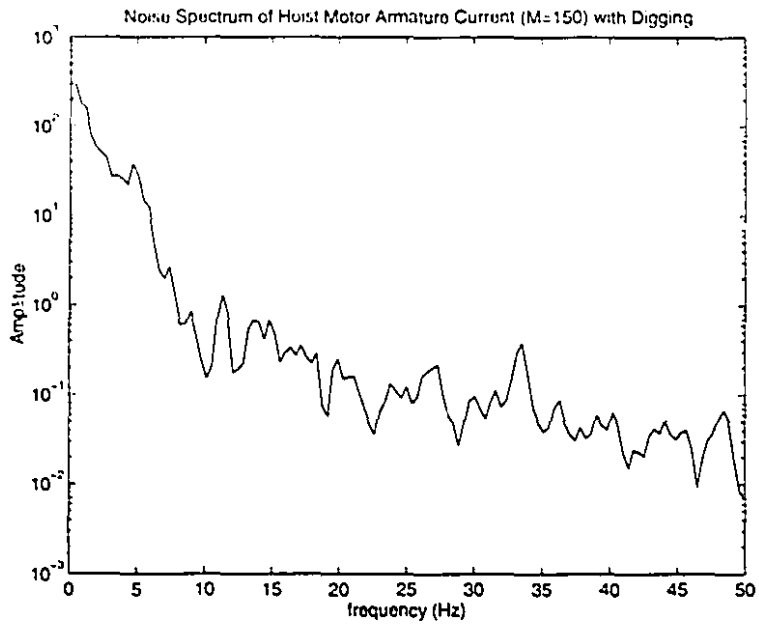

Figure 8.8: Noise Spectrum of Hoist Motor Armature Current (M=150)

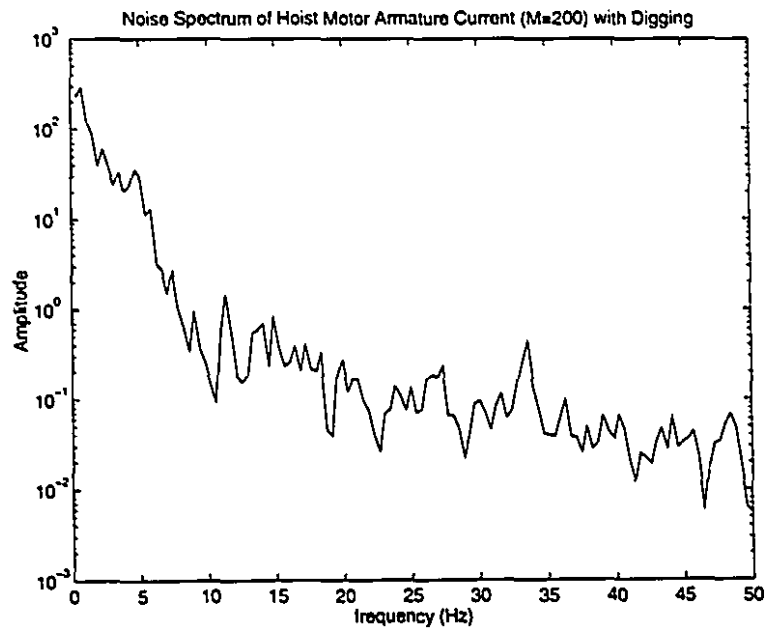

Figure 8.9: Noise Spectrum of Hoist Motor Armature Current (M=200)

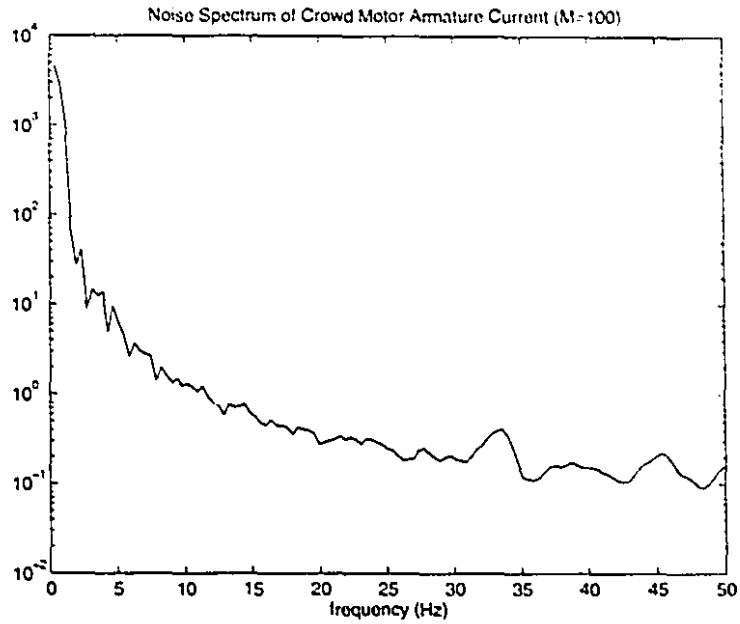

Figure 8.10: Noise Spectrum of Crowd Motor Armature Current (M=100)

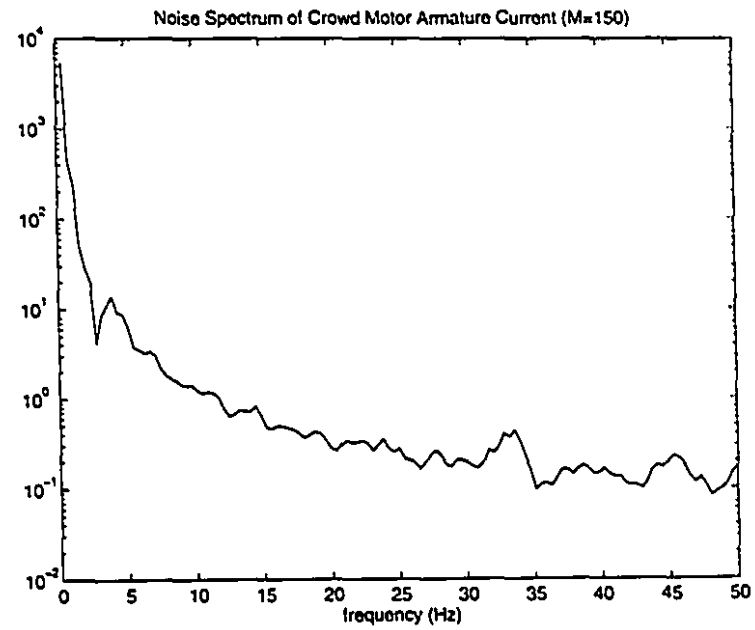

Figure 8.11: Noise Spectrum of Crowd Motor Armature Current (M=150)

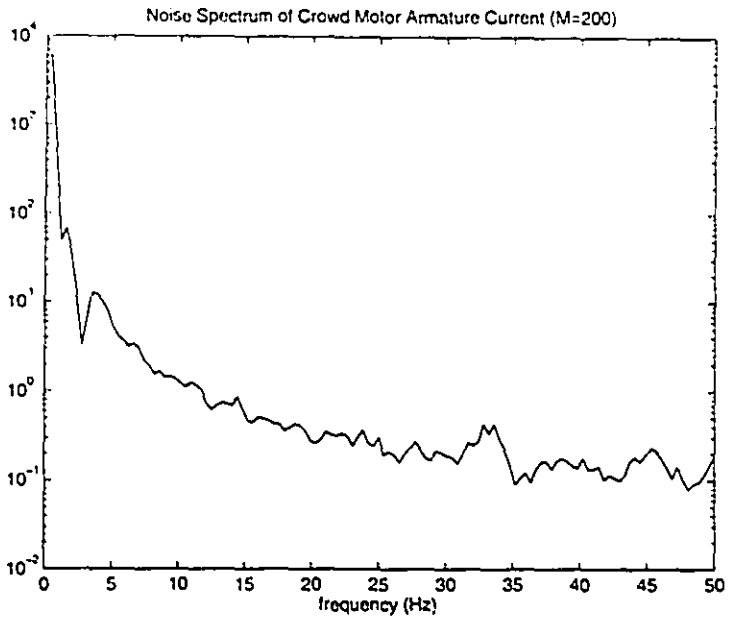

Figure 8.12: Noise Spectrum of Crowd Motor Armature Current (M=200)

8.4 Noise Spectrum Comparisons of Armature Currents with and without Digging

After we decide the lag window and its M parameter value equals 150, we begin to analyse the noise spectra of the armature currents of the DC motors. At first, let us see why we chose the armature currents as our objective of the nonparametric model estimation. We recall equations (5.2) and (5.3) as follows:

$$T_m = I_m\dot{\omega} + b\omega + T_d \tag{8.8}$$

$$T_m = k_1 i_a \tag{8.9}$$

From the two equations, we have:

$$T_d = k_1 i_a - I_m\dot{\omega} - b\omega \tag{8.10}$$

Under the conditions of certain ω and $\dot{\omega}$, the change of i_a reflects the change of T_d. Therefore, we concentrate the nonparametric identification in estimating each motor's armature current.

From all armature current spectra, we extract two typical parts: noise spectrum with digging process and noise spectrum without digging process for hoist and crowd motor cases. The relevant results are shown in Figures 8.13, 8.14, 8.15, and 8.16. From these figures, we can see: lower frequency parts have a higher gain and higher frequency parts have a smaller gain; there are larger gains between 30Hz and 35Hz for both motor cases and this indicates the shovel has vibration of non-rigid body in this frequency range.

Comparing the Figures, we also find that the noise with digging are larger than those without digging. This conclusion is in line with the actual circumstance, because during the digging process, there are two types of noise for each actuator, i.e. shovel body noise and digging noise. The differences in the noise spectra just reflect the difference between the whole noise spectrum and the rigid body noise spectrum.

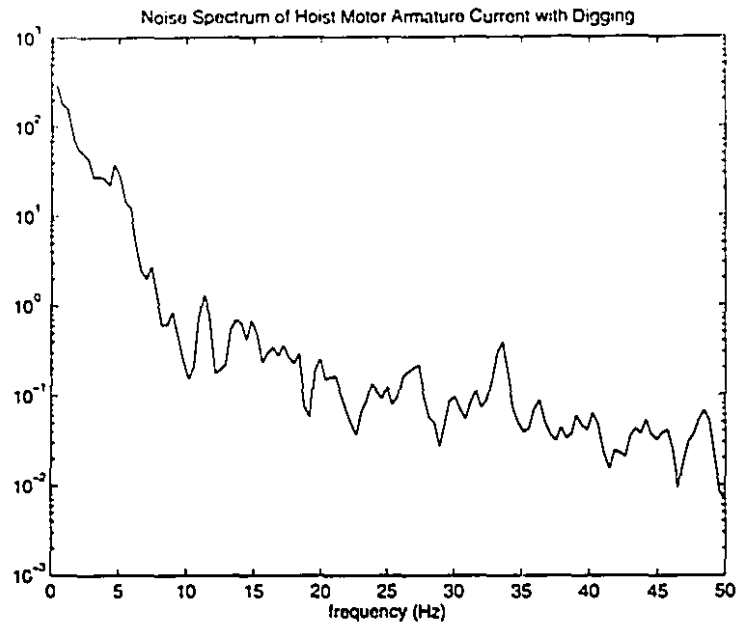

Figure 8.13: Noise Spectrum of Hoist Motor Armature Current with Digging

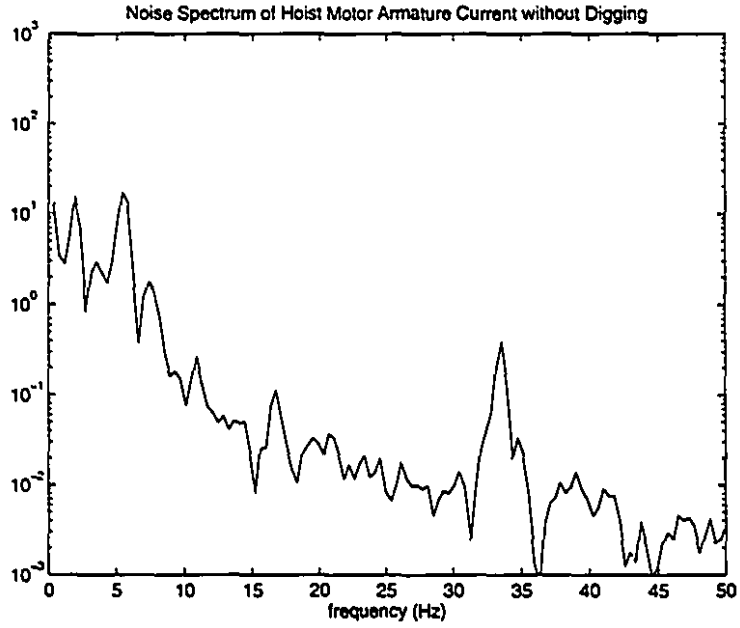

Figure 8.14: Noise Spectrum of Hoist Motor Armature Current without Digging

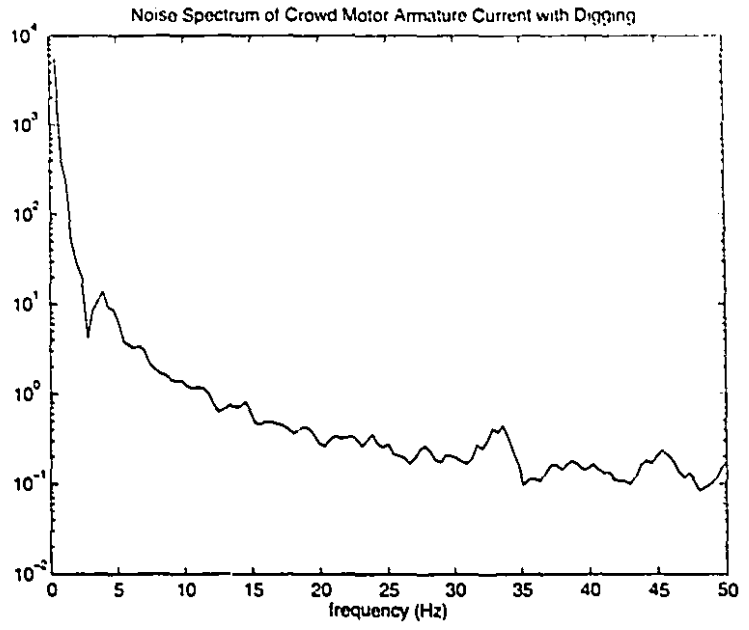

Figure 8.15: Noise Spectrum of Crowd Motor Armature Current with Digging

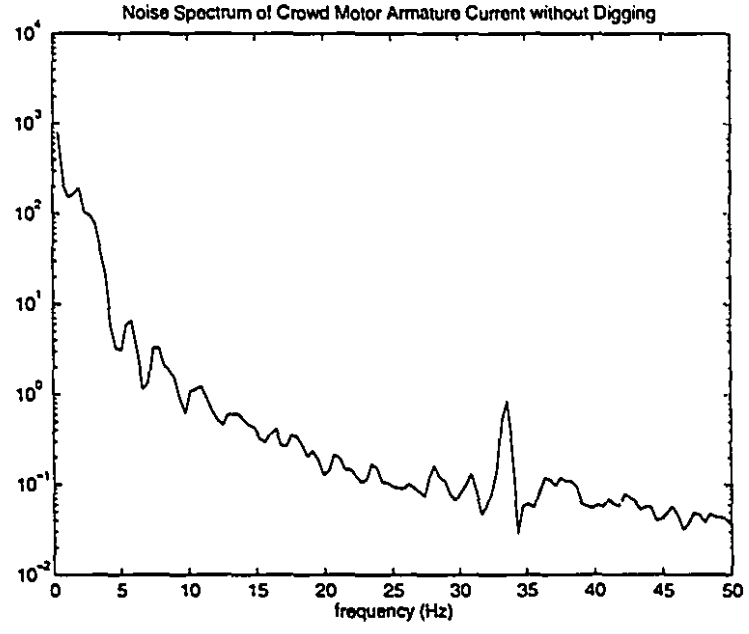

Figure 8.16: Noise Spectrum of Crowd Motor Armature Current without Digging

8.5 Noise Spectrum Comparisons of Armature Currents with Easy and Hard Digging

The easy and hard diggings can also have different effect on the armature currents, due to different interactional forces. The relevant results are shown in Figures 8.17, 8.18, 8.19, and 8.20.

Comparing the Figures, we also find that the noise with hard digging is larger than those with easy digging in low-frequency parts, but smaller in high-frequency parts. We believe that during the hard digging process, due to harder ore, interaction has slower process — this brings in larger low-frequency noise (impact) and smaller high-frequency noise into the armature currents.

8.6 Noise Spectrum Comparisons of Positions with and without Digging

In addtion to armature current noise spectra, we can estimate the position noise spectrum as well. It fully reflects the actual noise effect of the motor. Figures 8.21 and 8.22 show the noise spectra of the hoist motor rope position. Figures 8.23 and 8.24 show the noise spectra of the crowd motor arm extension, when we set $M = 150$.

The noise spectra of the positions have similar features to the noise spectra of the armature currents, except that the gains between 25Hz to 30Hz and 40Hz to 50Hz have larger values. That means the shovel has also vibration of non-rigid body in the two frequency ranges. From this phenomenon, we can recognize that the effects of non-rigid body truly exsit on the electric mining shovel.

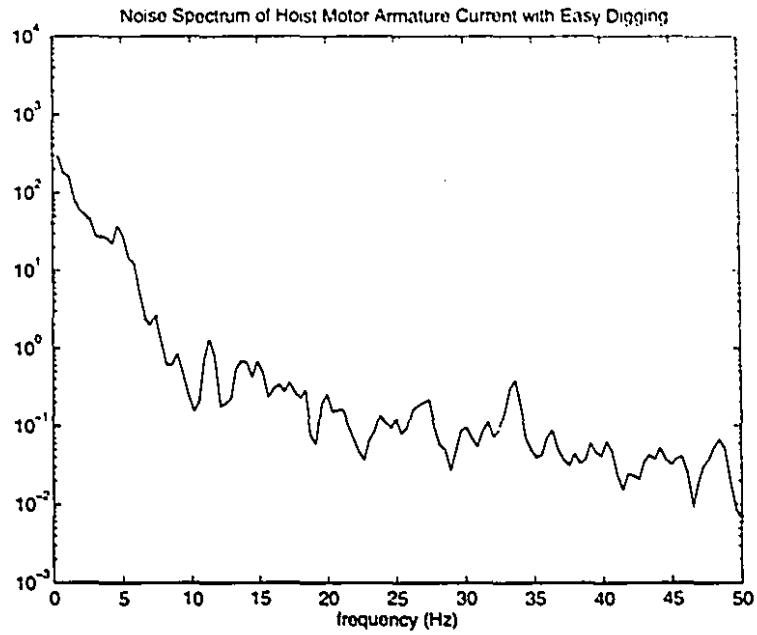

Figure 8.17: Noise Spectrum of Hoist Motor Armature Current with Easy Digging

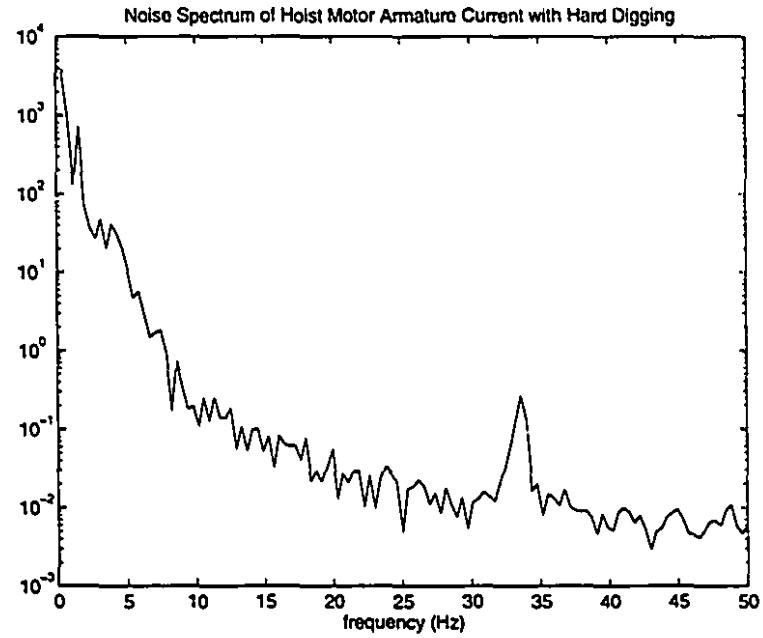

Figure 8.18: Noise Spectrum of Hoist Motor Armature Current with Hard Digging

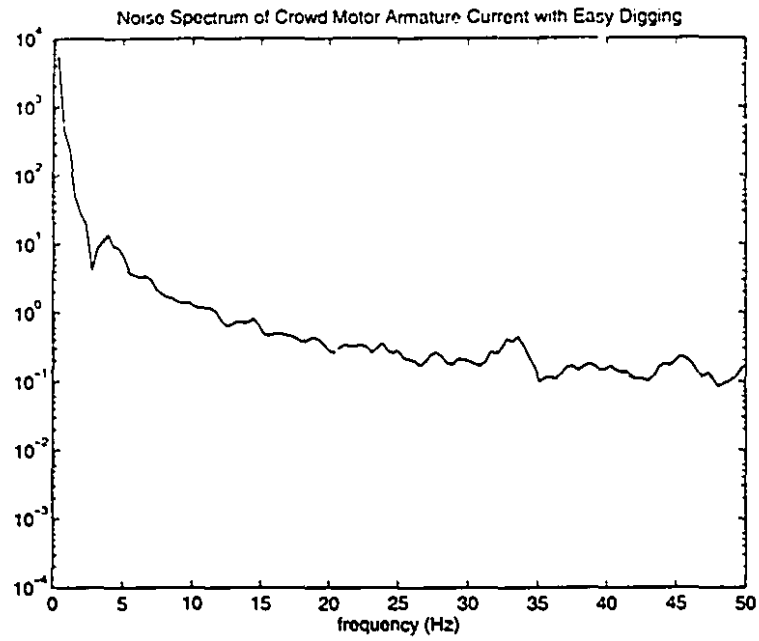

Figure 8.19: Noise Spectrum of Crowd Motor Armature Current with Easy Digging

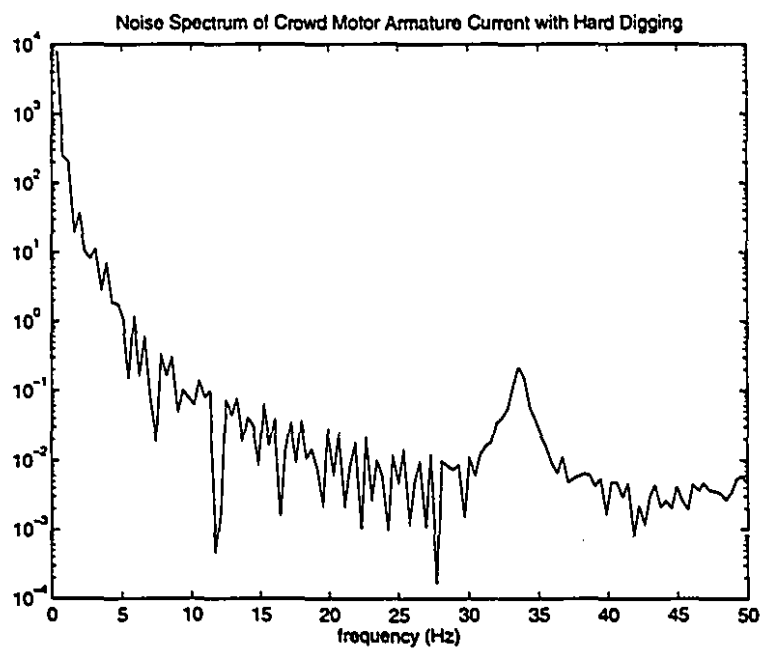

Figure 8.20: Noise Spectrum of Crowd Motor Armature Current with Hard Digging

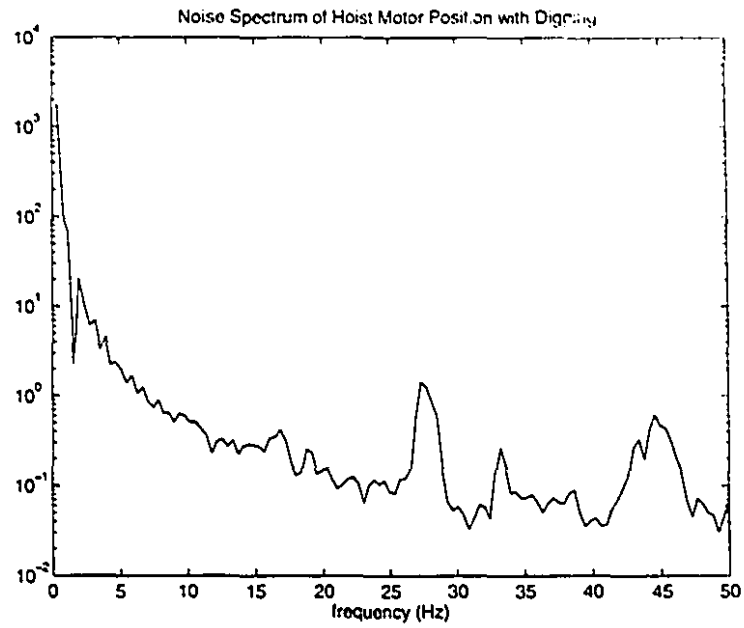

Figure 8.21: Noise Spectrum of Hoist Motor Rope Position with Digging

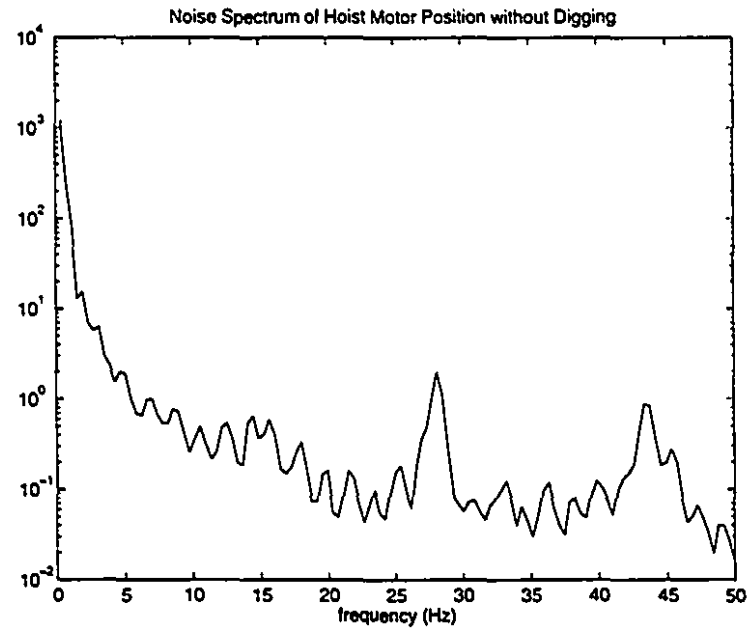

Figure 8.22: Noise Spectrum of Hoist Motor Rope Position without Digging

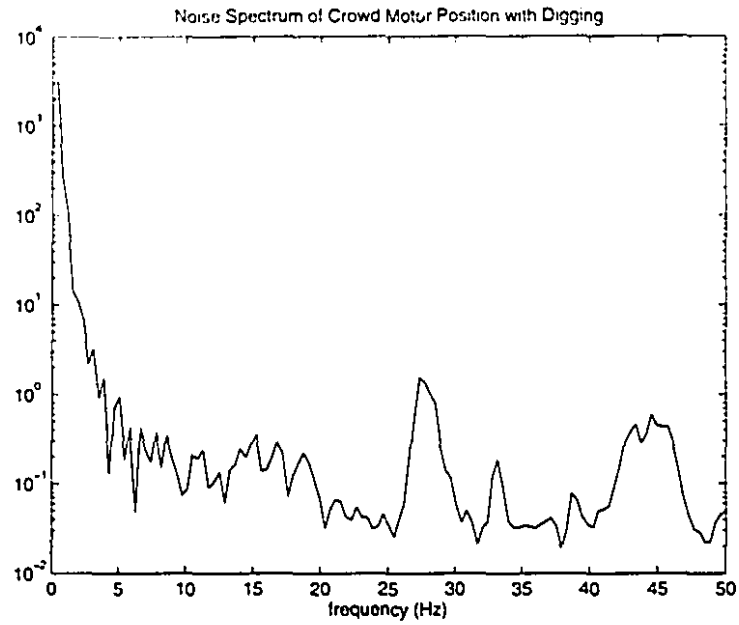

Figure 8.23: Noise Spectrum of Crowd Motor Arm Extension with Digging

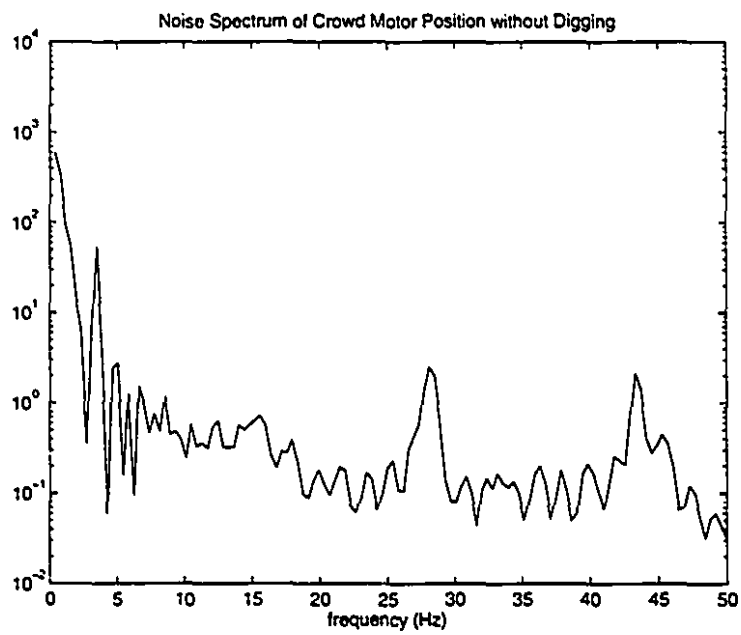

Figure 8.24: Noise Spectrum of Crowd Motor Arm Extension without Digging

Chapter 9

Simulating Methodology and Simulator

For the purposes of building a software simulator, all the models derived in the previous chapter must be integrated in a coherent manner which reflects the behaviour of the actual system, while remaining computationally efficient. SIMULINK, a simulation toolbox of MATLAB, is used in our system simulation. The general simulation system structure is shown in Figure 9.1.

9.1 Overall Machine/Process Model

The overall machine/process model includes the actuator dynamics, rigid body dynamics, and the interaction between bucket and muckpile.

In terms of the three actuators, one can obtain crowd, hoist, and swing motor dynamics, respectively. Using equations (5.10), (5.11), and (5.12), we have

$$\dot{x_1} = x_2 \tag{9.1}$$

$$\dot{x_2} = -\frac{1}{\tau_2}x_2 + \frac{k_1}{b\tau_2}x_3 - \frac{1}{b\tau_2}rT_d \tag{9.2}$$

$$\dot{x_3} = -\frac{k_2}{R_a\tau_1}x_2 - \frac{1}{\tau_1}x_3 + \frac{1}{R_a\tau_1}v \tag{9.3}$$

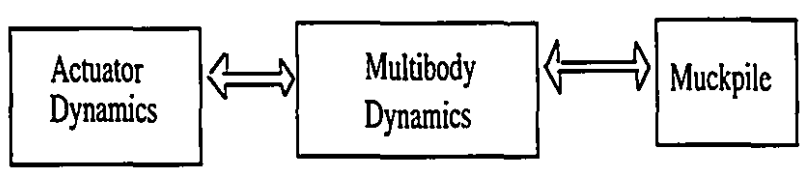

Figure 9.1: Simulation System Structure

Considering the three different parts, one can obtain the matrix representation form as follows:

$$\frac{d}{dt}\begin{pmatrix} x_1 \\ x_2 \\ x_3 \\ x_4 \\ x_5 \\ x_6 \\ x_7 \\ x_8 \\ x_9 \end{pmatrix} = \begin{pmatrix} 0 & 1 & 0 & 0 & 0 & 0 & 0 & 0 & 0 \\ 0 & -\frac{1}{\tau_2} & \frac{k_1}{b_1\tau_2} & 0 & 0 & 0 & 0 & 0 & 0 \\ 0 & -\frac{k_2}{R_{a1}\tau_1} & -\frac{1}{\tau_1} & 0 & 0 & 0 & 0 & 0 & 0 \\ 0 & 0 & 0 & 0 & 1 & 0 & 0 & 0 & 0 \\ 0 & 0 & 0 & 0 & -\frac{1}{\tau_4} & \frac{k_2}{b_2\tau_4} & 0 & 0 & 0 \\ 0 & 0 & 0 & 0 & -\frac{k_4}{R_{a2}\tau_3} & -\frac{1}{\tau_3} & 0 & 0 & 0 \\ 0 & 0 & 0 & 0 & 0 & 0 & 0 & 1 & 0 \\ 0 & 0 & 0 & 0 & 0 & 0 & 0 & -\frac{1}{\tau_6} & \frac{k_3}{b_3\tau_6} \\ 0 & 0 & 0 & 0 & 0 & 0 & 0 & -\frac{k_6}{R_{a3}\tau_5} & -\frac{1}{\tau_5} \end{pmatrix} \begin{pmatrix} x_1 \\ x_2 \\ x_3 \\ x_4 \\ x_5 \\ x_6 \\ x_7 \\ x_8 \\ x_9 \end{pmatrix}$$

$$+ \begin{pmatrix} 0 & 0 & 0 \\ 0 & 0 & 0 \\ \frac{1}{R_{a1}\tau_1} & 0 & 0 \\ 0 & 0 & 0 \\ 0 & 0 & 0 \\ 0 & \frac{1}{R_{a2}\tau_3} & 0 \\ 0 & 0 & 0 \\ 0 & 0 & 0 \\ 0 & 0 & \frac{1}{R_{a3}\tau_5} \end{pmatrix} \begin{pmatrix} v_1 \\ v_2 \\ v_3 \end{pmatrix} - \begin{pmatrix} 0 & 0 & 0 \\ \frac{r_1}{b_1\tau_2} & 0 & 0 \\ 0 & 0 & 0 \\ 0 & 0 & 0 \\ 0 & \frac{r_2}{b_2\tau_4} & 0 \\ 0 & 0 & 0 \\ 0 & 0 & 0 \\ 0 & 0 & \frac{r_3}{b_3\tau_6} \\ 0 & 0 & 0 \end{pmatrix} \begin{pmatrix} T_{d1} \\ T_{d2} \\ T_{d3} \end{pmatrix} \qquad (9.4)$$

The gearbox rates, r_1, r_2, and r_3 are brought into the system simulation. This is reflected in position and velocity outputs as well as disturbance inputs.

9.2 Continuous-Time Controller

The rotational velocities of all DC motors are controlled by analog electronic control circuits on shovel. In order to the purpose of simulation, one can design the controllers in terms of the electrical parameters of the three motors.

1. Analytical Model Controller

Recalling the parameters in Section 5.2, we have:

Swing Motor:

$$R_a = 0.41\ \Omega, \quad I = 24.22\ kg.m^2, \quad b = 226.31$$

$$k_1 = 2.383\ N.m/A, \quad k_2 = 0.27\ v.sec.$$

$$\tau_1 = 0.024\ sec., \quad \tau_2 = 0.107\ sec. \tag{9.5}$$

Hoist Motor:

$$R_a = 0.28\ \Omega, \quad I = 241.34\ kg.m^2, \quad b = 363.17$$

$$k_1 = 6.103\ N.m/A, \quad k_2 = 3.44\ v.sec.$$

$$\tau_1 = 0.036\ sec., \quad \tau_2 = 0.67\ sec. \tag{9.6}$$

Crowd Motor:

$$R_a = 0.32\ \Omega, \quad I = 26\ kg.m^2, \quad b = 337.12$$

$$k_1 = 5.726\ N.m/A, \quad k_2 = 0.68\ v.sec.$$

$$\tau_1 = 0.031\ sec., \quad \tau_2 = 0.077\ sec. \tag{9.7}$$

In order to design the controller, we change (5.10) and (5.11) into:

$$\dot{x_1} = -\frac{1}{\tau_2}x_1 + \frac{k_1}{b\tau_2}x_2 - \frac{r}{b\tau_2}T_d \tag{9.8}$$

$$\dot{x_2} = -\frac{k_2}{R_a\tau_1}x_1 - \frac{1}{\tau_1}x_2 + \frac{1}{R_a\tau_1}v \tag{9.9}$$

$$y = x_1 \tag{9.10}$$

The matrices are obtained by inspection of the above equations as:

$$A = \begin{pmatrix} -\frac{1}{\tau_2} & \frac{k_1}{\tau_2 b} \\ -\frac{k_2}{R_a\tau_1} & -\frac{1}{\tau_1} \end{pmatrix}, B = \begin{pmatrix} 0 \\ \frac{1}{R_a\tau_1} \end{pmatrix}, B_1 = \begin{pmatrix} -\frac{r}{\tau_2 b} \\ 0 \end{pmatrix} \tag{9.11}$$

$$C = \begin{pmatrix} 1 & 0 \end{pmatrix} \tag{9.12}$$

(1) Swing Motor Controller and Disturbance Compensation

Substituting the parameters from equation (9.5) into (9.11), we have

$$A = \begin{pmatrix} -9.35 & 0.098 \\ -27.44 & -41.67 \end{pmatrix}, B = \begin{pmatrix} 0 \\ 101.63 \end{pmatrix} \tag{9.13}$$

We define an additional state variable x_3 as

$$x_3 = \int_0^t (y - r)dt \tag{9.14}$$

i.e.,

$$\dot{x_3} = y - r = x_1 - r \tag{9.15}$$

The $\hat{A}$ and $\hat{B}$ matrices are

$$\hat{A} = \begin{pmatrix} -9.35 & 0.098 & 0 \\ -27.44 & -41.67 & 0 \\ 1 & 0 & 0 \end{pmatrix}, \hat{B} = \begin{pmatrix} 0 \\ 101.63 \\ 0 \end{pmatrix} \tag{9.16}$$

The controllability matrix is given by

$$Q = (\ \hat{B} \quad \hat{A}\hat{B} \quad \hat{A}^2\hat{B}\ ) = \begin{pmatrix} 0 & 9.9597 & -508.1456 \\ 101.63 & -4234.9221 & 176195.91 \\ 0 & 0 & 9.9597 \end{pmatrix} \tag{9.17}$$

The determinant of Q is nonzero. Its rank therefore is 3, and the pair $(\hat{A}, \hat{B})$ is controllable. The characteristic equation of the closed-loop system is given by

$$|sI - \hat{A} + \hat{B}k| = \begin{vmatrix} s + 9.35 & -0.098 & 0 \\ 27.44 + 101.63k_{11} & s + 41.67 + 101.63k_{12} & 101.63k_{13} \\ -1 & 0 & s \end{vmatrix}$$

$$= s^3 + (51.6297 + 101.63k_{12})s^2 + (392.3036 + 950.2405k_{12} + 9.9594k_{11})s + 9.9597k_{13} \tag{9.18}$$

The desired characteristic equation is

$$s^3 + 87.5s^2 + 5374.5s + 124969 = 0 \tag{9.19}$$

Matching equations (9.18) and (9.19), we obtain

$$k_{11} = 466.58, \quad k_{12} = 0.3529, \quad k_{13} = 12547.466 \tag{9.20}$$

In the first part of the equation (9.4), the disturbance compensation has the following form

$$\begin{pmatrix} \dot{x}_1 \\ \dot{x}_2 \\ \dot{x}_3 \end{pmatrix} = \begin{pmatrix} 0 & 1 & 0 \\ 0 & -9.35 & 0.098 \\ 0 & -27.44 & -41.69 \end{pmatrix} \begin{pmatrix} x_1 \\ x_2 \\ x_3 \end{pmatrix} + \begin{pmatrix} 0 \\ 0 \\ 101.63 \end{pmatrix} v_1 + \begin{pmatrix} 0 \\ -0.0413r_1 \\ 0 \end{pmatrix} T_{d1} \tag{9.21}$$

In the condition of steady-state, we have $\dot{x}_1 = 0, \dot{x}_2 = 0$, and $\dot{x}_3 = 0$. Therefore,

$$\begin{aligned} -9.35x_2^* + 0.098x_3^* - 0.0413r_1T_{d1}^* &= 0 \\ -27.44x_2^* - 41.69x_3^* + 101.63v_1^* &= 0 \end{aligned} \tag{9.22}$$

Solving the above equations, we have

$$v_1^* = 39.4077x_2^* + 0.1729r_1T_{d1}^* \tag{9.23}$$

By the state feedback law, $\Delta v = -K\Delta \mathbf{x}$, we have

$$v_1 = 39.4077x_2^* + 0.1729r_1T_{d1}^* - 0.3529x_3 + (466.58 + \frac{12547.466}{s})(x_2^* - x_2) \tag{9.24}$$

(2) Hoist Motor Controller and Disturbance Compensation

The $\hat{A}$ and $\hat{B}$ matrices are

$$\hat{A} = \begin{pmatrix} -1.49 & 0.025 & 0 \\ -341.27 & -27.78 & 0 \\ 1 & 0 & 0 \end{pmatrix}, \hat{B} = \begin{pmatrix} 0 \\ 99.2 \\ 0 \end{pmatrix} \tag{9.25}$$

The controllability matrix is given by

$$Q = (\hat{B} \quad \hat{A}\hat{B} \quad \hat{A}^2\hat{B}) = \begin{pmatrix} 0 & 2.48 & -72.5896 \\ 99.2 & -2755.776 & 75709.108 \\ 0 & 0 & 2.48 \end{pmatrix} \tag{9.26}$$

The determinant of Q is nonzero. Its rank therefore is 3, and the pair $(\hat{A}, \hat{B})$ is controllable. The characteristic equation of the closed-loop system is given by

$$|sI - \hat{A} + \hat{B}k| = \begin{vmatrix} s + 1.49 & -0.025 & 0 \\ 341.27 + 99.2k_{14} & s + 27.78 + 99.2k_{15} & 99.2k_{16} \\ -1 & 0 & s \end{vmatrix}$$

$$= s^3 + (29.27 + 99.2k_{15})s^2 + (49.924 + 147.808k_{15} + 2.48k_{14})s + 2.48k_{16} \quad (9.27)$$

Matching equations (9.27) and (9.19), we obtain

$$k_{14} = 2112.0213, \quad k_{15} = 0.587, \quad k_{16} = 50390.726 \quad (9.28)$$

In the second part of the equation (9.4), the disturbance compensation has the following form

$$\begin{pmatrix} \dot{x}_4 \\ \dot{x}_5 \\ \dot{x}_6 \end{pmatrix} = \begin{pmatrix} 0 & 1 & 0 \\ 0 & -1.49 & 0.025 \\ 0 & -341.27 & -27.78 \end{pmatrix} \begin{pmatrix} x_4 \\ x_5 \\ x_6 \end{pmatrix} + \begin{pmatrix} 0 \\ 0 \\ 99.2 \end{pmatrix} v_2 + \begin{pmatrix} 0 \\ -0.0041r_2 \\ 0 \end{pmatrix} T_{d2} \quad (9.29)$$

In the condition of steady-state, we have $\dot{x}_4 = 0, \dot{x}_5 = 0$, and $\dot{x}_6 = 0$. Therefore,

$$\begin{aligned} -1.49x_5^* + 0.025x_6^* - 0.0041r_2T_{d2}^* &= 0 \\ -341.27x_5^* - 27.78x_6^* + 99.2V_2^* &= 0 \end{aligned} \quad (9.30)$$

Solving the above equations, we have

$$v_2^* = 20.1921x_5^* + 0.046r_2T_{d2}^* \quad (9.31)$$

By the state feedback law, $\Delta v = -K\Delta \mathbf{x}$, we have

$$v_2 = 20.1921x_5^* + 0.046r_2T_{d2}^* - 0.587x_6 + (2112.0213 + \frac{50390.726}{s})(x_5^* - x_5) \quad (9.32)$$

(3) Crowd Motor Controller and Disturbance Compensation

The $\hat{A}$ and $\hat{B}$ matrices are

$$\hat{A} = \begin{pmatrix} -12.99 & 0.22 & 0 \\ -68.55 & -32.26 & 0 \\ 1 & 0 & 0 \end{pmatrix}, \hat{B} = \begin{pmatrix} 0 \\ 100.81 \\ 0 \end{pmatrix} \tag{9.33}$$

The controllability matrix is given by

$$Q = (\hat{B} \quad \hat{A}\hat{B} \quad \hat{A}^2\hat{B}) = \begin{pmatrix} 0 & 22.1782 & -1003.5634 \\ 100.81 & -3252.13 & 103393.4 \\ 0 & 0 & 22.1782 \end{pmatrix} \tag{9.34}$$

The determinant of Q is nonzero. Its rank therefore is 3, and the pair $(\hat{A}, \hat{B})$ is controllable. The characteristic equation of the closed-loop system is given by

$$|sI - \hat{A} + \hat{B}k| = \begin{vmatrix} s + 12.99 & -0.22 & 0 \\ 68.55 + 100.81k_{17}s & s + 32.26 + 100.81k_{18} & 100.81k_{19} \\ -1 & 0 & s \end{vmatrix}$$

$$= s^3 + (45.25 + 100.81k_{18})s^2 + (434.1384 + 1309.5219k_{18} + 22.1782k_{17})s + 22.1782k_{19} \tag{9.35}$$

Matching equations (9.35) and (9.19), we obtain

$$k_{17} = 198.0116, \quad k_{18} = 0.4191, \quad k_{19} = 5634.7675 \tag{9.36}$$

In the third part of the equation (9.4), the disturbance compensation has the following form

$$\begin{pmatrix} \dot{x}_7 \\ \dot{x}_8 \\ \dot{x}_9 \end{pmatrix} = \begin{pmatrix} 0 & 1 & 0 \\ 0 & -12.99 & 0.22 \\ 0 & -68.55 & -32.26 \end{pmatrix} \begin{pmatrix} x_7 \\ x_8 \\ x_9 \end{pmatrix} + \begin{pmatrix} 0 \\ 0 \\ 100.81 \end{pmatrix} v_3 + \begin{pmatrix} 0 \\ -0.038r_3 \\ 0 \end{pmatrix} T_{d3} \tag{9.37}$$

In the condition of steady-state, we have $\dot{x}_7 = 0$,$\dot{x}_8 = 0$,and $\dot{x}_9 = 0$. Therefore,

$$\begin{aligned} -12.99x_8^* + 0.22x_9^* - 0.038r_3T_{d3}^* = 0 \\ -68.55x_8^* - 32.26x_9^* + 100.81v_3^* = 0 \end{aligned} \tag{9.38}$$

Solving the above equation, we have

$$v_3^* = 19.5745x_8^* + 0.0553r_3T_{d3}^* \tag{9.39}$$

By the state feedback law, $\Delta c = -K\Delta \mathbf{x}$, we have

$$c_3 = 19.5745x_8^* + 0.0553r_3T_{d3}^* - 0.4191x_9 + (198.0116 + \frac{5634.7675}{s})(x_8^* - x_8) \quad (9.40)$$

2. Empirical Model Controller

Recalling the parameters in Section 7.4, we have:

Swing Motor:

$$R_a = 2.6242\ \ \Omega, \quad I = 24.22\ \ kg.m^2, \quad b = 346$$

$$k_1 = 106.73\ \ N.m/A, \quad k_2 = 2.725\ \ v.sec$$

$$\tau_1 = 0.0319\ \ sec., \quad \tau_2 = 0.07\ \ sec. \quad (9.41)$$

Hoist Motor:

$$R_a = 0.36\ \ \Omega, \quad I = 241.34\ \ kg.m^2, \quad b = 870.32$$

$$k_1 = 75.829\ \ N.m/A, \quad k_2 = 4.6997\ \ v.sec.$$

$$\tau_1 = 0.2454\ \ sec., \quad \tau_2 = 0.2773\ \ sec. \quad (9.42)$$

Crowd Motor:

$$R_a = 1.2925\ \ \Omega, \quad I = 26\ \ kg.m^2, \quad b = 313.25$$

$$k_1 = 70.577\ \ N.m/A, \quad k_2 = 0.984\ \ v.sec.$$

$$\tau_1 = 0.025\ \ sec., \quad \tau_2 = 0.083\ \ sec. \quad (9.43)$$

The matrices are obtained by inspection of the above equations as

$$A = \begin{pmatrix} -\frac{1}{\tau_2} & \frac{k_1}{\tau_2 b} \\ -\frac{k_2}{R_a\tau_1} & -\frac{1}{\tau_1} \end{pmatrix}, B = \begin{pmatrix} 0 \\ \frac{1}{R_a\tau_1} \end{pmatrix}, B_1 = \begin{pmatrix} -\frac{r}{\tau_2 b} \\ 0 \end{pmatrix} \quad (9.44)$$

$$C = (1 \quad 0) \quad (9.45)$$

(1) Swing Motor Controller and Disturbance Compensation

Substituting the empirical parameters from (9.41) into the equation (9.44), we have

$$A = \begin{pmatrix} -14.2542 & 6.6362 \\ -32.5403 & -31.3358 \end{pmatrix}, B = \begin{pmatrix} 0 \\ 11.941 \end{pmatrix} \tag{9.46}$$

We define an additional state variable x_3 as

$$x_3 = \int_0^t (y - r)dt \tag{9.47}$$

i.e.

$$\dot{x_3} = y - r = x_1 - r \tag{9.48}$$

The $\hat{A}$ and $\hat{B}$ matrices are

$$\hat{A} = \begin{pmatrix} -14.2542 & 6.6362 & 0 \\ -32.5403 & -31.3358 & 0 \\ 1 & 0 & 0 \end{pmatrix}, \hat{B} = \begin{pmatrix} 0 \\ 11.941 \\ 0 \end{pmatrix} \tag{9.49}$$

The controllability matrix is given by

$$Q = (\hat{B} \quad \hat{A}\hat{B} \quad \hat{A}^2\hat{B}) = \begin{pmatrix} 0 & 79.2429 & -3612.6775 \\ 11.941 & -374.18 & 9146.6419 \\ 0 & 0 & 79.2429 \end{pmatrix} \tag{9.50}$$

The determinant of Q is nonzero. Its rank therefore is 3, and the pair $(\hat{A}, \hat{B})$ is controllable. The characteristic equation of the closed-loop system is given by

$$|sI - \hat{A} + \hat{B}k| = \begin{vmatrix} s + 14.2542 & -6.6362 & 0 \\ 32.5403 + 11.941k_{21} & s + 31.3358 + 11.941k_{22} & 11.941k_{23} \\ -1 & 0 & s \end{vmatrix}$$

$$= s^3 + (45.59 + 11.941k_{22})s^2 + (662.6139 + 170.2094k_{22} + 79.2429k_{21})s + 79.2429k_{23} \tag{9.51}$$

The desired characteristic equation is

$$s^3 + 87.5s^2 + 5374.5s + 124969 = 0 \tag{9.52}$$

Matching equations (9.51) and (9.52), we obtain

$$k_{21} = 51.9224, \quad k_{22} = 3.5098, \quad k_{23} = 1577.0372 \tag{9.53}$$

In the first part of the equation (9.4) the disturbance compensation has the following form

$$\begin{pmatrix} \dot{x_1} \\ \dot{x_2} \\ \dot{x_3} \end{pmatrix} = \begin{pmatrix} 0 & 1 & 0 \\ 0 & -14.2542 & 6.6362 \\ 0 & -32.54 & -31.336 \end{pmatrix} \begin{pmatrix} x_1 \\ x_2 \\ x_3 \end{pmatrix} + \begin{pmatrix} 0 \\ 0 \\ 11.94 \end{pmatrix} v_1 - \begin{pmatrix} 0 \\ 0.24r_1 \\ 0 \end{pmatrix} T_{d1} \tag{9.54}$$

In the condition of steady-state, we have $\dot{x_1} = 0, \dot{x_2} = 0$,and $\dot{x_3} = 0$. Therefore,

$$\begin{aligned} -14.2542x_2^* + 6.6362x_3^* - 0.237r_1T_{d1}^* &= 0 \\ -32.5403x_2^* - 31.3358x_3^* + 11.941x_1^* &= 0 \end{aligned} \tag{9.55}$$

Solving the above equations, we have

$$v_1^* = 8.3631x_2^* + 0.0937r_1T_{d1}^* \tag{9.56}$$

By the state feedback law, $\Delta v = -K\Delta \mathbf{x}$, we have

$$v_1 = 8.3631x_2^* + 0.0937r_1T_{d1}^* - 3.5098x_3 + (51.9224 + \frac{1577.0372}{s})(x_2^* - x_2) \tag{9.57}$$

(2) Hoist Motor Controller and Disturbance Compensation

Substituting the empirical parameters (9.42), into the equation (9.44), we have

$$A = \begin{pmatrix} -3.6061 & 0.3142 \\ -53.0812 & -4.0743 \end{pmatrix}, B = \begin{pmatrix} 0 \\ 11.2947 \end{pmatrix} \tag{9.58}$$

The $\hat{A}$ and $\hat{B}$ matrices are

$$\hat{A} = \begin{pmatrix} -3.6061 & 0.3142 & 0 \\ -53.0812 & -4.0743 & 0 \\ 1 & 0 & 0 \end{pmatrix}, \hat{B} = \begin{pmatrix} 0 \\ 11.2947 \\ 0 \end{pmatrix} \tag{9.59}$$

The controllability matrix is given by

$$Q = (\hat{B} \quad \hat{A}\hat{B} \quad \hat{A}^2\hat{B}) = \begin{pmatrix} 0 & 3.5488 & -27.2562 \\ 11.2947 & -46.018 & -0.8835 \\ 0 & 0 & 3.5488 \end{pmatrix} \tag{9.60}$$

The determinant of Q is nonzero. Its rank therefore is 3, and the pair $(\hat{A}, \hat{B})$ is controllable. The characteristic equation of the closed-loop system is given by

$$|sI - \hat{A} + \hat{B}k| = \begin{vmatrix} s + 3.6061 & -0.3142 & 0 \\ 53.0812 + 11.2947k_{24} & s + 4.0743 + 11.2947k_{25} & 11.2947k_{26} \\ -1 & 0 & s \end{vmatrix}$$

$$= s^3 + (7.6804 + 11.2947k_{25})s^2 + (31.3704 + 40.7298k_{25} + 3.5488k_{24})s + 3.5488k_{26} \tag{9.61}$$

Matching equations (9.61) and (9.52), we obtain

$$k_{24} = 1416.9, \quad k_{25} = 7.067, \quad k_{26} = 35214.44 \tag{9.62}$$

In the second part of equation (9.4), the disturbance compensation has the following form

$$\begin{pmatrix} \dot{x}_4 \\ \dot{x}_5 \\ \dot{x}_6 \end{pmatrix} = \begin{pmatrix} 0 & 1 & 0 \\ 0 & -3.6061 & 0.3142 \\ 0 & -53.0812 & -4.074 \end{pmatrix} \begin{pmatrix} x_4 \\ x_5 \\ x_6 \end{pmatrix} + \begin{pmatrix} 0 \\ 0 \\ 11.295 \end{pmatrix} v_2 - \begin{pmatrix} 0 \\ 0.026r_2 \\ 0 \end{pmatrix} T_{d2} \tag{9.63}$$

In the condition of steady-state, we have $\dot{x}_4 = 0, \dot{x}_5 = 0$, and $\dot{x}_6 = 0$. Therefore,

$$\begin{aligned} -3.6061x_5^* + 0.3142x_6^* - 0.0256r_2T_{d2}^* &= 0 \\ -53.0812x_5^* - 4.0743x_6^* + 11.2947v_2^* &= 0 \end{aligned} \tag{9.64}$$

Solving the above equations, we have

$$v_2^* = 8.84x_5^* + 0.0294r_2T_{d2}^* \tag{9.65}$$

By the state feedback law, $\Delta v = -K\Delta \mathbf{x}$, we have

$$v_2 = 8.84x_5^* + 0.0294r_2T_{d2}^* - 7.067x_6 + (1416.9 + \frac{35214.44}{s})(x_5^* - x_5) \qquad (9.66)$$

(3) Crowd Motor Controller and Disturbance Compensation

Substituting parameters in equation (9.43) into (9.44), we have

$$\hat{A} = \begin{pmatrix} -11.9917 & 2.7145 & 0 \\ -30.4554 & -40.6672 & 0 \\ 1 & 0 & 0 \end{pmatrix}, \hat{B} = \begin{pmatrix} 0 \\ 30.9475 \\ 0 \end{pmatrix} \qquad (9.67)$$

The controllability matrix is given by

$$Q = (\ \hat{B} \quad \hat{A}\hat{B} \quad \hat{A}^2\hat{B}\ ) = \begin{pmatrix} 0 & 84.007 & -4423.72 \\ 30.9475 & -1258.55 & 48623.24 \\ 0 & 0 & 84.007 \end{pmatrix} \qquad (9.68)$$

The determinant of Q is nonzero. Its rank therefore is 3, and the pair $(\hat{A}, \hat{B})$ is controllable. The characteristic equation of the closed-loop system is given by

$$|sI - \hat{A} + \hat{B}k| = \begin{vmatrix} s + 11.9917 & -2.7145 & 0 \\ 30.4554 + 30.9475k_{27} & s + 40.6672 + 30.9475k_{28} & 30.9475k_{29} \\ -1 & 0 & s \end{vmatrix}$$

$$= s^3 + (52.6589 + 30.9475k_{28})s^2 + (570.34 + 371.1131k_{28} + 84.01k_{27})s + 84.01k_{29} \quad (9.69)$$

Matching equations (9.69) and (9.52), we obtain

$$k_{27} = 52.2124, \quad k_{28} = 1.1258, \quad k_{29} = 1487.5491 \qquad (9.70)$$

In the third part of the equation (9.4), the disturbance compensation has the following form

$$\begin{pmatrix} \dot{x}_7 \\ \dot{x}_8 \\ \dot{x}_9 \end{pmatrix} = \begin{pmatrix} 0 & 1 & 0 \\ 0 & -11.9917 & 2.7145 \\ 0 & -30.4554 & -40.67 \end{pmatrix} \begin{pmatrix} x_7 \\ x_8 \\ x_9 \end{pmatrix} + \begin{pmatrix} 0 \\ 0 \\ 30.95 \end{pmatrix} v_3 - \begin{pmatrix} 0 \\ 0.08r_1 \\ 0 \end{pmatrix} T_{d3} \quad (9.71)$$

In the condition of steady-state, we have $\dot{x}_7 = 0, \dot{x}_8 = 0$, and $\dot{x}_9 = 0$. Therefore,

$$\begin{aligned} -11.9917x_8^* + 2.7145x_9^* - 0.08r_3T_{d3}^* &= 0 \\ -30.4554x_8^* - 40.6672x_9^* + 30.9475v_3^* &= 0 \end{aligned} \tag{9.72}$$

Solving the above equations, we have

$$v_3^* = 6.7893x_8^* + 0.0387r_3T_{d3}^* \tag{9.73}$$

By the state feedback law, $\Delta v = -K\Delta \mathbf{x}$, we have

$$v_3 = 6.7893x_8^* + 0.0387r_3T_{d3}^* - 1.1258x_9 + (52.2124 + \frac{1487.5491}{s})(x_8^* - x_8) \tag{9.74}$$

9.3 Saturation

Due to the motor and power amplifier characteristics, the input current and generated torque cannot surpass certain values. Saturation functions on both these variables are used to replicate this behavior in the simulation. The limits on the input current and generated torque effectively limit the maximum velocity and acceleration of the motor.

9.4 Filter

The simulated trajectories of three DC motors had similar shapes to the actual trajectories, but the armature voltages and currents included a lot of high-frequency disturbance. In order to solve these problems, At first, we used FFT technique to check the frequency ranges of the actual voltages and currents. Then, according to the ranges, we designed the low-pass filters. Finally, we used the filters in our simulator for improving the output curves of the armature voltages and currents.

9.5 Disturbance

The disturbances to the actuators primarily arise from two sources: the rigid body cross coupling between components of the shovel itself and the interaction between bucket and muckpile during the course of digging and loading. For the first source, we can use formulae (4.53), (4.56), and (4.62) to represent the disturbance. For the second source, the disturbance is already included in τ_1, τ_3, and τ_4, identified as f_{51} and f_{53} in formulae (6.45) and (6.46).

9.6 Analytical Model Simulation

All three parts of the shovel simulator are integrated in a single simulation file which is shown at its most superficial level in Figure 1 in Appendix. The complexity of the overall software simulator is illustrated by examining the subroutine blocks which are shown in Appendix. Figure 9.2 and Figure 9.3 show the rotational angles and voltages of swing motor. Figure 9.4, Figure 9.5, and Figure 9.6 show the rope positions, voltages, and currents of hoist motor. Figure 9.7, Figure 9.8, and Figure 9.9 show the arm extensions, voltages, and currents of crwod motor. From these figures, we can see the actual and simulated curves of trajectories and voltages have very similar shapes; the basic shapes of the currents are also similar.

9.7 Empirical Model Simulation of Easy Digging

The empirical model simulation of easy digging has the same block diagram as the analytical model simulation except that the motor parameters are different. Figure 9.10 and Figure 9.11 show the rotational angles and voltages of swing motor. Figure 9.12, Figure 9.13, and Figure 9.14 show the rope positions, voltages, and currents of hoist motor. Figure 9.15, Figure 9.16, and Figure 9.17 show the arm extensions, voltages, and currents of crwod motor. From these figures, we can see the actual and simulated curves of both trajectories and voltages have very similar shapes; the basic shapes

of the currents are also similar. In actual application, we prefer to use the empirical model , due to that it better represents the actual situation.

9.8 Empirical Model Simulation of Hard Digging

The empirical model simulation of hard digging has same block diagram as that of easy digging except the system has different input data. Figure 9.18 and Figure 9.19 show the rotational angles and voltages of swing motor. Figure 9.20 , Figure 9.21, and Figure 9.22 show the rope positions, voltages and currents of hoist motor. Figure 9.23, Figure 9.24, and Figure 9.25 show the arm extensions, voltages, and currents of crowd motor. From these figures, we can see the actual and simulated curves of both trajectories and voltages have very similar shapes; the actual and simulated curves of currents have some differences, but the basic shapes are similar.

In general, from all simulations in above three sections, we can find that the trajectories are well simulated; the voltages are a little bit worse simulated; and the currents are worse simulated, because the actual trajectories have a little high frequency noise; the actual voltages have more high frequency noise; the actual currents have the most high frequency noise (in our simulators doesn't exist in this kind of high frequency noise).

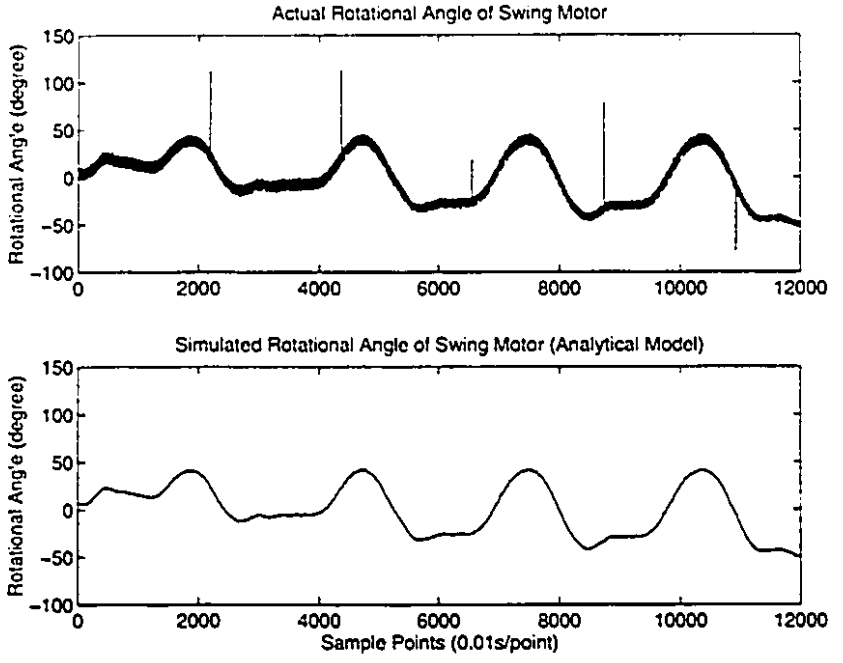

Figure 9.2: Actual and Simulated Rotational Angles of Swing Motor

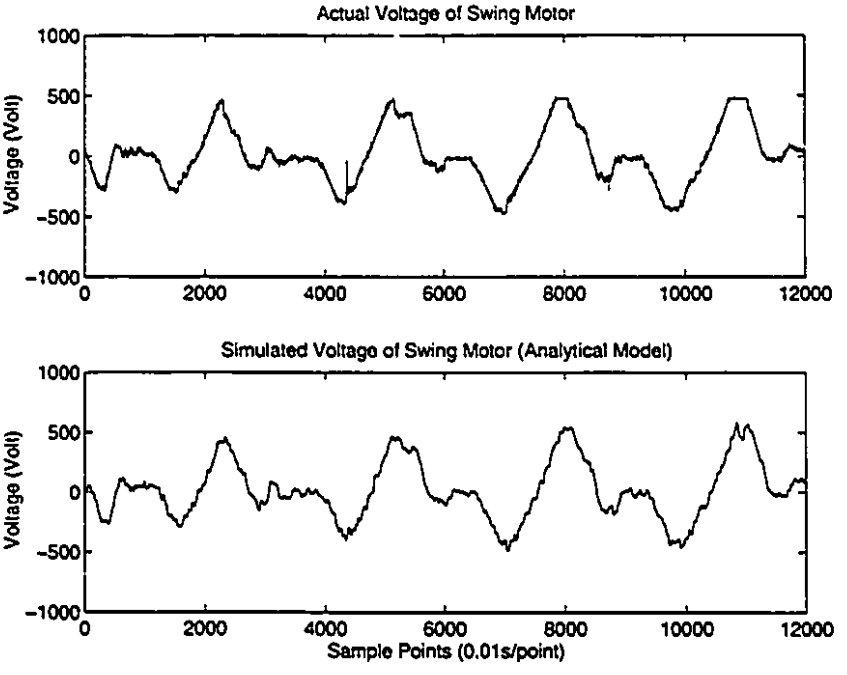

Figure 9.3: Actual and Simulated Voltages of Swing Motor

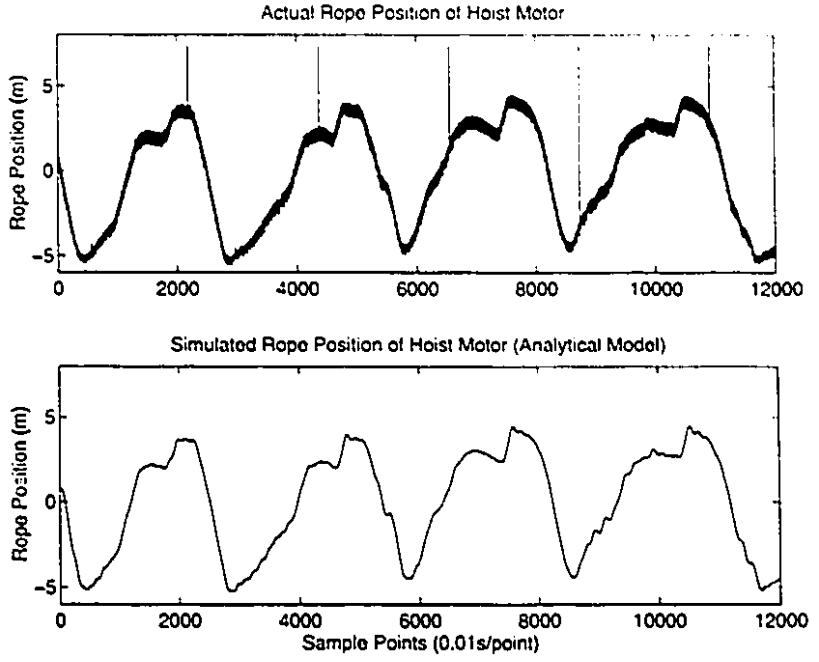

Figure 9.4: Actual and Simulated Rope Positions of Hoist Motor

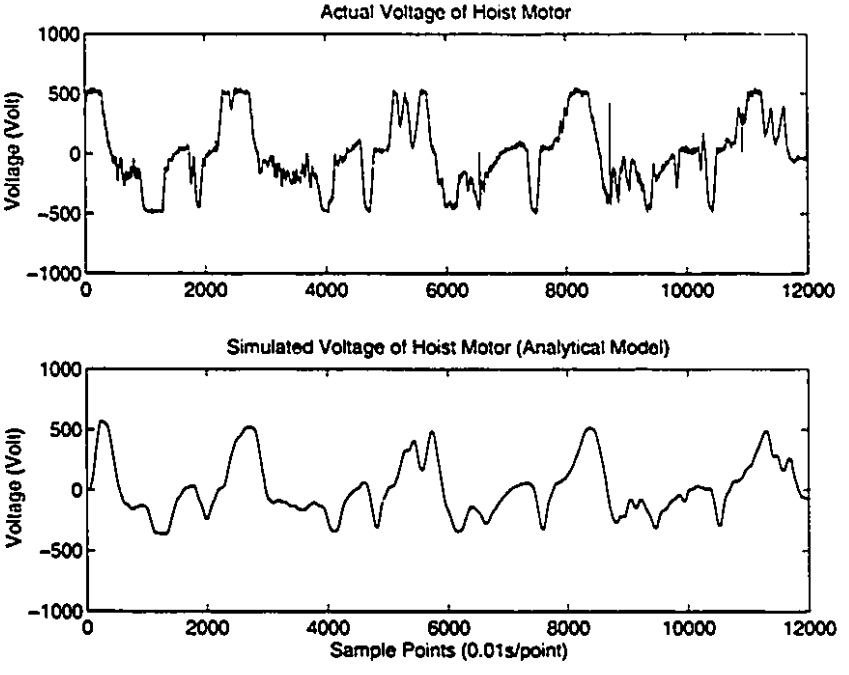

Figure 9.5: Actual and Simulated Voltages of Hoist Motor

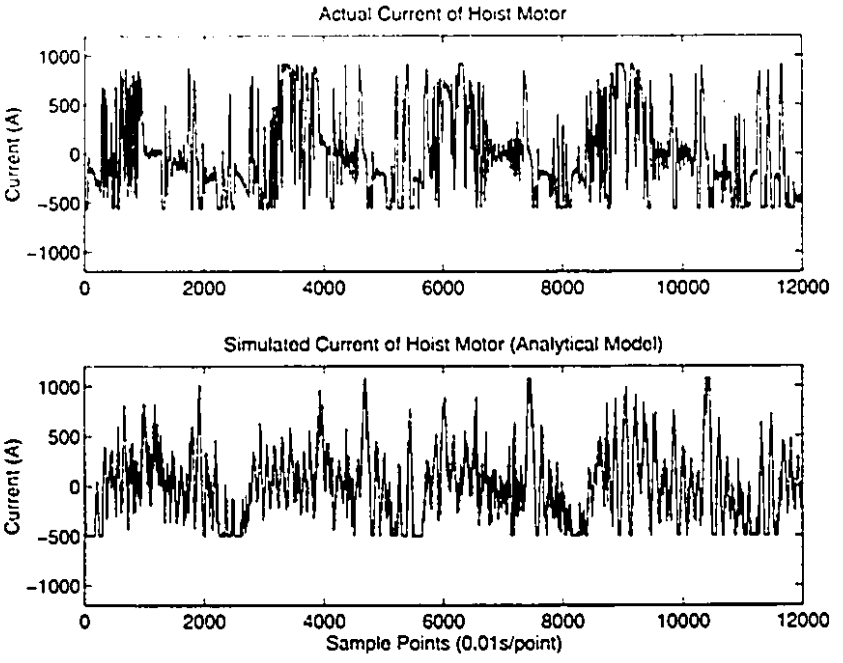

Figure 9.6: Actual and Simulated Currents of Hoist Motor

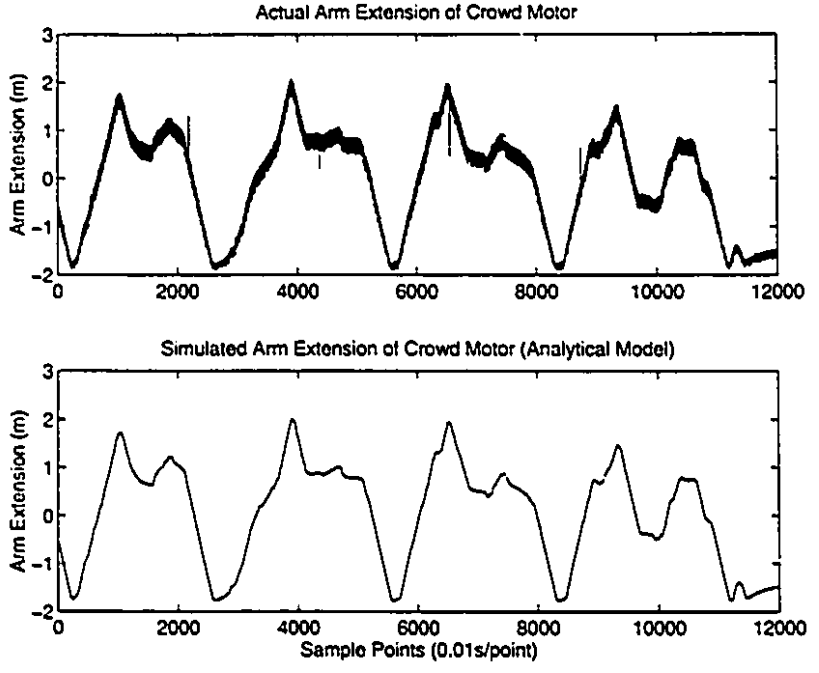

Figure 9.7: Actual and Simulated Arm Extensions of Crowd Motor

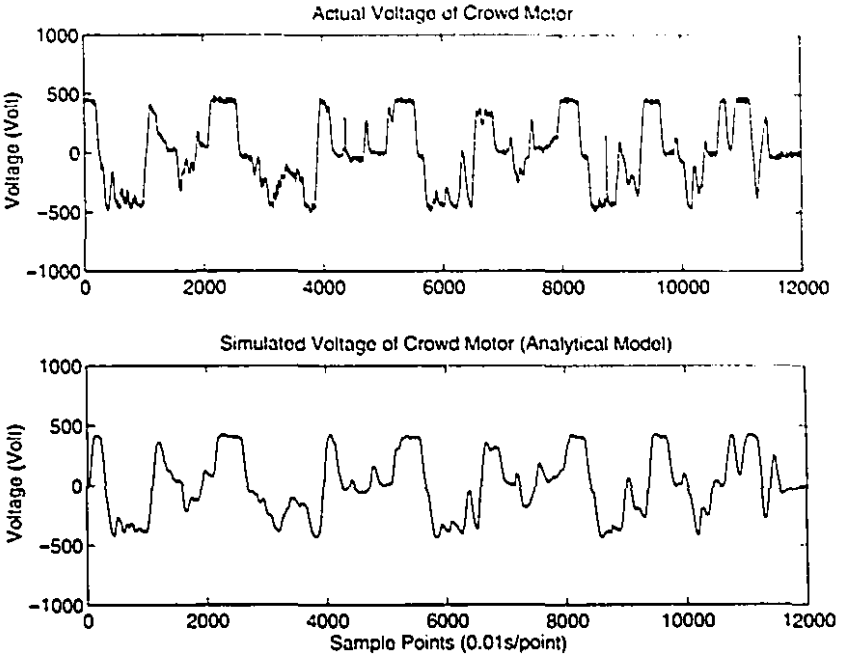

Figure 9.8: Actual and Simulated Voltages of Crowd Motor

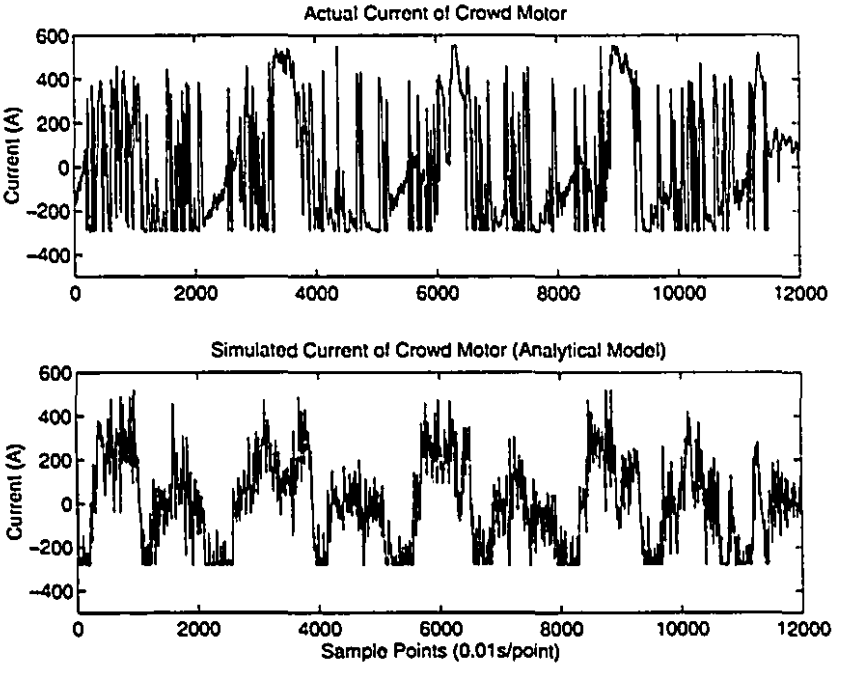

Figure 9.9: Actual and Simulated Currents of Crowd Motor

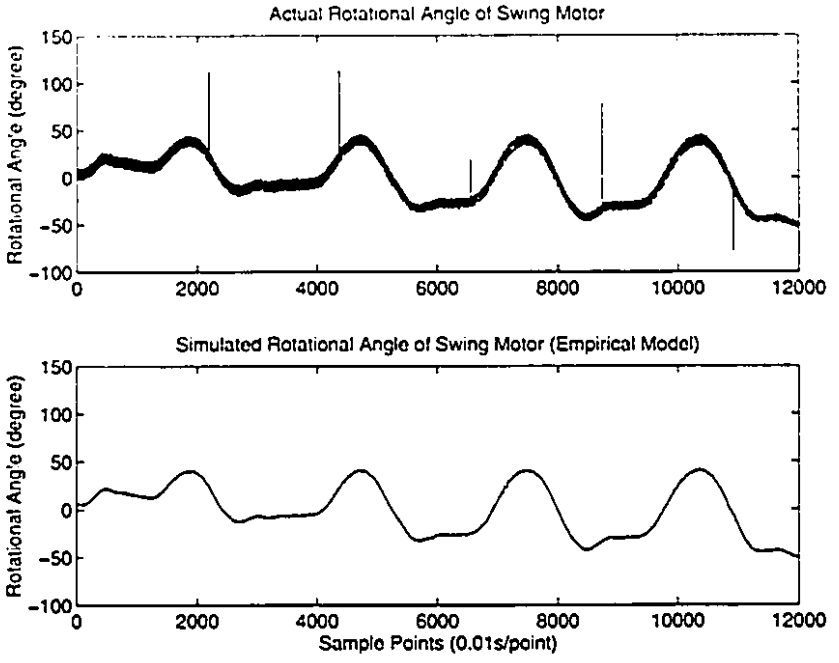

Figure 9.10: Actual and Simulated Rotational Angles of Swing Motor (Easy Digging)

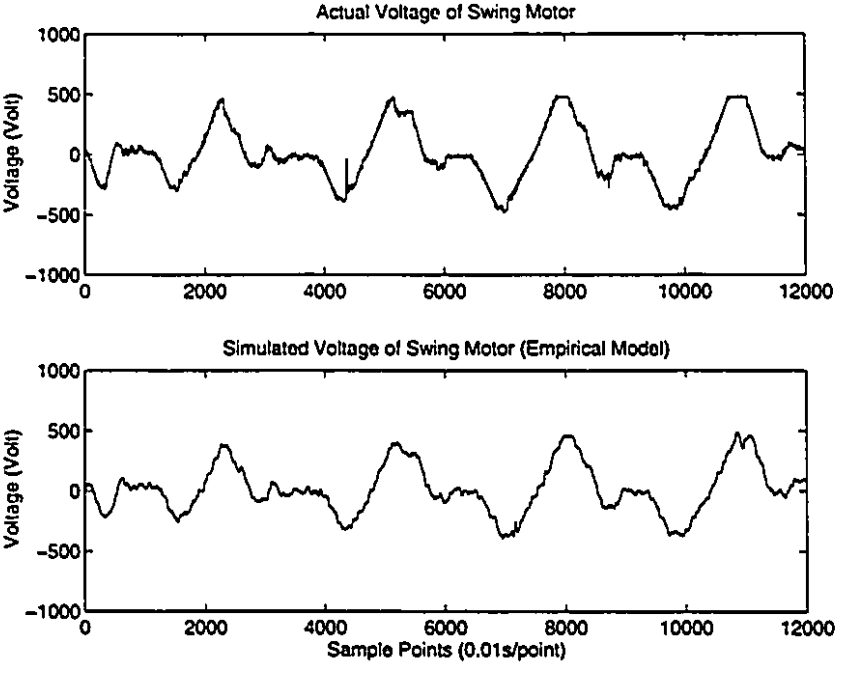

Figure 9.11: Actual and Simulated Voltages of Swing Motor (Easy Digging)

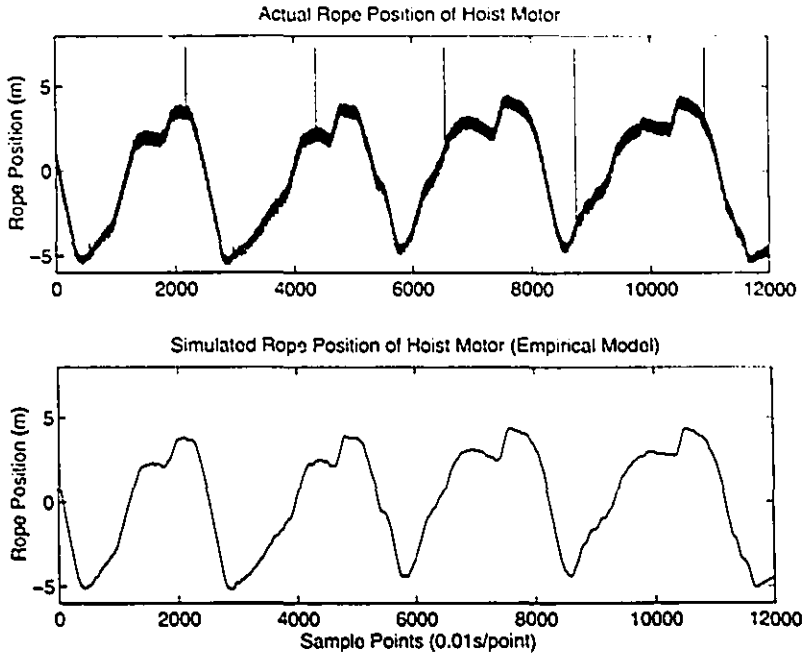

Figure 9.12: Actual and Simulated Rope Positions of Hoist Motor (Easy Digging)

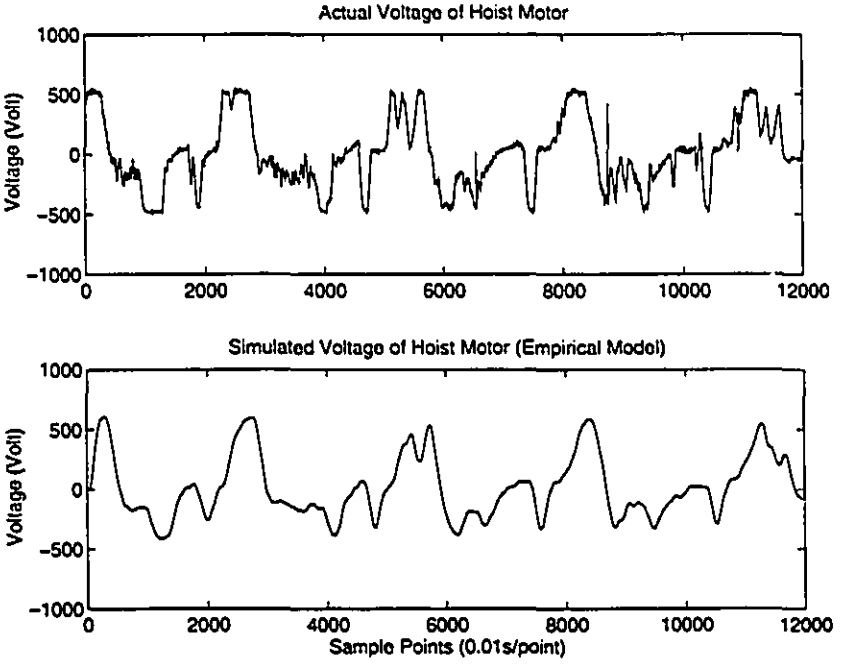

Figure 9.13: Actual and Simulated Voltages of Hoist Motor (Easy Digging)

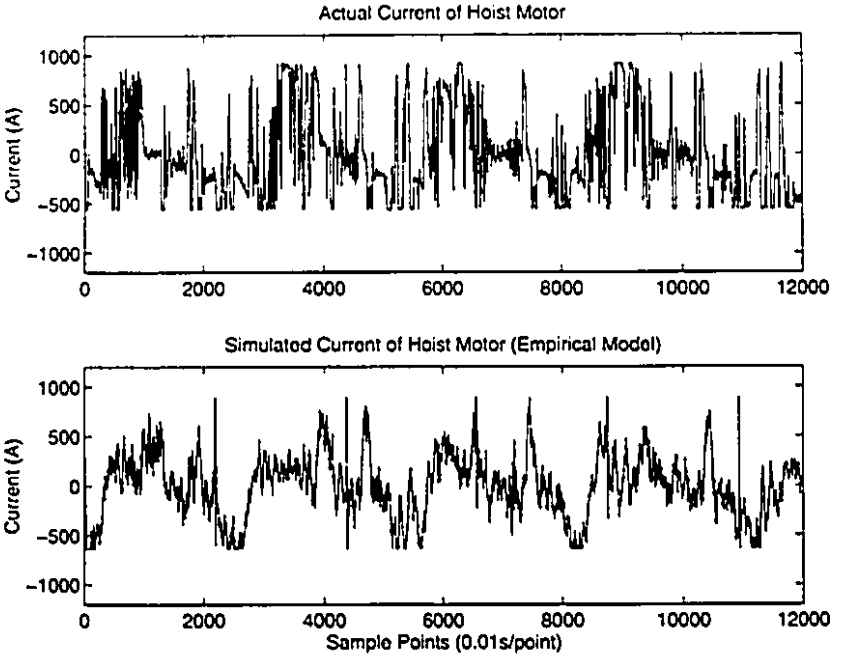

Figure 9.14: Actual and Simulated Currents of Hoist Motor (Easy Digging)

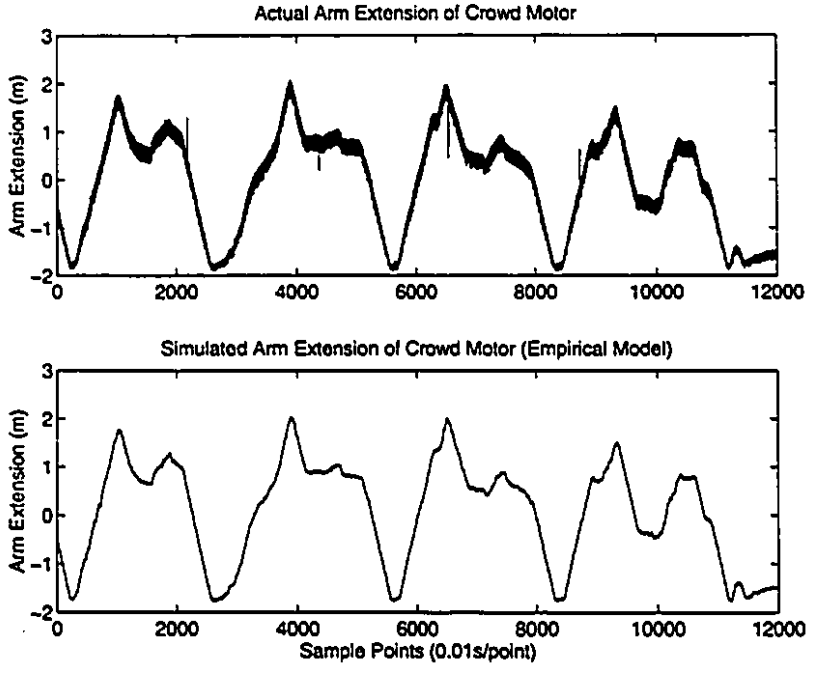

Figure 9.15: Actual and Simulated Arm Extensions of Crowd Motor (Easy Digging)

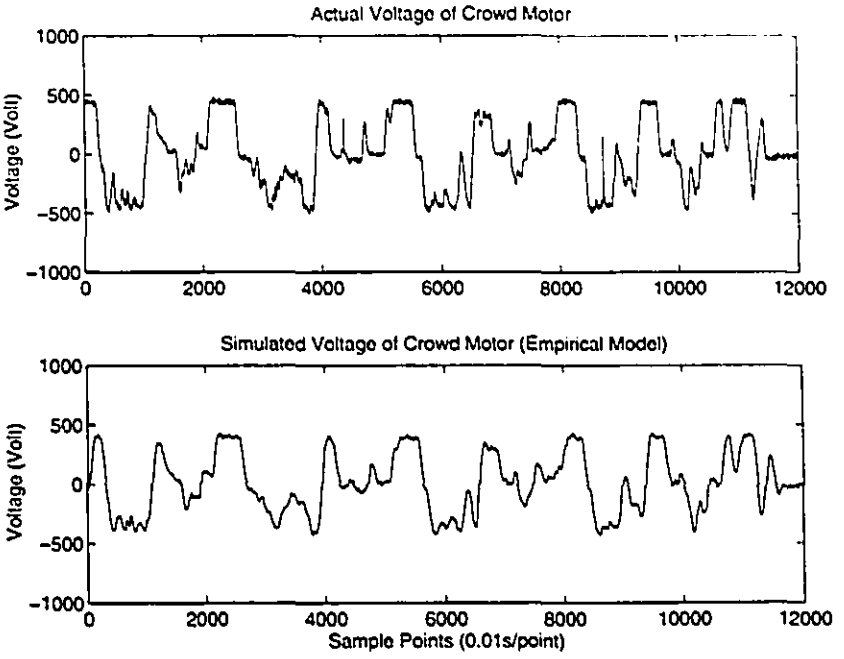

Figure 9.16: Actual and Simulated Voltages of Crowd Motor (Easy Digging)

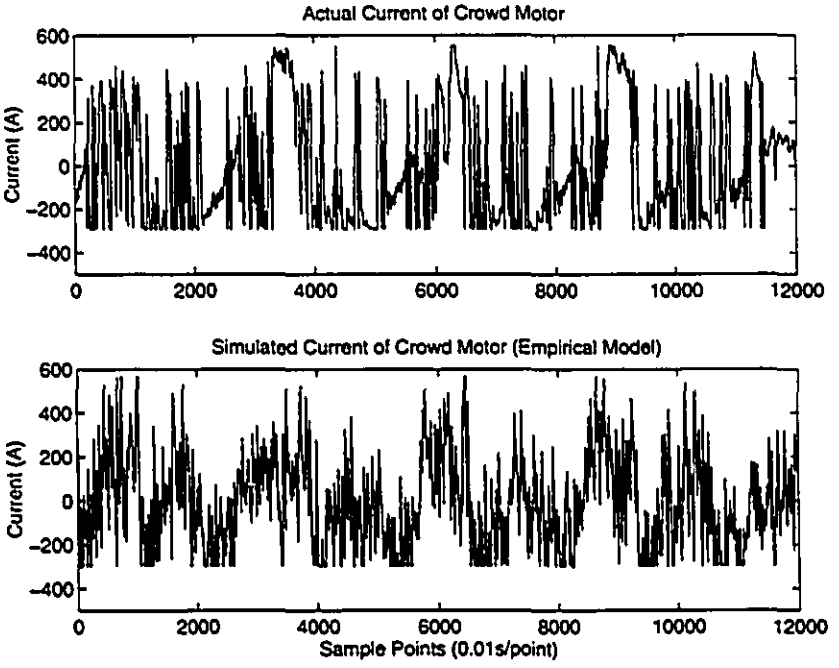

Figure 9.17: Actual and Simulated Currents of Crowd Motor (Easy Digging)

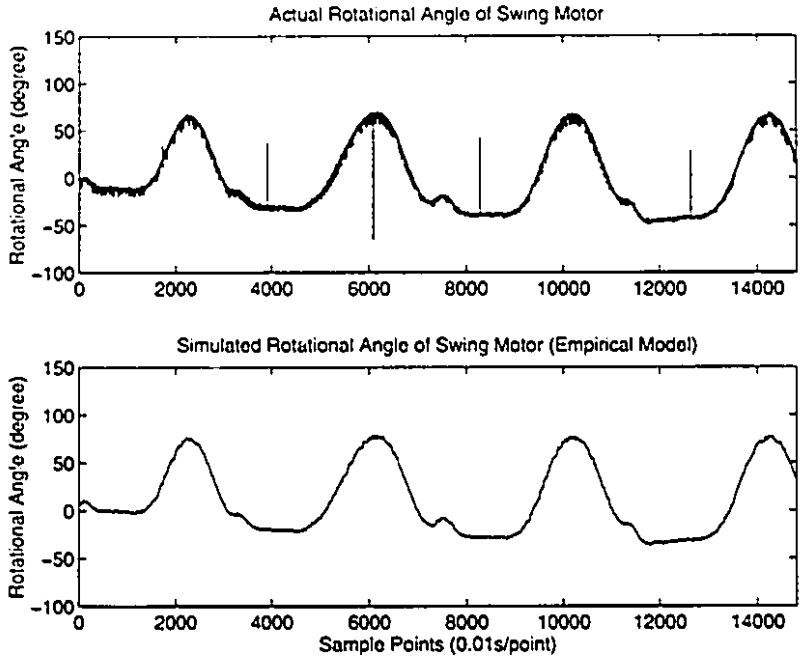

Figure 9.18: Actual and Simulated Rotational Angles of Swing Motor (Hard Digging)

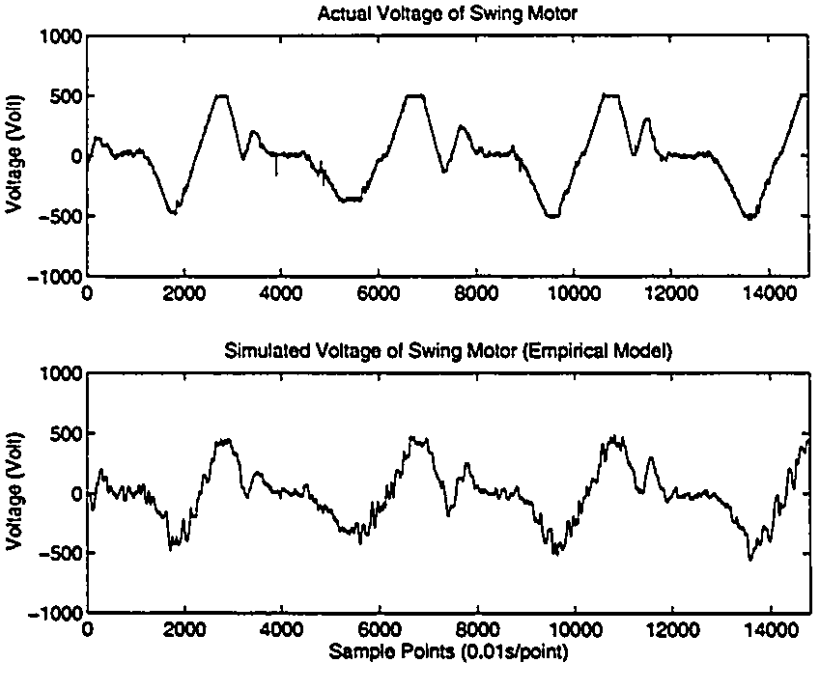

Figure 9.19: Actual and Simulated Voltages of Swing Motor (Hard Digging)

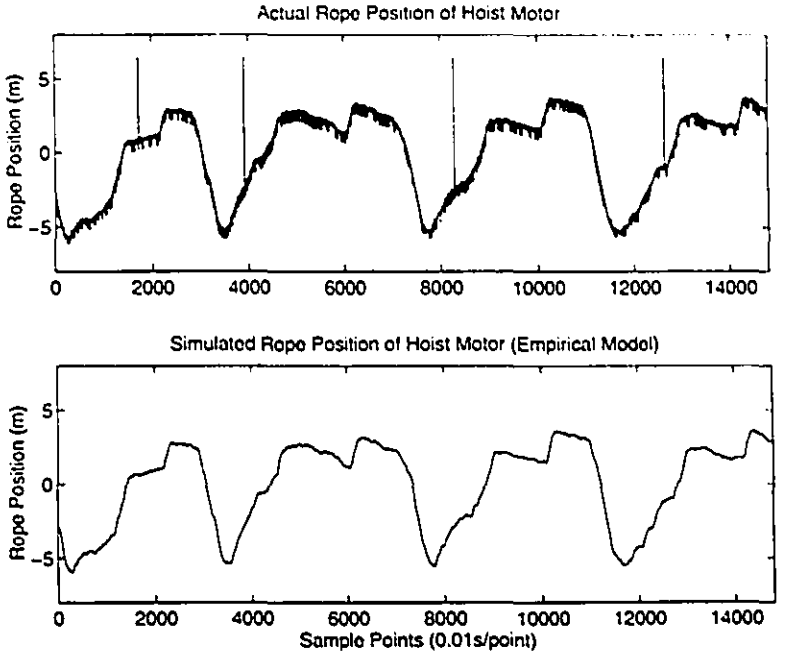

Figure 9.20: Actual and Simulated Rope Positions of Hoist Motor (Hard Digging)

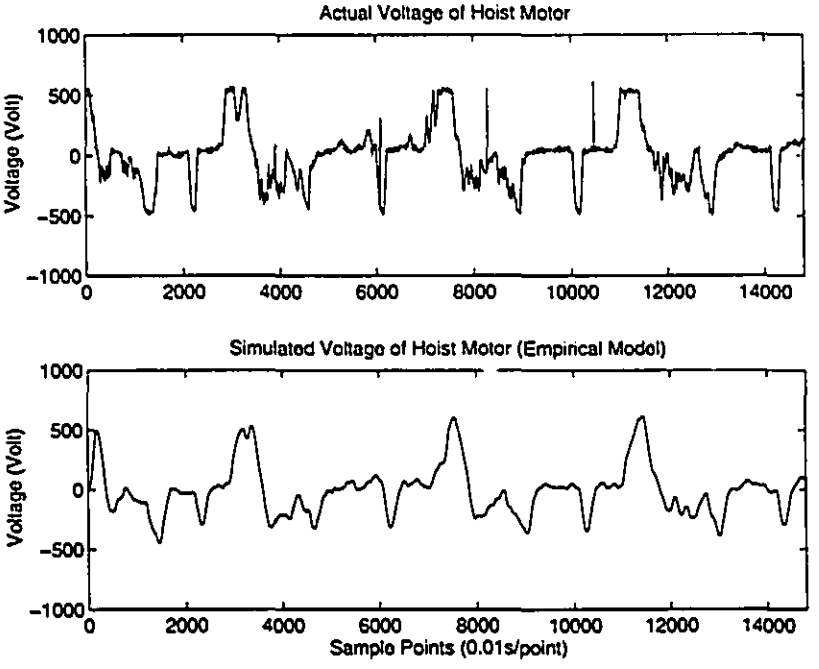

Figure 9.21: Actual and Simulated Voltages of Hoist Motor (Hard Digging)

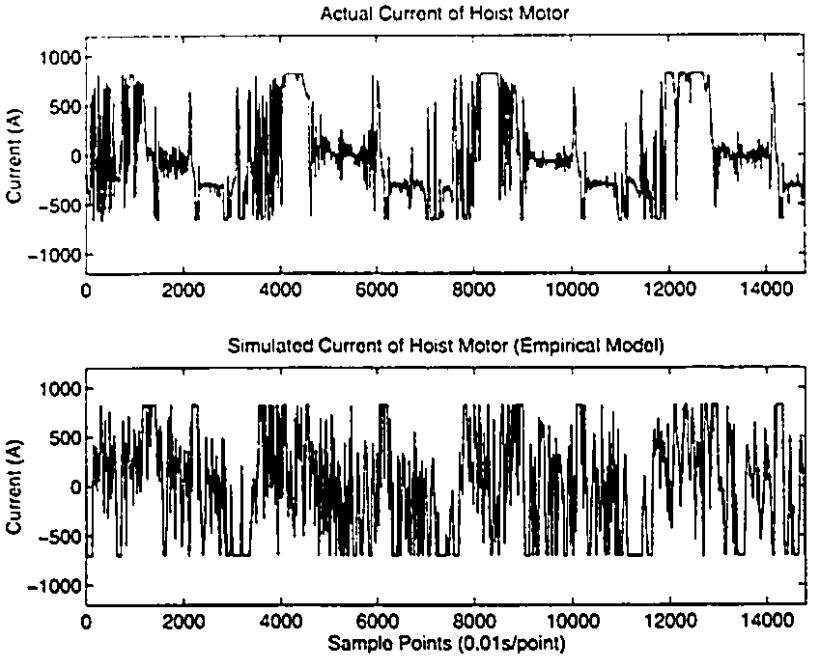

Figure 9.22: Actual and Simulated Currents of Hoist Motor (Hard Digging)

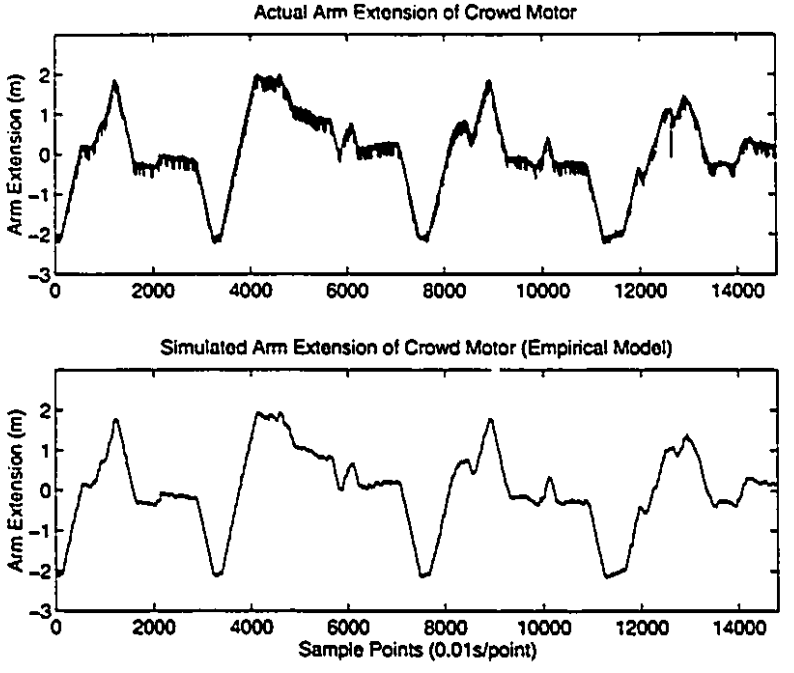

Figure 9.23: Actual and Simulated Arm Extensions of Crowd Motor (Hard Digging)

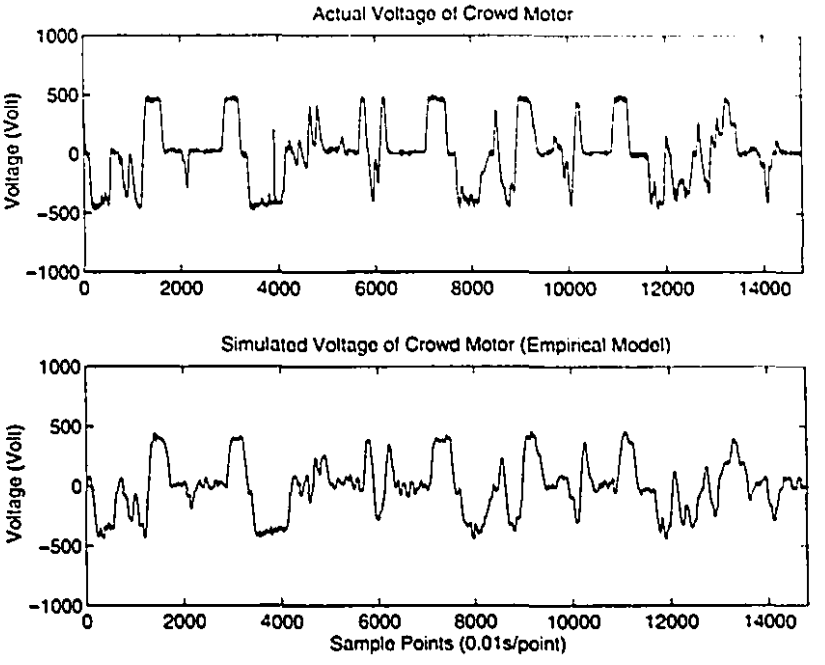

Figure 9.24: Actual and Simulated Voltages of Crowd Motor (Hard Digging)

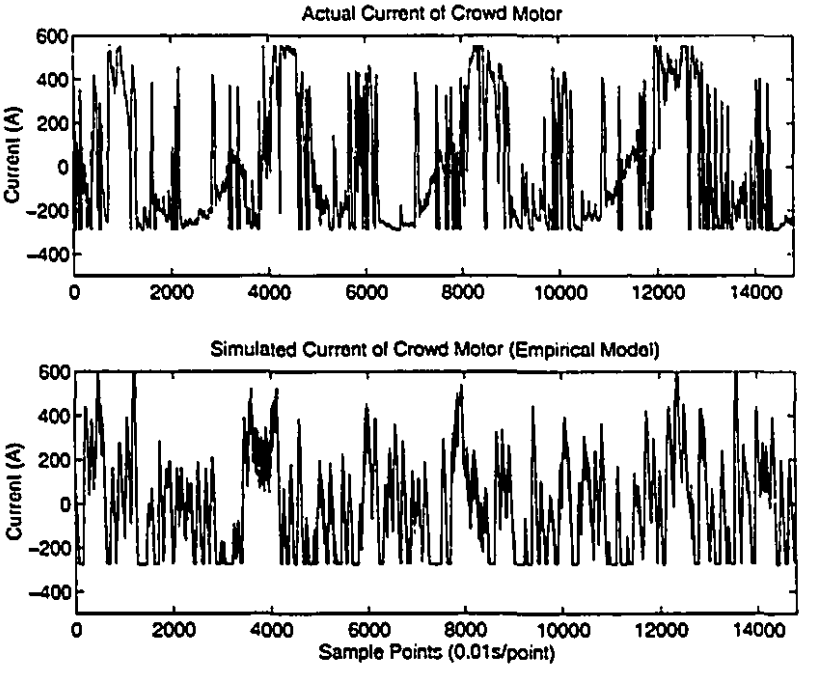

Figure 9.25: Actual and Simulated Currents of Crowd Motor (Hard Digging)

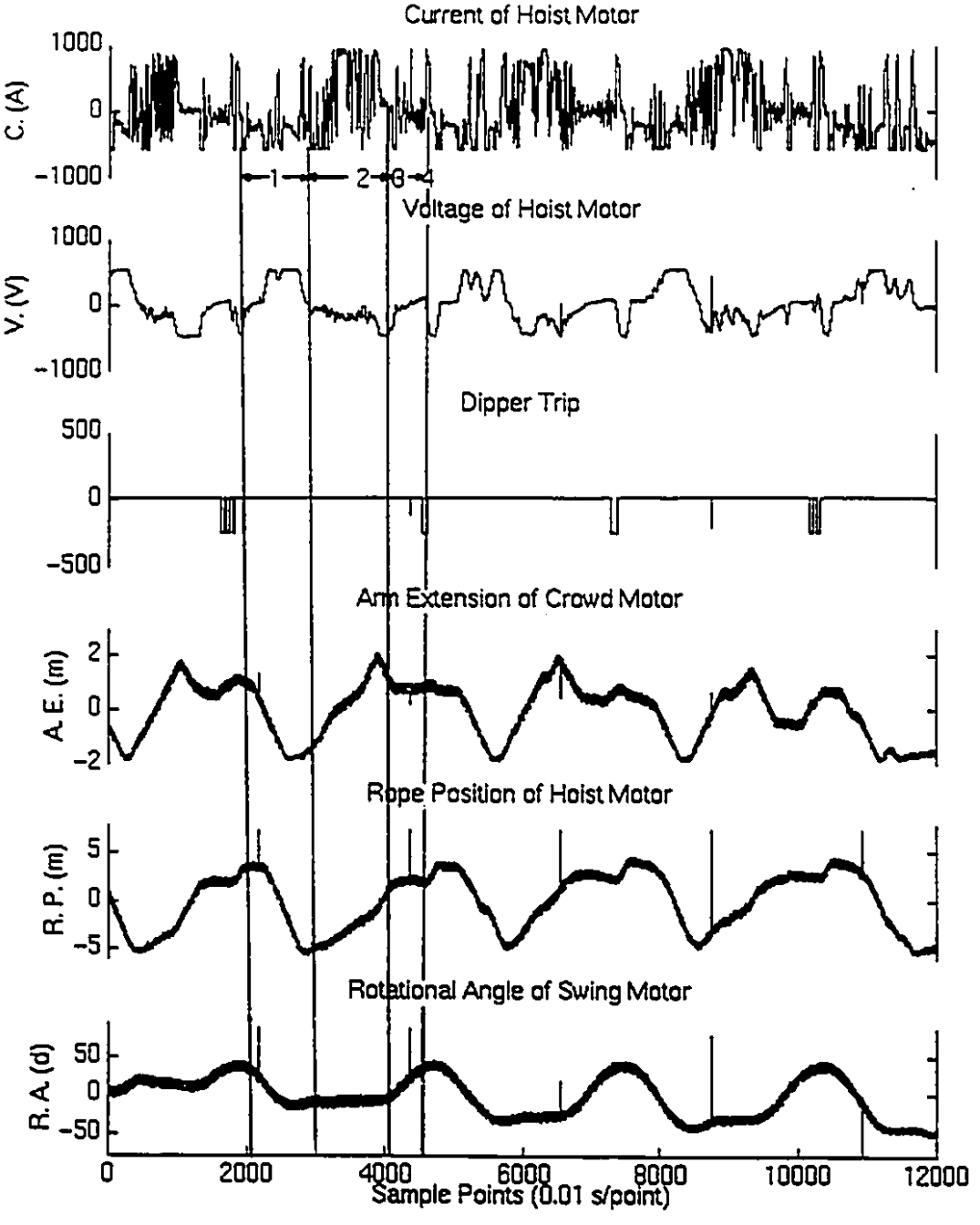

Figure 9.26: Main Variables of Electric Mining Shovel

9.9 Diggability Index

Figure 9.26 includes the main variables of the electric mining shovel. In this figure, the typical working phase of the electric mining shovel is swing from a truck to the face of a muckpile (phase 1), digging the muckpile (phase 2), swing from the face of the muckpile to the truck (phase 3), and dumping the ore or rock into the truck (phase 4).

Among the four phases, swing - digging - swing - dumping, except the digging phase, other three phases have little variance over different digging conditions. Therefore, we extract the digging phase for the hoist motor (Figure 9.27 and Figure 9.28) as well as the digging phase for the crowd motor (Figure 9.29 and Figure 9.30) from a whole shovel working phase, to investigate different digging conditions. In order to evaluate the different digging conditions, the diggability index had been established and used (Williamson, 1983, Mol 1987, and Hendricks 1989). The diggability index is a product of the ratios of the total vertical signal variations of both motor armature voltage and current, to the product of sampling time and these signals. The hoist based diggability index equation is given as follows [26]:

$$HDI = (\sum_{i=1}^{n} |HV_{i+1} - HV_i|)/(\sum_{i=1}^{n} |S * HV_i|) \times (\sum_{i=1}^{n} |HI_{i+1} - HI_i|)/(\sum_{i=1}^{n} |S * HI_i|)$$
$$= HVDI \times HCDI \qquad (9.75)$$

where n is number of reading taken during the dig cycle; HV is the hoist armature voltage; HI is hoist armature current; S is sampling time; HDI is hoist based diggability index; $HVDI$ is diggability index of hoist voltage; $HCDI$ is diggability index of hoist current. For a comparison purposes, the same approach was used in calculating a diggability index based on crowd motor responses. The crowd motor based diggability index equation is given as follows [26]:

$$CDI = (\sum_{i=1}^{n} |CV_{i+1} - CV_i|)/(\sum_{i=1}^{n} |S * CV_i|) \times (\sum_{i=1}^{n} |CI_{i+1} - CI_i|)/(\sum_{i=1}^{n} |S * CI_i|)$$
$$= CVDI \times CCDI \qquad (9.76)$$

where n is a number of reading taken during the dig cycle; CV is the crowd armature voltage; CI is the crowd armature current; S is the sampling time; CDI is crowd based diggability index; $CVDI$ is diggability index of crowd voltage; $CCDI$ is diggability index of crowd current. Using equations (9.75) and (9.76), one can obtain the different diggability indices shown in Table 9.1 ($*$ — analytical model).

From the table, one can find that the hard digging has larger diggability indices than has easy digging, in line with actual circumstance. Since the hard digging takes a longer time as well as the current and voltage traces of the hard digging are also more ragged (comparing Figure 9.27 with Figure 9.28), the absolute length of the traces will be much longer. Furthermore, the average value of the hoist current and voltage are lower. As a result, the equation (9.75) will produce a larger value. A similar explanation applies to the crowd motor.

From the table, one can find that the simulated values are less than the actual values. In those figures of Section 9.6, 9.7, and 9.8, we can find that the simulated curves have smoother shape than have the actual curves. As a result, we obtained lower diggability indices for simulated traces.

From the table, one can also find that although the diggability indices of the crowd motor in the hard digging are larger than those in the easy digging, they are less sensitive to variations in diggability than those of the hoist motor. This can be explained as follows: comparing Figure 9.27 and Figure 9.28 with Figure 9.29 and Figure 9.30, one can find that from the easy digging to the hard digging, the traces of the crowd motor change less than do those of the hoist motor. From Figure 2.1, it is evident that during the digging process, the force in X_5 direction is normally larger than that in Z_5 direction. The force in the X_5 direction is controlled by the hoist motor and the force in Z_5 direction is controlled by the crowd motor. The hoist motor is also more powerful (1450 H.P. @ 475 volts - 2250 peak H.P.) than the crowd motor (400 H.P. @ 475 volts - 630 peak H.P.) [26]. Therefore, The hoist motor contributes more to the digging action. Moreover, another important effect is due to the different transmission effects on the hoist and crowd motors. The crowd motor

is connected with a "V" belt transmission system, to transfer power from the crowd motor to the shipper shaft gear train. The net effect of these elastic belts is to absorb the high amplitude energy of the shocks from sudden impact loads, damp it and gradually transfer the dissipated energy to the crowd motor and drive mechanism. It is believed that the action of these energy absorptive belts is responsible for the relative lack of crowd motor responsiveness to variation in ground diggability [26]. The hoist motor is directly connected to the gear case. Hence, it offers no absorptive effects and the different digging conditions directly reflect on the hoist motor response. As a result, in order to compare the hard and easy diggings, we show more tables of the diggability indices in hoist motor (from tables 9.2 to 9.7).

EasyDigging1	*HVDI*	*HCDI*	*HDI*	*CVDI*	*CCDI*	*CDI*
ActualValue	0.7542	0.9700	0.7316	0.8940	0.7392	0.6669
SimulatedValue	0.4405	0.7851	0.3458	0.6717	0.7511	0.5046
*SimulatedValue**	0.4952	0.7618	0.3773	0.6018	0.7587	0.4565
HardDigging1	*HVDI*	*HCDI*	*HDI*	*CVDI*	*CCDI*	*CDI*
ActualValue	0.9342	1.4285	1.3345	0.9919	0.8502	0.8433
SimulatedValue	0.5272	1.1300	0.5892	0.7537	0.7902	0.5956
*SimulatedValue**	0.5852	1.2567	0.7354	0.6055	0.8168	0.4946

Table 9.1: Summary of Diggability Indices

EasyDigging2	*HVDI*	*HCDI*	*HDI*
ActualValue	0.9419	0.8055	0.7587
SimulatedValue	0.5164	0.6100	0.3150
*SimulatedValue**	0.5585	0.5647	0.3154

Table 9.2: Diggability Indices of Easy Digging 2

EasyDigging3	*HVDI*	*HCDI*	*HDI*
ActualValue	0.6348	0.6310	0.4006
SimulatedValue	0.3943	0.6715	0.2647
*SimulatedValue**	0.4022	0.7204	0.2899

Table 9.3: Diggability Indices of Easy Digging 3

HardDigging2	*HVDI*	*HCDI*	*HDI*
ActualValue	0.6452	1.8702	1.2067
SimulatedValue	0.8174	1.0020	0.8190
*SimulatedValue**	0.8625	0.9746	0.8407

Table 9.4: Diggability Indices of Hard Digging 2

HardDigging3	*HVDI*	*HCDI*	*HDI*
ActualValue	1.0117	1.3734	1.3895
SimulatedValue	0.5901	0.8699	0.5133
*SimulatedValue**	0.6381	0.8772	0.5598

Table 9.5: Diggability Indices of Hard Digging 3

HardDigging4	*HVDI*	*HCDI*	*HDI*
ActualValue	1.3166	1.5664	2.0623
SimulatedValue	0.4675	1.2542	0.5863
*SimulatedValue**	0.4262	1.0062	0.4289

Table 9.6: Diggability Indices of Hard Digging 4

HardDigging5	*HVDI*	*HCDI*	*HDI*
ActualValue	0.7902	1.2207	0.9647
SimulatedValue	0.5107	1.3070	0.6674
*SimulatedValue**	0.4970	0.9089	0.4517

Table 9.7: Diggability Indices of Hard Digging 5

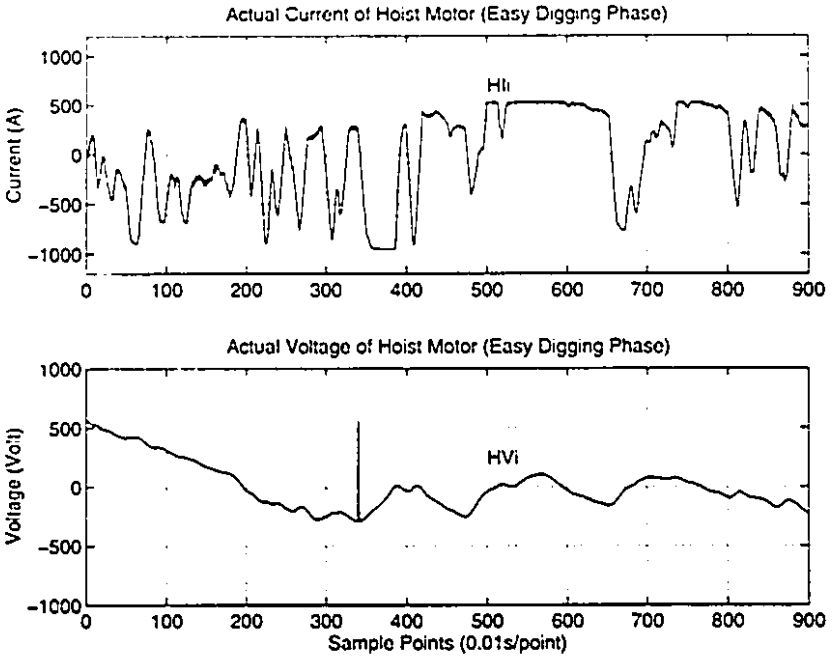

Figure 9.27: Actual Current and Voltage of Hoist Motor in a Easy Digging Phase

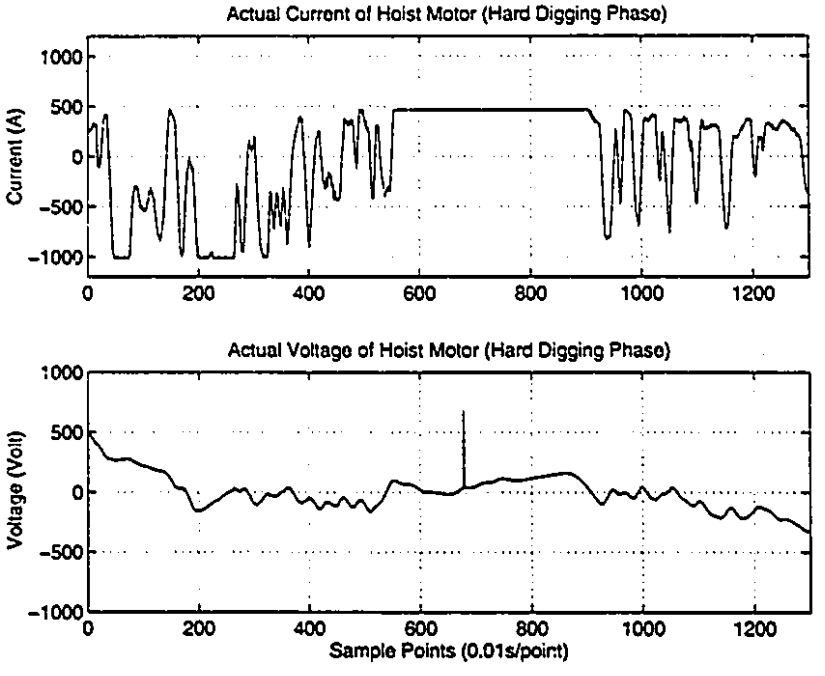

Figure 9.28: Actual Current and Voltage of Hoist Motor in a Hard Digging Phase

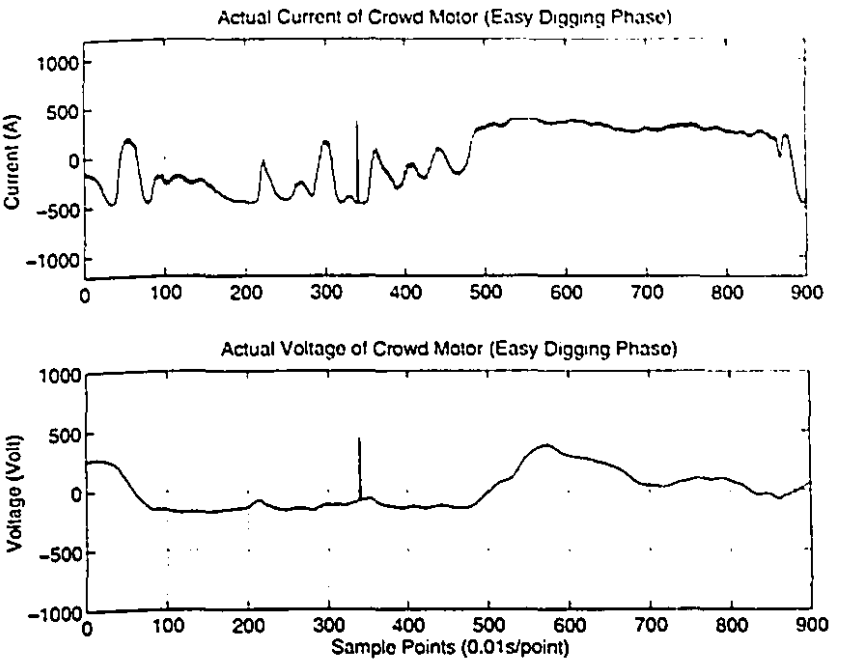

Figure 9.29: Actual Current and Voltage of Crowd Motor in a Easy Digging Phase

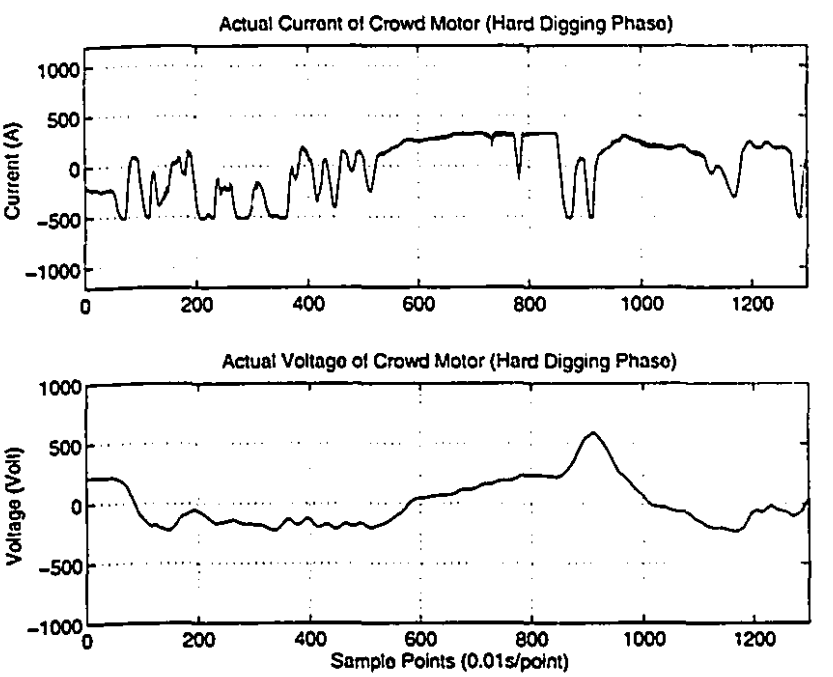

Figure 9.30: Actual Current and Voltage of Crowd Motor in a Hard Digging Phase

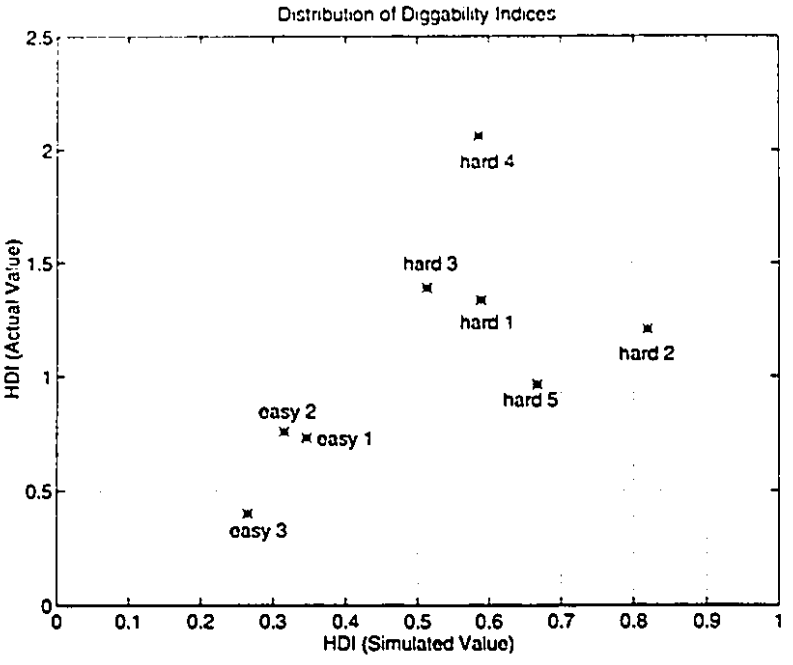

Figure 9.31: Distribution of Diggability Indices

Figure 9.31 shows the data in Tables 9.1, 9.2, 9.3, 9.4, 9.5, 9.6, 9.7. In this figure, we can see that the diggability indices in hard digging distribute in top-right area and the diggability indices in easy digging distribute in bottom-left area. From the distribution, we can conclude:

- Easy Digging HDI: $0.4 \sim 0.8$ (actual value)
- Easy Digging HDI: $0.2 \sim 0.4$ (simulated value)
- Hard Digging HDI: $0.9 \sim 2.1$ (actual value)
- Hard Digging HDI: $0.5 \sim 0.9$ (simulated value)

Chapter 10

Conclusions and Suggestions for Future Work

This thesis has used state-of-the-art robotics and control theory to investigate the electric mining shovels as well as established a simulator for this kind of machines. The conclusions and suggestions for future work are indicated in the following sections.

10.1 Conclusions

This thesis has comprised three main work activities: analytical modelling, empirical modelling, and simulator for the electric mining shovels. The analytical and empirical models have included kinematics, Jacobian, rigid body dynamics, actuator dynamics, interaction between bucket and muckpile, parametric system identification, and non-parametric system identification. All these models have contributed to establishing a simulator for electric mining shovels. The simulator was validated by using empirical data. In addition, because the diggability index is an important factor (usually used to evaluate the different digging conditions), the actual and simulated diggability indices have been used to validate the simulator. The simulator could contribute to the shovel manufacturers in their ability to improve their machine designs. The simulator could contribute to investigating the effects of different muckpile condition on shovel performance. The kinematics could contribute to a shovel operator's ability to optimize their trajectory and task planning. All these models could contribute to computer control design. Main achievements of the thesis are:

- An analytical model of the complete machine was derived, based upon rigid body assumptions. This included the crowd, hoist, and swing motor actuator models and kinematics, Jacobian, and rigid body dynamics.

- An analytical model of the bucket-muckpile interaction was derived. Based upon Rowlands' friction model of a dragline bucket, a more advanced friction model of the shovel bucket was obtained. In addition, the impact effects relevant to larger fragments of rock were considered.

- In the empirical modelling part, system identification methods are used. In addition to a typical ARX estimate, used for identification of the transfer functions, the maximum likelihood estimate was employed for identification of the state space models, which were used in the system simulation. Furthermore, the disturbances acting on the three actuators were identified by using nonparametric model estimation. The digging/non-digging, and easy digging/hard digging effects were also considered, as governed by the fragmentation characteristics.

- An integrated model of the complete process, i.e. the machine and its interaction with the muckpile, was constructed based on all the previous models.

- The individual models, as well as the integrated model, were implemented in software, using MATLAB and its toolbox SIMULINK, and validated by simulation.

- The analytical model and empirical models were simulated, accounting for easy digging and hard digging conditions which were compared.

- The diggability indices of the actual and simulated armature voltages and currents were calculated, in order to further validate the simulator.

10.2 Suggestions for Future Work

Certain improvements could be made to the modelling, simulation and analysis of the machine:

- The models could be extended to include non-rigid body effects of the machine structure.

- The empirical models can be revised by using more input-output data and their identifications in order to obtain more accurate models.
- The control problem could be posed as a coupled multivariable problem. This should be a more accurate reflection of the coupled nature of the process.
- Since the system parameters are changing with respect to time, adaptive control could be used on the shovel control system.
- The interaction between the bucket and muckpile may be able to be extended to include the cohesion issue when digging a wet muckpile.
- Elements of structural design could be reconsidered, e.g. using parallel instead of serial kinematics, which would greatly enhance machine rigidity and reduce the disturbance loading of the actuators, while likely reducing the weight and size of the electric mining shovel.

APPENDIX A

Appendix: Simulink Simulators

The simulink simulators include the main routine, "Electric Shovel Main System", and some subroutines, which are mainly three disturbance blocks, T_{d1}, T_{d3}, and T_{d4}.

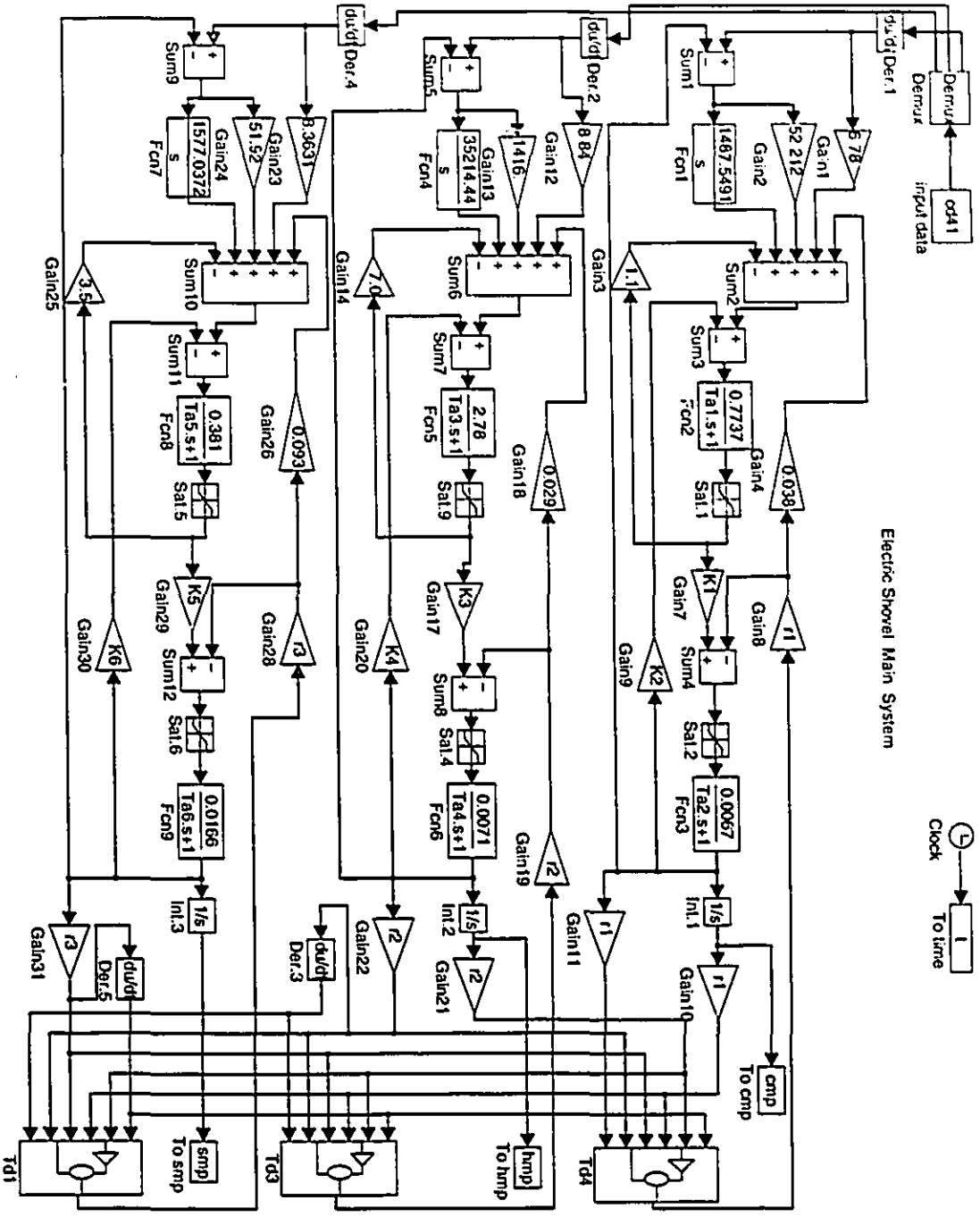

Figure A.1: Electric Shovel Main System

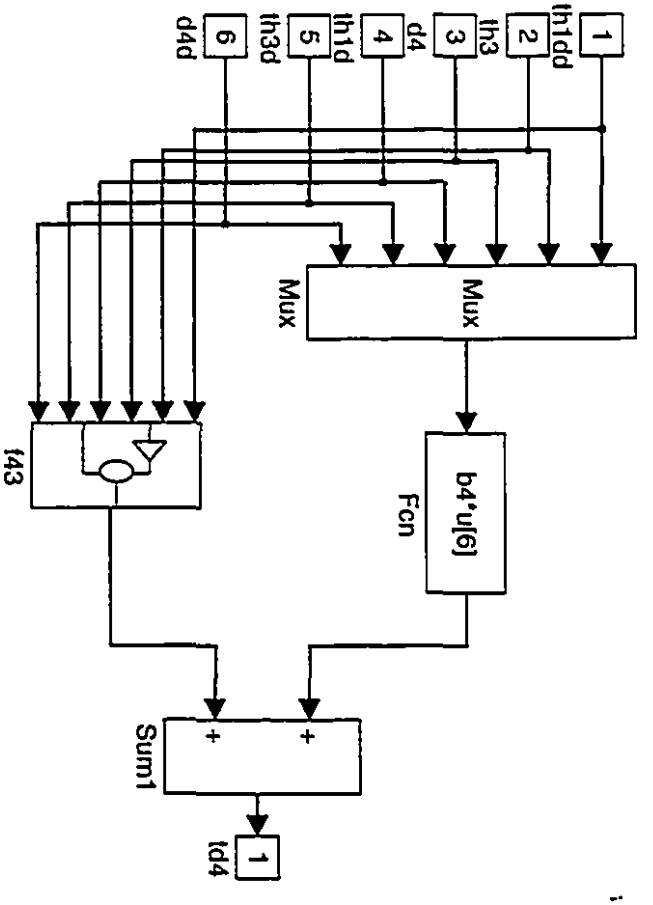

Figure A.2: Td4 subroutine

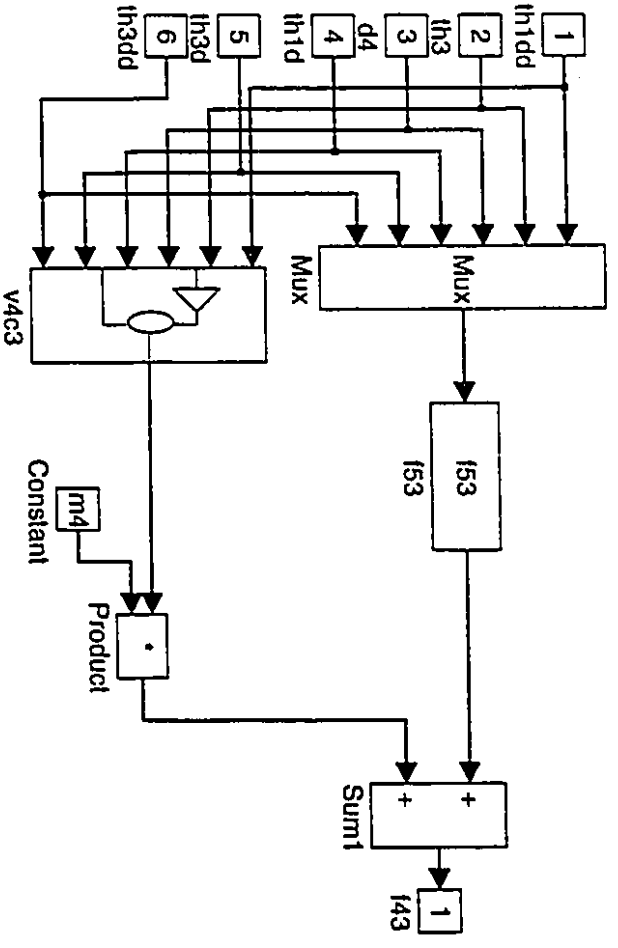

Figure A.3: f43 subroutine

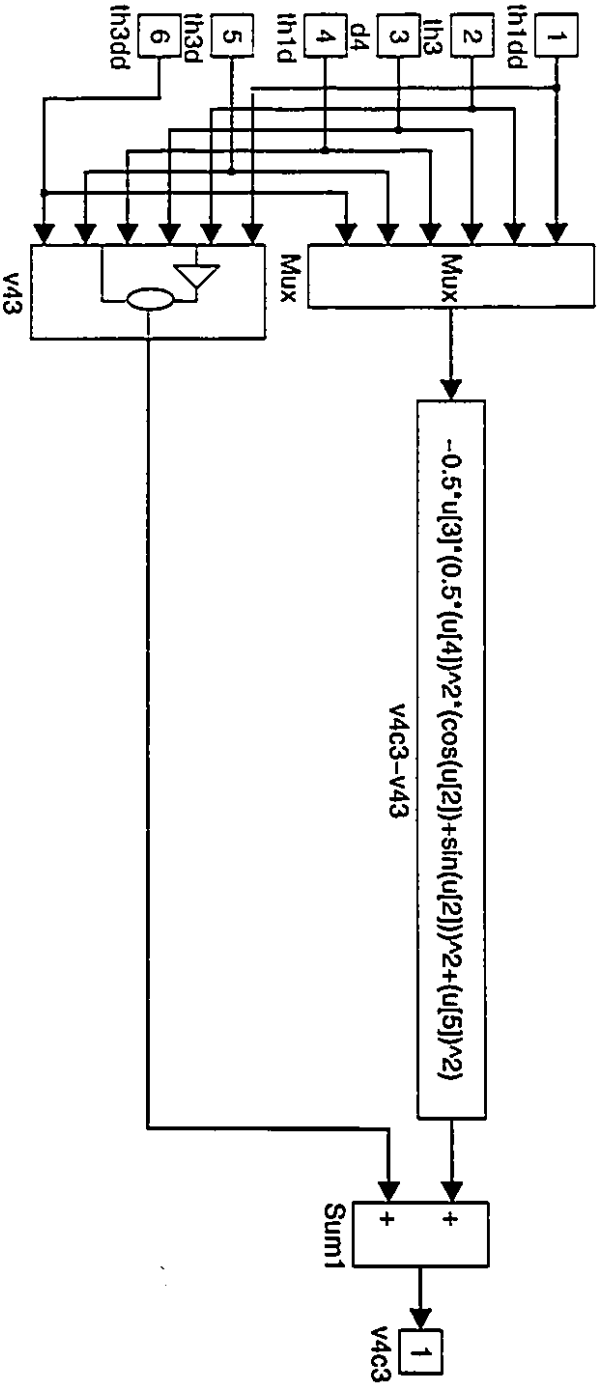

Figure A.4: v4c3 subroutine

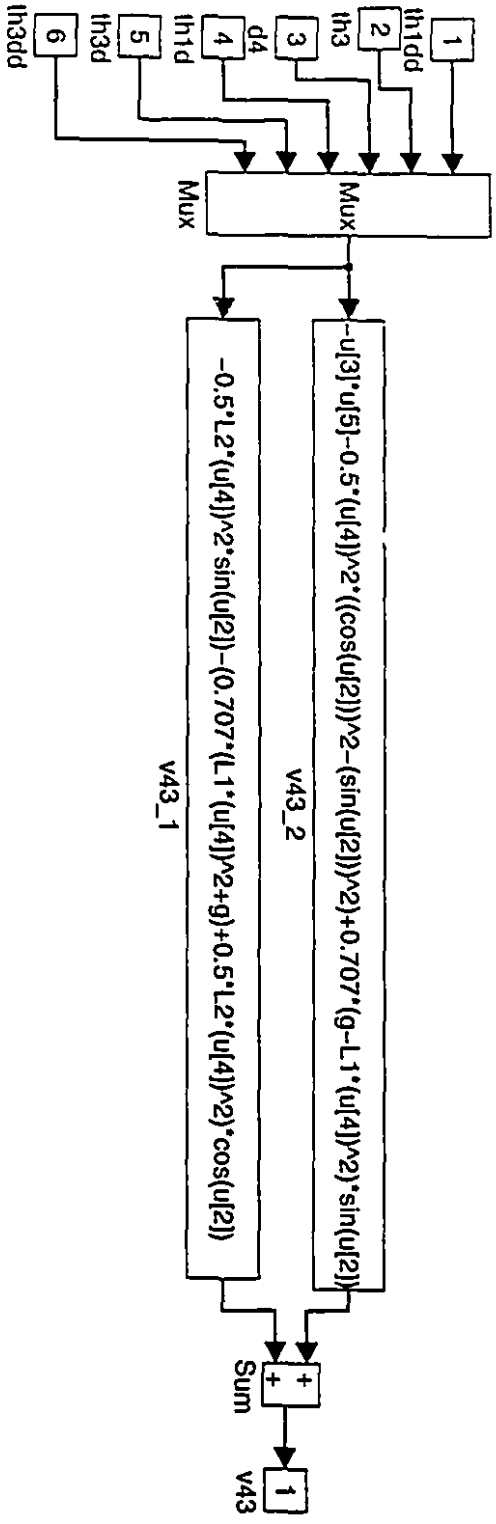

Figure A.5: v43 subroutine

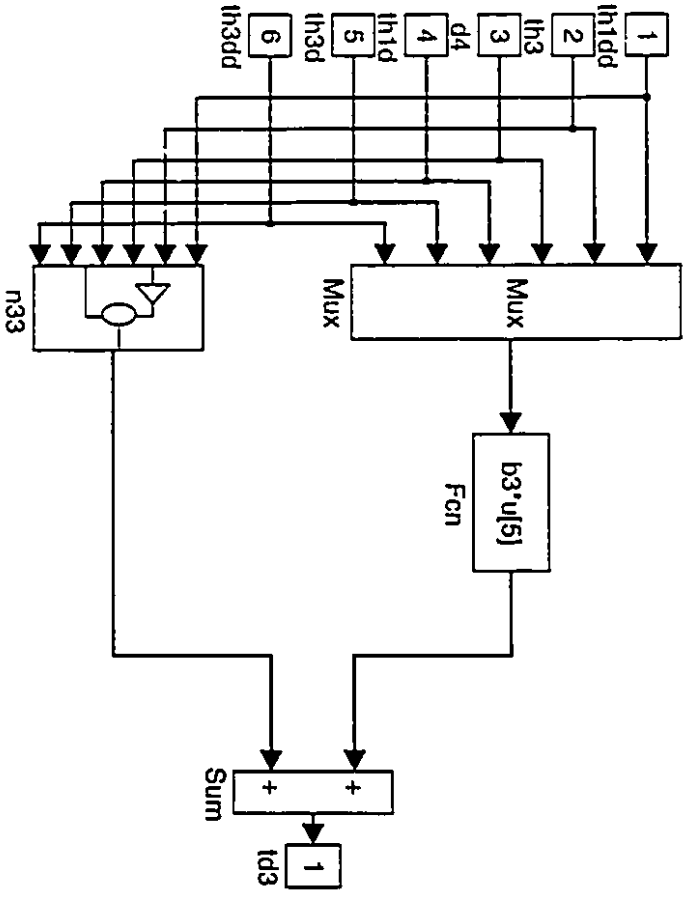

Figure A.6: Td3 subroutine

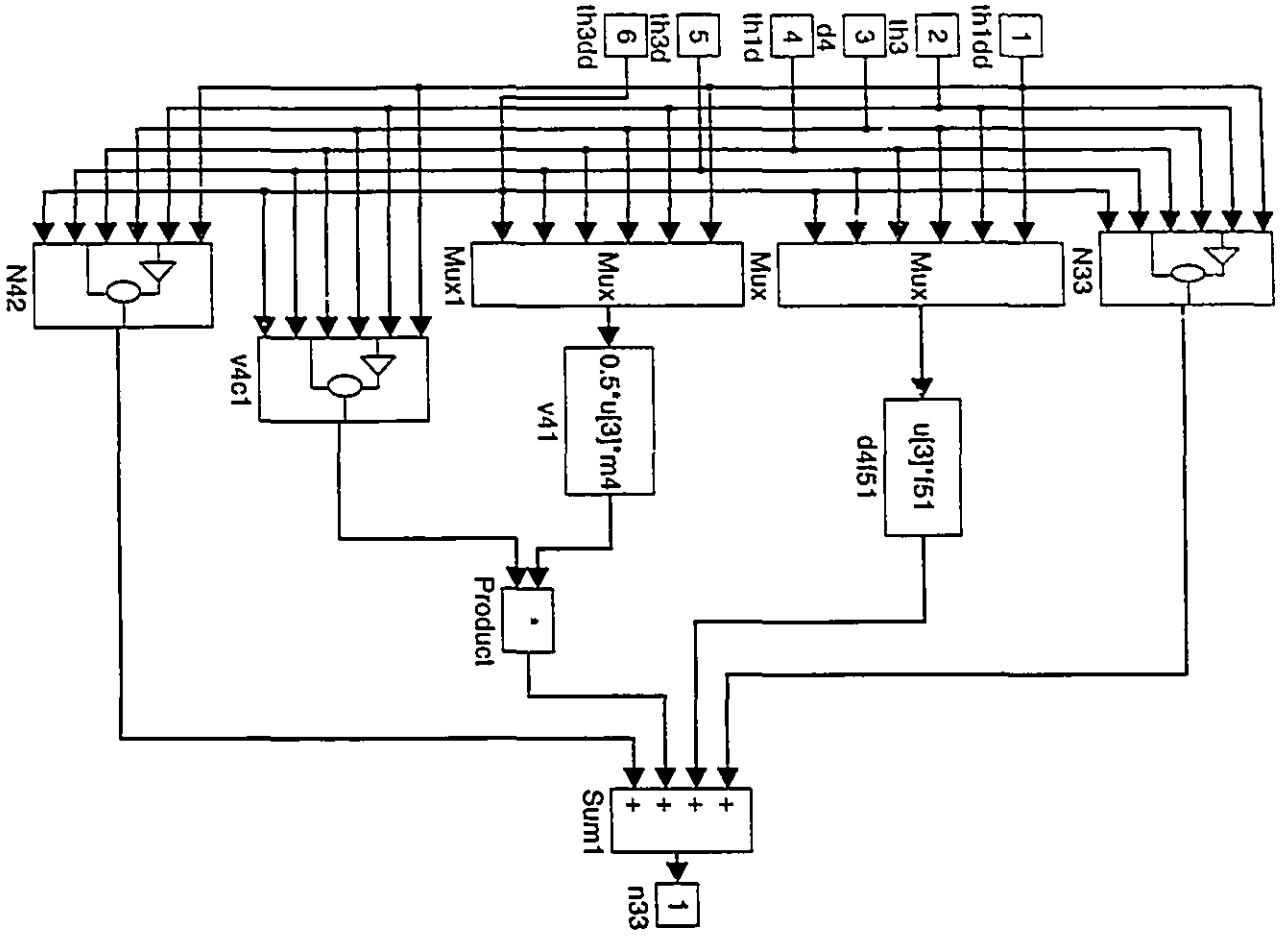

Figure A.7: n33 subroutine

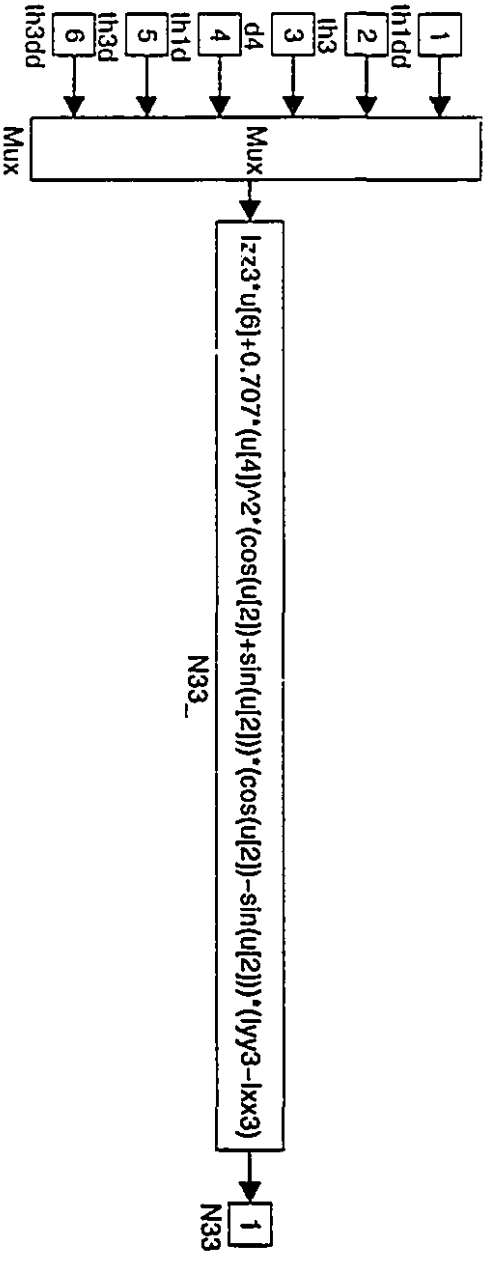

Figure A.8: N33 subroutine

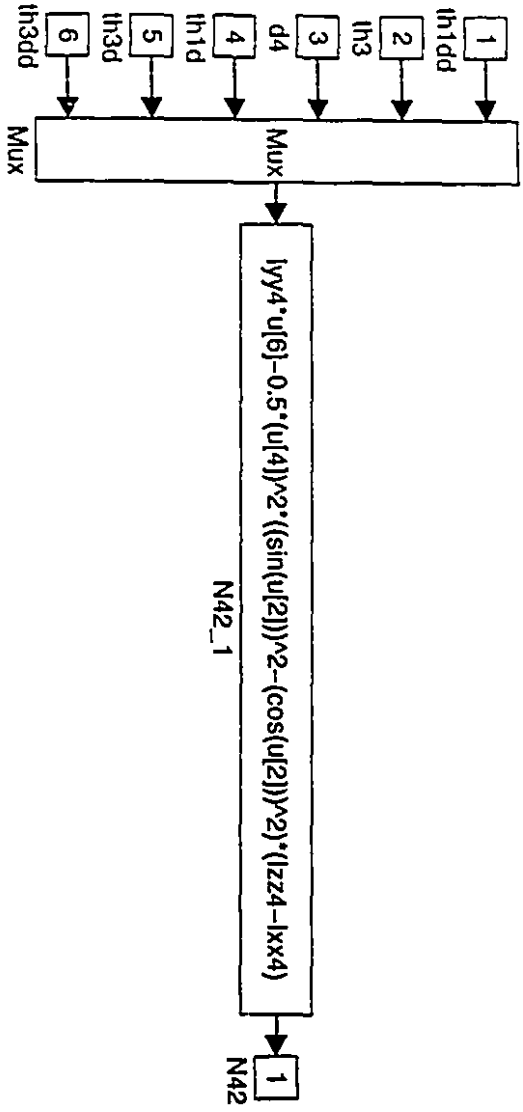

Figure A.9: N42 subroutine

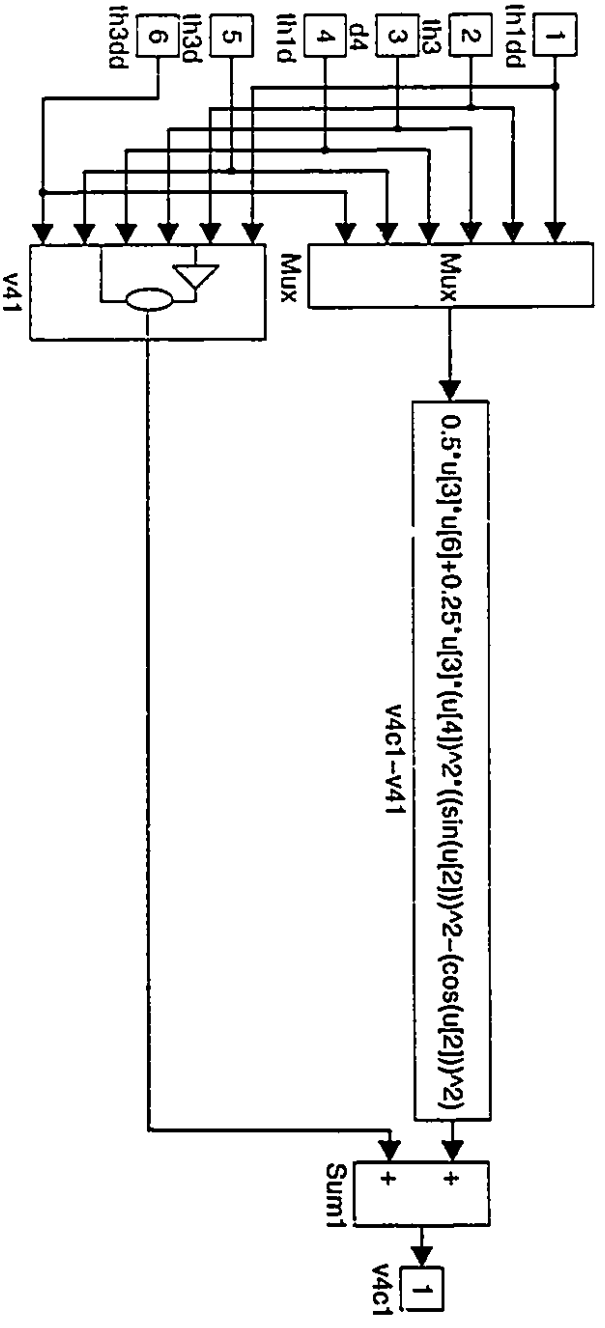

Figure A.10: v4c1 subroutine

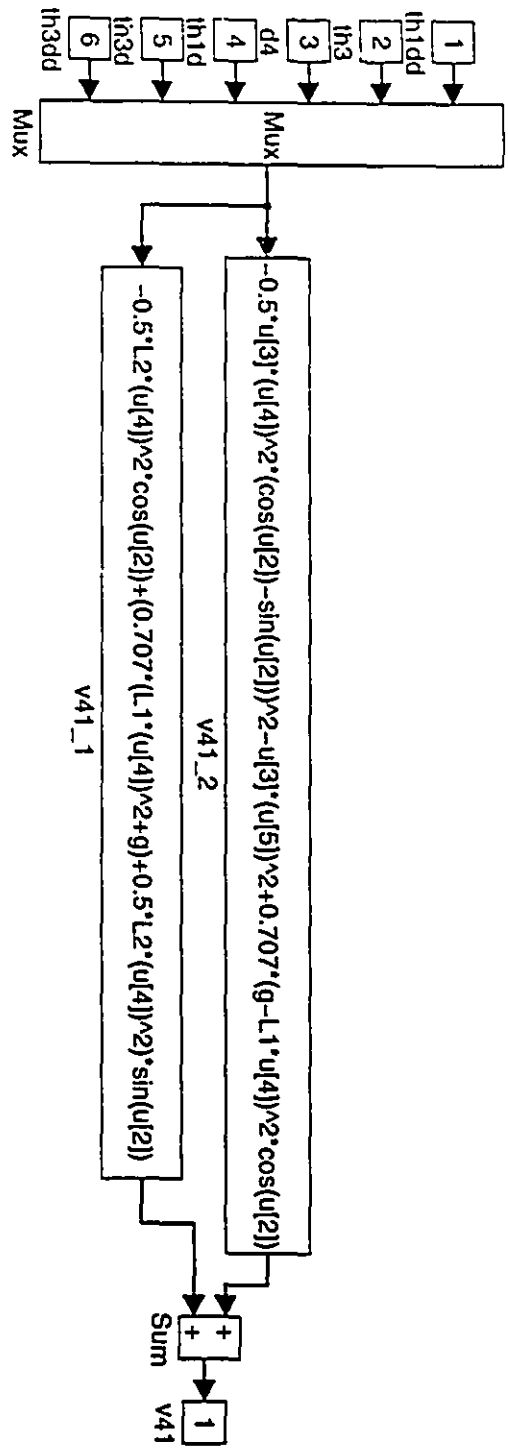

Figure A.11: v41 subroutine

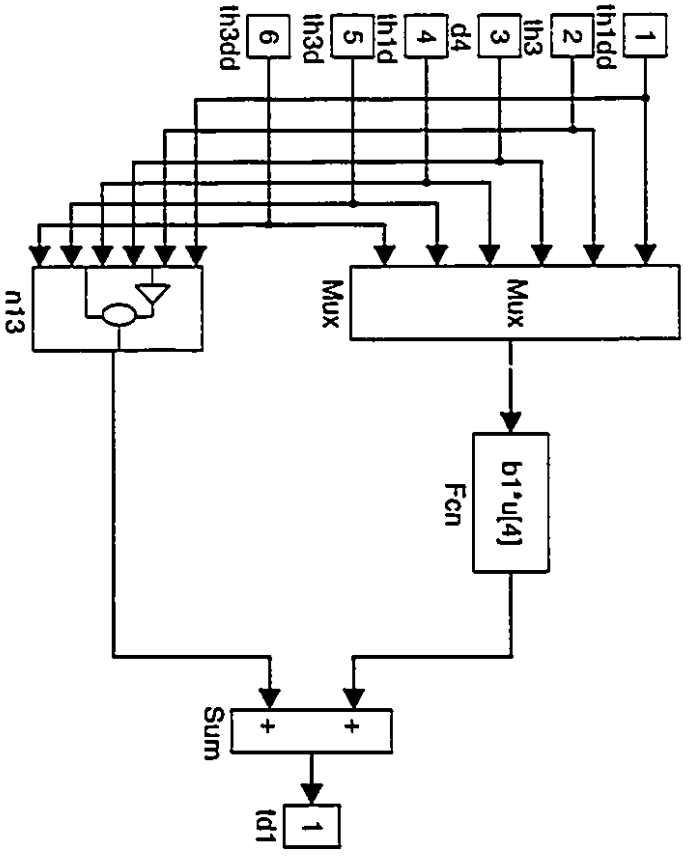

Figure A.12: Td1 subroutine

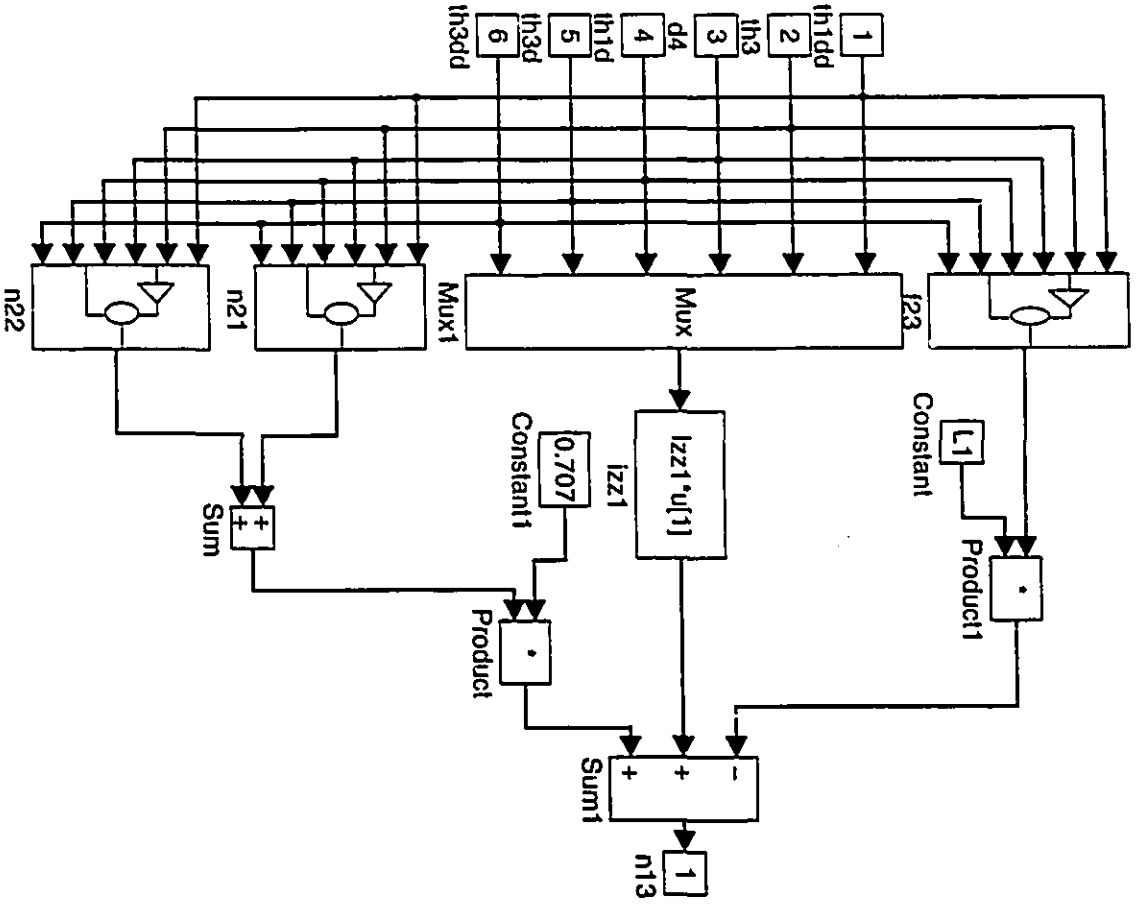

Figure A.13: n13 subroutine

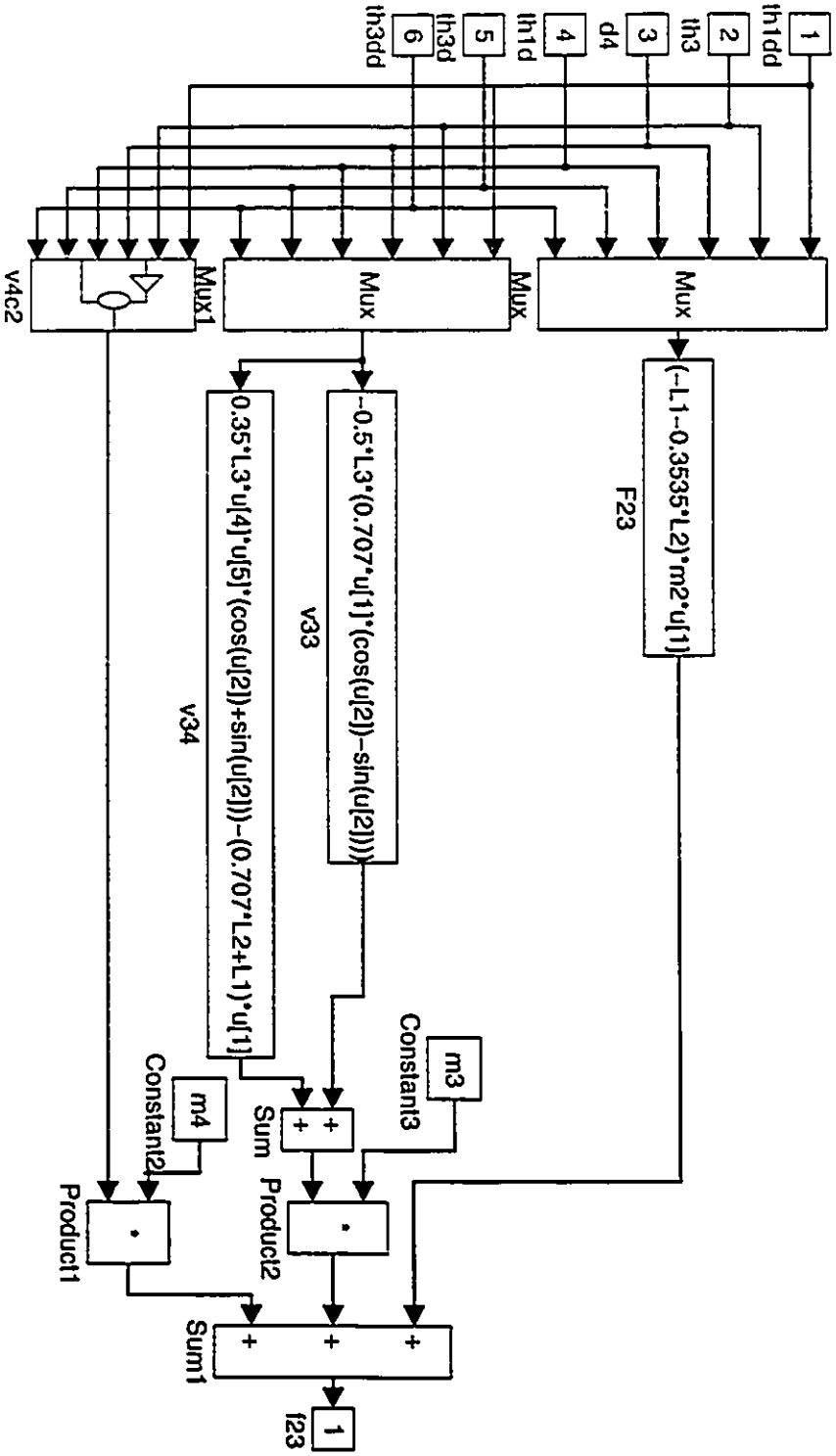

Figure A.14: f23 subroutine

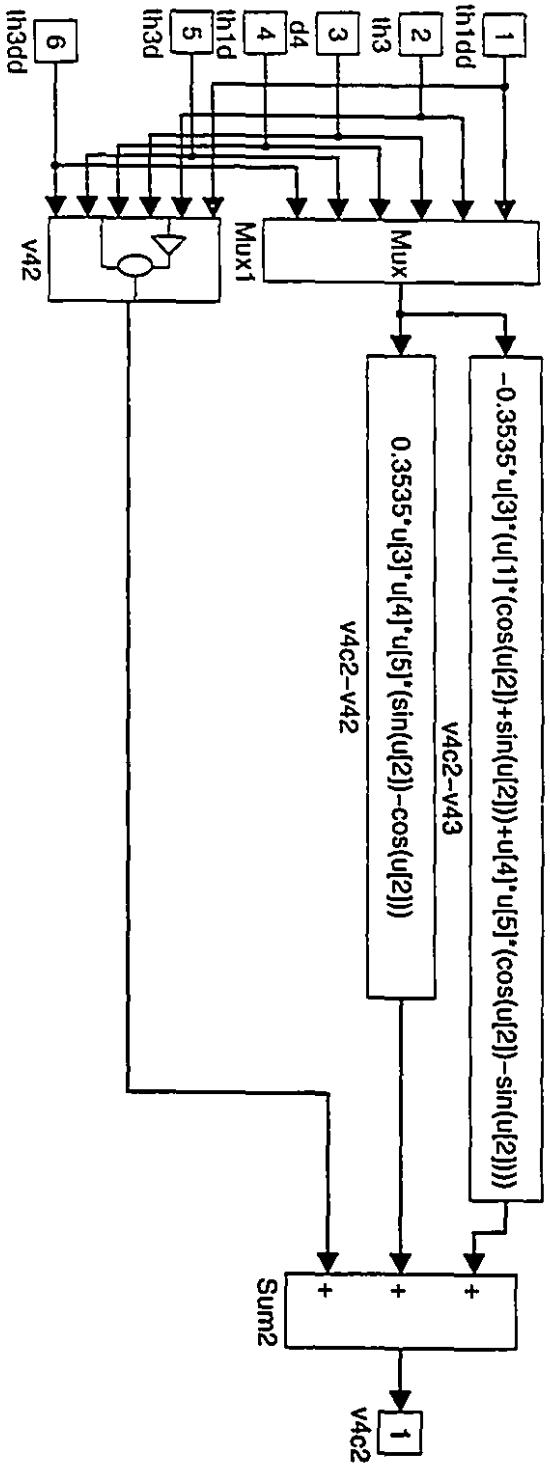

Figure A.15: v4c2 subroutine

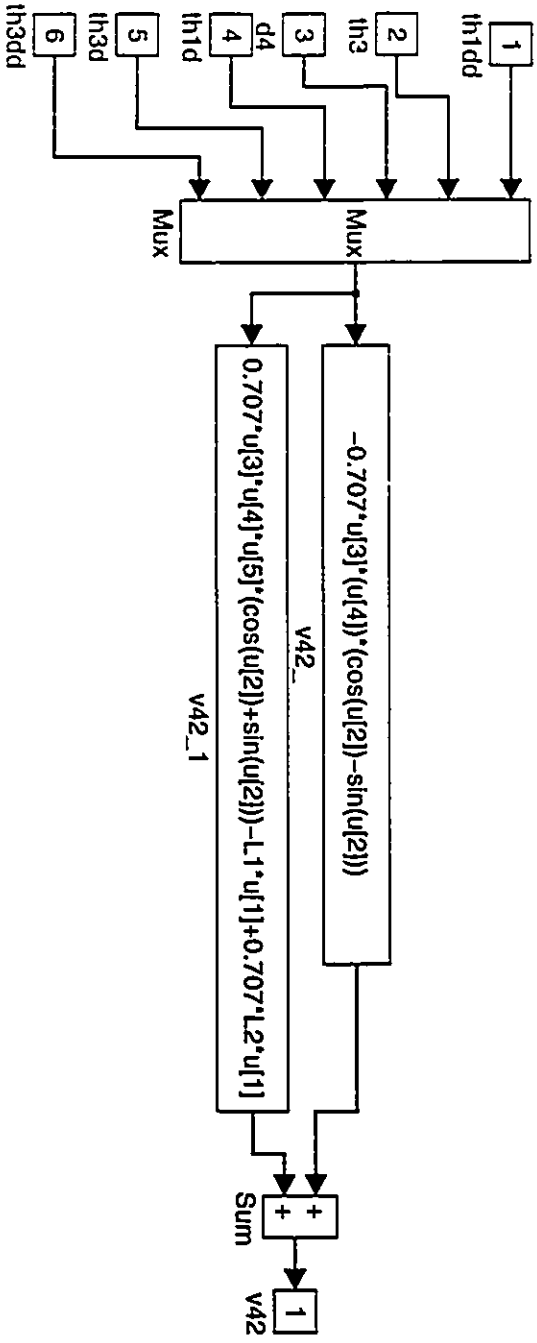

Figure A.16: v42 subroutine

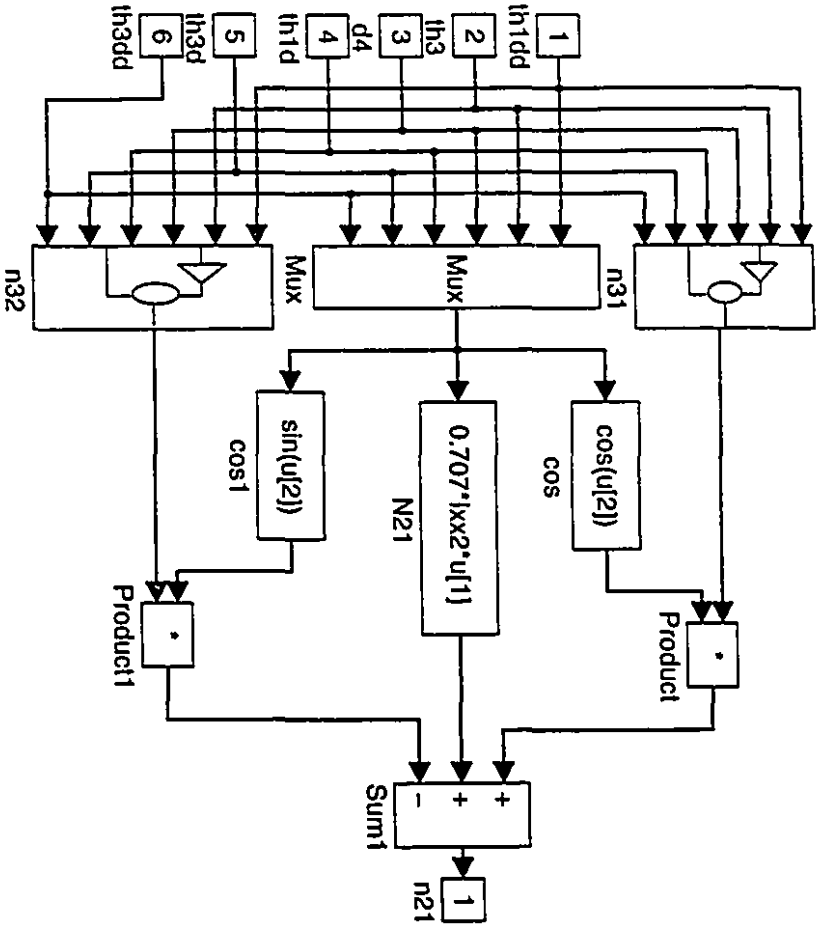

Figure A.17: n21 subroutine

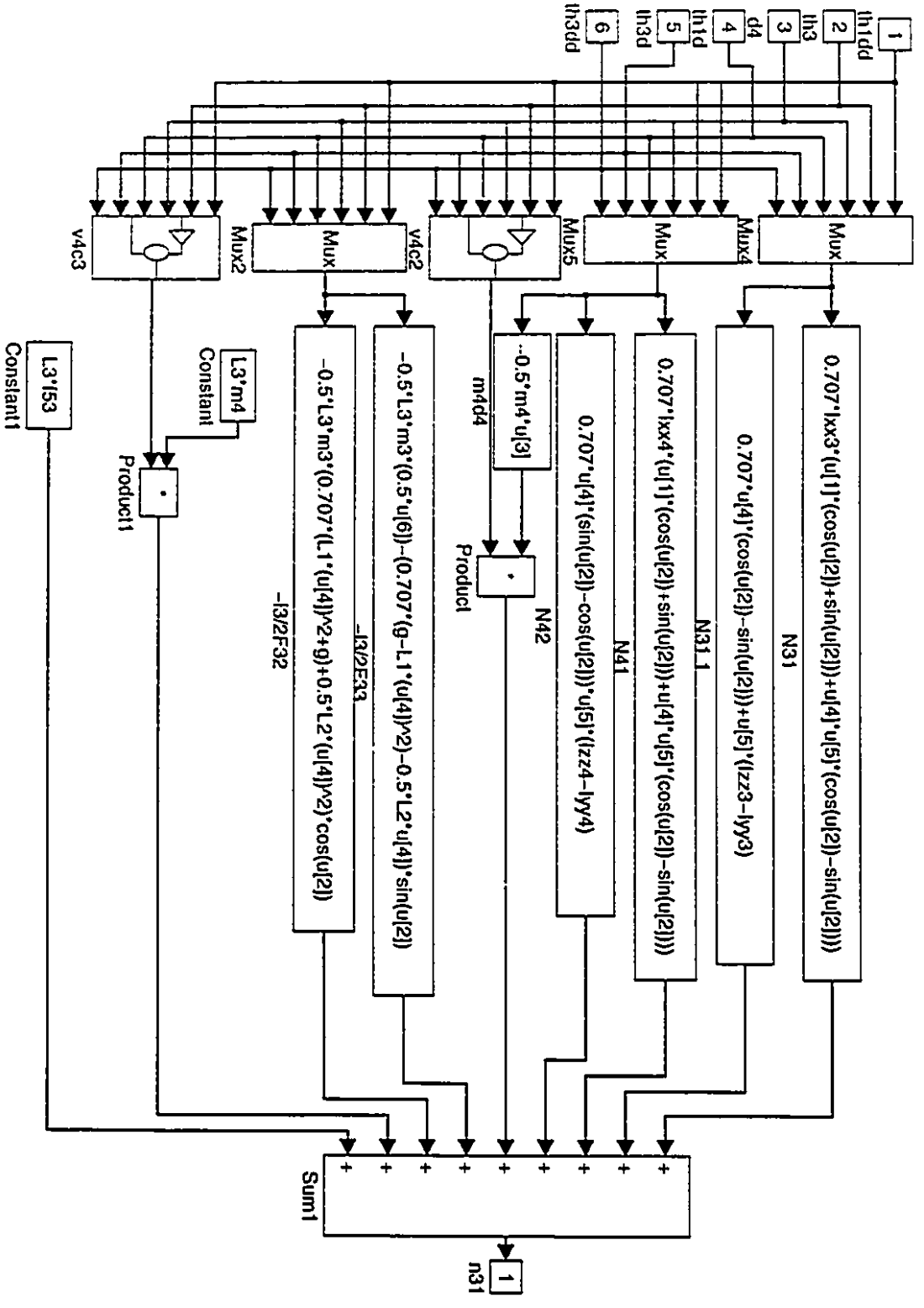

Figure A.18: n31 subroutine

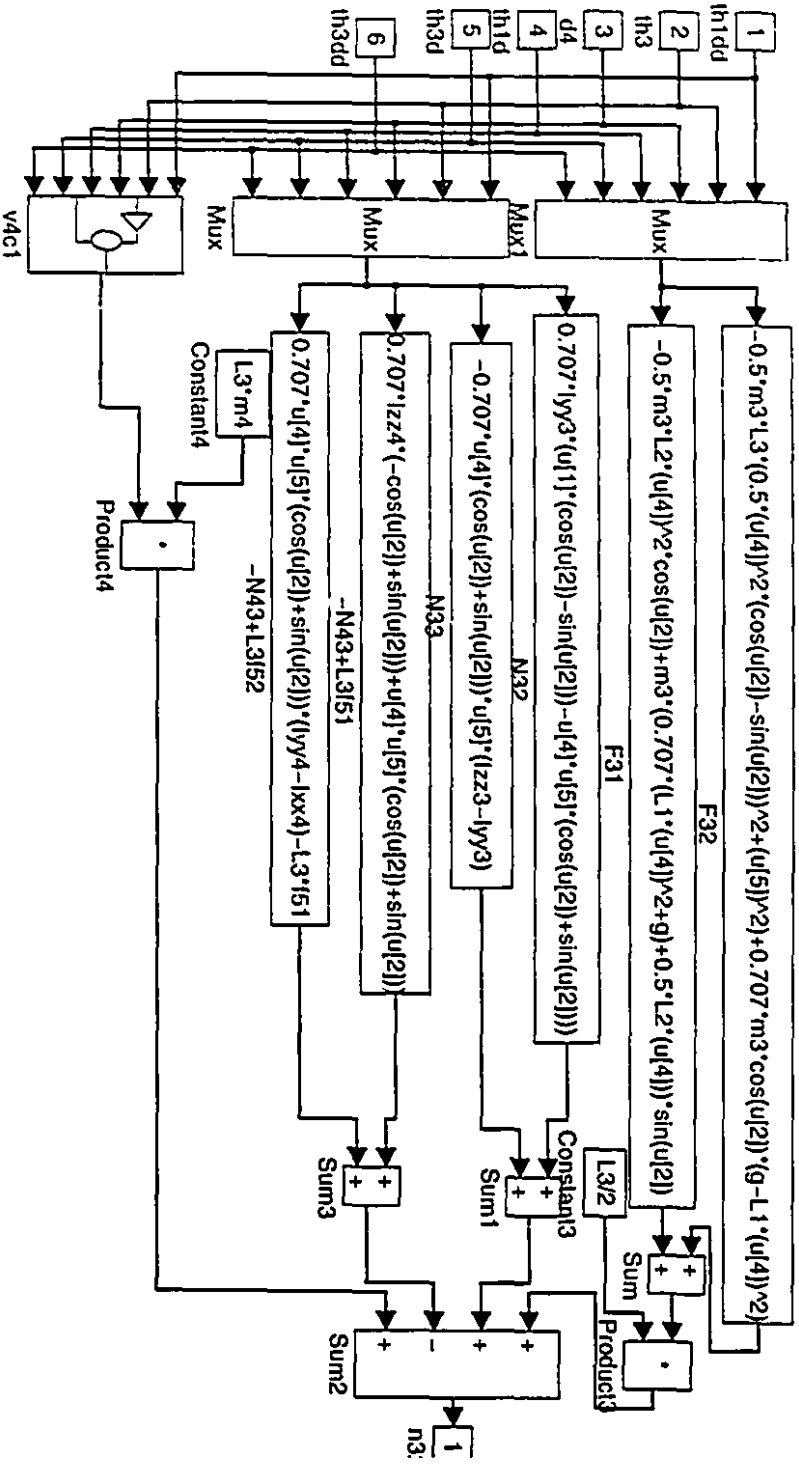

Figure A.19: n32 subroutine

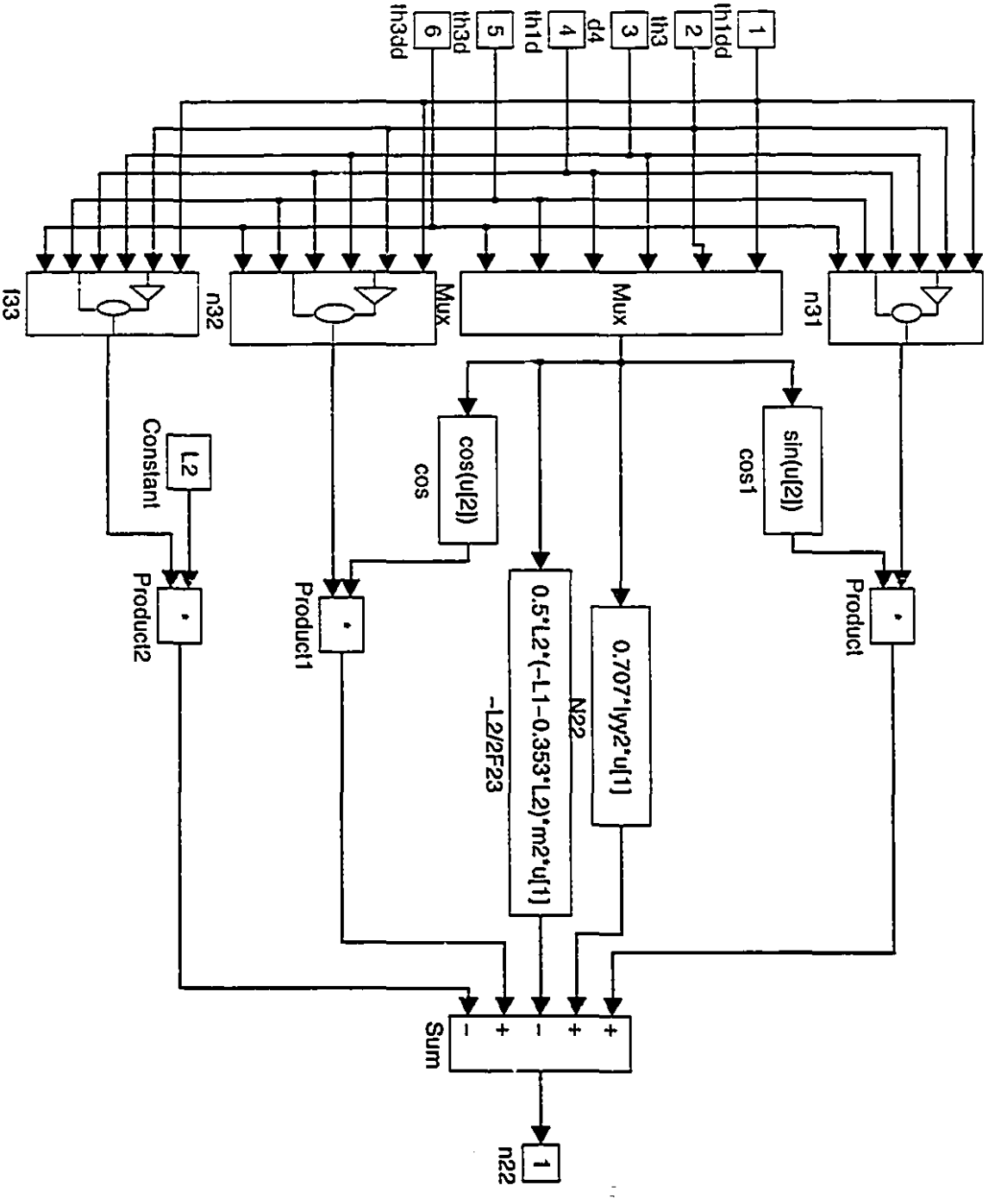

Figure A.20: n22 subroutine

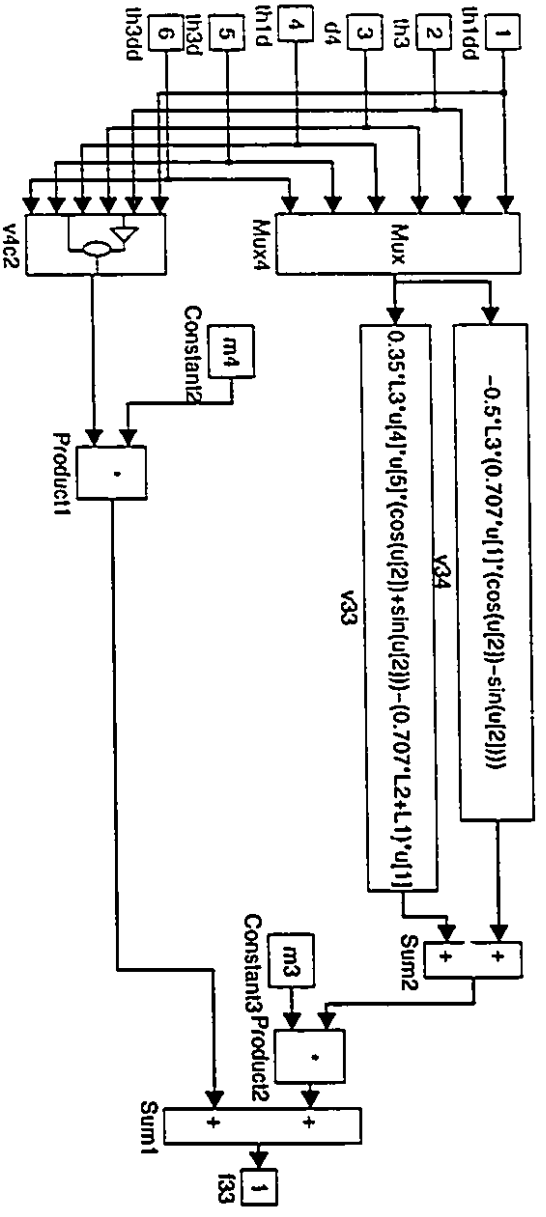

Figure A.21: f33 subroutine

Bibliography

[1] Anderson,W., *Controlling Electrohydraulic Systems*, Marcel Dekker, INC., 1988.

[2] Astrom, K. J., *Computer Controlled Systems: Theory and Design*, Prentice-Hall, Second edition, 1990.

[3] Astrom, K. J., *Introduction to Stochastic Control Theory*, Academic Press, Inc., 1970.

[4] Belanger, P.R., *Control Engineering Text*, Fall 1990.

[5] Bollinger, J.G., Duffie, N.A., *Computer Control of Machines and Processes*, Addison-Wesley Publishing Company, 1988.

[6] Brady, B.H.G., Brown, E.T., *Rock Mechanics for Underground Mining*, Boston:Allen and Unwin, 1985.

[7] Chapnik, B.V., Heppler, G.R.,Aplevich, J.D., *Controlling the Impact Response of a One-Link Flexible Robotic Arm*, Proceeding of the International Conference on Robotics and Automation, IEEE, 1990, pp. 1444-1449.

[8] Clarke, A.B., Disney, R.L., *Probability and Random Processes for Engineers and Scientists*, John Wiley & Sons Inc., 1970.

[9] Chung, K.L., *Elementary Probability Theory with Stochastic Processes* Transaction of the Institution of Mining and Metallurgy, 1979.

[10] Colgate, E., Hogan, N., *An Analysis of Contact Instability in Terms of Passive Physical Equivalents*, Proceeding of the International Conference on Robotics and Automation, IEEE, 1989, pp. 404-409.

[11] Cotton, B.B., *Electrics and Hydraulics on Roadheader Machinery*, IMechE, 1985, pp. 13-22.

[12] Craig, J.J., *Introduction to Robotics*, second edition, Addison-Wesley Publishing Company, 1989.

[13] Daneshmend, L.K., and Pak, H.A., *Model Reference Adaptive Control of Feed Force in Turning*, Trans. ASME, J. Dyn. Sys. Meas. and Control, Vol.108, September 1986, pp. 215-222.

[14] Daneshmend, L., Hendricks, C., Wu, H. and Scoble, M., Design of a Mining Shovel Simulator, Proceedings of the International Congress on Mine Design, Kingston, Ontario, Canada, 1993, pp. 551-561.

[15] Daneshmend, L., Scoble, M., etc., *6th Canadian Symposium on Mining Automation*, Montreal, Canada, Oct. 16th-19th, 1994.

[16] Davenport, W.B., *Probability and Random Processes, an introduction for applied scientists and engineers*, McGraw-Hill Book Company, 1970.

[17] D'Souza, A.F., *Design of Control System*, Prentice Hall, Inc., 1988.

[18] D'Souza, A.F. and Garg, U.K., *Advanced Dynamics: Modeling and Analysis*, Prentice-Hall, Inc., 1984.

[19] Franklin, G.F., Powell, J.D., and Workman, M.L., *Digital Control of Dynamic Systems*, Addison-Wesley Publishing Company, 1990.

[20] Goldsmith,W. *Impact: The Theory and Behaviour of Colliding Solids*, Edward Arnold Ltd., London 1960.

[21] Goodwin, G.C., and Sin, K.S., *Adaptive Filtering Prediction and Control*, Prentice-Hall, 1984.

[22] Grenier, A., Chevrette, G., and Coache, C., *Noranda Automatic Guidance System Architecture Overview*, 6th Canadian Symposium on Mining Automation, Sept.1994, pp. 116-119.

[23] Guru, B.S., Hiziroglu, H.R., *Electric Machinery and Transformers*, Harcourt Brace Jovanovich, Inc., 1988.

[24] Hadjigeorgiou, J., *Studies of Machine - Ground Interaction in Surface Mines*, Ph.D. thesis, McGill University, 1993.

[25] Hemami, A., Goulet, S., and Aubertin, M., *On the Resistance of Particulate Media to Bucket Loading*, 6th Canadian Symposium on Mining Automation, Sept. 1994, pp. 171-178.

[26] Hendricks, C., *Performance Monitoring of Electric Mining Shovels*, Ph.D. thesis, McGill University, 1990.

[27] Hendricks, C., Daneshmend, L., Wu, H., and Scoble, M., *Design of a Simulator for Productivity Analysis of Electric Mining Shovels*, Proceedings of the Second International Symposium on Mine Mechanization and Automation, Lulea University of Technology, Sweden, 1993, pp. 329-336.

[28] Hendricks, C., Scoble, M., and Peck, J., *Performance Monitoring of Electric Mining Shovels*, Transactions Institute of Mining and Metallurgy. 1989, pp. A151-A159.

[29] Herceg, E.E., *Handbook of Measurement and Control*, Pennsauken N.J.: Schaevitz Engineering, 1972.

[30] Hettiaratchi, D.R.P., and Reech, A.R., *The Calculation of Passive Soil Resistance*, Géotechnique 24, No.3, 289-310, 1974.

[31] Hollerbach, John M., *A Recursive Lagrangian Formulation of Manipulator Dynamics and a Comparative Study of Dynamics Formulation Complexity*, IEEE Transactions on System, Man, and Cybernetics, Vol.SMC-10, No.11, Nov.1980.

[32] Hostetter, G.H., Savant, C.J.Jr, and Stefani, R.T, *Design of Feedback Control Systems*, Saunders College Publishing, 1989.

[33] Huculak, M., *Compliant Motion with Impact, Time Constraints and Uncertainty*, M.Eng. thesis, McGill University, Sept. 1990.

[34] Izaguirre, A., Hashimoto, M., Paul, R., Hayward, V., *A New Computational Structure for Real-Time Dynamics*, The International Journal of Robotics Research, pp. 346-361, Aug. 1992.

[35] Johnson, C.D., *Theory of Disturbance-Accommodating Controllers*, Control and Dynamic Systems: Advances in Theory and Applications, Vol.12, C.T. Leondes, editor, Academic Press, New York, 1976.

[36] Kahng, J., Amirouche, F.M.L., *Impact Force Analysis in Mechanical Hand Design*, Proceeding of the International Conference on Robotics and Automation, IEEE, 1987, pp. 2061-2067.

[37] Karnopp, D. and Rosenberg, R. *System Dynamics: A Unified Approach*, 1975

[38] Knuth, D.E., *The TEXbook*, Addison-Wesley, 1984.

[39] Kosow, I.L., *Control of Electric Machines*, Englewood Cliffs, N.J.:Prentice-Hall, 1973.

[40] Kuo, B.C., *Digital Control Systems*, Srl, Illinois, 1977.

[41] Kuo, B.C., *Automatic Control Systems*, fourth edition, Prentice-Hall, Englewood Cliffs, 1982.

[42] Lamport, L., *LATEX: A Document Preparation System*, Addison-Wesley, 1986.

[43] Learmont, T., *Current Developments in Surface Mining Excavators*, International Conference on Mining and Machinery, 1979.

[44] Lee, C.S.G., *Robot Arm Kinematics, Dynamics, and Control*, IEEE Computer 1982, pp.62-80.

[45] Lever, P.J.A., Wang, F.Y., and Shi, X., *An Intelligent Task Control System for Dynamic Mining Environments*, For presentation at the SME Annual Meeting, Albuquerque, New Mexico, Feb. 14-17, 1994.

[46] Ljung L., *System Identification: Theory for the User*, Prentice-Hall, 1987.

[47] Ljung L., *System Identification Toolbox*, The Math Works, 1991.

[48] Ljung L., Soderstrom T., *Theory and Practice of Recursive Identification*, The MIT Press, Cambridge, Massachusetts, 1983.

[49] Luh, J.Y.S., Walker, M.W., and Paul, R.P.C., On-Line Computational Scheme for Mechanical Manipulators, Journal of Dynamic Systems, Measurement, and Control, June 1980, Vol.102, pp. 69-76.

[50] Maciejowski, J.M., *Multivariable Feedback Design*, Reading, Mass.: Addison-Wesley, 1989.

[51] Ogata, K., *Modern Control Engineering*, Prentice-Hall, 1990.

[52] Ogata, K., *System Dynamics*, Prentice-Hall, Englewood Cliffs, New Jersey 07632, 1978.

[53] Palm, W.J., Modeling, Analysis, and Control of Dynamic System, New York: Wiley, 1983.

[54] Papoulis, A., *Probability, Random Variables and Stochastic Processes*, McGraw-Hill, New York, 1990.

[55] Patton,R., Frank,P., Clark,R., *Fault Diagnosis in Dynamic Systems*, Prentice Hall, 1989.

[56] Phillips, C.L., Nagle, H.T.,Jr., *Digital Control System Analysis and Design*, Prentice-Hall, Englewood Cliffs, N.J.1984.

[57] Piche, A., *Perspectives of Mine Automation in Canada*, 3rd Canadian Symposium on Mining Automation, Sept.1988, Montreal, pp. 5-6.

[58] Raven, F.H., *Automatic Control Engineering*, 3rd edition, McGraw-Hill, 1978.

[59] Readman, M.C., *Contributions to the Control of Compliant-Joint Manipulators*, Ph.D. thesis, McGill University, 1992.

[60] Reece, A.R., *A Rational Approach to the Design of Earth-Moving Machines*, Journal of Terramechanics, Vol.21, No.1, ; p. 69-79, 1984.

[61] Rose.D.P., *Hydraulic, Electrical, Pneumatic Control-Which Way to Go?*, IMechE 1985, pp. 23-30.

[62] Rowlands, Jeffery C., *Dragline Bucket Filling*, University of Queensland, Ph.D thesis, 1991.

[63] Sarata, S., *Concept of an autonomous system for piled ore shoveling*, Mine Mechanization and Automation, June 1993, Sweden.

[64] Savant, C.J., Stefani, R.T., *Design of Feedback Control Systems*, N.Y.:Saunders College Pub., 1989.

[65] Shinners, S.M., *Modern Control System Theory and Application*, Reading, Mass.:Addison-Wesley Pub.Co., 1978.

[66] Silva, C.W.D., *Control Sensors and Actuators*, Prentice Hall, Englewood Cliffs, New Jersey 07632, 1989.

[67] Soderquist, B.A.T., Wernersson, A., *Information for Assembly from Impacts*, Proceeding of the International Conference on Robotics and Automation, IEEE, 1992, pp. 2012-2017.

[68] Spong, Mark W., Vidyasagar, M., *Robot Dynamics and Control*, John Wiley and Sons, 1988.

[69] Takahashi, Y., Rabins, M.J., Auslander, D.M., *Control and Dynamic Systems*, Addison-Wesley Publishing Company, 1970.

[70] Taylor, D.W., *Fundamentals of Soil Mechanics*, John Wiley and Sons, 1948.

[71] The Math Works, Inc. *Simulink User's Guide*, 1992.

[72] Thornhill, R.J., Smith C.C., *Impact Force Prediction Using Measured Frequency Response Functions*, Journal of Dynamic Systems, Measurement, and Control, Dec. 1983, Vol.105, pp. 227-231.

[73] Timoshenko, S., *Strength of Materials*, 3rd edition, N.Y.: R.E.Krieger Pub.Co., 1976.

[74] Walker, I.D., *The Use of Kinematic Redundancy in Reducing Impact and Contact Effects in Manipulation*, Proceedings of the International Conference on Robotics and Automation, IEEE, 1990, pp. 434-439.

[75] Wang, Yu, Mason, M.T., *Modelling Impact Dynamics for Robotic Operations*, Proceeding of the International Conference on Robotics and Automation, IEEE, 1987, pp. 678-685.

[76] Weaver, W., Timoshenko, S.P., and Young,D.H., *Vibration Problems in Engineering*, , 5th edition, N.Y.: Wiley, 1990.

[77] Wu, H., *Dynamic Modelling, Simulation, and Control of a Vertical Turret Tunnelling Machine*, McGill University M.Eng. thesis, 1992.

[78] Wu, H., Daneshmend, L., *Dynamic Simulation and Computer Control of a Boom-Type Tunnelling Machine*, Proceedings of the International Congress on Mine Design, Kingston, Ontario, Canada, 1993, pp. 539-549.

[79] Wu, H., Daneshmend, L., *Dynamic Control of a Vertical Boom Type Tunnelling Machine*, Proceedings of APCOM XXIV International Symposium on the Application of Computers and Operations Research in the Mineral Industries, Montreal, Quebec, Canada, 1993, pp. 560-567.

[80] Youcef-Toumi, K., Gutz, D.A., *Impact and Force Control*, Proceeding of the International Conference on Robotics and Automation, IEEE, 1989, pp. 410-416.